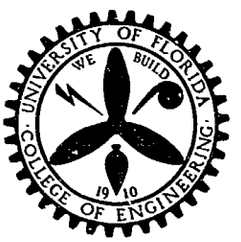

ENGINEERING AND INDUSTRIAL EXPERIMENT STATION

College of Engineering

University of Florida

Gainesville

Final Report

October 31, 1968

Prediction of Explosive Yield and Other Characteristics of Liquid Propellant Rocket Explosions

Contract No. NAS 10-1255

Prepared for
Launch Operations Center
Facilities Engineering and Construction Division
Cocoa Beach, Florida

Prepared by

Dr. E. A. Farber, Principal Investigator
Prof. F. W. Klement
Mr. C. F. Bonzon

University of Florida
Florida Engineering and Industrial Experiment Station
Department of Mechanical Engineering
Gainesville, Florida

Abstract

The study reported upon here was initiated in 1964 to develop a method or methods by which the explosive hazards of liquid propellant rockets can be assessed and the explosive yield predicted.

To be able to do this became of great importance as the rocket sizes increased and the liquid propellant quantities reached levels of millions of pounds, making experimental evaluation practically impossible, necessitating other methods since the hazards to astronauts, launch support personnel, launch support facilities and surrounding communities become potentially enormous.

The work reported upon can be divided into four parts:

Part I. The Mathematical Model

This section of the report includes the development of a mathematical model which can satisfy the presently available experimental information (which is all small scale and very sparse), and at the same time is flexible enough to be able to incorporate future information as it becomes available.

In addition to the above requirements this model has to satisfy the statistical requirements to allow valid estimation procedures to determine the parameters involved and to allow statistical analysis as to probability distributions, probability regions, and confidence limits.

The mathematical model developed and described here is then used to predict such things as the peak value of the probability distributions, the average yield (with half of the yield predictions falling below and half of them falling above this value), the 95 (or any other) percent confidence limit (the yield values below which 95 (or any other) percent of all predicted yield values fall), confidence regions of both the yield and the mixing function, etc.

The mathematical model contains four parameters. For the prediction of yields three of them become fixed, the fourth is allowed to vary with propellant weight so as to become a scaling factor.

The mathematical model with its parameters based upon experiments designed to produce high explosive yields, has been shown to be conservative where predictions from it could be compared with explosive experiments or actual liquid propellant rocket failures for which yield estimates are available. It is believed that the model is also conservative in its predictions where at present no information is available.

Part II. The Seven Chart Approach

This systematic method for the analytical analysis and prediction of the yield from liquid propellant explosions is referred to by the writer and his associates as the "Seven Chart Approach." This name is appropriate since the results of this stepwise investigation can be summarized in seven charts leading to the explosive yield prediction in the last one.

This section contains a more detailed study of what actually takes place and what the phenomena are which contribute to producing or controlling the explosive yield. Naturally this detailed study produces more information and results and answers but it also requires considerably more input information and knowledge about liquid propellant rockets. This information is in many cases not yet available and therefore must be covered, for the time being at least, by assumptions.

The rather complicated problem of the explosive yield prediction was, for the purpose of this study, divided into three parts which can be investigated separately and independently and then when combined give the

desired results. These parts are:

A. The Yield Potential. It is defined as the maximum theoretical explosive yield which can be produced at any time t if the propellants present are mixed in the most favorable manner.

This function can be calculated for given propellants, for selected fuel to oxidizer ratios from Chemical Kinetics, and as a function of time based upon heat transfer theory and some knowledge of the mode of failure and the original configuration of the missile.

Normalized yield potential curves are presented for a few cases in this report.

B. The Mixing Function. This function, referred to by the writer as "Spill" function in his earlier work and publications, is defined as the fraction of the propellants which is actually mixed at any time t. Only this portion can take part in producing the explosive yield.

This fraction can be defined in terms of volume, modified by factors which give the degree to which mixing has progressed, or in terms of contact area between fuel and oxidizer, or in terms of profile surface again modified by proper factors, etc.

The mixing function is controlled by the type of propellants, the rocket size and configuration, and the mode of failure. It will always start at zero at the time of failure, reach a maximum and then decrease again if ignition does not occur. If ignition takes place, the mixing function is terminated at the time of ignition, giving the value controlling the explosive yield.

The mixing function multiplied by the yield potential gives the expected yield as a function of time for the propellants, missile configuration, and mode of failure under consideration.

C. Ignition Time. The ignition time, the third factor, determines what the explosive yield will be of all the possible values, since it gives the point at which the expected yield curve is terminated. Early ignition means a low explosive yield and so does late ignition. Somewhere between, ignition at the right time will produce the maximum explosive yield possible for this combination of propellants, missile configuration, and mode of failure.

It seems that only small quantities of propellants which are presently used, allow control of the ignition time. Propellant quantities of 25,000 lb or more in present missile configurations seem to auto-ignite rather early during the mixing process, producing low explosive yield values. This auto-ignition phenomenon is or can be due to many factors which act as ignition source, such as electrostatic phenomena (one of the prime suspects), failure of electrical systems, cold glow, crystal fracture, failure of structural members, hot engine parts, etc.

Actual rocket failures of larger propellant quantities, than could be used in experiments, produced even lower explosive yield values since relatively little time is available for the mixing process. It takes longer to mix larger quantities of propellants to the same degree. With hypergolic propellants a very short and essentially constant delay time is characteristic and so the yield is determined by how much of the propellants can be mixed during this time interval. With cryogenic propellants the process is more random since the ignition delay time is random in character.

Thus from the above discussion it is possible, when knowing the propellant type and quantity, the missile configuration and the ignition time, either controlled or statistically, to predict the expected yield

in ranges of missile size where experimental results are impossible to obtain.

Part III. Fireball Hypothesis, and Experimental Verification, Describing the Reaction Front and Shock Wave Behavior in Liquid Propellant Explosions.

For better understanding of the phenomena which lead to the production of explosive yield it is advantageous to know what goes on after ignition in a liquid propellant mixture. In collecting information to support and verify the work of Part I and Part II, instrumentation was installed in two 25,000 lb LOX/RP explosive experiments and one 200 lb LOX/RP cold flow and explosive experiment.

First a hypothesis was developed, estimating what should be expected and this was then verified by taking the necessary data.

Such things as

1. The three-dimensional mixing front of a particular constituent
2. The degree of mixing at a particular point
3. The degree of turbulence at a particular point
4. The location of the point or points of ignition
5. The time delay from start of mixing to ignition
6. The propagation of the reaction front
7. The propagation of the shock front
8. The separation of the shock and reaction fronts
9. The fireball and combustion products cloud history, etc.

were discussed and measured by the methods developed in Part II for the experimental determination of the mixing function. Some of the measurements taken are believed to be the first of their kind.

Part IV. Fireball and Post-Fireball Combustion Products Cloud History and Composition

To complete the picture of liquid propellant explosions the information from the other parts of this work was taken and the Fireball and the Combustion Products Cloud further investigated.

The composition as a function of time was determined for a number of fuel/oxidizer combinations using the pressure, temperature and volume time history (all verifiable quantities) as input.

The composition becomes of great interest when toxic propellants are involved in the liquid propellant explosion since new hazards are added which need to be predicted as well as possible and their magnitude assessed.

It is believed that the work presented in this report will materially help the Space Program and provide new information with regard to liquid propellant explosion characteristics and allow the prediction of such things as explosion yields in ranges of propellant quantities where experimentation is not practical if not impossible.

Acknowledgements

It is with sincere appreciation that the authors thank the many faculty members in Engineering, Mathematics, Statistics, and Chemistry who have worked on this project, the many graduate students who have given assistance with the experimentation and the many engineering students who have helped with the computations, preparation of graphs, etc.

Thanks are given to the personnel of the computer center who have given helpful advice in connection with the computer programs developed for this work.

The help given by a group at the Air Force Rocket Propulsion Laboratory, Edwards Air Force Base made it possible to carry out the explosive experiments.

Last but not least NASA personnel, especially Mr. J. H. Deese and Mr. J. P. Claybourne greatly contributed through administrative action to the execution of this contract.

Table of Contents

Table of Contents (Continued)

Table of Contents (Continued)

Table of Contents (Continued)

Table of Contents (Continued)

Table of Contents (Continued

Table of Contents (Continued)

Table of Contents (Continued)

Table of Contents (Continued)

Table of Contents (Continued)

Table of Contents (Continued)

Table of Figures

Table of Figures (Continued)

Table of Figures (Continued)

Table of Figures (Continued)

Table of Figures (Continued)

Table of Figures (Continued)

Table of Figures (Continued)

Table of Figures (Continued)

Table of Tables

Definitions and Symbols
(In order of use)

Part I

y	Explosive Yield
c	Constant
x	Mixing Function
d	Parameter (Constant), Differential Operator
k	Constant
E	Expected Value
f	Function
∞	Infinity
<	Inequality
>	Inequality
b	Parameter (Constant)
c	Parameter (Constant)
a	Parameter (Function)
Γ	Gamma Function
u	Transformation Variable
v	Transformation Variable
Σ	Summation Sign
n	Number of Terms
ψ	Euler's Digamma Function
-	Average Value ($\overline{V}$)
ln	Logarithm (Base e)
P	Probability
V	Volume
r	Error

Definitions and Symbols (Continued)

Subscript	1	First Term
	2	Second or Last Term
	i	ith Term

Part II

y_p	Yield Potential
$\underline{S}O_2$	Solid Oxygen
$\underline{S}$RP-1	Solid RP-1
P	Parameter
$\mathcal{F}$	Group Factor

Part IV

C	Carbon
F, LF_2	Fluorine, Liquid Fluorine
H_2, LH_2	Hydrogen, Liquid Hydrogen
O_2, LO_2	Oxygen, Liquid Oxygen
N	Total Number of Moles of Products of Reaction
N_2	Nitrogen
P	Total Pressure
P_i	Partial Pressure of Constituent i
RP-1	Rocket Fuel
T	Temperature
V	Total Volume
V_i	Partial Volume of Constituent i
W	Total Weight
W_i	Partial Weight of Constituent i

Definitions and Symbols (Continued)

Δ	Incremental Change
∂	Partial Derivative

All other symbols used in the text are defined where they are used.

PART I

Part I

A Mathematical Model for the Prediction of Explosive Yield of Liquid Propellant Explosions.

Introduction

The explosive yields produced by liquid propellant rockets or their estimation did not pose much of a problem as long as the propellant quantities involved were small.

With the size of the rockets increased and the liquid propellant quantities reaching levels of millions of pounds the knowledge of the potential explosive hazard is of utmost importance. The determination of the explosive yield by experimental means is out of question, so other means must be made available to assess the explosive hazards to astronauts, launch support personnel, launch support facilities and surrounding communities, hazards which are potentially enormous.

In Part I of this report a Mathematical Model is developed which can be used in predicting the explosive yield of liquid propellant explosions. How this was accomplished and the results obtainable is explained in the following.

This mathematical model is able to use available data and predict yields, and even give the effects of such things as propellant quantities, propellant type, rocket configuration, mode of failure, etc. upon the explosive yield. A minimum of input data is required.

Analysis of the Mathematical Model, a statistical function, allows the determination of such things as the average value or the peak value of the explosive yield, of the mixing, and the setting of confidence limits as well as the determination of probability regions.

Probably the most useful result of this section is the presentation of the expected yield as a function of propellant quantity. Data which has become available since the model was developed is also shown (Fig. I-8) and they show that the model is very conservative, predicting values somewhat higher than the ones actually encountered.

This mathematical model, having four parameters, is able to use one of them, expressed as a function to bring out the dependency of explosive yield upon such factors as propellant quantity or missile size, propellant type, missile configuration, mode of failure, etc., even in regions for which no information is available.

The mathematical model developed here predicts for rockets such as the Atlas, Titan, Centaur, Jupiter and S-IV, an average explosive yield of about 4 percent of the theoretical maximum and that 95 percent of all explosive yields for this group fall below 11 percent. For the almost six million pounds of liquid propellants of the Saturn V the mathematical model predicts an average yield of 3.8 percent of the theoretical maximum and 95 percent of all explosive yield values are predicted to fall below 9.6 percent of the theoretical maximum.

Theory of Approach

The approach used in the development of the mathematical model was to first look at the data available at that time and then to try to analyze this data mathematically so as to extract the maximum amount of information from it. The goal was the ability to predict the explosive yield from liquid propellant explosions.

Yield and Mixing Function

Since the determination of the explosive yield was the ultimate objective of this study it was defined for the purpose of this study as the fraction of the theoretically maximum explosive yield based upon the total propellant quantity present at the beginning of the experime... or at launch of an actual missile.

Since the yield is dependent upon the mixed portion of propellants the Mixing Function is defined as the fraction mixed, of the propellants present. This Mixing Function can be expressed in terms of volume, modified by factors giving the degree of mixing which has occurred, in terms of contact area between oxidizer and fuel, or in terms of profile surface again modified by various factors, etc.

This method of defining the explosive yield and the mixing function[1,2,3,4,5] eliminates the necessity of relating one propellant type to another or one explosive to another which is a very difficult problem since the pressure-time traces from different propellant explosions are different.

TNT Equivalency

Since much of the work on liquid propellants is reported in terms of "TNT Equivalent Yields," it was suggested that the investigators provide some indication on how the yield values obtained here could possibly be converted into equivalent TNT values.

The explosive yields defined as the fraction of the theoretical maximum (Normalized Yields) can be changed into "TNT Equivalent Yields" using the method given by Arthur D. Little, Inc.[6] The results presented on page 70 of the above reference lead to the following correlation:

A. 1 lb of LOX/RP propellant in a 2.25/1 weight ratio is potentially equivalent to 1.23 lb of TNT.

B. 1 lb of LOX/LH_2 propellant in a 5/1 weight ratio is potentially equivalent to 1.52 lb of TNT.

C. 1 lb of LOX/RP/LH_2 propellant in a weight composition of 0.75/0.18/0.07 (Saturn C-2 Configuration) is potentially equivalent to 1.355 lb of TNT.

D. 1 lb of LOX/RP/LH_2 propellant in a weight composition of 0.721/0.244/0.035 (Saturn V Configuration) is potentially equivalent to 1.29 lb of TNT.

Caution must be used when this is done since not enough is known at this time of how to properly equate the pressure-time traces of different propellant and explosives to each other. This is especially true when damage indeces are attached to these yield values because even though the explosive yield value may be the same, due to the difference in pressure-time trace, different propellants can be expected to do a different amount and type of damage.

Yield and Mixing Data

The data found most promising for the desired analysis and almost the only data available was that of the Arthur D. Little Spill Test series[6] where tanks with fixed quantities of liquid propellants were dumped into a general spill area. Calibration of the quantity spilled as a function of time could give information of what was later defined as the "spill function"[1,2] and the "yield function"[1,2,3,4,5]. The spill function is now referred to as the "mixing function."

The data is presented in Table I. Different propellant quantities were used, 45, 60, 110, 220, 320, 530 and approximately 44,000 lb.

The propellant types used were LOX/RP, LOX/LH_2, and LOX/RP/LH_2. In general the data indicated that the more of the propellants were mixed the higher was the explosive yield obtained, suggesting a relationship between yield and mixing.

Controlled and Auto-Ignition

A significant difference in behavior was noticed in the data. The small propellant quantity experiments could be detonated at will producing yields according to the portion mixed at that time. If ignition was initiated early a low yield was obtained, when very late also a low yield was obtained. In between these times the values were higher and so for the purpose of the analysis here the highest observed explosive yield values were taken since they could be obtained at will.

In the 44,000 lb experiments auto-ignition occurred in each case much before the planned initiation time thus limiting the yield and producing much lower yields. This auto-ignition phenomenon was observed in later experiments and seems to occur with statistical certainty for quantities of 25,000 lb and above. The actual critical weight is probably below this figure but no data is available between 1000 and 25,000 lb.

This auto-ignition phenomenon, which will be discussed in greater detail in Part II, seems to be a very significant limiting factor in the explosive yield obtainable with large liquid propellant rockets.

Yield - Mixing Relationship

It is clear that when none of the propellants are spilled and no mixing has occurred no reaction can take place and therefore no explosive yield can result. Thus when the mixing function is zero the yield must be zero.

In the small scale experiments with liquid propellants the time of ignition and thus detonation could be controlled and so any desired yield up to the maximum (a function of fuel/oxidizer ratio) could be obtained. So as to be on the conservative side the theoretically possible maximum yield value was taken for the explosive yield. This gave an explosive yield value of 0.78 for a mixing function of 1.

The above two points form the limiting values and the other three, the J series of experiments fall between them. The data is presented in Table I and is also plotted on Fig. I-1. Closer inspection of the data suggests an exponential functional relationship between the yield and mixing function of the type

$$y = C\, x^{d} \qquad (1)$$

The Mathematical Model

From the above it seemed that an exponential function can properly express the yield - mixing function relationship with flexibility enough to satisfy new data when it becomes available.

Having this relationship the next step was to develop a mathematical function which could incorporate this relationship and at the same time could satisfy all the statistical requirements necessary to allow valid estimating procedures for the parameters involved and then allow statistical analysis of the function so as to obtain explosive yield predictions of average values, peak values, confidence limits and confidence regions in terms of propellant quantities or rocket size.

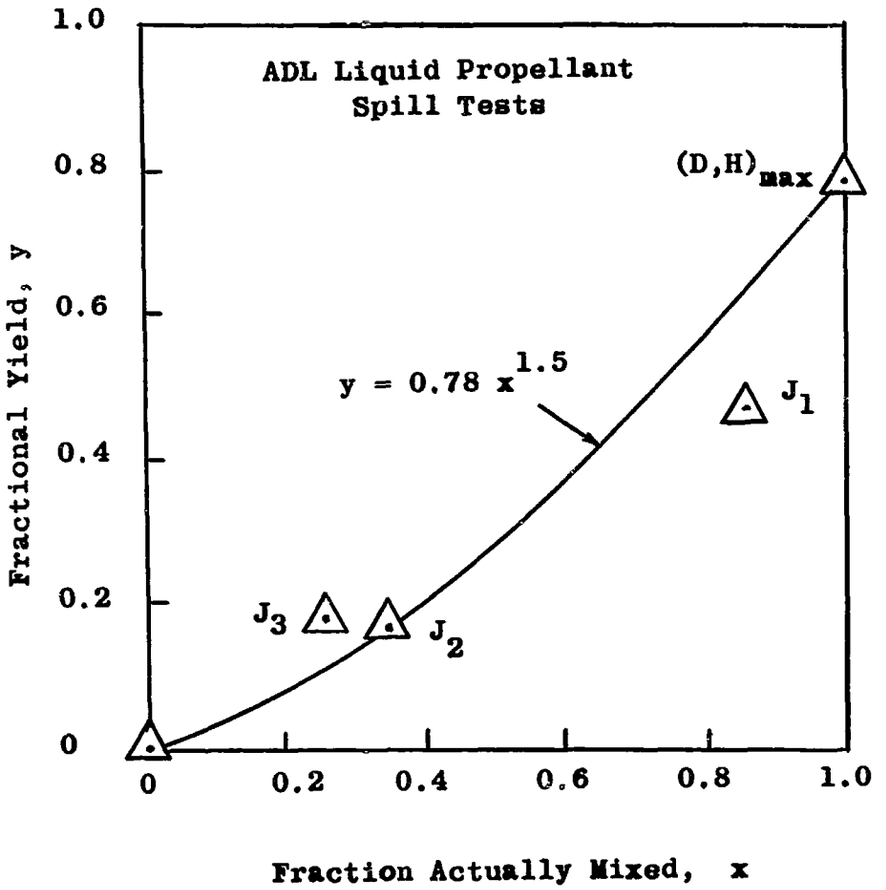

Figure I-1 "Yield Function - "Mixing" Function Relationship

Information Available

From the above it is obvious that the given information, the explosive yield function (y) and the spill mixing function (x) constitute two random variables such that

$$0 \leq x \leq 1$$
$$0 \leq y \leq k \qquad (2)$$
$$k < 1$$

and that the expected value of the yield function (y) for any value of the mixing function (x) is

$$E(y/x) = \text{some appropriate non-linear function of } x$$
$$= C\, x^d \text{ based upon available data} \qquad (3)$$

The mathematical problem was to find a Bivariate Probability Density Function satisfying these conditions.

Requirements

The statistical requirements for this function needed here are that the expected (or mean) value of y for any given x value is

$$E(y/x) = C\, x^d$$
$$= \int_0^1 y \, \frac{f(x,y)}{\left[\int_0^{x^d} f(x,y)\, dy\right]} \, dy \qquad (4)$$

Search for a Suitable Function

No ready made, suitable function to satisfy the above relationship could be found.

The usual Gaussian function is not suitable since the limits are $(-\infty, +\infty)$ and $E(y/x)$ = Linear function of x.

The usual Dirichlet Bivariate function (see Wilks: Mathematical Statistics)[7] has limits

$$\begin{aligned} 0 \leq x \leq 1 \\ 0 \leq y \leq 1 \\ 0 \leq x-y \leq 1 \end{aligned} \qquad (5)$$

but again $E(y/x)$ is a linear function of x.

However the Dirichlet Bivariate function can be modified to make $E(y/x)$ equal to a non-linear function of x, in particular

$$E(y/x) = C\, x^d \qquad (6)$$

This is a non-linear function that seems to meet the Engineering requirements of the problem.

Development of the Function

In the theory of definite multiple integrals one can find a class of integrals known as the Liouville-Dirichlet Integrals. These are described by SERRET ("Cours de Calcul Differentiel et Integral," Paris 1907)[8] and by GRADSHETEYN & RYSHIK[9] in the "Tablitsy Integralov" Moscow 1963 (Integrals Number 4.631 to 4.648).

S. S. WILKS (mathematical Statistics, 1962)[7] uses one of these integrals to define a multivariate probability density function and this is called the DIRICHLET Distribution (p. 177).

Its Bivariate form becomes

$$f(x,y) = \frac{\Gamma(a+b+c)}{\Gamma(a)\Gamma(b)\Gamma(c)} x_1^{a-1} x_2^{b-1} (1-x_1-x_2)^{c-1} \qquad (7)$$

with $x_1>0$, $x_2>0$, $x_1-x_2<1$

To adapt the Dirichlet Distribution to the problem at hand the following change in variables is made. Let

$$\begin{aligned} x_1 &= 1 - x^d \quad \text{where } x \text{ is the Mixing function} \\ x_2 &= y \quad \text{where } y \text{ is the Yield function} \end{aligned} \qquad (8)$$

After mathematical manipulation and simplification the desired function in x and y is obtained both satisfying the physical data and the statistical requirements. It is

$$f(x,y) = \frac{d\Gamma(a+b+c)}{\Gamma(a)\Gamma(b)\Gamma(c)} x^{d-1}(1-x^d)^{a-1}y^{b-1}(x^d-y)^{c-1} \qquad (9)$$

The only restrictions on this equation are that

$y>0$, $x>0$, $y \leq x^d$, $d \neq 0$

Carrying out the mathematical operation indicated in equation (4)

$$E(y/x) = \int_0^1 y \; \frac{f(x,y)}{\left[\int_0^{x^d} f(x,y)\, dy\right]} \, dy = \frac{b}{b+c} \; x^d \qquad (10)$$

The last expression, equation (10) shows that the mathematical function developed here satisfies all the statistical requirements as well as the functional relationship, connecting the yield function (7) and the mixing function (x).

Confidence Regions

To enable the construction of a confidence region for (x,y) use is now made of the fact that the transformed variables

$$\begin{aligned} u &= 1 - x^d && 0 \leq u \leq 1 \\ v &= \frac{y}{x^d} && 0 \leq v \leq 1 \end{aligned} \qquad (11)$$

both independently follow the BETA distributions

$$f_1(u) = \frac{\Gamma(a+b+c)}{\Gamma(a)\Gamma(b+c)} \; u^{a-1}(1-u)^{b+c-1} \qquad (12A)$$

$$f_2(v) = \frac{\Gamma(b+c)}{\Gamma(b)\Gamma(c)} \; v^{b-1} \; (1-v)^{c-1} \qquad (12B)$$

so that

$$f_3(u,v) = f_1(u) \; f_2(v) \qquad (13)$$

or in other words that the function of both u and v is equal to the function of u multiplied by the function of v (equation 12A times equation 12B).

Given the numerical values of the parameters a, b, and c the two sided 95 percent confidence interval can be found from (12B)

$$\text{Prob. } (v_1 \leq v \leq v_2) = 0.95$$

where v_1 and v_2 can be determined from the Beta Tables.

Substituting for v we find the 0.95 confidence interval for the yield function (y)

$$\text{Prob. } (v_1 x^d \leq y \leq v_2 x^d) = 0.95 \qquad (14A)$$

From (12A) one has

$$\text{Prob. } (u_1 \leq u \leq u_2) = 0.95$$

where u_1 and u_2 are determined from tables.

Substituting for u one finds the 0.95 confidence interval for the mixing function (x)

$$\text{Prob. } \left((1-u_2)^{\frac{1}{d}} \leq x \leq (1-u_1)^{\frac{1}{d}} \right) = 0.95 \qquad (14B)$$

Combining (14A) and (14B) one obtains the Joint Confidence region as shown in Fig. 1-2.

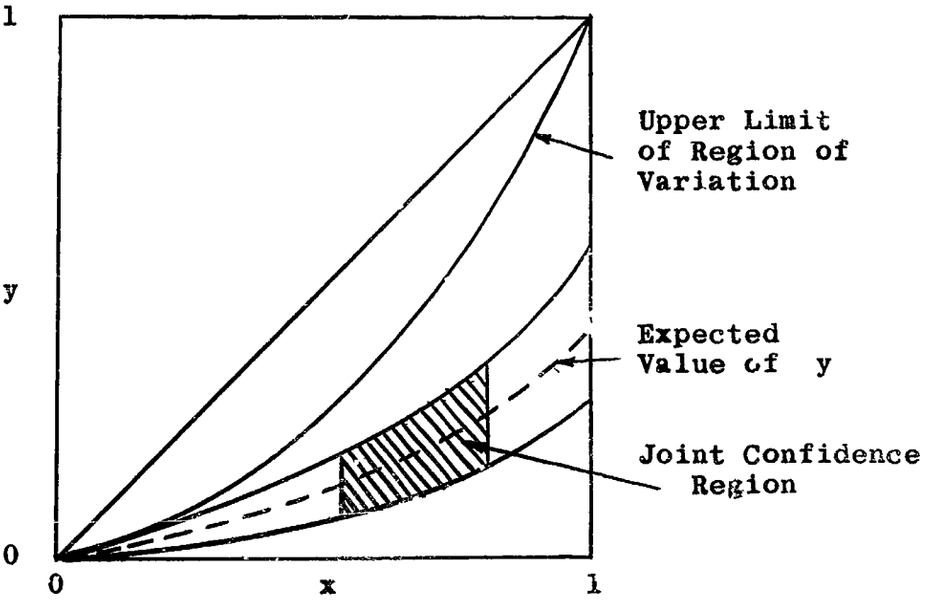

Figure I-2 "Yield" - "Mixing" Confidence Region

Estimation of Pa ameters

As shown in equation (9) the Modified Dirichlet Distribution de· ·d here is characterized by four parameters a, b, c, and d. The next step is to estim. e these from observed data.

Many of the standard methods of estimation have been shown to be unreliable when functions like the Dirichlet are involved.

The usual method of Maximum Likelihood estimation leads to intractable equations and the estimates derived are biased to an unknown degree.

The other method of Moments also leads to difficult equations and is known not to be very reliable in functions like the Dirichlet.

Mostly for the sake of simplicity the following procedure was developed.

Parameter "d"

First . imate the parameter "d" from relation (10). Taking logarithms one obtains

$$\ln E(y/x) = \ln \frac{b}{b+c} + d \ln x \qquad (15A)$$

and identifying this with the data by writing

$$\ln y = \ln \frac{b}{b+c} + d \ln x \qquad (15B)$$

Since both x and y and hence $\ln x$ and $\ln y$ are random variables, the ordinary least square method of estimating "d" is not advisable nd WALD's method[10] is recommended, (A. Wald, ANNALS of Mathemat· ·l Statistics 1·, 1940, p. 284[10]) leading to the relationship

$$d = \frac{\sum_{n+1}^{2n} \ln y_i - \sum_{1}^{n} \ln y_i}{\sum_{n+1}^{2n} \ln x_i - \sum_{1}^{n} \ln x_i} \qquad (16)$$

In the procedure described in the reference leading to equation (16) it is only necessary to arrange the x_i's in order of their magnitude.

The equation can be applied directly to an even number of observations or can be modified to apply to an odd number.

Equation (16) when applied to a small number of observations gives the parameter d with an inherent degree of conservativeness and the result can be compared with results from other estimating procedures.

Parameters "b" and "c"

Having obtained a numerical value for "d" from the above procedure the observed data (x_i, y_i) can be transformed to (u_i, v_i).

$$u_i = 1 - x_i^d$$

$$v_i = \frac{y_i}{x_i^d} \qquad (17)$$

Returning to relationship (12B) the expected value of v is calculated

$$E(v) = \int_0^1 v\, f(v)\, dv = \frac{b}{b+c} \qquad (18)$$

and

$$\ln [\, E(v)] = \ln b - \ln (b+c) \tag{19}$$

Also calculate

$$\begin{aligned} E(\ln v) &= \int_0^1 \ln v \, f(v)\, dv \\ &= \psi(b) - \psi(b+c) \end{aligned} \tag{20}$$

The properties of Ψ (Euler's Digamma Function) are given in the National Bureau of Standards "Handbook of Mathematical Functions"[11] or in the Jahnke-Emde-Loesch "Tables of Higher Functions."[12]

Identifying the above results with observed data by replacing $E(v)$ by $\bar{v}$ (mean of observed data v_i) and $E(\ln v)$ by $\overline{\ln v}$ (mean of logs of observed data v_i) one obtains

$$\overline{\ln v} = \Psi(b) - \Psi(b+c) \tag{21}$$

$$\ln \bar{v} = \ln (b) - \ln (b+c) \tag{22}$$

Equations (21) and (22) become the estimation equations for the parameters "b" and "c."

Parameter "a"

Repeating the above procedure for u leads to equations involving parameter "a" and these become the estimation equations for that parameter. They are:

$$\overline{\ln u} = \Psi(a) - \Psi(a+b+c) \tag{23}$$

$$\ln \bar{u} = \ln (a) - \ln (a+b+c) \tag{24}$$

Applying the above procedures all four parameters can be evaluated in terms of the available data.

The Mathematical Model is now ready with the parameters a, b, c, and d giving it its characteristic configuration, and analysis of the resulting statistical surface produces a wealth of new information.

Characteristics of the Mathematical Model

The parameters a, b, c, and d give the mathematical model, expressed by the function of equation (9) its characteristics, which can be brought out by proper mathematical analysis. Some of the most significant results with regard to this investigation are the

A. Probability Distribution of the Yield, P_y

B. Probability Distribution of the Mixing, P_x

C. Confidence Regions for the Yield and Mixing Functions

D. Confidence Limits for the Yield Function

E. Confidence Limits for the Mixing Function

A discussion of how these characteristics can be extracted from the mathematical model follows.

A. Probability Distribution for the Yield, P_y

To obtain the probability distribution for the yield function it is only necessary to determine the ordinate of the probability distribution for each value of y.

This ordinate for a particular value of y represents the cross-sectional area of the mathematical model at this value of y and

perpendicular to the x-y plane. This area can be obtained graphically, or by integration requiring a large scale computer.

The integral representing the probability ordinate is

$$P_y(y) = \int_{\underline{y}^d}^{1} f(x,y)\, dx \qquad (25)$$

The lower limit of this equation (25) is the value at which f(x,y) becomes positive for the chosen value of y. The function f(x,y) is given in equation (9).

B. Probability Distribution for the Mixing Function, P_x

To obtain the probability distribution for the mixing function the procedure is the same as in the above section except that the variables x and y are interchanged so as to obtain the integral

$$P_x(x) = \int_0^{x^d} f(x,y)\, dy \qquad (26)$$

Here the upper limit is the value of y at which f(x,y) becomes negative for a chosen value of x.

C. Confidence Regions for Yield and the Mixing

To obtain the probability regions for the mixing (x) and the yield (y) it is necessary to determine the volume under the probability surface, and then to establish the regions which contain a desired subvolume.

In this manner the regions are obtained representing the intersections of planes, parallel to the x-y plane, with the surface which define the

subvolumes. These intersections projected as regions simulate contour lines on a topographical map representing the various elevations.

The above analysis can be made by building a physical model of the mathematical function (using clay, putty, wood, and so forth) and by determining the total and subvolumes by sectioning, submersion in liquid, etc.: it can also be done mathematically by double integration, again necessitating a large-scale computer. The integrals to be solved are

$$V_{x,y} = \int_0^1 \int_0^{x^d} f(x,y)\, dy\, dx \tag{27}$$

for the total volume and with different limits for the subvolumes. The limits of the integrals have to give the required subvolumes to include the desired percentages of x and y surface values.

D. Confidence Limits for the Yield Function

To obtain confidence limits for the yield function it is necessary to work with fractional areas under the yield probability distribution.

The fraction of the total area under the probability distribution lying between values of y represents the fraction of all y values in this interval. If the highest statistically expected yield value is desired with a confidence, let us say, of 95 percent, then the value of y has to be found for which 95 percent of the area under the probability distribution curve lies to the left of it. Many other questions of this type can be answered in this manner.

E. Confidence Limits for the Mixing Function

The same information regarding the mixing function can be obtained as were described above for the yield. The procedure is the same except that the mixing probability distribution curve is used in this case.

Information in addition to the above, can be extracted from the mathematical model by sectioning it and subsectioning it physically or mathematically in various ways.

Application of the Mathematical Model

In this section it will be shown how the mathematical model developed above can be used on available information.

The only data reported for which complete mixing and yield information is available is shown in Table I-I.

Table I-I

Experimental Data of Liquid Propellant Explosions[6]

1.	$(D,H)_{max}$	Test Series	Y = 0.78	x=1
2.	J_1	Experiment	0.47	0.85
3.	J_2	Experiment	0.17	0.35
4.	J_3	Experiment	0.18	0.25

The writer of this report and his associates have made a great number of inert mixing studies, discussed later in this report as well as installed thermocouple grid instrumentation in two 25,000 lb LOX/RP liquid propellant explosion experiments and in one 200 lb LOX/RP cold flow and liquid propellant explosion experiment, performed under project PYRO. The thermocouple grid was installed in the fuel tanks where most

of the mixing occurred. The results strongly support the yield function-mixing function relationship exhibited by the data in Table I-I. This fact gives credence to the assumption that the yield - mixing relationship is a characteristic of the propellants themselves.

The first step in giving the mathematical model the specific characteristics exhibited by the data is to evaluate the parameters a, b, c, and d.

Estimation of the Parameters

Parameter "d"

Three methods for the estimation of this parameter were employed here even though some of them have been shown not to be reliable when functions of the Dirichlet type are involved.

Method of Averages

The basis for this method is that the error of a particular data point from the true value is to be made as small as possible. Thus if

$$r_i = f(x_i) - y_i \tag{28}$$

the best curve fit is obtained when

$$\Sigma r_i = 0 \tag{29}$$

This method applied to the data of Table I results in a curve

$$y = \frac{b}{b+c}\ x^d = 0.78\ x^d \tag{30}$$

with a "d" value too high and thus a curve too low (thus not conservative) to be a good fit for the data.

Method of Least Squares

This widely used method often gives the most probable equation, best fitting the data, assuming that the residues follow the Gaussian Law of Error. Again this method has been shown not to give very good results for functions like this one. If applied however

$$r_i = \bar{y} - y_i \tag{31}$$

and the best fit is obtained when

$$\Sigma r_i^2 = 0 \tag{32}$$

This method applied to the data of Table I-I results in a curve

$$\bar{y} = \frac{b}{b+c} x^d = 0.78\ x^d \tag{33}$$

with the value of "d" better but still too high, resulting in average values too low (again not conservative). Plotting the resulting curve over the data reveals this by simple inspection.

Wald's Method

For functions like the Dirichlet, Wald[10] recommends the method previously discussed, culminating in equation (16). Applying this equation to the data of Table I-I a value for "d" is obtained which is too small, resulting in the curve

$$y = \frac{b}{b+c} x^d = 0.78\ x^d \qquad (34)$$

which falls too high when plotted over the data (thus over conservative).

Combining the three methods of estimation results in the curve

$$y = 0.78\ x^{1.5} \qquad (35)$$

which with the d = 1.5 giving the best fit.

If more data had been available the estimation procedure would have been much better and the confidence in the resulting value of "d" would be increased.

Parameters b and c

The next step is the evaluation of the parameters "b" and "c." The relationship

$$y = \frac{b}{b+c} x^{1.5} = 0.78\ x^{1.5} \qquad (36)$$

is not enough since it gives one equation with two unknowns. It was however shown earlier that two estimation equations could be derived and they were given as equation (21) and (22). Use only the J series data from Table I-I, since the two anchor points of the curve lead to undefined values for u and v. The first anchor point of this curve had actually already been used. With the numerical values the equations (21) and (22) become respectively (37) and (38)

$$-0.30 = 1.2 - 1.5 \qquad (37)$$

$$-0.28 = 1.37 - 1.65 \qquad (38)$$

for values of b = 4, and c = 1.1.

Parameter "a"

It has been shown above that all parameters except "a" have been determined using the available data. To evaluate the parameter "a" for a given set of data the value for "a" can be calculated, and when applied with the other parameters to the Dirichlet Distribution the analysis of this function will give results characteristic of all the data.

If however there are basic differences according to which the data may logically be grouped then the parameter "a" becomes a function which can describe the effects of the differences. If for instance, the various data points represent different propellant weights then the function of "a" will become a scaling function. This same procedure can be applied to propellant type, missile configuration, missile failure mode, etc.

Analysis of the Experimental Data by Means of the Mathematical Model

Using the data in Table I-I, a weighted value of 3.5 is assigned to data point (1, 0.78) since this point represents a great number of experiments of small scale involving three separate Oxidizer/Fuel combinations, LOX/LH_2, LOX/RP, $LOX/RP/LH_2$, and several different propellant quantities. The J series points and anchor point (0,0) were given a weighted value of 1.

Utilizing the estimation equations for parameter "a" namely (23) and (24), a value for "a" = 3.1 is obtained. Having all the parameters the Dirichlet distribution, equation (9) becomes

$$f(x,y) = \frac{1.5\ \Gamma(8.2)}{\Gamma(3.1)\Gamma(4.0)\Gamma(1.1)}\ x^{0.5}(1-x^{1.5})^{2.1}y^{3.0}(x^{1.5}-y)^{0.1}$$

(39)

which is the mathematical model describing this data and it can be analyzed as discussed earlier.

The function has a very characteristic shape as shown in Fig. I-3 and is referred to by the writer and his associates as "Shark Fin."

This mathematical model has been programmed on the IBM 360 computer and gives probability distribution, confidence limits and confidence regions for different values of the parameters.

Fig. I-4A, I-4B, and I-4C give the results for the parameters

$$a = 3.1,\ b = 4.0,\ c = 1.1,\ d = 1.5$$

which represents all the experimental data in Table I-I. They give the yield probability distribution, the mixing probability distribution and the yield - mixing confidence regions.

From the probability distributions the peak values can be found, the average values (the value of yield or mixing which divides the area under the probability distribution in half), the 95 percent confidence interval (the value of yield or mixing below which 95 percent of all expected yield or mixing values will fall - the value to the left of which 95 percent of the area under the probability distribution lies). The probability regions around the peak value include 50, 70, 83, 93, and 100 percent of all yield and spill values. Further information is given in reference 2.

Analysis of Missile Failures by Means of the Mathematical Model

The above procedure of applying the mathematical model to the experimental data exhibited a wealth of information which can be extracted by such analysis.

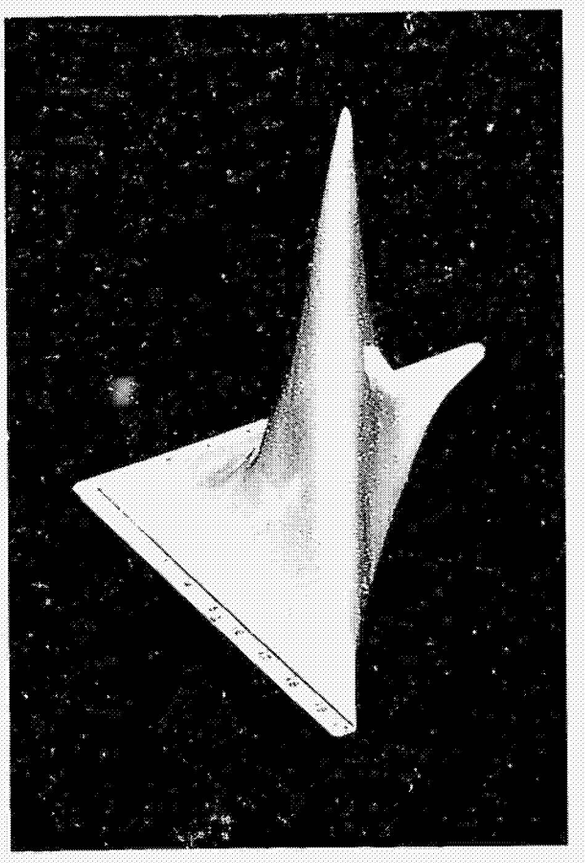

Figure I-3 The Mathematical Model Represented by a Statistical Surface

The Mathematical Model, a = 3.1, b = 4.0, c = 1.1, d = 1.5

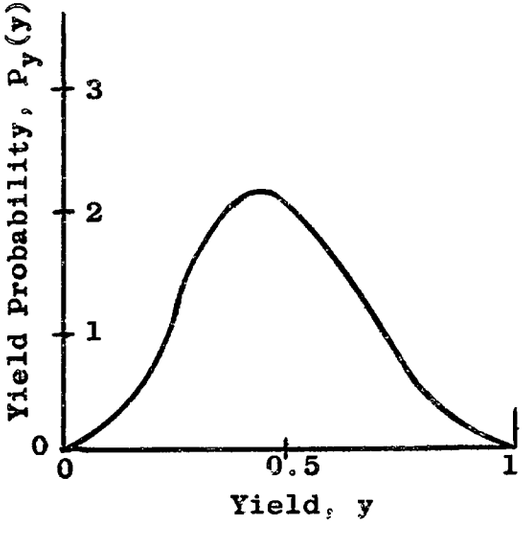

Figure I-4A Probability Distribution for the Yield Function (Experimental Results)

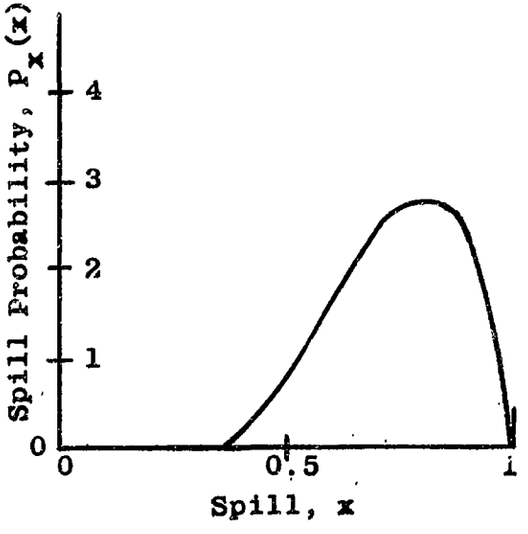

Figure I-4B Probability Distribution for the Spill Function (Experimental Results)

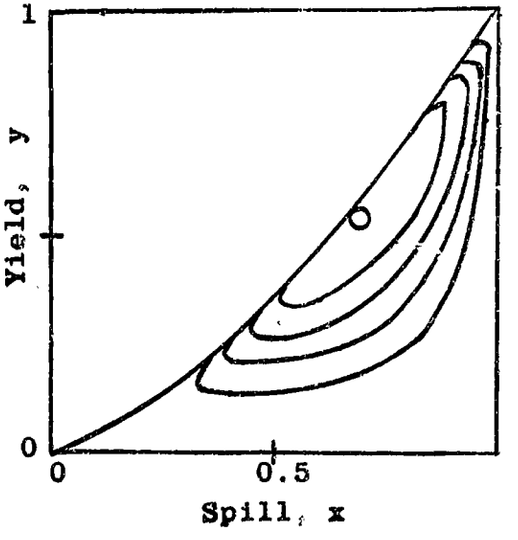

Figure I-4C Yield-Spill Probability Regions (Experimental Results)

In this section the mathematical model will be used on yield estimates of actual missile failures, presented in Table I-II.

To be able to use this data since only yield could be estimated it was necessary only to assume that the yield - mixing relationship, a basic propellant characteristic, holds for this data. Theoretically this is a good assumption which is further supported by two 25,000 lb PYRO experiments which were partially instrumented by the writer and his associates to establish in addition to other things this very fact.

Evaluation of the parameters for the missile failures as presented in Table I-II (using TNT values to be conservative) give

$$a = 70,\ b = 4.0,\ c = 1.1,\ d = 1.5$$

and the analysis based upon the mathematical model controlled by these values for the parameters is presented in Fig. I-5A, I-5B and I-5C.

A closer look at these figures shows that the average yield value for this group as predicted by the model is 4 percent and 95 percent of all the yields fall below 11 percent.

Only the 80 percent confidence region is presented in Fig. I-5C since it already is very small indicating that rather close grouping of the expected yields and mixing will result.

Scaling by Means of the Mathematical Model

If the effect of the size or quantity of propellants (on board at launch) is desired the data can be grouped according to propellant quantity and the parameter "a" can be calculated for each group.

It must be realized that with already sparse data, by doing this, some uncertainty is introduced since each "a" value is based upon fewer

Table I-II

Yield Estimates and Data of Missile Failures[2]

				Yield, TNT	Yield, Norm.
5.	Atlas 9-C	LOX/RP	250,000 lb	0.18	0.147
6.	Atlas 48-D	LOX/RP	250,000 lb	0.08	0.065
7.	Atlas	LOX/RP	250,000 lb	0.06	0.049
8.	Titan 1 (Impact)	Hyp.	230,000 lb	~0.02	0.016
9.	Titan 1	Hyp.	230,000 lb	~0.01	0.008
10.	Atlas	LOX/RP	250,000 lb	0.0088	0.008
11.	Centaur	LOX/LH_2	282,000 lb	0.029	0.024
12.	Jupiter # 9 (Impact)*	LOX/RP	120,000 lb	0.11	0.09
13.	S-IV Failure	LOX/LH_2	100,000 lb	0.01	0.008
14.	S-IV Test (PYRO)	LOX/LH_2	92,000 lb	0.03-0.06	0.036

* y Based upon propellant quantity at time of impact

The Mathematical Model, a = 70, b = 4.0, c = 1.1, d = 1.5

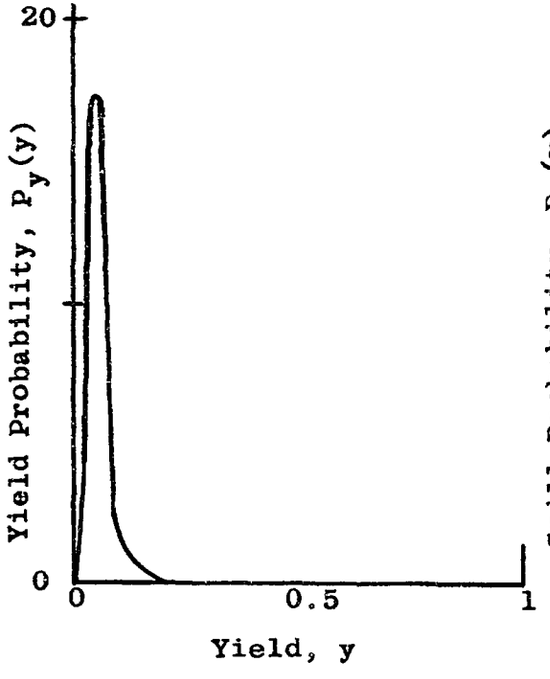

Figure I-5A Probability Distribution for the Yield Function (Missile Failures)

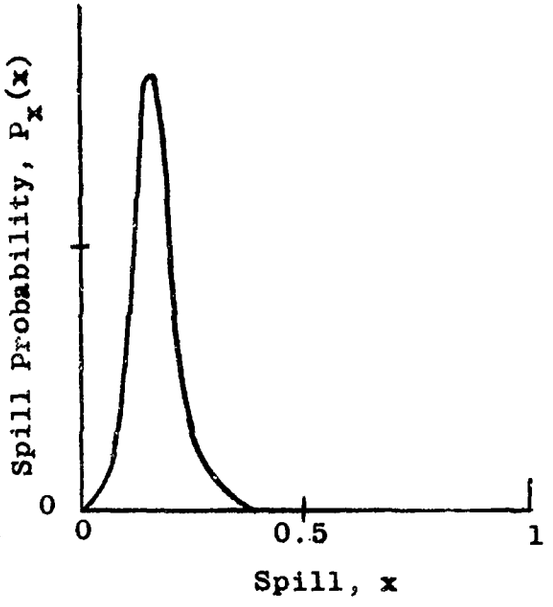

Figure I-5B Probability Distribution for the Spill Function (Missile Failures)

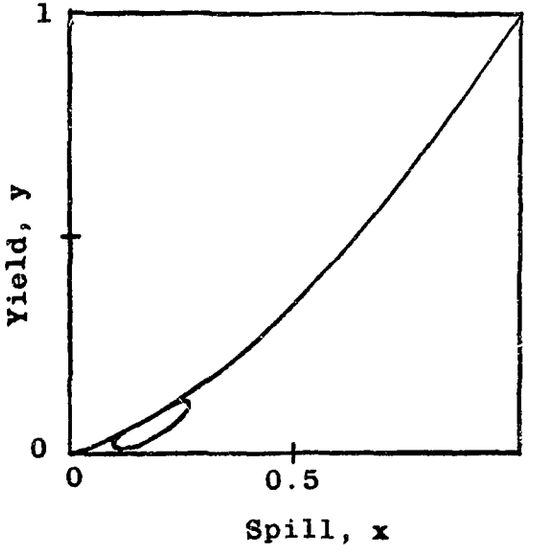

Figure I-5C Yield-Spill Probability Regions (Missile Failures)

points. This problem will however correct itself as more data become available.

Using the small experiments of about 200 lb average the "a" value when calculated as outlined above is less than 2.

For the J test series of almost 44,000 lb of propellants the "a" value becomes 7.5.

In the about 100,000 lb class the best point, since it is based upon actual measurements, is the S-IV Test, and the highest explosive yield value is used for analysis. It gives a value for "a" of 60. Point 14 in Table I-II is an estimate and point 12 gives a yield which was based upon an estimate of the propellant quantity on board at the time of impact, thus giving too high a value as compared to the launch quantity of propellants. The writer could not find out what the impact quantity was so did not feel it advisable to use another value.

For the 250,000 lb class or group points 5 through 11 of Table I-II were used resulting in an "a" value of 70.

For these calculations as those of the previous section the yield values were taken as reported rather than normalized since the accuracy of the estimates is not known and this procedure will keep the analysis on the conservative side.

The results are summarized in Table I-III

Table I-III

Parameter "a" as a Function of Propellant Weight

200 lb	a = 2
44,000 lb	7.5
100,000 lb	60
250,000 lb	70

These results are graphically represented in Fig. I-6 which shows that the parameter "a" as a function of propellant weight forms a distorted S curve indicating that an increase in propellant weight increases the value "a" and thus decreases the yield values predicted. It indicates further that the curve still increases beyond the last known point but at a decreasing rate.

Studying Fig. I-6 the value of "a" can be bracketed ~~in for, let us~~ say, propellant quantities of the Saturn V class. It is shown that the value is definitely higher than it is at the last known point. On the other hand since the curve continues at a decelerating rate a straight line between the last two known points will, when intersected with the Saturn V propellant quantity, overshoot or give a value of "a" too large. So the true value of "a" can be expected to lie between these two extremes. In this case between 70 and 97.

If the mathematical model is taken and the value "a" varied in the computer program the effect of "a" on the yield prediction can be found. Fig. I-7 presents the effect of "a" upon the average yield value. It shows that at the higher values of "a" the predicted yield values changes little or in other words that the yield sensitivity with respect to the parameter "a" at higher values of "a" is low. Thus even inaccuracy in the value "a" due to insufficient data will have little effect on the explosive yield predicted.

From Fig. I-7 and the "a" values obtained from Fig. I-6 the predicted average yield value for the Saturn V based upon the mathematical model is between 3.5 and 4 percent.

Fig. I-8 presents the results in the most useful form, showing the average expected yield value and the 95 percent confidence limit as

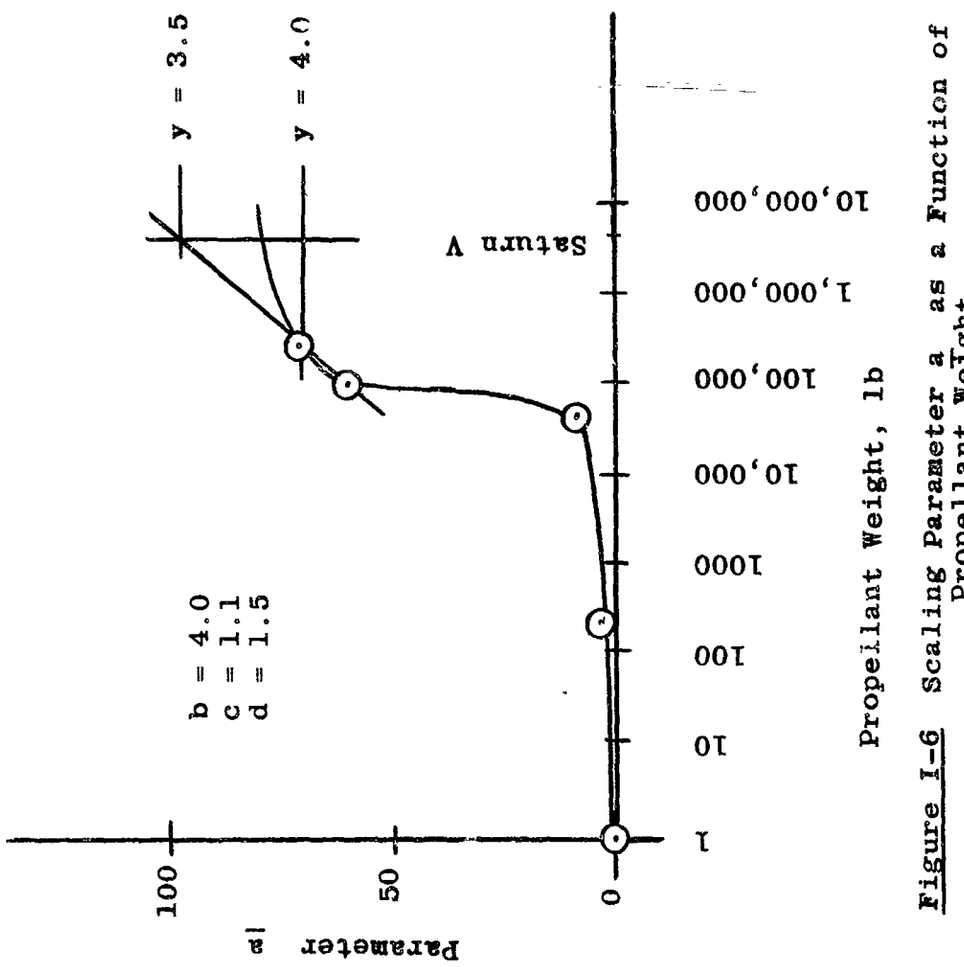

Figure I-6 Scaling Parameter a as a Function of Propellant Weight

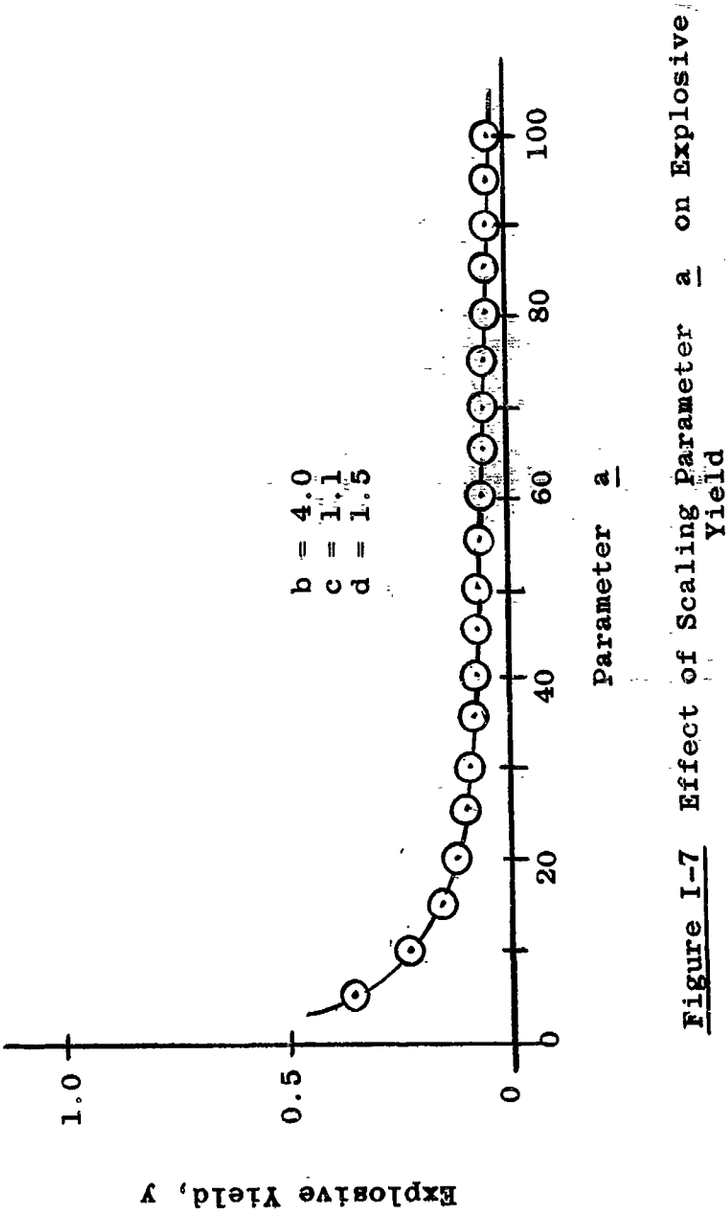

Figure I-7 Effect of Scaling Parameter a on Explosive Yield

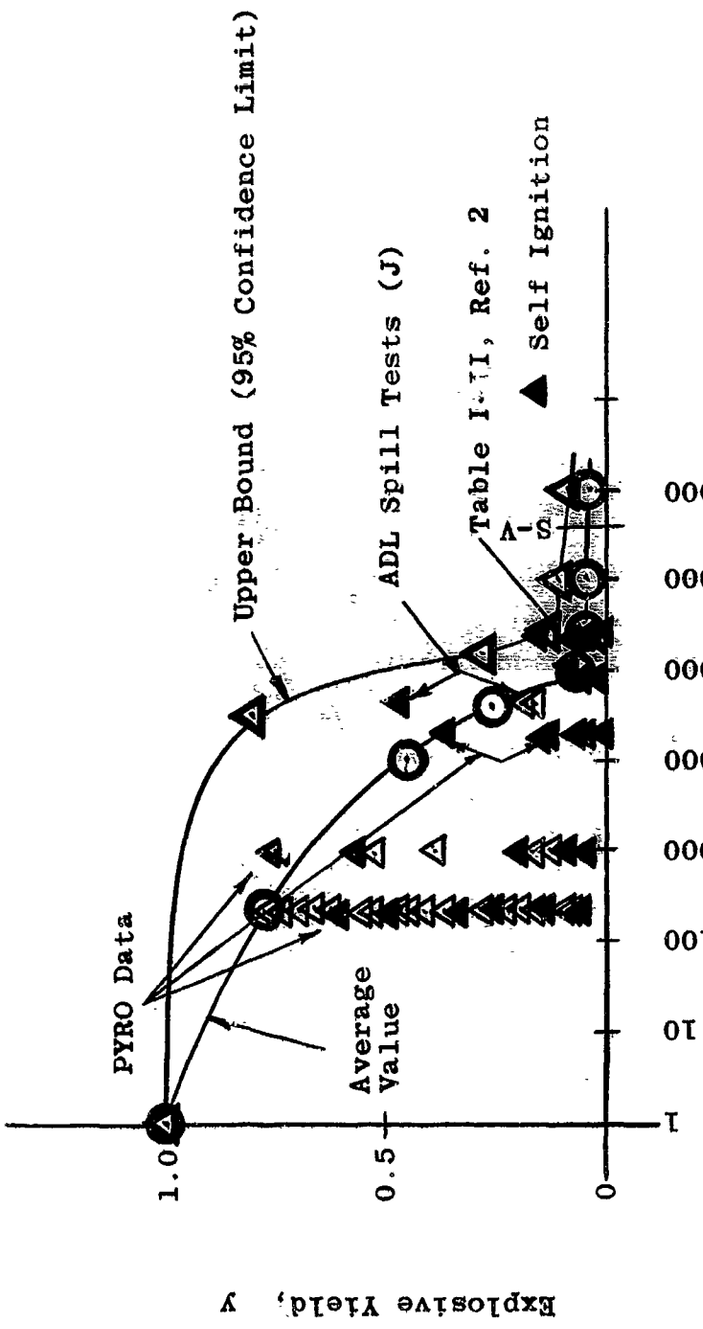

Figure I-8 Estimated Explosive Yield as a Function of Propellant Weight

predicted by the mathematical model as a function of propellant weight. From this Fig. the prediction for the Saturn V would be that the average expected yield value is about 3.8 percent and 95 percent of all the expected yield values will fall below 9 percent.

In addition to the prediction from the mathematical model by analysis many actual yield data points are plotted on Fig. I-8 so that a comparison between predictions and actual results can be made.

The mathematical model as used here included all types of propellants, presently used, all modes of failures and or experiments, it thus represents our knowledge based on experiments and upon the case history of missile failures. The model is found to be conservative in its predictions since the conservative route was taken in its development and use of data.

Other Analyses Which can be Carried Out With the Mathematical Model

In the above analysis it was shown that the data can be grouped according to some known variation and parameter "a" can then be used to indicate this variation through its functional characteristic. So the data could be grouped not only according to weight but also according to propellant type, missile configuration, mode of failure, ignition time, etc.

If for any such set of data the parameters a, b, c, and d are evaluated the predicted average explosive yields should be better in such cases and the confidence limits will be found, in general, closer to the average value.

Evaluation of the Mathematical Model

The development of the mathematical model as described in Part I resulted in a very flexible tool which can utilize a minimum amount of

data and extract from it a wealth of information. Its four parameters give it this flexibility and allow one or more of them to vary, if desired, to investigate certain characteristics of the data.

The data used for the predictions here were taken conservatively so that the explosive yield predictions are on the high side of the unknown true value. Fig. 8 bears this out since most of the available data falls even below the predicted average value.

Since the mathematical model is shown to be conservative in the range where information is available it is also believed to be conservative in its predictions in the regions where no data is presently available. So it is believed that the predictions for the Saturn V, based upon this mathematical model are on the high side.

Inspite of this very conservative nature of the model it predicts yield values for propellant quantities of the Saturn V size, much, much lower than the values presently used. In this last statement lies, the writer believes, the most significant contribution of this model.

In closing it might be added that for large liquid propellant rockets, it may be desirable to control the mode of failure with a properly designed destruct system, so that in case launch abort becomes necessary, a minimum explosive yield is produced. With such a procedure the explosive yield value can be lowered still further and the explosive yield prediction reliability increased.

Part II

"The Seven Chart Approach"

A Systematic Approach for the Analysis and Prediction of the Yield from Liquid Propellant Explosions

Introduction

It was pointed out in Part I that in an effort to assess and minimize the hazards from liquid propellant explosions as a result of missile failures to astronauts, launch support personnel, launch facilities, and surrounding structures it is of utmost importance to be able to predict the most probable expected yield.

An approach, considering the over-all characteristics of liquid propellant explosions, to predict the explosive yield, spill or mixing, probability distributions, confidence regions, confidence limits, and so forth, by means of a mathematical model was presented in Part I as well as in reports and papers[1,2,3,4,5] by the writer. The method described there accomplished the ultimate goal of leading to a valid prediction procedure of yield, spill or mixing, and so forth, of liquid propellant explosions; it did not provide an insight into the physical phenomena producing this yield, mixing, and so on.

The present approach, that of Part II of this report, suggests a more fundamental approach to this problem by considering the physical phenomena in detail which go into producing the explosive yield, mixing, etc. This approach therefore can, through understanding of the physical processes and phenomena, provide the information necessary to control these processes.

The approach presented here is referred to by the authors as the "Seven Chart Approach" since the procedure can be summarized in seven charts, constituting a complete, well planned program, outlining the necessary steps to be followed.

Furthermore, the "Seven Chart Approach" uses presently available information regarding these poorly understood phenomena producing the liquid propellant explosion yield; it points out where more theoretical and experimental work is needed, and what information it should provide. In this manner an ideal balance is obtained between theory guiding the experimental work and the results from the experiments modifying the theory. For this reason the recommended procedure is able to reach the desired goals along a most direct route in the shortest possible time and at a minimum cost.

Previous theoretical and experimental investigations reported in the literature[1,2,3,4,5,15,16] suggest that the actual phenomena producing the yield in liquid propellant explosions can be divided into groups which lend themselves to separate study, both theoretically and through small-scale experimentation.

For the purpose of the "Seven Chart Approach," suggested here for the prediction of the expected explosive yield, etc., for liquid propellant explosions, the problem is divided into three such groups of phenomena which can be studied separately but when combined allow the desired prediction. The groups revolve around

A. The Yield Potential Function

B. The Mixing Function

C. Delay and Detonation Times

and allow the incorporation of the basic characteristics of the particular

propellants involved, of the missile design configuration, and the mode of failure.

The yield potential function (A) is basically controlled by chemical kinetics, the mixing function (B) by the principles of hydrodynamics modified by heat transfer, and the delay and detonation times (c) by characteristic functions for some propellants such as hypergolics or by random processes for others.

The separate studies can be combined by taking the yield potential, when expressed as a time function, and multiplying it by the mixing function to obtain the expected yield at any time after the start of the failure or after the mixing has begun. This mixing function will be different for different modes of failure and missile configurations.

The actual expected yield can be determined by superimposing the delay and detonation times upon the above expected yield function, either as a fixed value where applicable or as a statistically most probable value with proper confidence limits. These delay and detonation times are characteristics of the propellants such as hypergolics, or cryogenics, modified by the propellant quantities, missile configuration, modes of failure, and so forth.

The total procedure can be summarized, with the seven charts supplying the necessary information, as the relationship

$$y = (y_p \cdot x)_{t^*} \qquad \text{(II-1)}$$

where y expected yield value at time*

y_p yield potential value at time*

x mixing function

t^* detonation time (controlled or statistically most probable)

The development of the seven charts follows: conditions were assumed so that quantitative results could be calculated for cases which were investigated experimentally and for which results are reported in the literature[2,6,13] or for which results were obtained as part of this investigation.[3]

These quantitative results give more meaning to the procedures suggested, and allow comparison of predicted values from the "Seven Chart Approach" with actual experimental results. The approach is the same if other initial conditions, than those presented here, other propellants or other configurations are used.

A. The Yield Potential Function

The yield potential function is defined for this investigation as the theoretical maximum yield obtainable if the liquid propellants present are mixed in the most favorable manner to produce the maximum possible value. The explosive yields are then normalized with respect to the maximum theoretical yield obtainable with the original propellant quantities.

The yield potential function for any propellants or combinations of them as a function of time can be obtained from theoretical considerations in four steps as follows:

1. Maximum Theoretical Energy Release (Chart 1)

The maximum amount of energy which can be released from any particular liquid propellant fuel-oxidizer mixture can be calculated employing the basic laws of chemical kinetics.

Figures II-1A and II-1B (in greater detail) show the results from such calculations for the three-component propellant mixture, $LO_2/LH_2/RP\text{-}1$.

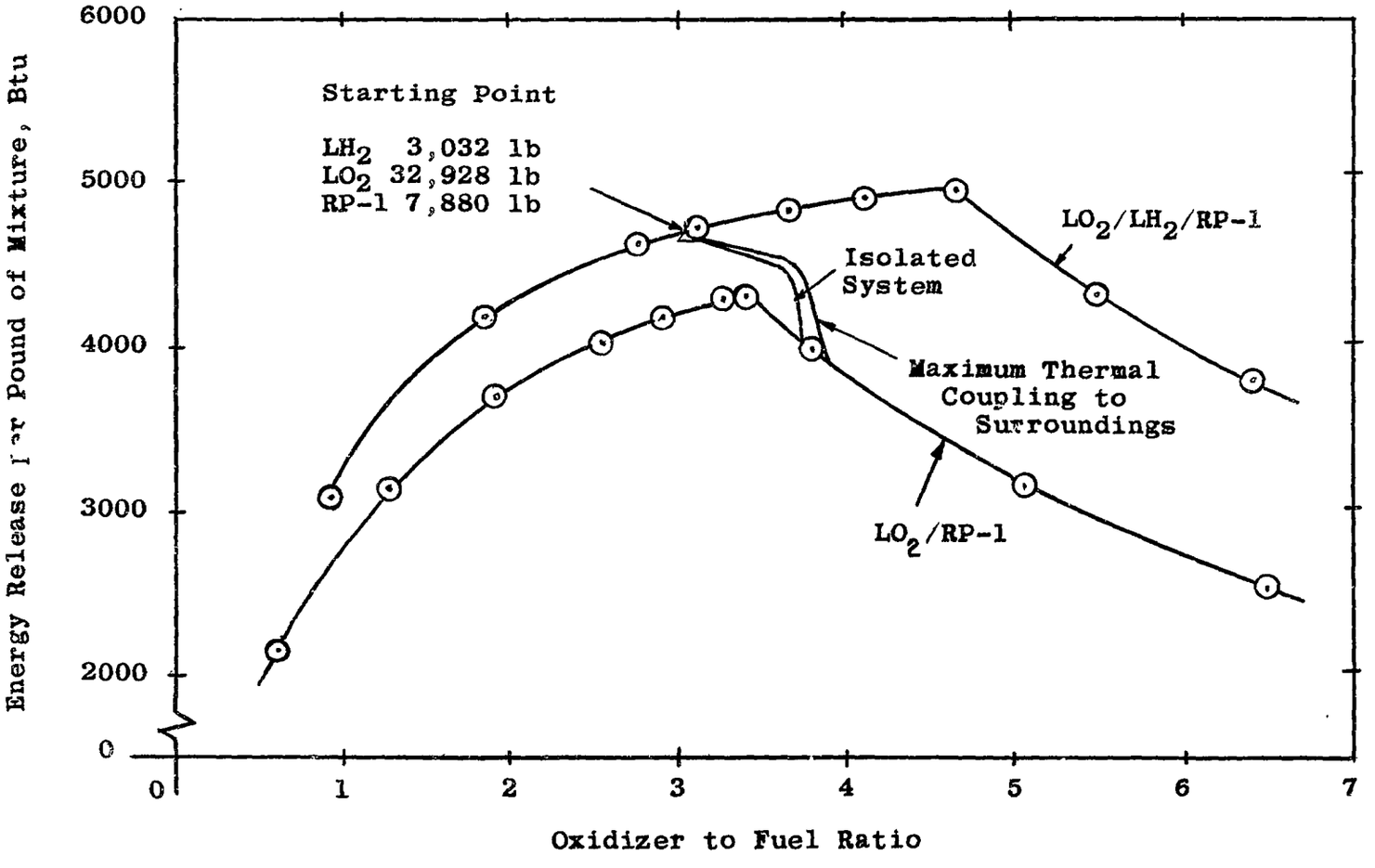

Figure II-1A Maximum Amount of Energy Release for a Three Component Liquid Propellant Mixture

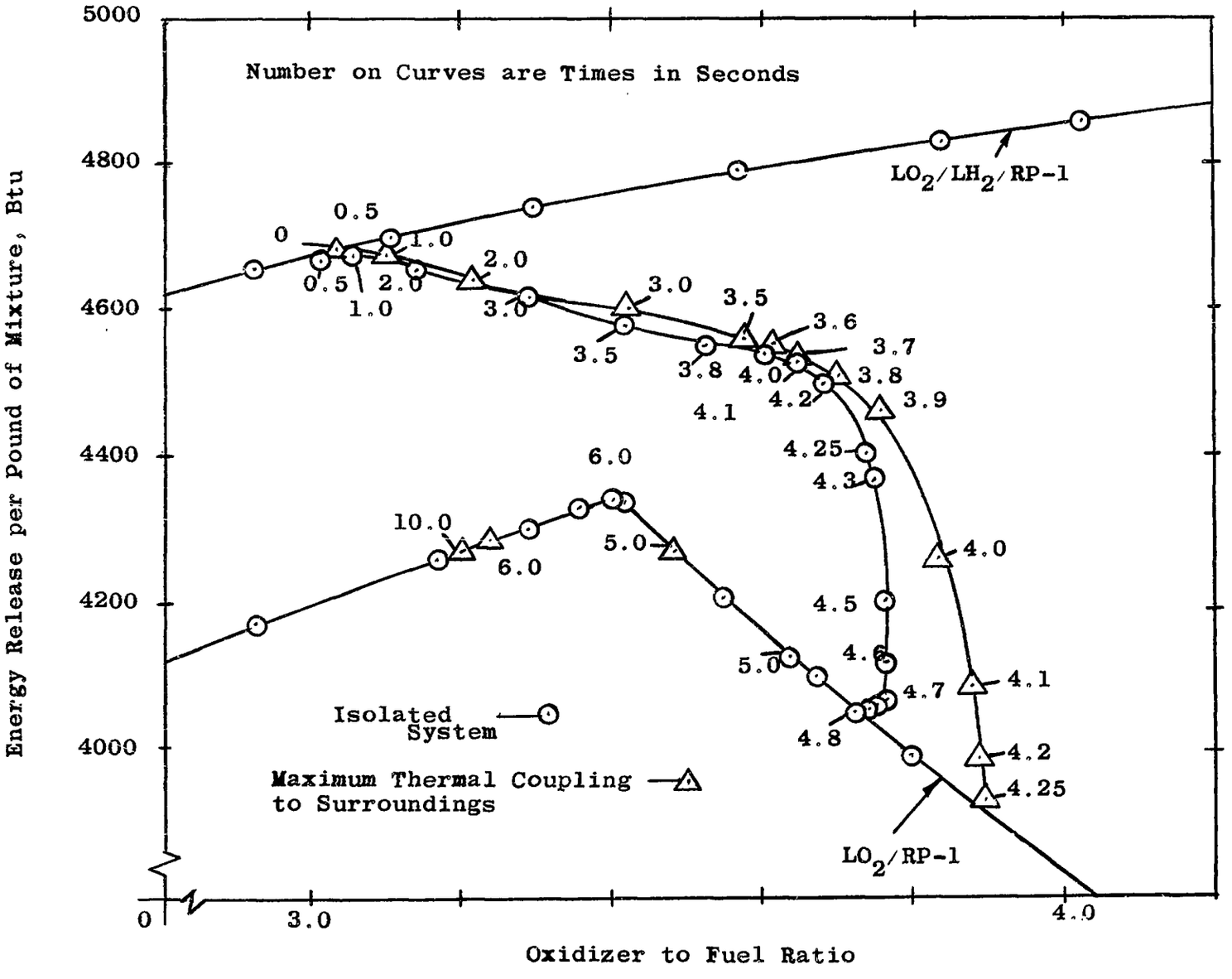

Figure II-1B Maximum Amount of Energy Release for a Three Component Liquid Propellant Mixture

Figures II-8A and II-8B (in greater detail) show the results from such calculations for the three-component propellant mixture, $LF_2/LH_2/RP\text{-}1$.

The upper curve in these figures is the result of the three-component mixtures $LO_2/LH_2/RP\text{-}1$ or $LF_2/LH_2/RP\text{-}1$, with the ratio of LH_2 to RP-1 held constant. In arriving at the numerical values it was assumed that all the LH_2 reacts, and as much of the RP-1 as can be supplied by the oxidizer. Atmospheric oxygen could also be included if desired without any particular difficulty.

The lower curve is the result of two-component mixtures $LO_2/RP\text{-}1$ or $LF_2/RP\text{-}1$, again presented here without atmospheric oxygen contribution. This curve is applicable to a two-component mixture or can be considered the condition after all LH_2 of the three-component mixtures has evaporated.

Thus any three-component mixture will have its starting point on the upper curve and will, due to evaporation of both the LH_2 and the LO_2 or LF_2, follow a path from the upper curve to the lower curve and then toward the origin, if reaction does not occur somewhere along this path terminating the process. The actual path depends upon the changes in the relative quantities of each component present. Two such paths for the $LO_2/LH_2/RP\text{-}1$ and two for the $LF_2/LH_2/RP\text{-}1$ mixture are shown in the above mentioned figures.

How they are calculated will be explained later, but it might be mentioned at this time that the $LO_2/LH_2/RP\text{-}1$ mixture was the one used in field experiments.[3] One path assumes that the mixture is thermally isolated from the surroundings and the other path assumes that maximum thermal interaction between the system and the surroundings occurs.

That the two paths are not as much different as might be expected indicates that the effect of the surroundings is minor.

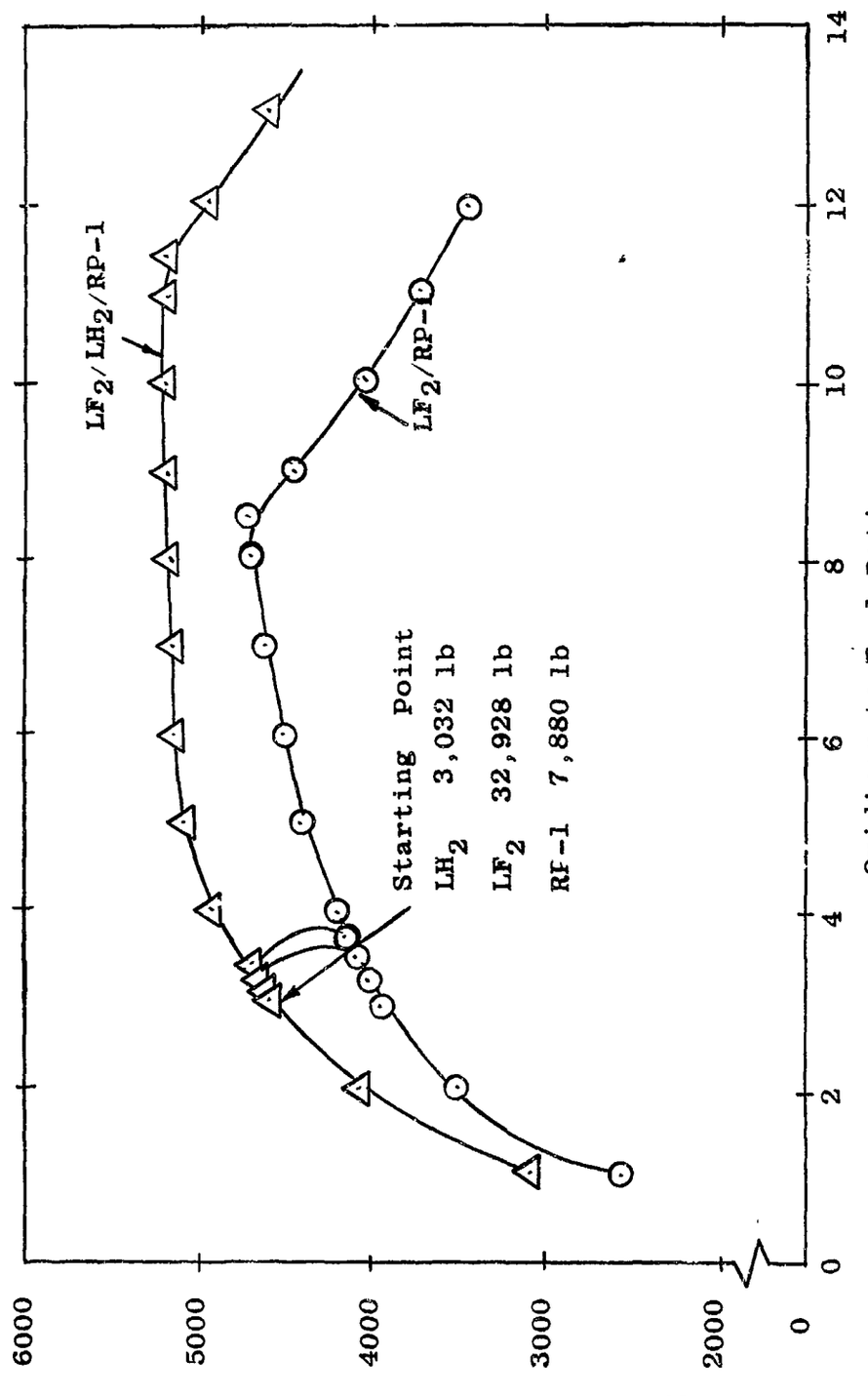

Figure II-8A Maximum Amount of Energy Release for a Three Component Liquid Propellant Mixture

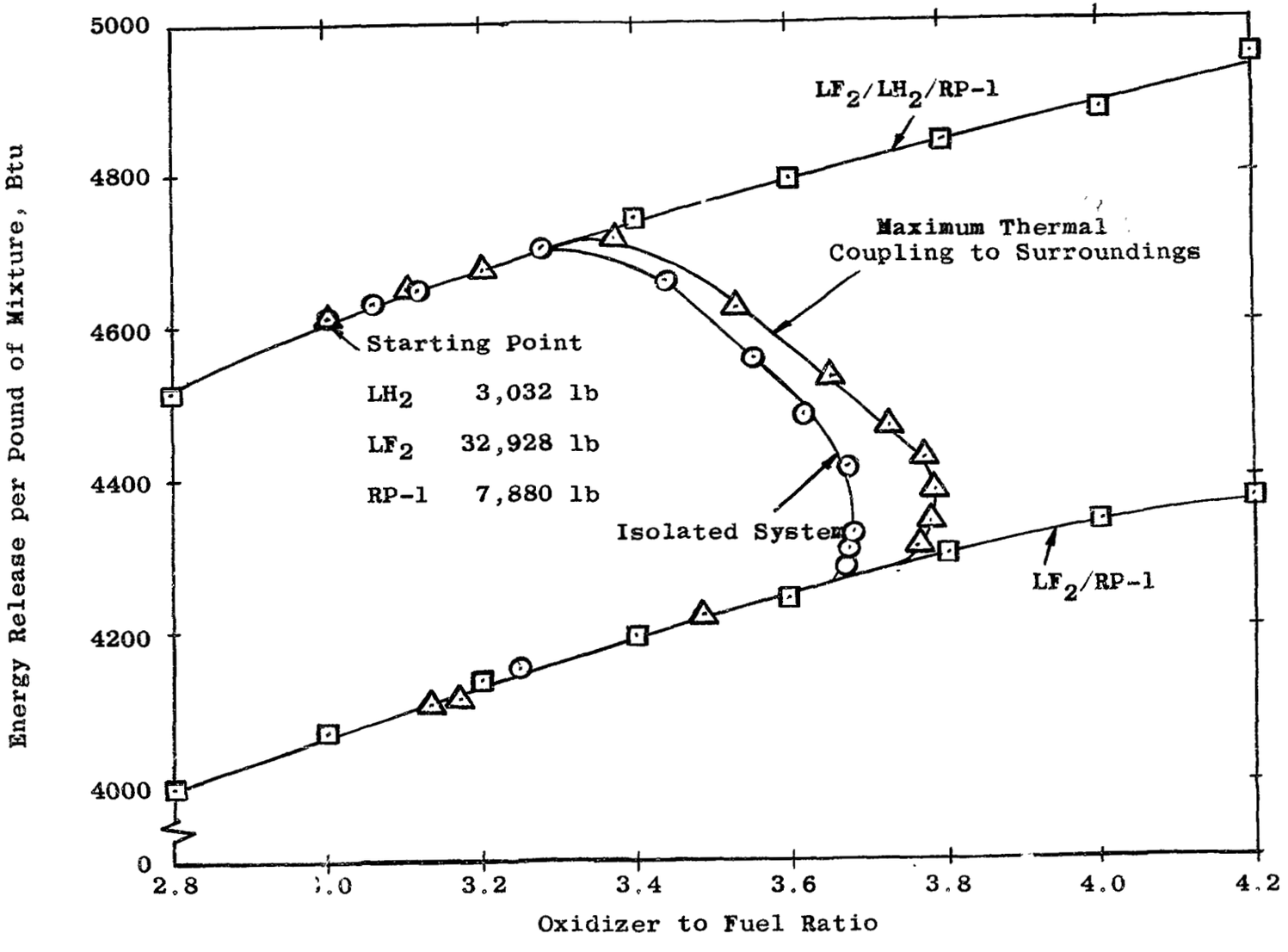

Figure II-8B Maximum Amount of Energy Release for a Three Component Liquid Propellant Mixture

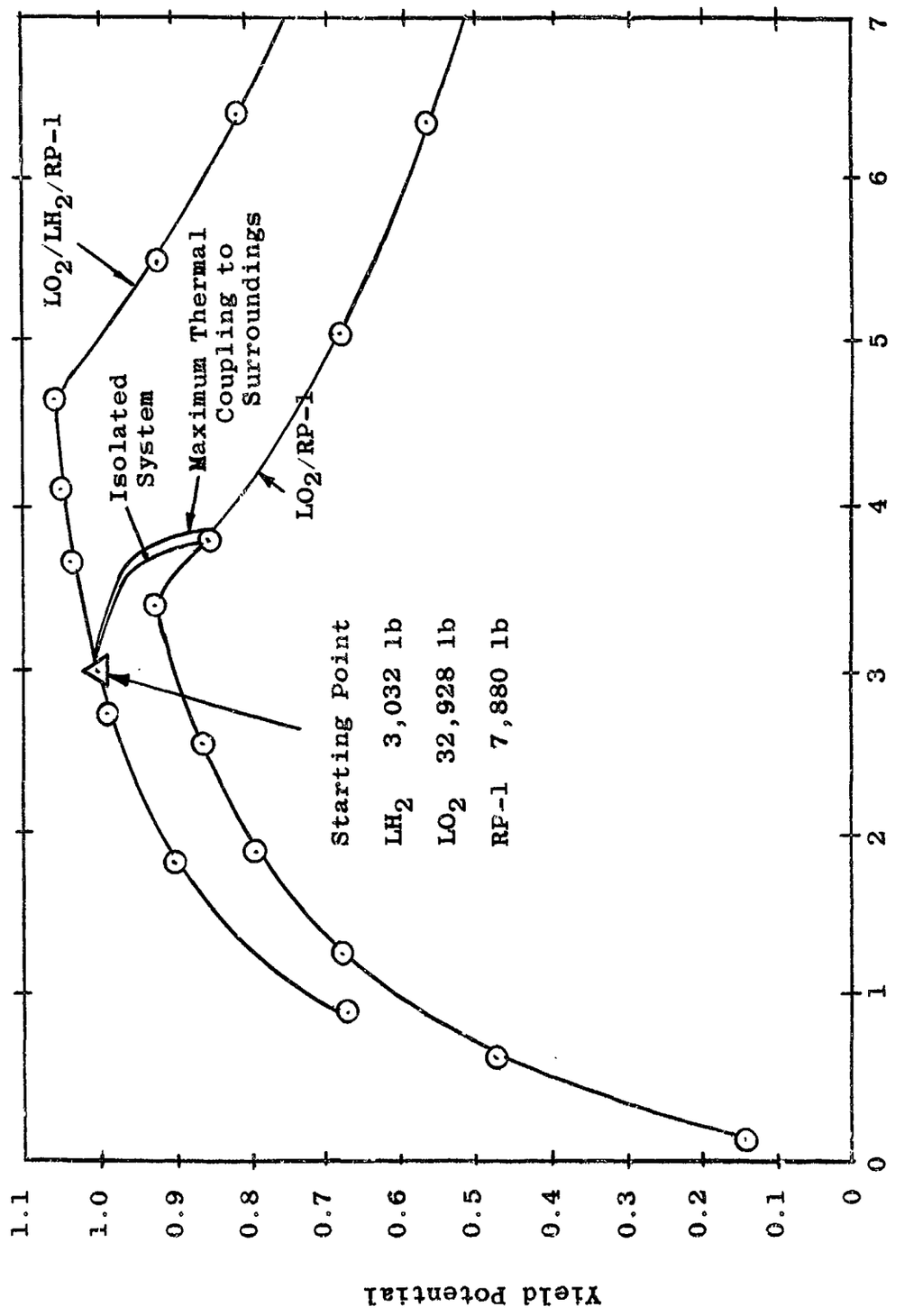

Figure II-2 Yield Potential for a Three Component Liquid Propellant Mixture

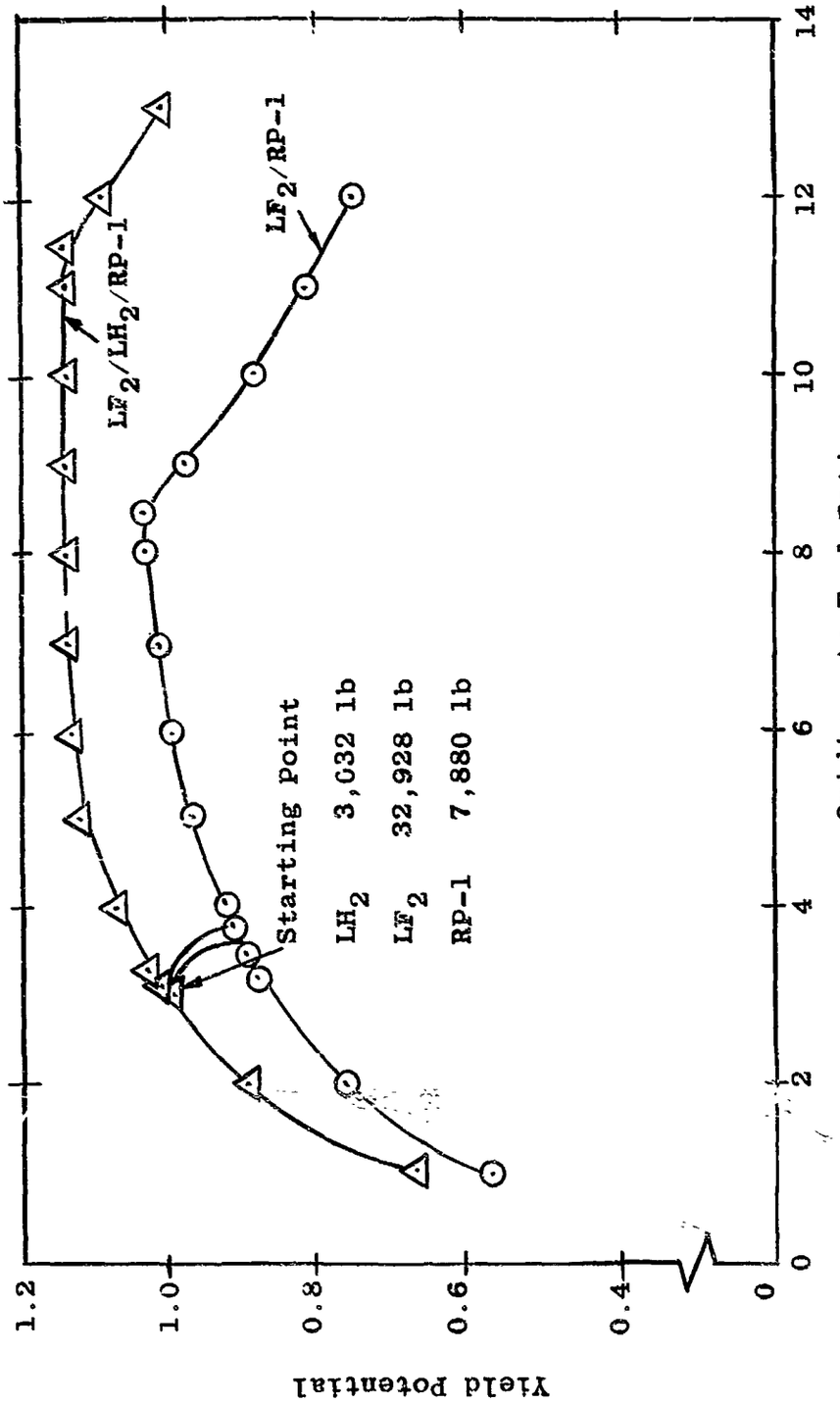

Figure II-9 Yield Potential for a Three Component Liquid Propellant Mixture

2. Yield Potential as a Function of Oxidizer to Fuel Ratio (Chart 2)

The explosive yield of the liquid propellants will depend not only upon the quantity of energy released, but also upon the rate at which this energy is released. Because of lack of information as to the variation of the reaction rates with propellant composition it was assumed for these calculations that the reaction rate remains essentially constant throughout the Oxidizer/Fuel ratios under consideration.

With this assumption, which should be replaced by reaction rate information as it becomes available, and the information of Figures II-1A, II-1B and II-8A, II-8B, the yield potential can be calculated and normalized in terms of the theoretical maximum of the original propellant quantities (propellant quantities used in an experiment or propellant quantities on board of a rocket at launch). The results are presented in Fig. II-2 for the LO_2/LH_2/RP-1 combination and in Fig. II-9 for the LF_2/LH_2/RP-1 combination.

3. Mass-Fraction Time Relationship for LO_2, LF_2 and LH_2 (Chart 3)

To determine the actual paths as previously discussed and shown in Figs. II-1A, II-1B, II-2, and II-8A, II-8B, II-9 it is necessary to know the LH_2/LO_2 and LH_2/LF_2 ratio and its variation. This is easiest obtained from calculations of the quantities of LH_2 and LO_2, and LH_2 and LF_2 respectively present at any time.

The calculations are more or less standard, involving the principles of thermodynamics and heat transfer, but are long and tedious. They involve simultaneous heat balance and heat transfer relationships, which with the proper heat transfer coefficients allow, through step-by-step and iterated calculations, the estimation of the quantities of cryogenics

vaporized, escaping, or again condensed in the mixture, the quantities of fuel and oxidizer frozen and portions remelted, and so forth. Some simplifying assumptions were made wherever it seemed advantageous in reducing the large amount of computations without appreciably effecting the results. Where quantities were encountered which had the same order of magnitude, but the opposite sign and were relatively small, they were sometimes cancelled against each other. These actions helped tremendously in reducing the scope of the necessary computations.

Contact area variations based upon mixing studies both at the University of Florida in connection with the study of explosive hazards of liquid propellants, and information found in literature, were used in the heat transfer equations together with the best available heat transfer coefficients to obtain the mass-fraction for LO_2/LH_2 and LF_2/LH_2.

The information needed and used, aside from that supplied by supporting studies at the University of Florida, are referenced in Table II-I but only some of the assumptions and the results from the calculations can be presented here because of space limitations.

Information for Mass Fraction Calculations

To calculate the mass fractions, by first calculating the quantities actually present at any time, it is necessary to assume a pnysical configuration and a mode of failure.

For the purpose of this investigation a model was chosen which leads to reactions less violent than spilling the propellants together as was done in the ADL test series, which was used as the data for the Mathematical Model in Part I.

The three propellants, LH_2, LO_2, and RP-1 were assumed to be contained in a 12 ft diameter cylinder with the LH_2 on top, the LO_2 in the middle and the RP-1 on the bottom.

At time zero the partitions between the propellants are removed and the initial contact areas between the propellant components are the plane, horizontal interfaces. It is assumed that no chemical reaction or combustion takes place for the calculation of the mass fraction curves. If ignition and combustion would occur the result would be the termination of the curve at the point of ignition.

Two cases are taken for purpose of illustration where the three propellant constituents are

1. Thermally isolated from the surroundings
2. Thermally coupled to a maximum with the surroundings (container temperature 75 F and constant).

Initial Conditions

T_o LH_2	= 36.5 R	m_o LH_2	= 3,032 lb
T_o LO_2	= 162.3 R	m_o LO_2	= 32,928 lb
T_o RP-1	= 528 R	m_o RP-1	= 7,880 lb

Interfacial contact areas between components at time t = 0 are the plane areas respectively.

Assumptions

1. The heat transfer rate between the LH_2 and the LO_2 is constant and 1140.5 Btu/hr ft^2 R.
2. The heat transfer rate between the LO_2 and the RP-1 is constant and 7776 Btu/hr ft^2 R.
3. The heat transfer rate between LH_2 and the container is constant and 757.3 Btu/hr ft^2 R.

4. The heat transfer rate between LO_2 and the container is constant and 632.0 Btu/hr ft^2 R.
5. The heat transfer from the container to the RP-1 is zero.
6. RP-1 has the same heat transfer characteristics as kerosene.
7. The interfacial contact area between LH_2 and LO_2 is governed by the relationship

$$A = 113.1 + 218\ t^2$$

8. The interfacial contact area between LO_2 and RP-1 is governed by the relationship

$$A = 113.1 + 31\ t^2$$

9. The bulk process for the localized intersurface regions involves a height of 0.66 ft (5,380 lb) between LH_2 and LO_2, and a height of 0.66 ft (5,380 lb) plus 0.34 ft (1,946 lb) between the LO_2 and the RP-1.
10. The heat of vaporization for LH_2 is 191 Btu/lb.
11. The heat of vaporization for LO_2 is 91.7 Btu/lb.
12. The specific heat at constant pressure for LO_2 is constant in the range of investigation and at 0.228 Btu/lb R.
13. The specific heat at constant pressure for RP-1 is constant in the range of investigation and at 0.51 Btu/lb R.
14. All the LH_2 which vaporizes, escapes.
15. Of the LO_2 which vaporizes, 25% escapes, 25% solidifies and is suspended in the LH_2, and 50% condenses. The portion which

condenses is first condensed in the LO_2 cooled localized region, any left over amounts are condensed in the LH_2 and fall back into the LO_2.

16. No heat is transferred between the $\underline{S}O_2$ and the LH_2.
17. The latent heat of fusion of RP-1 is 70 Btu/lb.
18. The GO_2 that is formed at the lower interface does not reach the upper interface until one time interval later.
19. The latent heat of fusion for LO_2 is 5.9 Btu/lb.
20. The heat transfer from $\underline{S}$RP-1 to LO_2 is so slow and small that it is negligible for the time intervals chosen here.
21. The specific heat at constant pressure of $\underline{S}$RP-1 is constant in the range of this investigation and at 0.255 Btu/lb R.
22. The thermal conductivity of LRP-1 in the range of this investigation is constant and at 0.086 Btu/hr ft R.
23. Thermal conductivity of gases is inversely proportional to temperature and the thermal conductivity of $\underline{S}$RP-1 is constant at 0.1183 Btu/hr ft R.
24. The density of $\underline{S}$RP-1 is 50 lb/ft^3.

Identical assumptions were used for the three propellant component system which was thermally isolated from its surroundings with the exceptions that the container tank walls were considered adiabatic so that no heat was transferred to it from external sources.

With the above assumptions, many of the sources of which are referenced in Table II-1, and the standard equations of Conduction, Convection and Radiation Heat Transfer the amounts of constituents present at any time t and their respective phases can be calculated.

The results are presented in Figs. II-3A and II-3B for the LO_2/LH_2/RP-1 propellants of the above quantities.

Using similar information as the above for the LO_2/LH_2/RP-1 mixture but for the LF_2/LH_2/RP-1 mixture results as presented in Figs. II-10A and II-10B result.

4. Yield Potential - Time Relationship (Chart 4)

Using the information developed in Fig. II-3A and II-3B or the corresponding Figs. for the Fluorine propellants a time scale can be superimposed upon Figs. II-1A, II-1B and II-2 or II-8A, II-8B and II-9.

With these time scales as shown on Figs. II-1B and II-8B, these curves can be replotted giving the yield potential versus time relationship as seen in Fig. II-4 and II-11 respectively.

These curves represent the theoretical maximum yield which could be obtained at any time t from the above propellants due to the quantities of the constituents which are present at that time t. One curve again represents the yield potential for the isolated system and the other for the system which has the maximum theoretical thermal interaction with the surroundings.

Since the curves of the last Figs. give the yield for propellants when perfectly (or better most advantageously) mixed to produce maximum yield, these results must be modified by the mixing function, the actual amounts (fraction of the maximum amounts) which are mixed at time t.

B. The Mixing (or Spill) Function (Chart 5)

While the yield potential function as calculated above for a specific case establishes the actual quantities of the various constituents present and the maximum theoretical yield, if all these

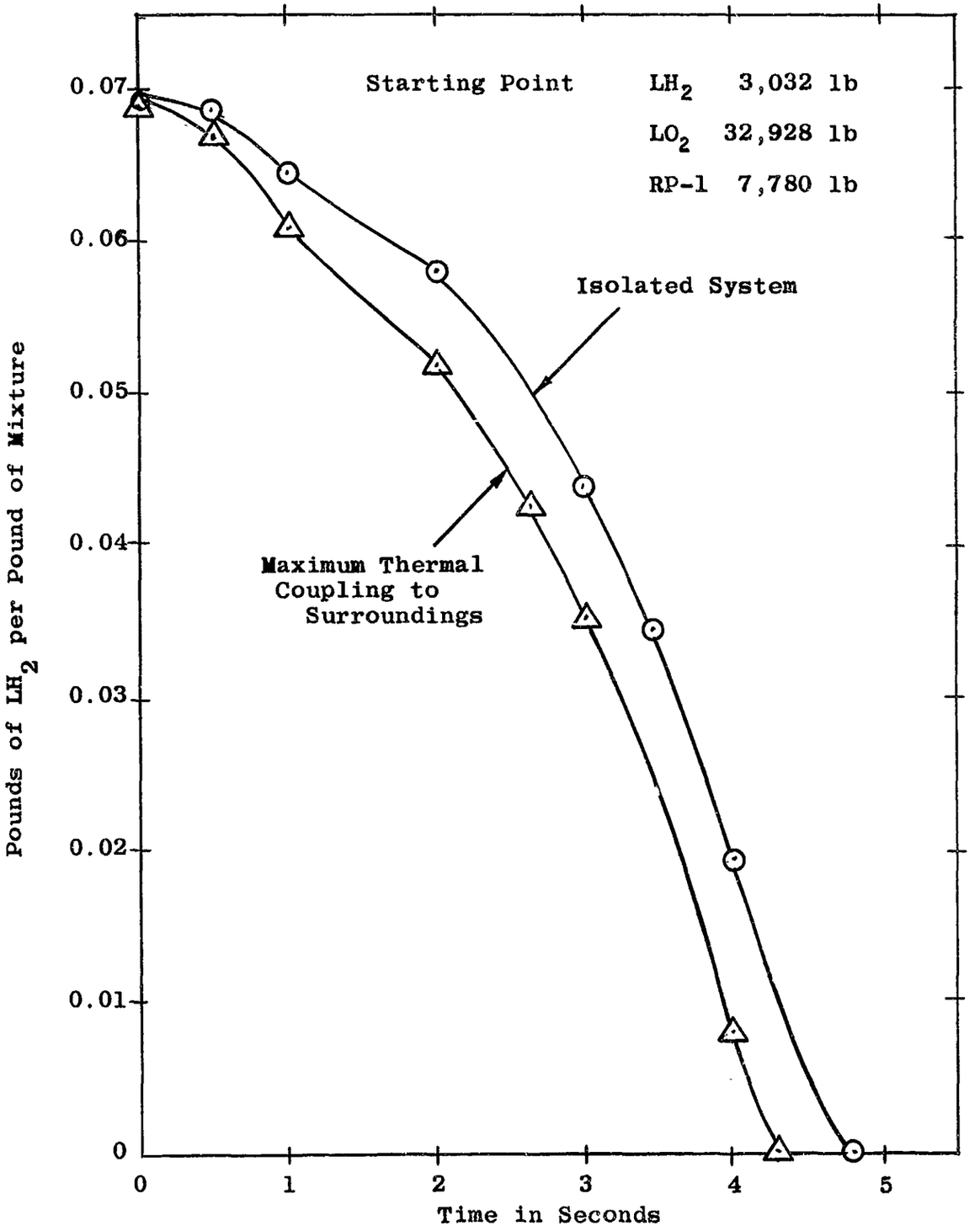

Figure II-3A Amount of LH_2 Present at Time t

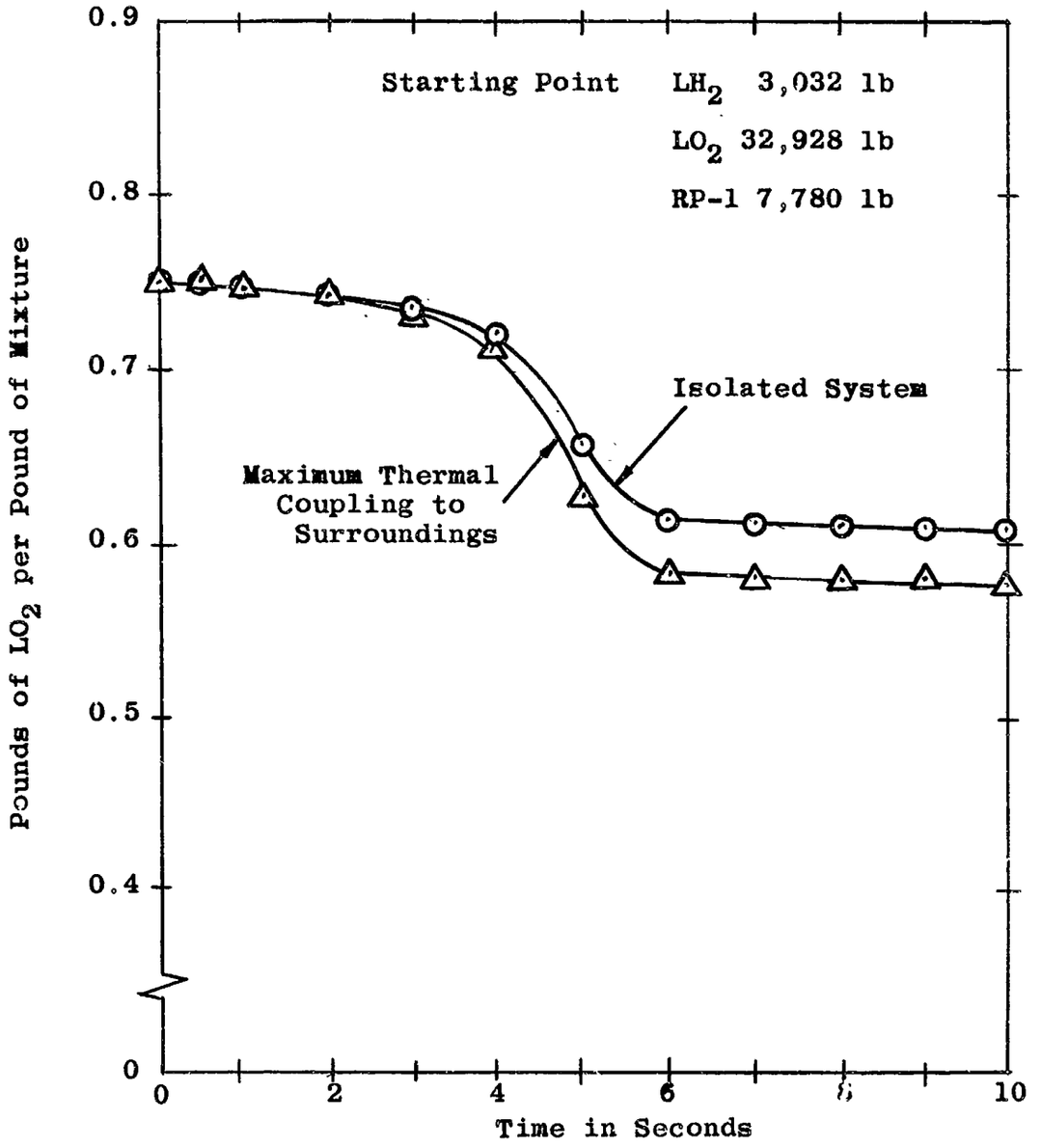

Figure II-3B Amount of LO_2 Present at Time t

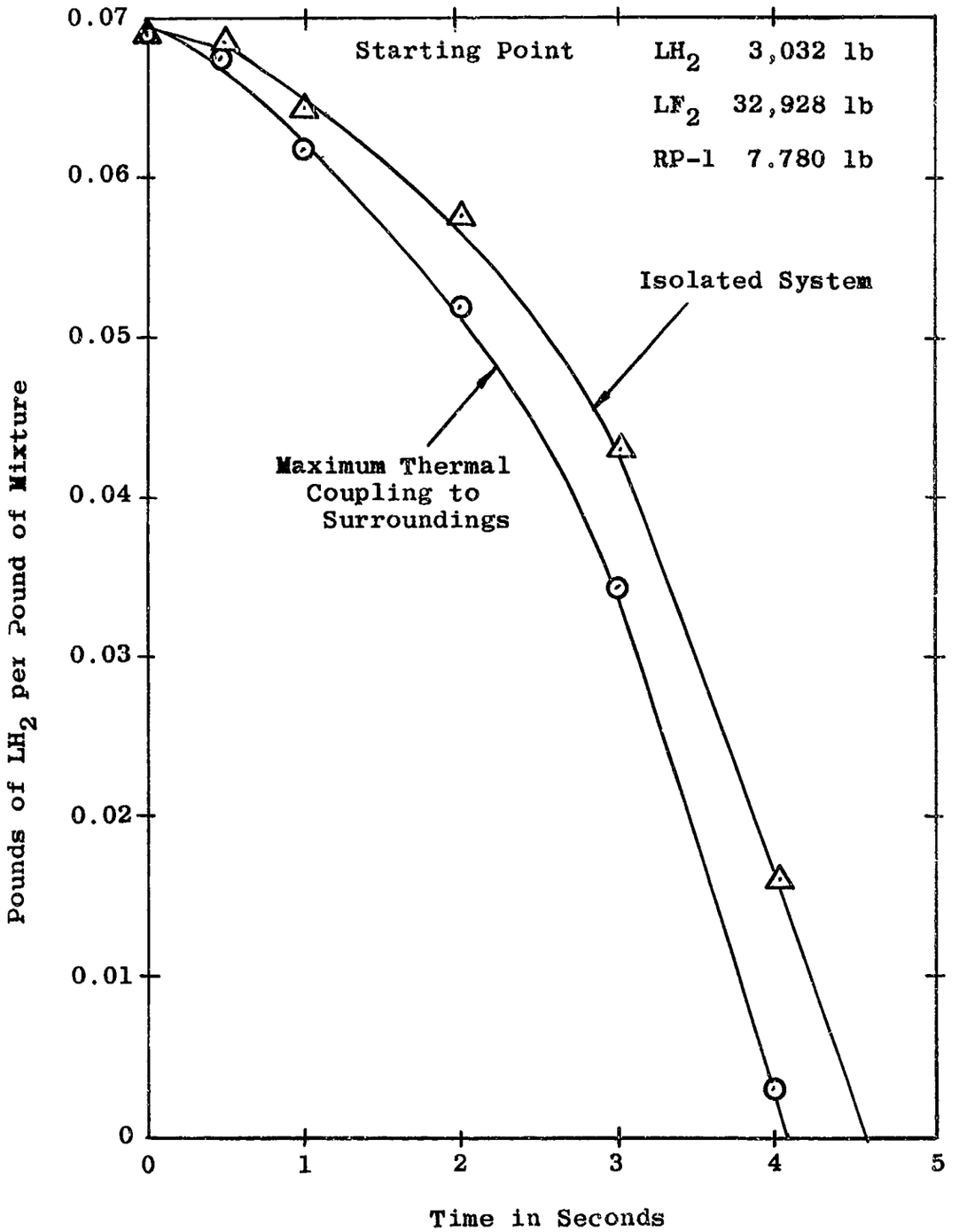

Figure II-10A Amount of LH_2 Present at Time t

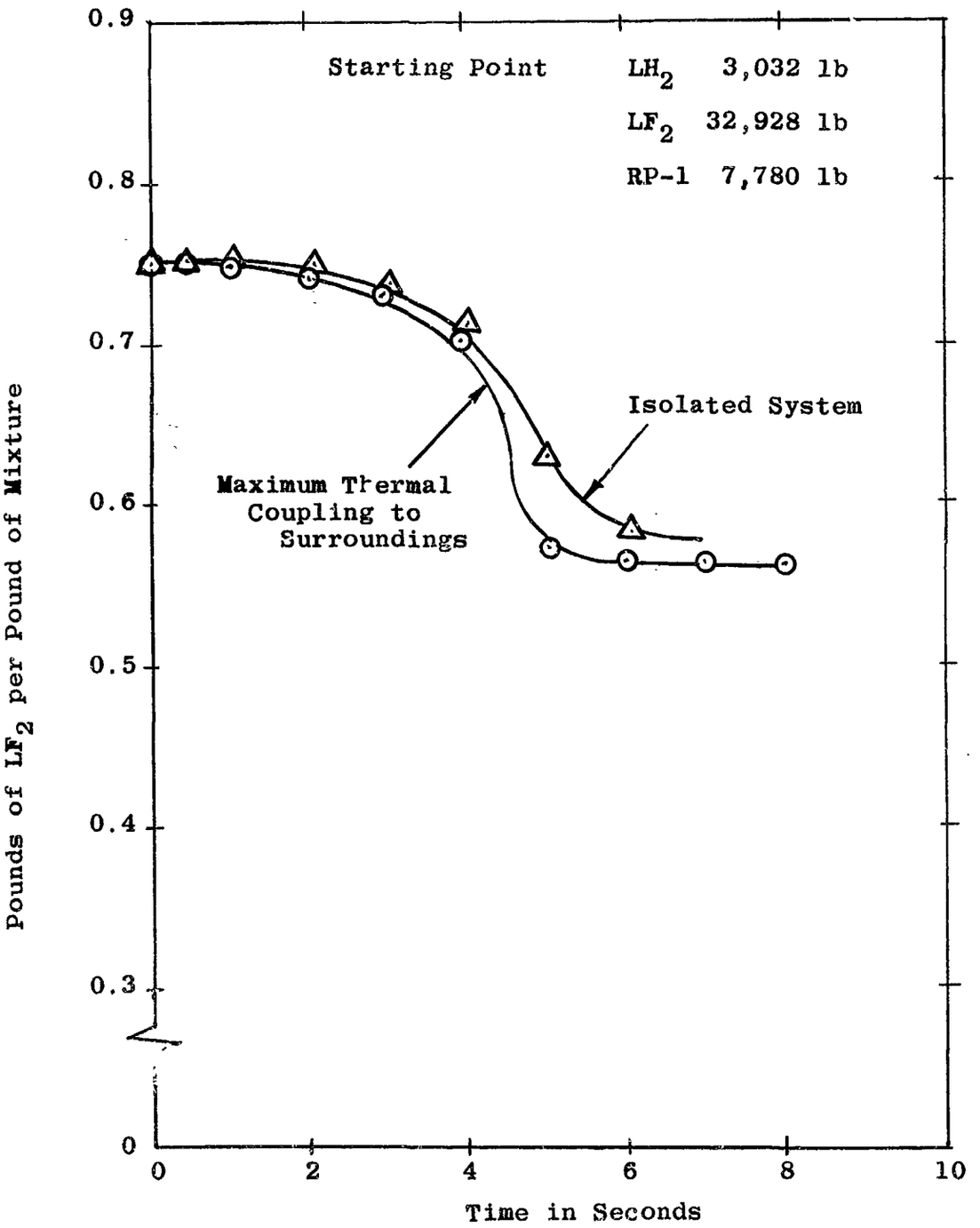

Figure II-10B Amount of LF_2 Present at Time t

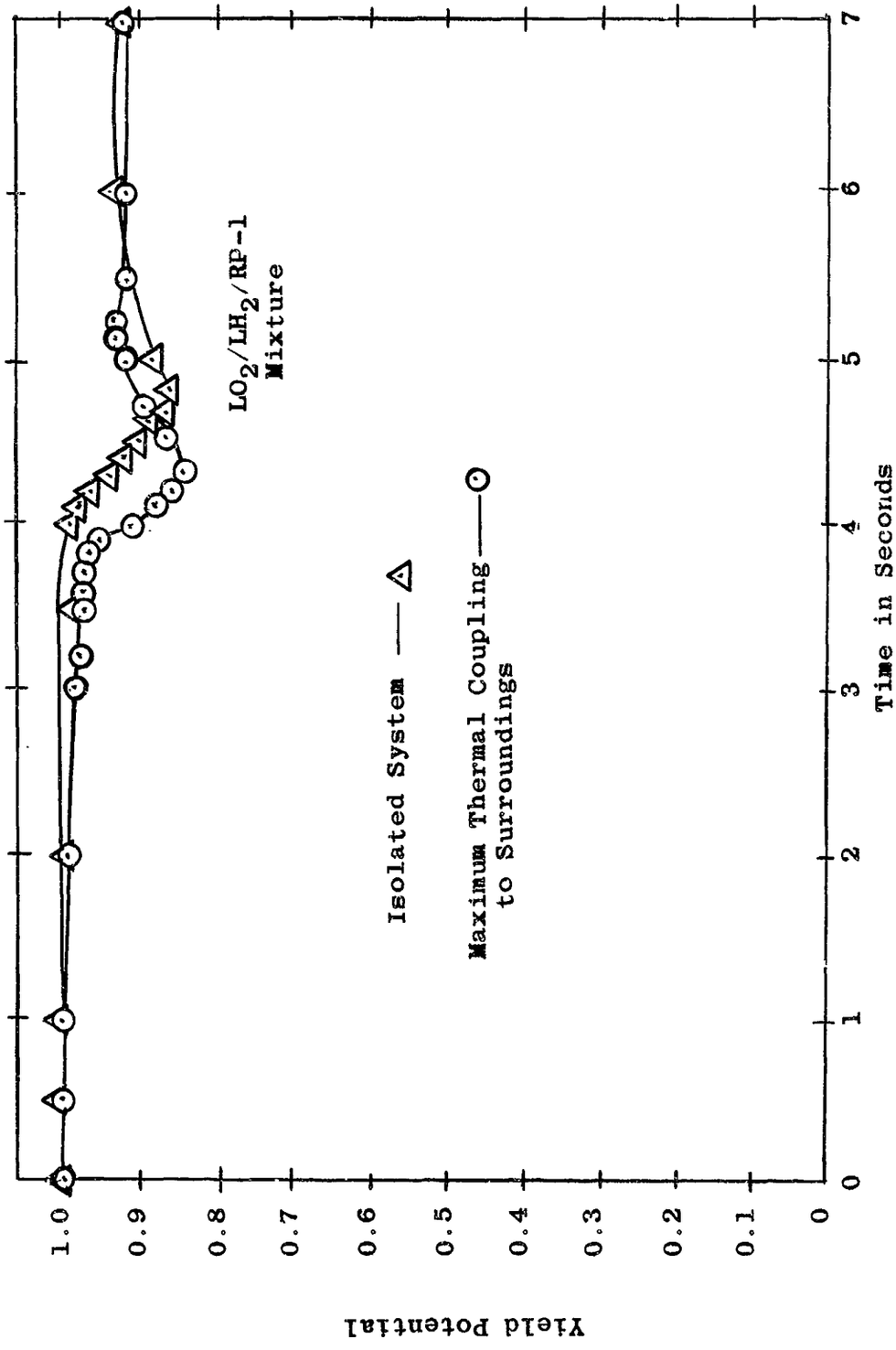

Figure II-4 Yield Potential as Time Function

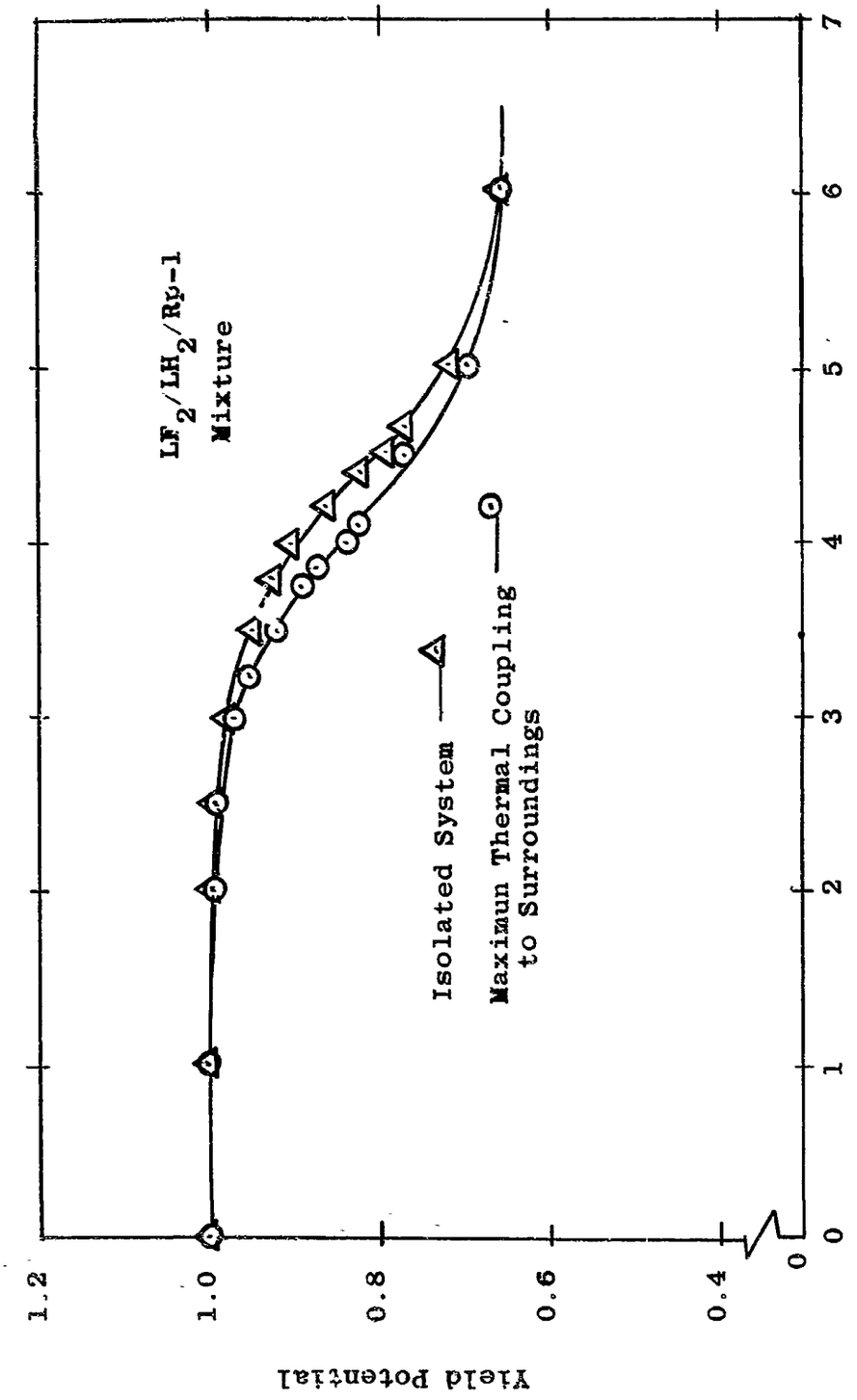

Figure II-11 Yield Potential as Time Function

Table II-I

List of Literature References Used in Support of the Calculations for the Results Presented in Figures II-1A through II-3B

SUBJECT	REFERENCES
Average Chemical Formulas for Kerosene, RP-1	37, 43, 44, 46
Average Heat of Combustion for Kerosene	37, 38, 45
Heat of Combustion for Hydrogen	38
Propellant Proportion used in Heat Transfer Calculations	6
LAN/RP-1 Contact Area versus Time Data for LO_2/RP-1 Analogy	22
Film Coefficients for LAN/RP-1 Interface	22
Film Coefficients for LN_2/LH_2 Interface and LN_2/LH_2 Contact Area versus Time Data for LO_2/LH_2 Analogy	22
Latent Heat of Evaporation for H_2 and Specific Heat for GO_2	39
Specific Heat for L JP-1 to simulate RP-1	28
Latent Heat of Evaporation for O_2	39, 28
Latent Heat of Fusion for O_2	39
Approximation of Latent Heat of Fusion for RP-1	46
Approximation of Specific Heat of Solid Kerosene	40, 41, 42

constituents are mixed most effectively, it does not give any information as to the actual degree of mixing of the constituents.

For example, at time zero when the constituents are not yet mixed or at best just beginning to mix, none of them are actually mixed and therefore an explosion could not be produced. Thus at time zero while the yield potential function has its maximum value the mixing function has the value zero. The product of the yield potential and the mixing function at time zero gives the true or expected yield.

The mixing function is essentially a hydrodynamic function, however complicated by high rates of heat transfer. This makes the analytical approach very difficult, and an experimental approach for determining this function was chosen which is more promising since questionable assumptions are not involved.

1. Analytical Approach

The basic problem to be solved here is the interaction of two or more liquids which come together due to a particular mode of failure. These liquids are at different temperatures and upon contact energy is transferred between them resulting in phase changes and extreme turbulence. At least one and probably more of the constituents will as a result be present in solid, liquid and vapor or gas phases making the analysis of the phenomena involved in this interaction one of extreme complicity.

Many variables and factors must be used to describe the behavior and even if the differential equations are set up presumably describing these processes no method has yet been found to solve them. As a matter of fact much simpler equations involving only a small part of these phenomena have never been solved. Such are three dimensional heat transfer involving

all the factors of our problem or the problem of fluid flow alone of the type which we are encountering.

The next best thing would be analytical approximate solutions and two approaches will be briefly discussed.

a. The Grid Cell Approach

It is possible to divide the field under study into a grid of cells (cubes, or curvilinear volumes). Then the amounts of each constituent in each of its three phases crossing into and out of each cell and the energy quantities crossing the cell boundary can be expressed. Thus a great number of equations can be set up expressing this interaction between the cells. The solution to the problem will be the state for the system as a whole, at a particular time t when everything balances. This process must then be repeated for each successive time. A tremendous task requiring an extremely large computer with tremendous storage capability, requiring uncountable numbers of iterations.

Thus even though this method is straight forward and certainly feasible it was not considered best for this investigation, and after setting up some of the relationships expressing the physical problem. Section (b) will give further support to this statement.

b. The MAC Method[17]

The Marker-And-Cell technique was developed at Los Alamos by a team of scientists for solving fluid flow problems. The method is appropriate with a high-speed digital computer. The fluid is incompressible, viscous, and moves through large-amplitude contortions in several space dimensions. There may be a free surface upon which waves

can form and break, or the flow may be entirely confined by walls. The motions are calculated by using the complete Navier-Stokes equations, including all non-linear terms. The only approximations arise from the finite-difference representation.

The above problem is one of approximate solutions already requiring a computer larger tnan what most Universities possess and this program does not include other than liquid phases and only one or two components. Naturally energy transfer such as heat transfer is excluded.

Only two dimensional examples are presented by the authors.

When one considers the amount of work which goes into such an analysis, the tremendous facilities and expense in carrying through such a program and in addition the boundary condition assumptions which must be fed into the program, the results obtainable are rather questionable.

2. Semi-Empirical Approach

When analytical approaches become too difficult, long, or impractical economically or time-wise, then often methods can be employed which combine theoretical work with a minimum of experimentation.

One such method which has been proven very powerful is Dimensional Analysis. This method is based upon the realization that when an expression has physical meaning it has to be dimensionally consistent. This method is able to give the relationships between the variables describing the phenomena under study, and then can usually be grouped in terms of dimensionless terms or numbers. The coefficients, exponents, or in more complicated case functions have to be found by experimentation. The experimentation is thus reduced since the relationship of the variables is already established.

Usually this method can save considerable time and has very successfully been applied in cases where only a limited number of variables were involved.

In the problem under consideration here the number of variables is so great and the experimental measurement of them difficult requiring expensive instrumentation. Because of the time involved in doing this it was decided to determine the mixing function experimentally for various modes of failure and liquid combinations.

3. Experimental Approach

As mentioned above and for the reasons cited the experimental approach was chosen to give the answers needed for analysis of the explosive yield prediction in the shortest possible time and with the greatest reliability. No questionable assumptions have to be made and the approach can be applied to the propellants, missile configuration and mode of failure desired.

To measure the fraction of the propellants mixed and the degree of mixing, methods had to be developed to be able to do this.

a. Definition of the Mixing (or Spill) Function

For the purposes of this investigation the mixing function, as mentioned earlier, is defined as the fraction of the propellants which are actually mixed at any time t. This can be expressed as

$$x = \frac{P_M}{P_P} F_T F_B F_F F_L = \frac{P_M}{P_P} \mathcal{F} \qquad \text{(II-1)}$$

P_M Mixed Propellant Parameter such as: Volume, Envelope Surface, Contact Area, etc.

P_P Total Propellant Parameter corresponding to P_M such as: Volume, Envelope Surface, etc.

F_T Turbulence Factor

F_B Boiling Factor

F_F Freezing Factor

F_L Loss Factor

In the work presented here the parameter P was taken as the contact area or most frequently as the mixing volume.

The factors modifying the parameters were determined most of the time as a group modifier ($\mathcal{F}$), by inert laboratory experiments, utilizing such fluids as water and oil, hot wax and water, hot oil and water, LN_2 and kerosene, etc.

It was shown, that in the early stages of the mixing, these factors have a value near one for the volume as parameter and thus the spill or mixing function x is in this range the normalized parameter.

This method allows the study and prediction of the mixing function as it occurs in the actual liquid propellant explosions through inert, non-destructive experiments, which are able to predict the actual phenomena.

The mixing function can thus be determined for the real missile without producing an explosion only by running mode of failure simulation experiments. Furthermore these experiments do not have to be full scale since hydrodynamic scaling has been proven in many fields as valid.

The approach and the mixing functions obtained in inert laboratory experiments on small configurations was substantiated by actual life tests[3] under project PYRO.

While the complete function could be obtained in the inert experiments only the first part of the curve could be obtained in the life tests since auto-ignition and detonation terminated the mixing process and explosion phenomena took over.

b. Experimental Methods for Obtaining the Mixing Function

Four methods have been developed in connection with the over-all systematic approach to implement the execution. These four methods allow the detailed study of the mixing process and phenomena producing the mixing function of liquid propellants and have been used with great success. In the preliminary studies, often applying two methods to the same experiment, these methods have independently produced results which are in excellent agreement. These methods are:

Film Analysis

A high speed photographic technique giving by use of mirrors a three-dimensional picture of the mixing process on the same film frame. Special analysis of these frames as to mixing profile, mixing volume, and modifying factors allows the determination of contact area, degree of mixing, etc.

Wax Cast Analysis

By use of hot wax and cold liquids the mixing process can be "frozen" at different stages of the mixing by varying the hot and cold temperatures. The "frozen" state of the mixing process can then be studied at leisure at any time later. These casts can be analyzed as to profile outside area by projection or coating methods; they can be serially sectioned to give the total contact area, volume, modifying factors, and so on.

Vibration Mixing Analysis

This method consists of mounting a particular configuration on a vibration table, simulating the various propellant components by particles of different color, size, density, shape, etc., and by partially or completely shaking the system to make these solid particles behave like liquids. Flotation of these particles with air or other gases can make them flow from simulated rocket tanks like the corresponding liquids would. When reaching the vibrating base of either plane or launch pad configuration (or any other desired simulation), the components will mix and the degree of mixing can be checked periodically at desired locations. Evaporation or other losses can be simulated by removing programmed quantities or numbers of particles at desired locations and prescribed intervals.

The arbitrary time scale of the vibration analysis is correlated through theoretical calculations or liquid calibration experiments.

Thermocouple Grid Analysis

This method of analysis employs a three-dimensional grid of fine thermocouples with each junction being monitored continuously. The traces give information regarding the mixing front, the degree of mixing at a particular point, the degree of turbulence at a point, the location of the point or points of ignition, the time delay from the start of mixing (or time of failure) to ignition, the propagation of the reaction front, the propagation of the shock front, the separation of the shock front from the reaction front, and so forth.

This method is certainly the most powerful of the four since it directly relates the mixing phenomena with the yield obtained all in

one and the same experiment. It is however, considerably more expensive than the others.

Instrumentation for high speed monitoring of the individual junctions is expensive and the reduction of the data obtained time-consuming.

However, this thermocouple grid method is capable of taking measurements in liquid propellant mixtures from the start of failure up to and after ignition. If the grid is extended beyond the original boundaries of the propellant configuration, information can be obtained as to fireball growth rate, extent, temperature, shock wave strength, shock wave velocity, and so on.

More detail and some of the results of the four methods are presented in Appendix B-III.

The analyses undertaken more recently have used the mixing volume as the mixing function parameter, modified by the various factors mentioned earlier. Actually during the time interval of greatest interest these factors have a value near 1 so that their actual value distribution is mostly academic. Auto-ignition terminates the mixing function curve rather early in its history so that only that part is of importance in predicting the volume mixed and thus the expected yield.

Four cases are presented here for which the mixing function was determined and for which the results at least in the beginning stages could be checked against actual live tests.

ADL J Test Series

These tests, three in number involved about 44,000 lb of propellants each which were poured together from tanks, spaced on a circle 120° apart so that the LH_2, the LOX and the RP-1 spilled into a splash area in the

center. Auto-ignition occurred in all three experiments and the resulting yields were measured. Calibration experiments of the flow from the tanks gave some information as to the quantities in the spill area at the time of ignition.

This arrangement was simulated in the laboratory with the vibration mixing analysis and the mixing function curve which resulted is shown in Fig. II-5A.

The statistical variation in repeated simulation experiments is indicated.

S-IV Explosion Experiment (PYRO)

In this experiment a S-IV configuration was taken filled with 92,800 lb of propellants (LH_2/LOX) and then a ram fired from the bottom to cut an eighteen inch hole into the common bulkhead between the LH_2 and the LOX. 200 milli-seconds after the ram was fired, auto-ignition occurred stopping the mixing process and detonating the propellants.

This type or mode of failure was again simulated in the laboratory with a three inch diameter tank configuration. The mixing function for this case is presented in Fig. II-5B, showing the point at which the actual live experiment was terminated by auto-ignition.

The double hump of this mode of failure is typical since a slug of the upper fluid falls into the lower one penetrating to a maximum then retracts somewhat and then surges again. This behavior was observed in all failure modes of this type.

The very early auto-ignition showed again that relatively little time was available for the mixing process to occur. Also noteworthy is that the mixing function never reached a very high value, never exceeded about 17 percent.

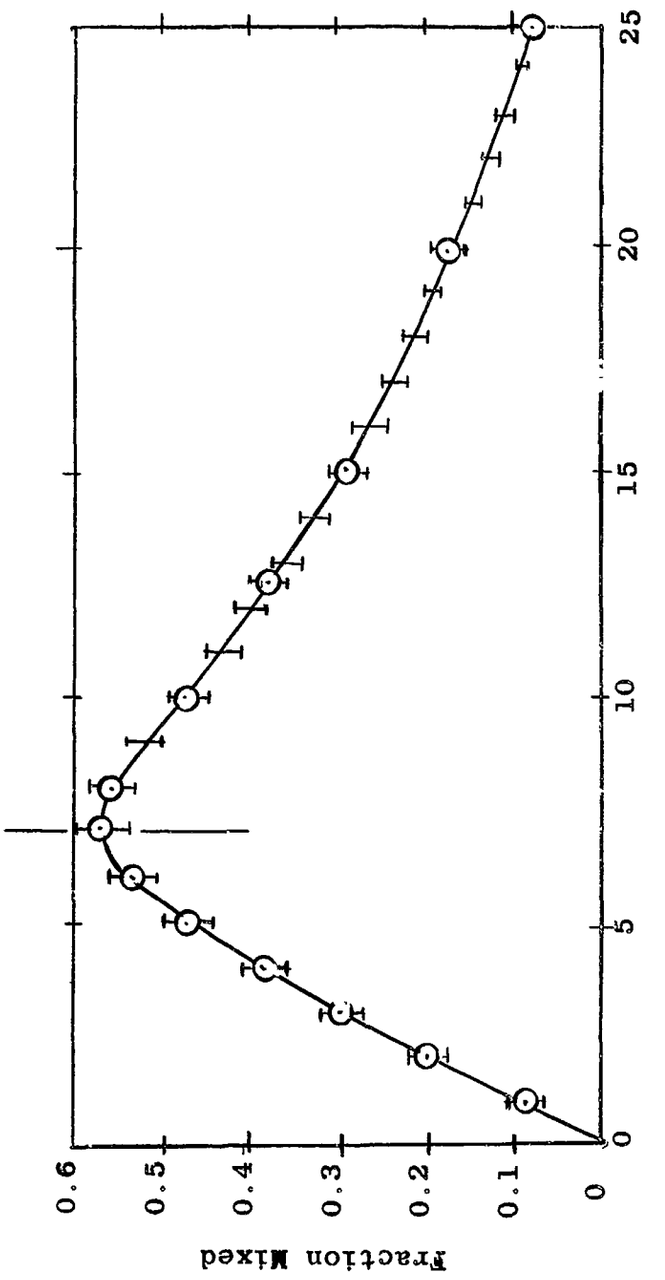

Figure II-5A Mixing Function or Spill Function for Three Component Liquid Propellant Spill Tests

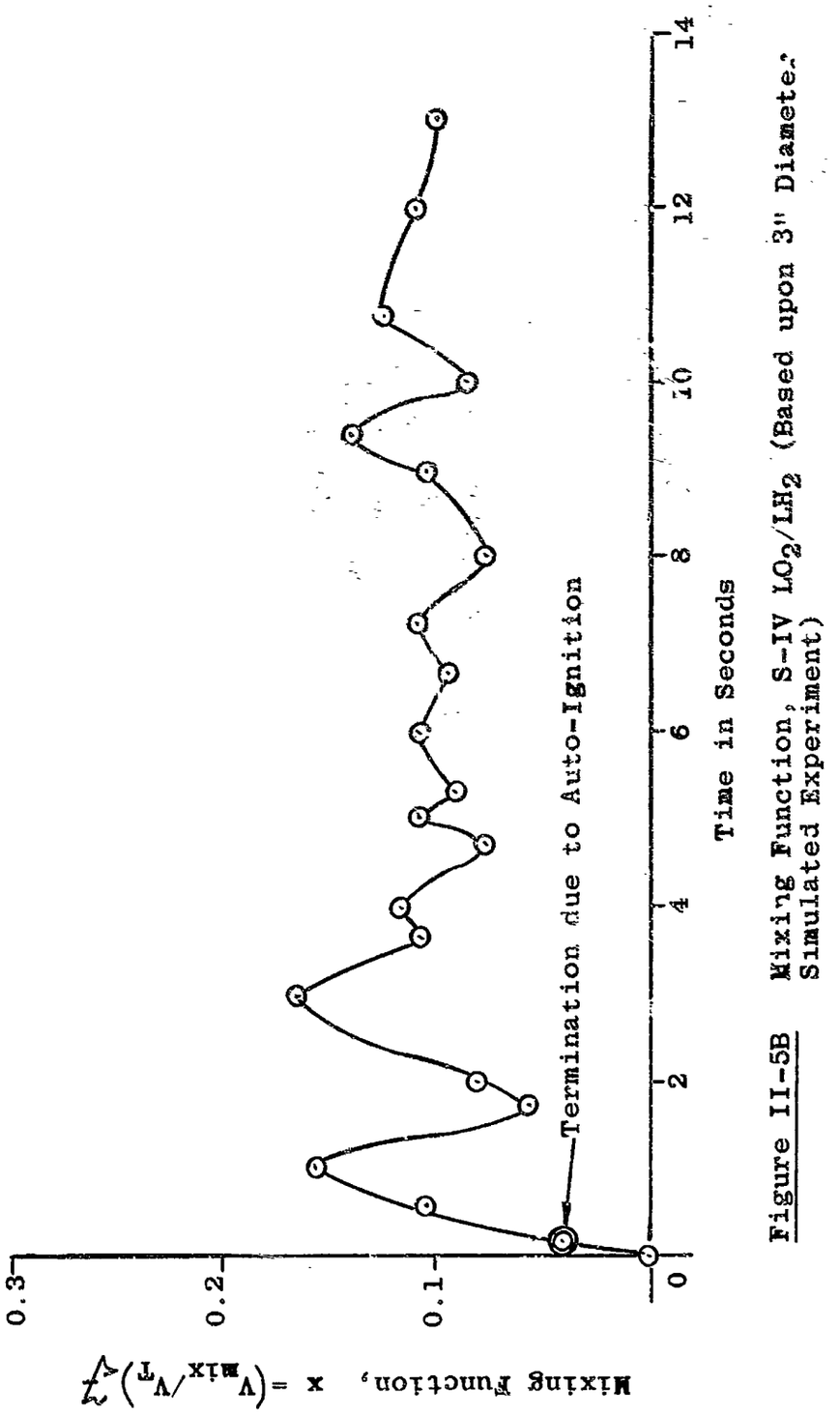

Figure II-5B Mixing Function, S-IV LO_2/LH_2 (Based upon 3" Diameter Simulated Experiment)

25,000 lb Explosion Experiments (PYRO)

These experiments were carried out under project PYRO but were carefully instrumented by Dr. Farber's group with thermocouple grids inside the RP-1 tanks. Measurements, believed to be the first of this kind, were taken and information obtained on the mixing phenomena, the ignition phenomena, shock wave and reaction front behavior. The results are presented in detail in Appendix C-V.

Since again auto-ignition occurred in the two experiments 540 and 580 milli-seconds after initiation of the failure respectively, relatively little time was available for the mixing which could not proceed to its maximum potential.

Again this mode was simulated in the laboratory with a 1 1/2 inch, a 3 inch and a 6 inch configuration giving essentially the same results, presented in Fig. II-5C. Again the characteristic double hump can be seen.

200 lb Cold Flow and Explosion Experiment

At the end of the PYRO project series a 200 lb LOX/RP-1 system was instrumented and a glass diaphragm in the common bulkhead broken just like in the 25,000 lb experiments. Auto-ignition did not occur, as is usual with these smaller quantities, and the mixing process was followed for 73 seconds at which time, with the mixing essentially stopped by solid RP formation, the mixture was detonated by two explosion bolts.

This test was similar to the 25,000 lb experiments, but with ignition controlled and much later in the process. The mixing progressed to a higher peak value than the 25,000 lb experiments and then dropped with relatively small fluctuations superimposed, very similar to the S-IV curve. Fig. II-5D.

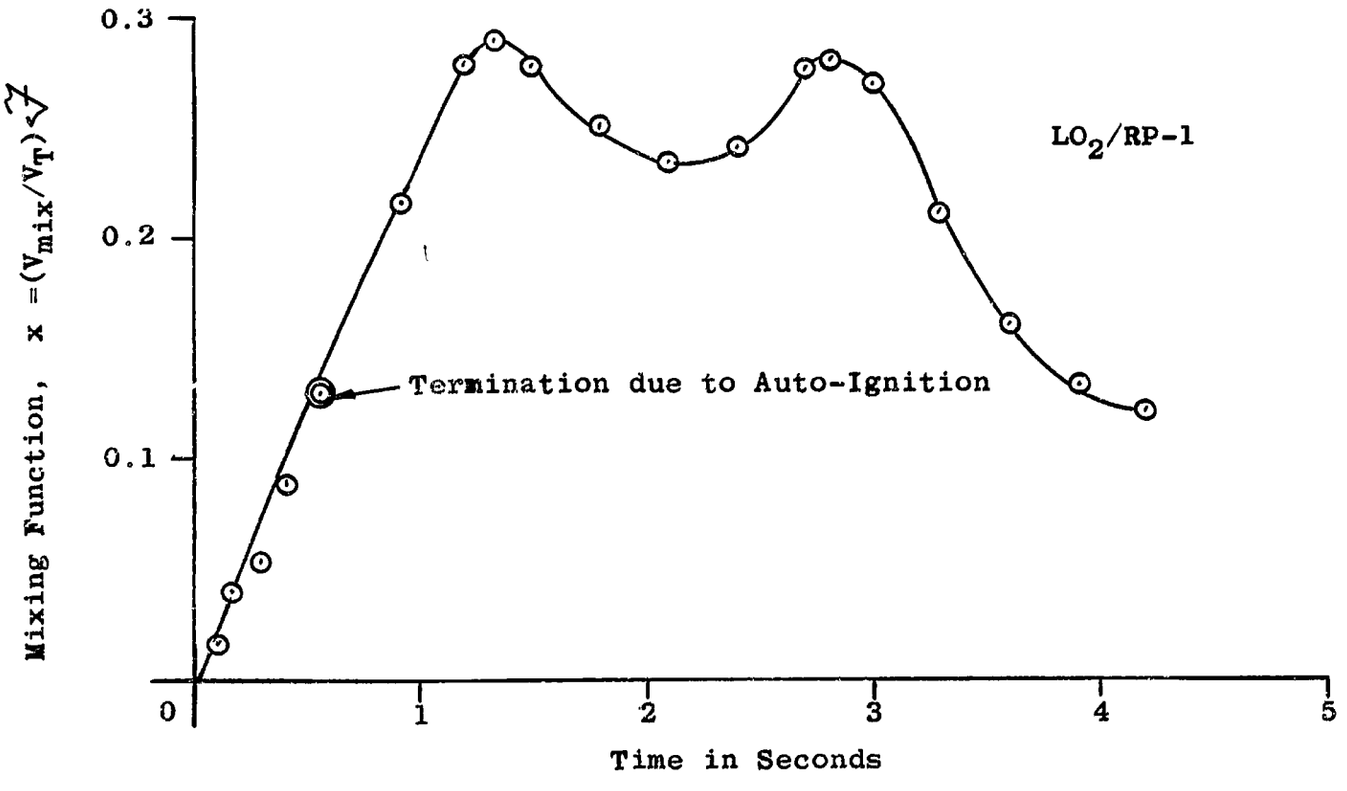

Figure II-5C Mixing Function, 25,000 lb Explosion Experiment (Based Upon 3" Diameter Simulated Experiment)

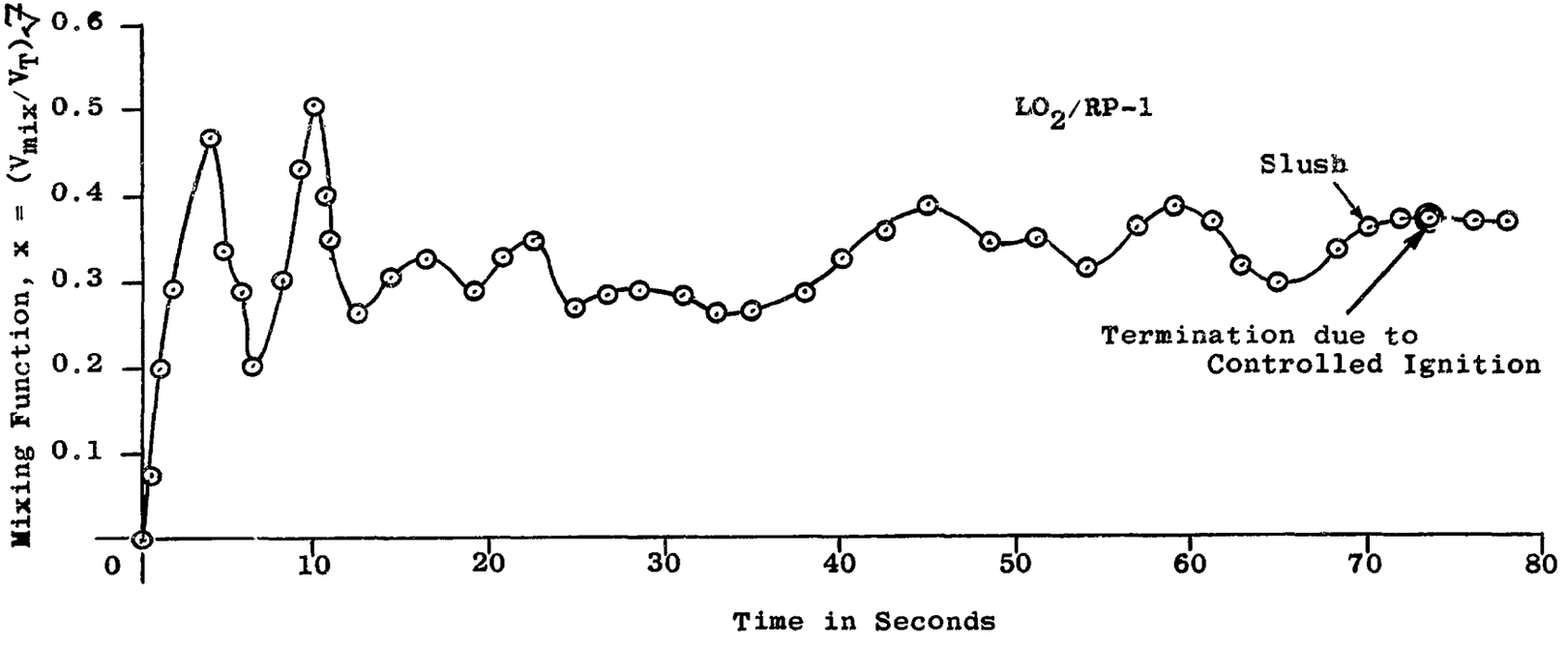

Figure II-5D Mixing Function, 200 lb Cold Flow Experiment
(Based Upon 3" Diameter Simulated Experiment)

C. Expected Yield as a Function of Time (Chart 6)

Taking the yield potential curve for a particular failure mode and multiplying it by the mixing function results in the expected yield curve, indicating what yield one could expect at any time t at which ignition occurs.

Fig. II-6A gives the Expected Yield curve for the ADL J series experiments. Experiments analyzed for which ignition, (auto-ignition) was delayed an appreciable amount.

From all the work and the Yield Potential curves, the Mixing Function curves and the resulting Expected Yield curves it is seen that the expected yield starts at zero at time zero (it may remain there for some time until the propellants come together and start to mix) then increases reaching a maximum and then decreases again with time. How high the maximum is depends upon the mode of failure and the violence with which the propellants are brought together.

Fig. II-6B gives the expected yield-time curve for the 200 # LO_2/RP-1 cold flow and explosion experiment.

D. Delay and Detonation Times

From the above work the Expected Yield curve was obtained giving information on what to expect at time t when ignition and subsequent detonation occurs. If this time can be pinned down then the Actual Yield is found and the objective of this study obtained.

The simplest case is the one where ignition is initiated under controlled conditions by igniting the propellant mixture at will.

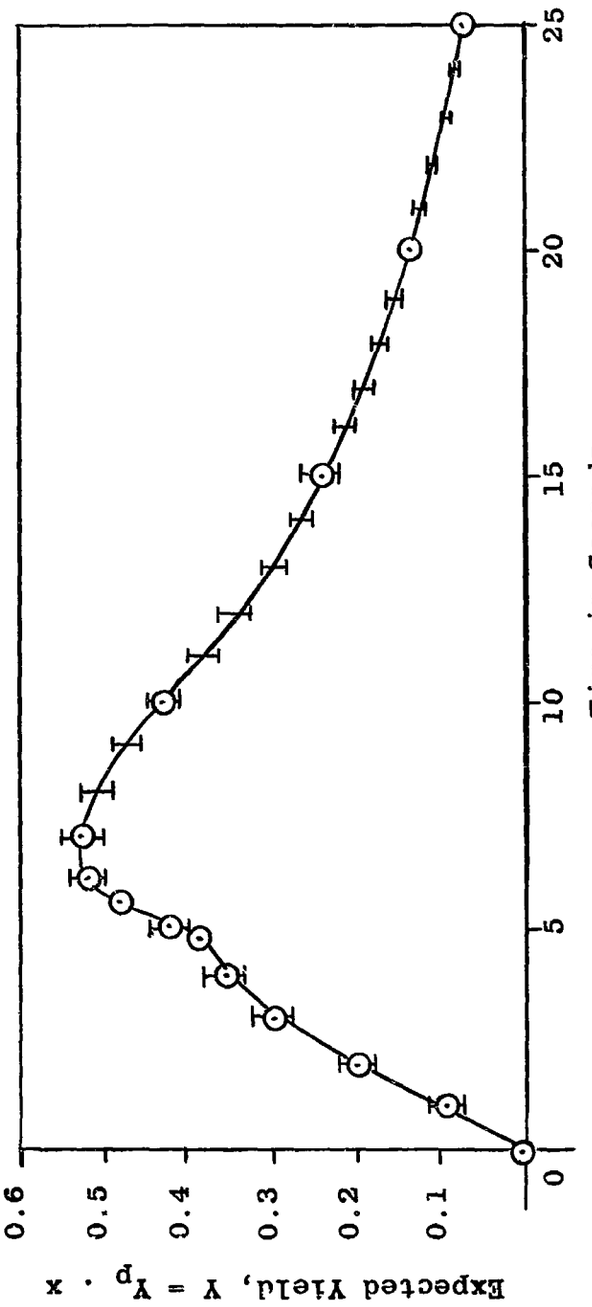

Figure II-6A Expected Yield as a Time Function (ADL J Series)

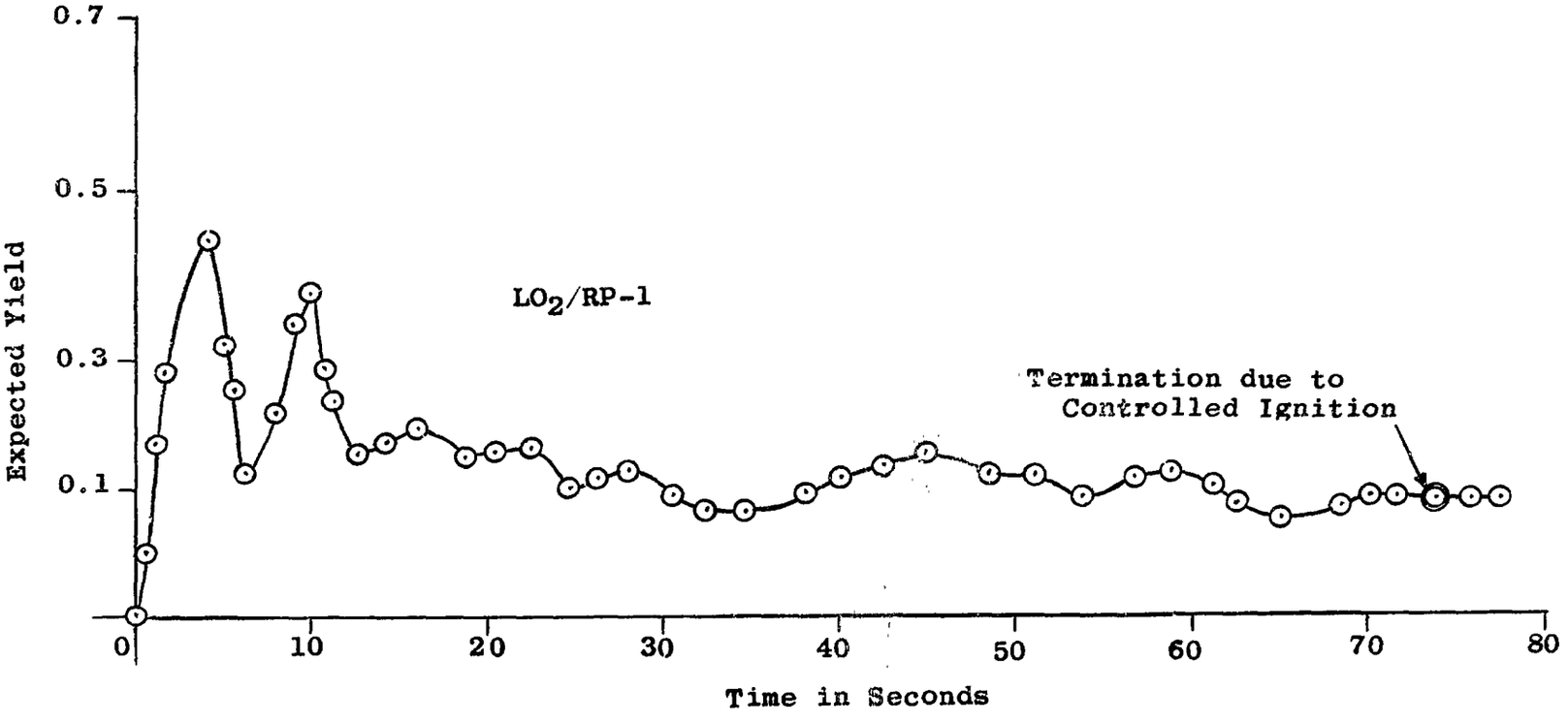

Figure II-6B Expected Yield as a Time Function
(200 lb Cold Flow and Explosion Experiment)

In this manner any desired yield can be obtained up to the maximum for the particular mode of failure involved.

This was done in some of the small scale ADL and small scale PYRO experiments. As soon as the quantities get larger controlled ignition becomes more and more difficult and auto-ignition phenomena take over. Some of this will be discussed in more detail below.

1. Ignition

a. Sources

There are many phenomena which can act as ignition initiators.

It is obvious that in a rocket failure there will or may be hot surfaces or even flames or fires.

Due to the collapse of the structural system falling members have enough energy and may through impact or by striking sparks when scraping other members, ignite the propellants.

Fluids which are good insulators when flowing across each other or solid surfaces can produce tremendous electro-static charges, which when discharging can easily ignite a combustible mixture. This particular phenomenon has been investigated in detail and is described below.

Crystal fracture of the thermally stressed solids formed by freezing the RP or even LOX when cracking release enough energy to act as an ignition source.

Silent glow, slow reaction between fuel and oxidizer may produce a hot spot setting off the mixture.

Phase changes may produce initiation centers (bubble compression, etc.) to start detonation in the stoichiometric mixture.

Many others could be named but the above are considered the most likely ones and any one of them will certainly be present in an actual missile failure.

Electrostatic Charge and Voltage Generations

This source is considered the most likely one since it is produced by the mixing propellants. Especially with cryogenics which exhibit considerable differences in temperature the mixing process is very violent producing high voltages and rather large charges in very short time.

Laboratory experiments with small quantities of RP-1 and LN_2 indicate that charges large enough and voltages high enough to cause sparking and then ignition can easily be produced by the mixing process.

According to the literature[18] in unusual cases hydrogen has been ignited by 1300 volts and 0.2 milli-joule. Usually it takes more and voltages of 14,000 and 20,000 are quoted. Some authorities according to the above source consider it necessary to have an electric field strength of 76,000 volts/inch before sparking can occur.

Using the laboratory results which for small quantities and bulkhead failure type experiments are presented in Fig. II-7 for voltages produced and in Fig. II-8 for charges, approximate critical mix masses can be calculated.

For LOX/LH_2 (weight ratios 5 to 1) this could be as low as 13 lb under unusual conditions but average about 2300 lb for LOX/LH_2 and about 2800 lb for LOX/RP-1 (weight ratio 2.25 to 1). These results assume an average spark gap of about 1/4 inch which is the average bubble size as determined in earlier experiments.

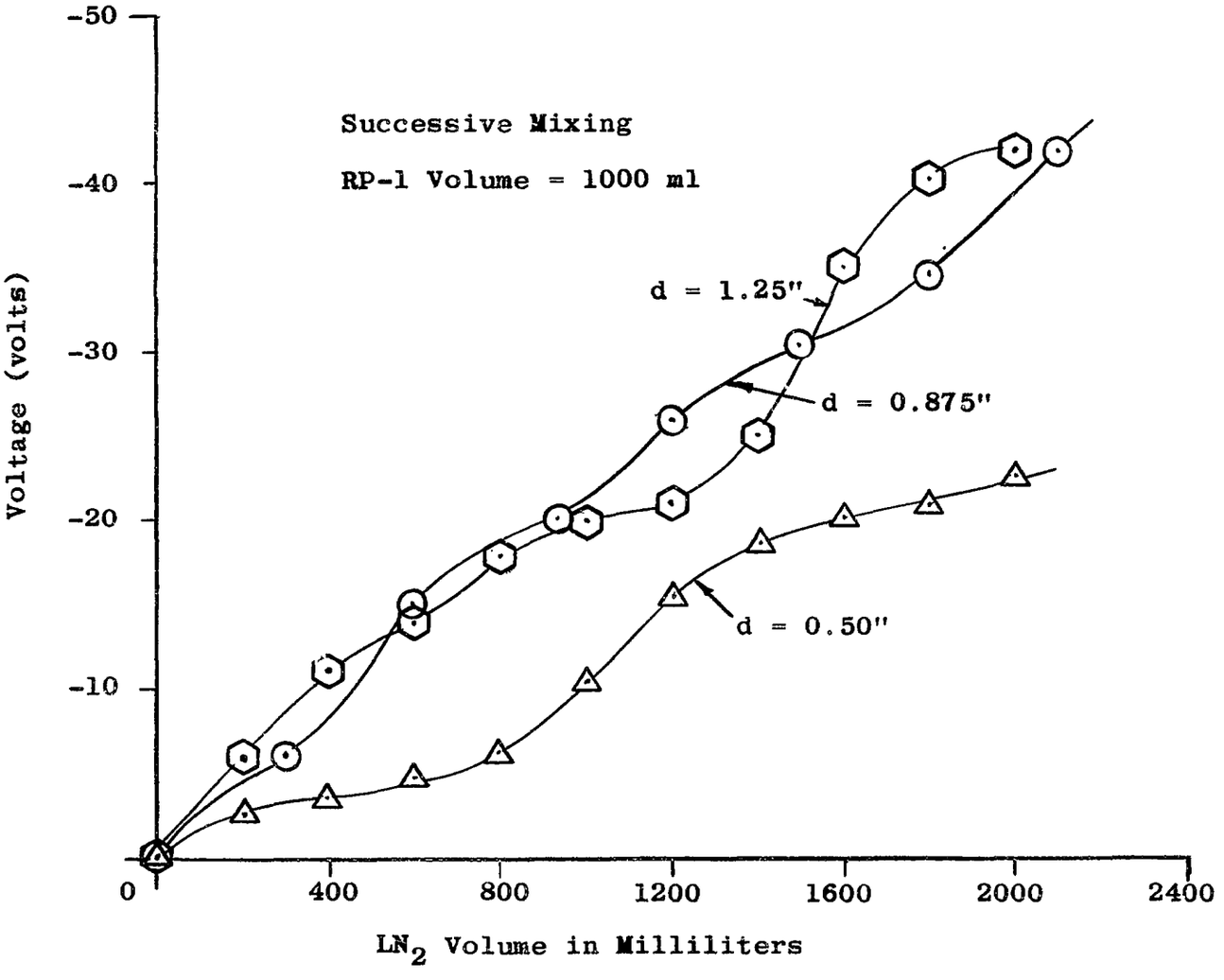

Figure II-7 Typical Voltage-Volume Relationship as a Function of Electrode Spacing

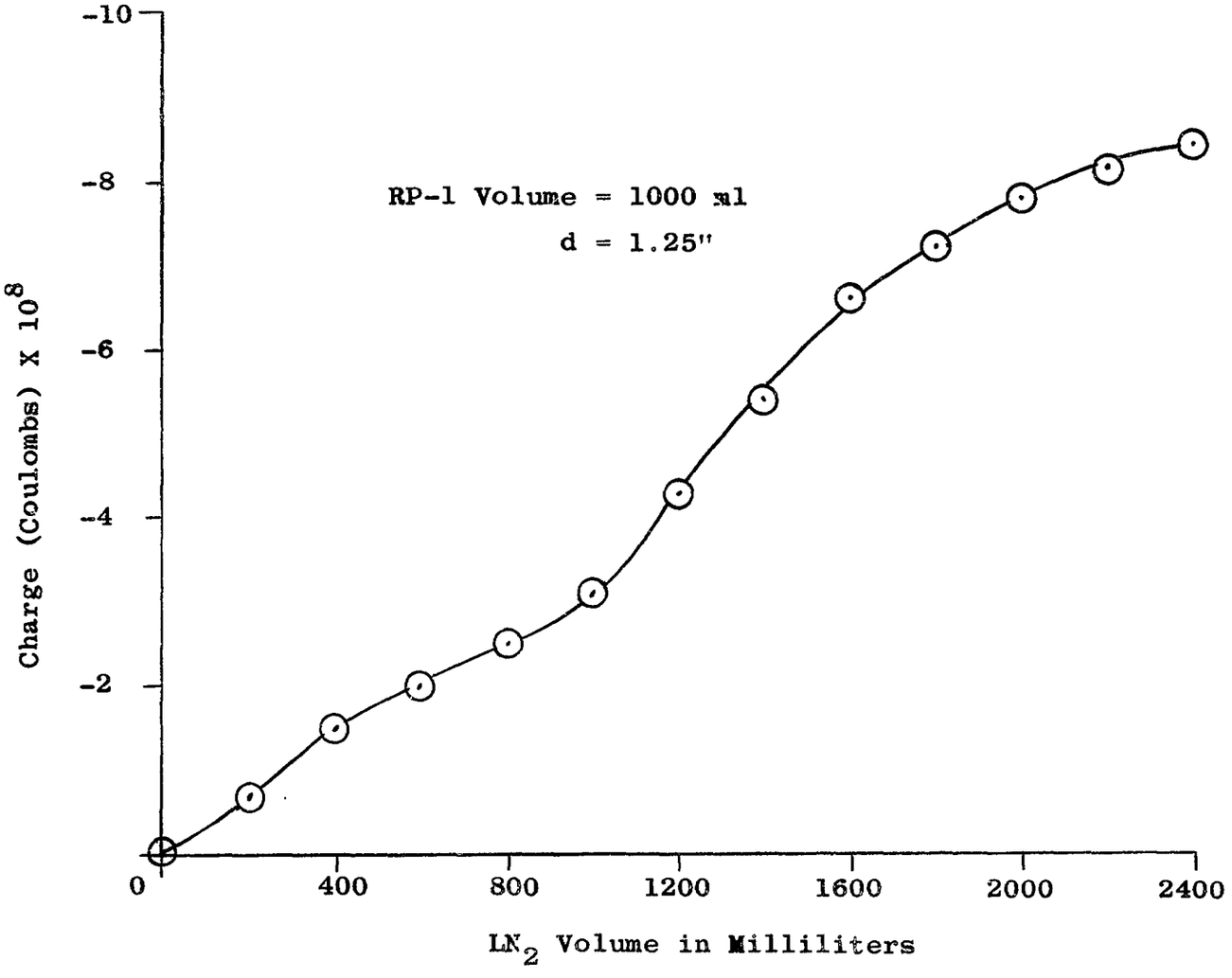

Figure II-8 Typical Charge-Volume Relationship

If the above results are assumed to be applicable, one can estimate the average expected yields for such failures, obtaining about 3 percent for the S-IV PYRO experiment and about 11 percent for the 25,000 lb LOX/RP explosion experiments.

b. Propellant Type

As was already mentioned in part (a) the characteristics of the particular propellants have a pronounced influence upon the results. The example cited above shows that it is much easier to ignite and produce detonation in a LOX/LH_2 mixture than in a LOX/RP-1 mixture.

Some propellants, one might say, have their ignition sources built in, such as hypergolics which ignite upon contact (more accurately a very short and essentially constant time after contact).

c. Propellant Quantity

As also already discussed above the ignition seems to be dependent upon the quantities of propellants involved. The ADL[6] experiments, the PYRO project experiments[13] and actual liquid propellant rocket failures[2] demonstrated this fact.

It seems possible to control the ignition of small quantities using any of the many available ignition methods but one seems to be unable to do this with large quantities of propellants due to the phenomena of auto-ignition. There seems to be a critical mass (actually a range or transition zone) below which controlled ignition is possible and above which auto - or self - ignition occurs.

2. Delay Time

a. Propellant Type

How late, after the fuel and oxidizer come together, ignition occurs

depends upon the type of propellant. Hypergolics will initiate their own ignition soon after they come in contact and their behavior upon mixing can be predicted better. Cryogenic propellants, on the other hand, will ignite with a random time delay, at least in the quantities actually encountered. Estimates regarding this time delay are possible in terms of the mixing volume as described under ignition. Only with small quantities does it seem possible to control the time delay.

b. Propellant Quantity

All the phenomena are interwoven, so that singling out any one parameter is next to impossible since the others effect it. So is it with propellant quantity. Hypergolic propellants will ignite with a more or less fixed time delay independent of the quantity involved. Cryogenic propellants have different characteristics so that the time delay can be controlled for small quantities of propellants but the delay time is set by the auto-ignition phenomena when large quantities are involved.

c. Mode of Failure

The mode of failure in producing or effecting the yield from liquid rocket propellant explosions will determine how violently the propellants are brought together. With propellants of hypergolic characteristics, where the delay time is essentially fixed, how much of the fuel and oxidizer can be mixed in the time interval from contact to ignition is determined by this mode of failure. It is obvious that more mixing will occur with more violence so that a nose impact will generally give a greater explosive yield than a simple bulkhead failure.

With cryogenic propellants, where the time delay is more random, the same basic criteria exists. The more violent failures will produce

more mixing during the time delay than less vigorous action. The delay time itself may be effected by the mode of failure occurring often earlier in more violent modes of failure, since generally more ignition sources are produced by this action.

One can also conceive the case where a particular mode of failure does not allow the propellants to mix such as if only let us say a fuel tank ruptures.

The configuration of the missile has a pronounced influence upon the delay time since it may take a relatively long time before the propellants even come together. Such may be the case in a tall rocket if the propellant tanks rupture with fuel flowing out on one side and the oxidizer on the other. It will take considerable time for the propellants to reach the ground and then more time for them to flow together. All this has to happen before they can mix.

3. Detonation Time

Is defined here as the time it takes after ignition until detonation waves are formed. It again depends upon many factors. Some materials only produce deflagration phenomena while others almost instantly form detonation waves. Again the characteristics of the propellants involved and the ignition source or method must be taken into account when considering this very involved question.

The Bureau of Mines has some publications[19] which discuss these phenomena in greater detail.

E. Actual Explosive Yield (Chart 7)

The actual yield can be found from the expected Yield-Time relationship (chart 6) if the ignition time is known. The ignition

time can either be controlled (only possible with small liquid propellant quantities), have a more or less fixed time delay as with Hypergolics, or be a random function as with cryogenic propellants.

The termination of the expected yield - time relationship is the actual yield and this point can be determined in terms of tne ignition time or in terms of the volumes mixed which most likely will produce auto-ignition.

1. ADL J Series Spill Tests

These experiments involving about 44,000 lb of LOX/LH_2/RP-1 each are represented by Fig. II-9 the expected yield - time relationship. Since the times of ignition were known for these experiments they could be marked upon the curve, determined by small scale laboratory experiments, as termination points or actual yields as predicted for each of the tests.

The actual yields as obtained experimentally by the J tests are marked as triangles on the graph and it is shown that the agreement between predicted and actual results is good.

The average ignition time from the three test was calculated and the standard deviation and the two sigma confidence region indicated.

Agreement between the predicted expected yield curve and the experimental results can only be checked up to J_1 but since it is good up to this point it is believed that the prediction relationship is also valid throughout the remainder of the range.

2. 25,000 lb Explosion Experiment Series

Two 25,000 lb LOX/RP-1 experiments carried out under project PYRO were instrumented by Dr. Farber's group with a thermocouple grid inside the RP-1 tank. This instrumentation allowed the determining of the mixing

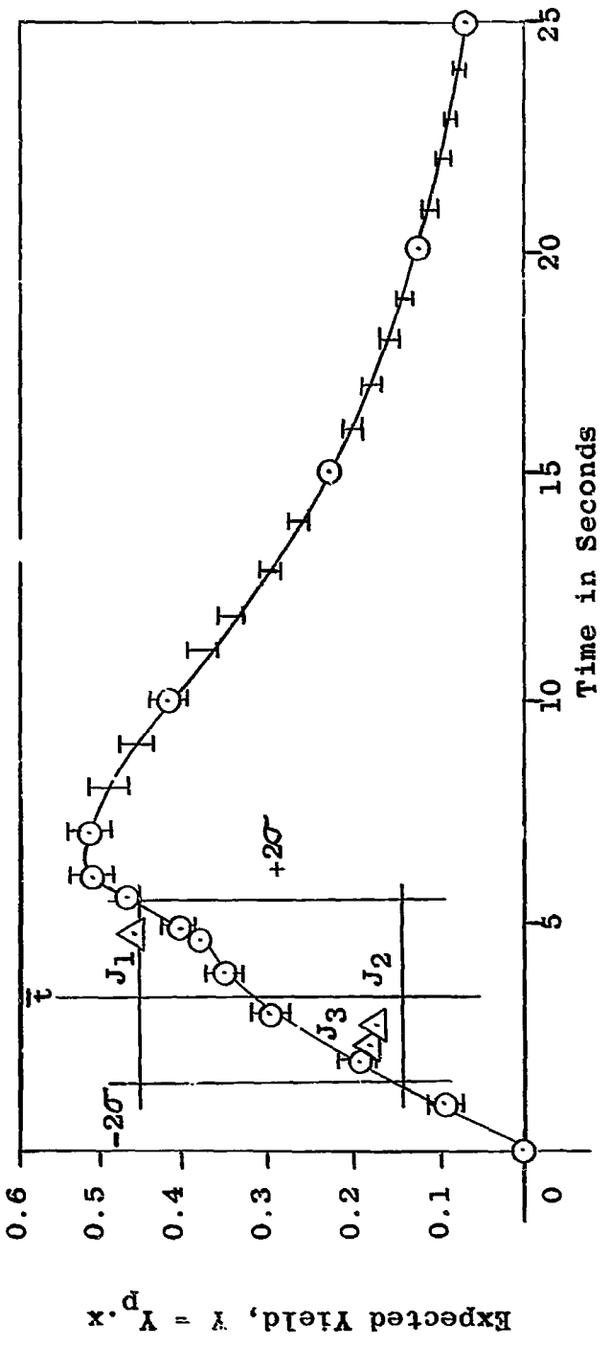

Figure II-9 Actual Yield for Random Ignition and Detonation Showing the Upper and Lower Limits of the Statistical Confidence Regions for Liquid Propellant Spill Tests

region as a function of time up to the point of ignition.

Due to the relatively early ignition (auto-ignition) in both of the instrumented experiments only the very first part of the mixing and thus expected yield curve could be obtained. The results however agree well with the mixing curve determined by 1 1/2 inch, 3 inch and 6 inch simulation experiments using Kerosene and LN_2. The mixing curve for these simulation experiments was presented in Fig. II-5C. Since the modifying factors in the early stages of the mixing process are essentially one the mixing curve actually represents in this range the expected yield - time relationship.

This curve indicates that for this mode of failure the yield would not have exceeded about 30 percent, with the peak values reached within the first three to four seconds.

3. S-IV Explosion Test

The S-IV tank configuration tested under project PYRO produced a yield of about 4 percent. Earlier in Fig. II-5B the mixing time relationship was shown as determined for this configuration in the laboratory. Again since ignition (auto-ignition) occurred early, and since the modifying factors up to ignition, are near one, the first part of the mixing curve is identical with the expected yield - time relationship and the actual yield point can be plotted on it.

Studying this curve in greater detail it can be seen that based upon the model study the explosive yield would never have exceeded 16 percent no matter when ignition would have occurred and again that the peak values of yield would have occurred during the first four seconds.

4. 200 lb Cold Flow and Explosion Experiment, LOX/RP

This controlled ignition experiment, since it went for 73 seconds before ignition, required the determination of the expected yield - versus time curve since the modifying factors deviate from their early value of one. Fig. II-6B gives this relationship.

Seventy-three seconds after the firing of the ram and when the mixing process was essentially completed (RP-1 slush formation) the mixture was fired with two explosion bolts.

The actual yield value as predicted from the simulation curve and the known time of ignition is about 0.14. The value obtained by actual measurement is estimated at 0.12. The above results indicate that the agreement between prediction and actual experiment is very good.

The above analyses were made by having the prediction curve obtained by small scale experiments and an anchor point for the prototype which can be superimposed upon this curve to give the corresponding time scale.

For the ADL J series spill tests the time scale was determined from calibration runs. For the 25,000 lb LOX/RP explosion experiments the data obtained from the thermocouple grid gave the points corresponding to the mixing function obtained by the small scale experiments. For the S-IV experiment the knowledge obtained from the 25,000 lb experiments was used, namely that the yield is in the early stages proportional to the volume mixed, and having the yield the point on the mixing function curve could again be plotted.

In addition to the above an analysis was made as to the relative mixing times of the various sizes involved for the bulkhead type failure and the [illegible] for three respective normalized mixing volumes are plotted against

the weights involved. Fig. II-10. The relationship is not simple and actually varies depending upon the percentage mixed but can be used for approximate scaling times. A reference point on the prototype is a better piece of information.

Closure

In Part II of this report it was demonstrated how the Yield Potential can be obtained for a particular configuration and mode of failure, how the mixing function can be found and how these two curves can be combined to give an expected yield - time relationship.

Then it was shown how the actual yield can be obtained from a knowledge of the ignition time or the range within which the ignition time will fall. If this information is not available the mixing function or volume or mass mixed which is most likely to be initiated by electrostatic phenomena can be estimated. And last but not least a time scale relationship is presented.

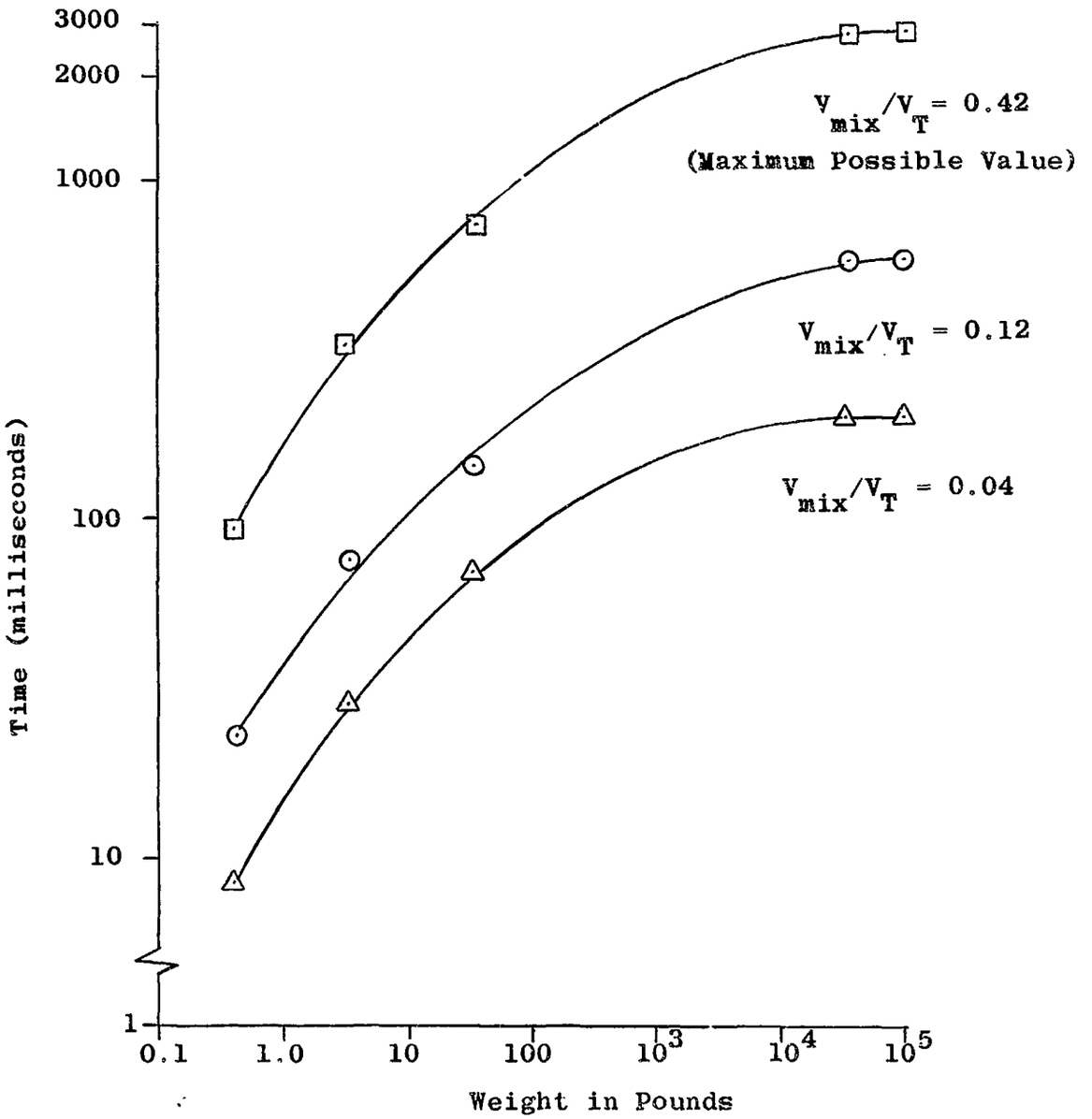

Figure II-10 Mixing Time-Scaling Relationship

Part III

Fireball Hypothesis Describing the Reaction Front and Shock Wave Behavior in Liquid Propellant Explosions.

Introduction

Part II of this report dealt with the criteria which have to be known for the prediction of the explosive yield from liquid propellant explosions by the "7 Chart Approach." For this purpose the problem was divided into three parts, the investigation of the Yield Potential, the Mixing Function and the Ignition Time. The knowledge of these three criteria made it possible to estimate the actual explosive yield.

For the above results the information as to where ignition occurred, at how many points, how after ignition detonation waves were formed and at what velocities these waves or fronts moved through the propellants or emerged from the rocket tanks, what and how large a fireball was formed, etc. was not needed.

Fireball Hypothesis

In this, the third part of the investigation, some of these factors are looked at. Since little information was available at the time this investigation was started, a fireball hypothesis was developed and presented as shown in Appendix B-II.

The phenomena were divided into four regions which together form the fireball hypothesis. These four regions are:

I. The region where ignition produces phenomena which develop into the detonation phenomenon.

II. The region where the reaction front and the shock front travel through the propellants.

III. The liquid propellant-air interface - actually the region where the liquid boundary begins to move and where the reaction front forming the fireball and the shockwave wave separate.

IV. The region in which the shock wave travels through the atmosphere as an air shock and where the fireball grows and develops separately behind the shock wave.

To get an idea of what results the fireball hypothesis predicts one should turn to Fig. 6 of Appendix B-II where the hypothesis is described in detail.

Characteristics of the Fireball Hypothesis

The fireball hypothesis predicts a very rapid rise of pressure, temperature and velocity after ignition. Due to confinement, by the propellants surrounding this region which are not mixed and the tank, a peak is reached, and then because of lessening of confinement as the phenomena travel toward the surface, attenuation of pressure, temperature, and velocity occur. The shock front and reaction front traveling together in the combustible mixture may separate when entering the unmixed liquid regions, generally with rather abrupt changes in their properties.

When reaching the liquid propellant or different phase interface, the tank, or the air interface, jumps in velocity and the other properties occur due to the change in density of the carrier media. Once in the air the shock wave will travel away from ground zero, and some distance behind, the reaction front will form the fireball and later the combustion products cloud.

For greater detail the reader is referred to Appendix B-II.

At the time this hypothesis was proposed it was not known whether and how soon it would be possible to carry out experiments which could lead to verification or modification of the fireball hypothesis for the various regions.

Proposed Verification of the Fireball Hypothesis

Later on in the performance of this project, in connection with Part II, it was proposed to instrument some of the explosion experiments carried out under project PYRO and to get as much information as possible to substantiate this hypothesis.

It was hoped for, by employing the methods developed - especially the thermocouple grid analysis, to:

1. Correlate the mixing phenomena of true propellants with laboratory experiments employing inert fluids for simulation.

2. To substantiate experimentally part or all of the "Fireball Hypothesis" proposed earlier in this study.

The specific objectives were to determine by this experimental procedure part or all of the following:

After failure but before ignition:

1. The three dimensional mixing front or boundary of the mixing region.

2. The degree of mixing at a particular point.

3. The degree of turbulence at a particular point.

After ignition:

4. The location of the point or points of ignition.

5. The time delays from initiation of failure to start of mixing, to ignition.

6. The propagation of the reaction front

7. The propagation of the shock front.

8. The separation of the shock front and the reaction front.

9. Other phenomena and events obtainable by detailed analysis.

Experimental Verification of the Fireball Hypothesis

Two 25,000 lb LOX/RP-1 explosion experiments were instrumented and one 200 lb cold-flow and explosion experiment.

The data obtained by recording, with Oscillographs, the signals from No. 36 gage copper-constan thermocouples, shellacked and teflon coated, were excellent. The junctions of the thermocouples were prepared by welding the wires together so that the junction was not distinguishable from the rest of the wire. The thermocouple ends were then put into small plastic tubes with only the junction protruding. This allowed mounting of the thermocouples and at the same time gave support to the junctions.

The response of these fine thermocouples between room temperature and LN_2 boiling temperature (-320 F) is about 0.0002 sec/F. With a greater temperature impulse the rate would even be higher.

It should be pointed out here that only in (2) and (3) of the above proposed verification list do the thermocouple response characteristics have to be considered. In all other cases only relative time differences are needed.

For the configuration detail and execution of the experiments the reader is referred to the Appendix C. In this reference the tankage configuration is shown, a photograph of a thermocouple presented, the thermocouple positions pinpointed and the thermocouple grid shown as installed in the 78 inch diameter tank.

Some of the traces obtained from the 25,000 lb LOX/RP experiments No. 278 and No. 282 are shown. These two experiments proved to be amazingly alike, truly reproducible in every respect.

Experimental Results and Analyses

Careful analysis of the data showed among the many important results:

Mixing Volume

Practically all the mixing up to the time of ignition was confined to the volume swept through by the star cutter. Not much mixing occurred after ignition.

This volume as determined from the data for the two 25,000 lb LOX/RP explosion experiments was about 12 percent of the total, based upon the RP, giving an upper yield estimate of about 12 percent of the theoretical maximum.

Ignition Point

In both the 25,000 lb LOX/RP experiments there was only one ignition point in each case. The location of it was determined and turned out to be in almost the same location for both experiments. See Fig. 6A and 6B in Appendix C. After ignition occurred at one point, reaction and the other phenomena were so rapid that not enough time seemed to be left for another ignition point to be formed.

Time Delays

The time delays between various events can be determined from the traces. If projected on a screen these times can be read to a 1/1000 of a milli-second. The time delay from failure or firing of the ram to ignition in experiment 278 was 543 milli-seconds, and in experiment 282

it was 580 milliseconds (read to the closest milli-second. Greater accuracy can be obtained if desirable).

Film Speed Determination or Check

To tie together the events inside the exploding liquid propellant tanks with events occurring later outside it is essential that both groups of phenomena are based upon the same absolute time scale. Since some of the phenomena such as the firing of the ram and the appearing of the reaction front when breaking through the tank walls could be recorded both by the thermocouple grid and the high speed film coverage, accurate film speeds could be determined. This proved to be essential for the analysis of the phenomena from failure to formation of the combustion products cloud.

Fine Structure

Many of the phenomena can be interpreted from the over-all appearance or characteristics of the traces but much more information can be obtained by studying the fine structure of the high speed thermocouple traces. At least three typical traces can be found. They are schematically shown in Fig. III-1.

The fine structure of the traces reveals that some of the glass fragments from the shattered diaphragm hit thermocouple junctions in the uppermost of the four layers, but did not damage them, so that the thermocouples recorded this and later events. The glass fragments did not penetrate during their high energy state to the lower layers since the attenuation in the liquid was too great.

Fig. III-1 shows a trace where LOX arrives at the thermocouple, makes it dip, followed by the reaction front which produced a rapid rise

Sketches of Typical Thermocouple Traces
(Temperature versus Time)

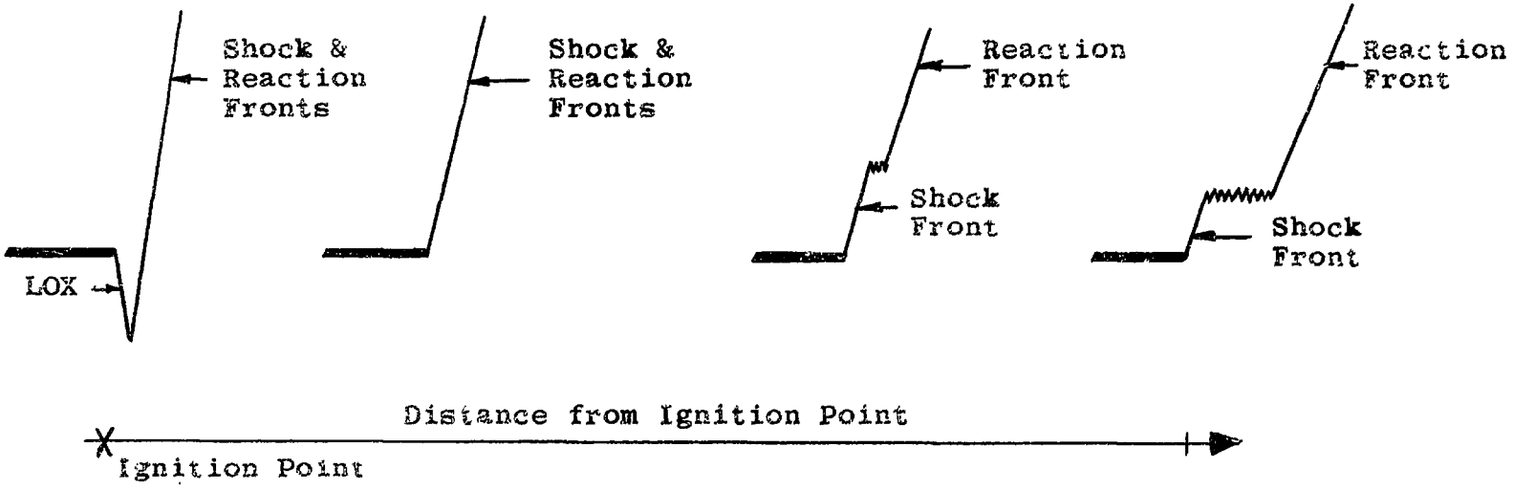

Figure III-1 Typical High Speed Thermocouple Traces

in temperature. Some of the thermocouples in the unmixed RP region never see LOX and they first sense the reaction front with the rapid rise in temperature until destruction through melting of the thermocouple occurs. The third typical curve is the one where the thermocouple records the passing of the shock front and then the passing of the reaction front. The further from the mixed region in the inert fluid the thermocouple was located the weaker was the shock front and the greater the time interval between the passing of the shock front and the passing of the reaction front, indicating an increasing separation of the two phenomena. Near the walls on some traces reflection of the shock front from the tank walls is indicated.

The interpretation of this fine structure of the traces had to be done with a knowledge of the respective location of the thermocouples. Some of this was made more difficult by the added turbulence and short exposure to some small slugs of LOX which enveloped the thermocouple for very short times and the passage of bubbles which under compression indicate some heating. The rates of the changes, however, allowed interpretation of which phenomena were involved.

25,000 lb LOX/RP Explosion Experiment No. 278

Experiment No. 278 was undertaken rather conservatively with the thermocouples placed so that they would have the best chance for recording and survival long enough. The recorders were operated at their maximum reliable speeds. In this manner it was hoped that some data could be obtained which has never been obtained before.

25,000 lb LOX/RP Explosion Experiment No. 282

Experiment No. 282 was undertaken as an all out effort to obtain the best possible data accepting some risks. This was possible since this

experiment was originally planned in case something went wrong with experiment No. 278.

Since excellent data was obtained in experiment No. 278 the thermocouples were moved closer to the ram and the recorders were operated at top speed in experiment No. 282. Even if something would have gone wrong in this test the data of experiment No. 278 supplied all the information needed. Since everything worked perfectly however, in experiment No. 282 excellent data was obtained, very close to the star cutter and in the mixing region and the resolution of the recorder charts was at its maximum.

200 lb LOX/RP Cold-Flow and Explosion Experiment

Essentially the same procedure was repeated for a 200 lb LOX/RP cold-flow experiment. In this case the ignition could be controlled and thus the complete mixing curve obtained for comparison with the laboratory inert fluid simulations. After the mixing had gone to near completion, and settled down to a more or less steady state, the system was ignited with two explosion bolts. Information was thus obtained on both the mixing process without ignition and then the phenomena recorded following controlled ignition.

Results of the 25,000 lb LOX/RP Liquid Propellant Explosion Experiment

The results of the two 25,000 lb experiments are generally better than the results of the 200 lb experiment mainly because the distances between the thermocouples were greater giving larger time delay and thus better resolution for analysis.

The two experiments No. 278 and No. 282 turned out to be almost identical thus giving a double check on some of the results.

In both cases auto-ignition occurred, a phenomenon typical for large scale liquid propellant rocket failures for which information was to be obtained through this study.

The results for these experiments are shown in Fig. III-2, III-3 and III-4, giving distance from point of ignition versus time for the shock wave and the reaction front, the velocities of these two phenomena versus time and distance from point of ignition. The data up to the liquid propellant - air interface were obtained by the thermocouple grid and the data outside the tank with high speed films. The absolute time scale was obtained by observing events such as firing of the ram and emergence of the fireball with both measurements.

After ignition it is seen that the velocity of the reaction front increases very rapidly to a velocity of between 7000 and 8000 feet per second. These values are or may be low since they are averages between neighboring thermocouples. With thermocouples closer together the variations could be determined better. The values obtained here are lower than those corresponding to the Von Neumann spike or the Chapman-Jouquet condition[19], but they represent actual measurements. As the reaction front, by now supporting a shock front, emerges from the mixed propellants into the unmixed RP, the velocities are attenuated severely with the shock front separating from the reaction front.

The shock front arrives slightly before the reaction front at the tank wall, where giving off some energy producing an outward movement of the tank wall it is reflected back toward the reaction front. Meeting the reaction front it is again reflected outward toward the by now moving tank wall. Here the earlier process is repeated and the total phenomena repeated until finally both the shock wave and the reaction front emerge

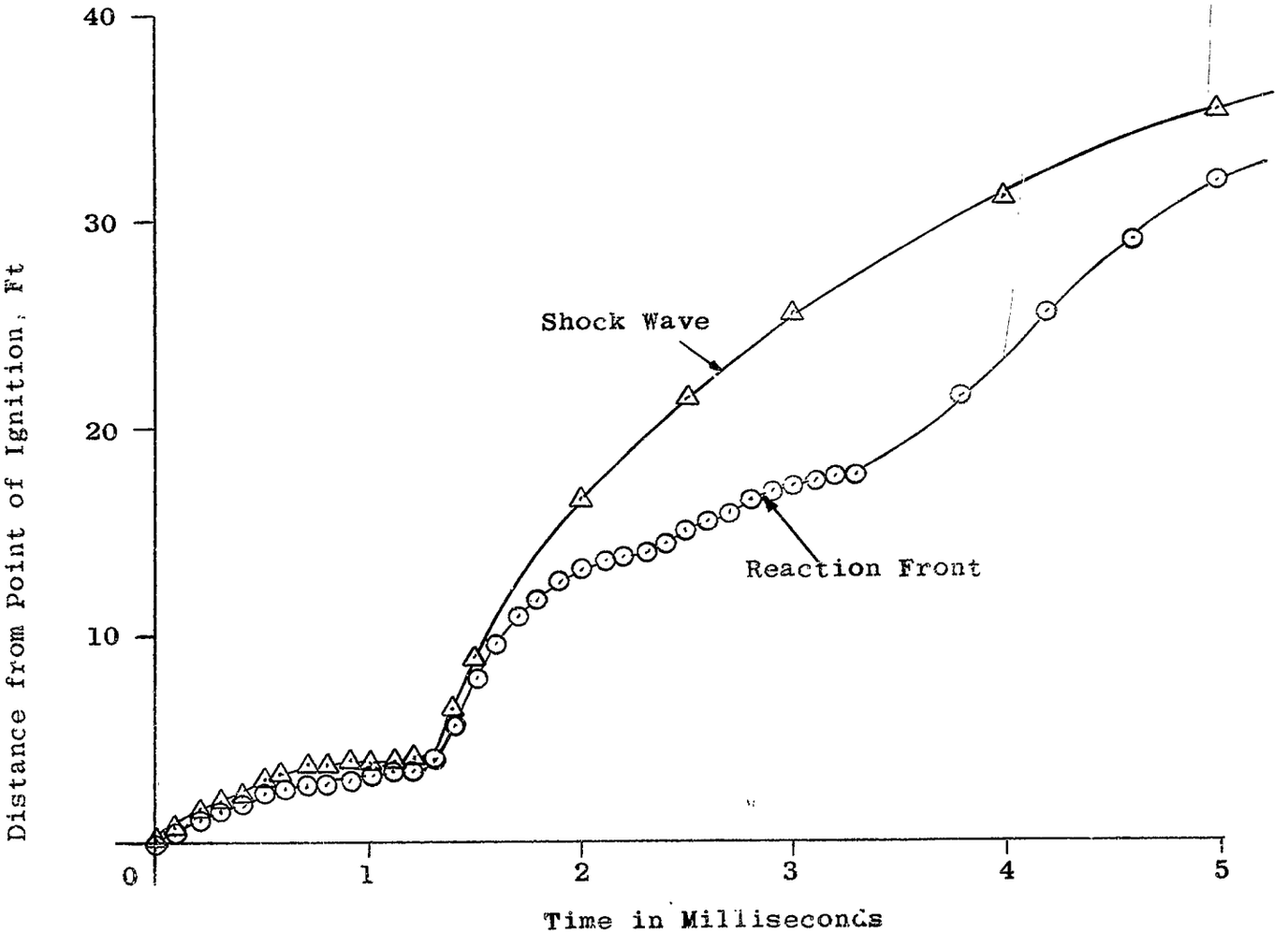

Figure III-2 Distance versus Time of Shock Wave and Reaction Front (25,000 lb LO_2/RP-1 Explosion Experiment)

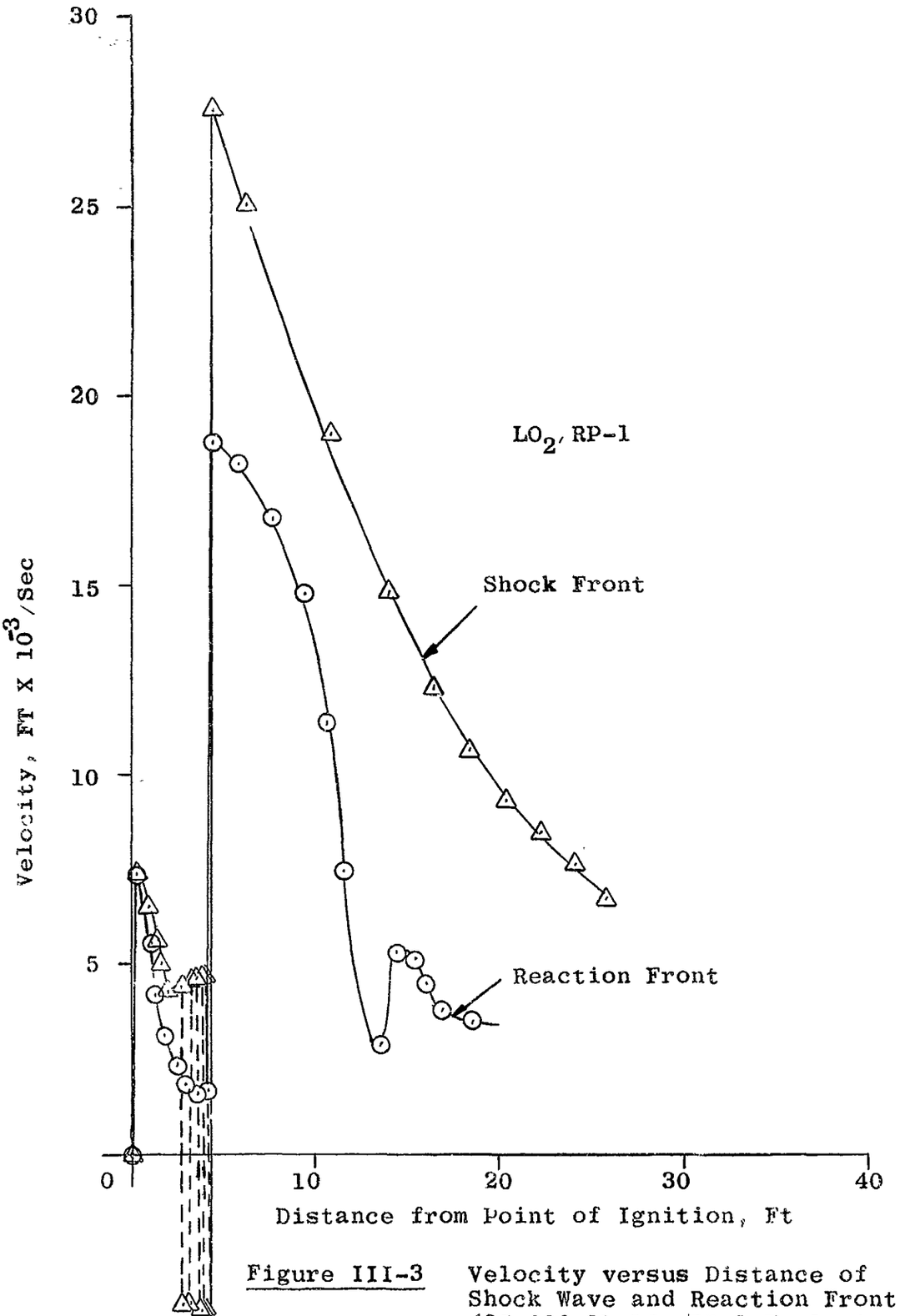

Figure III-3 Velocity versus Distance of Shock Wave and Reaction Front (25,000 lb LO_2/RP-1 Explosion Experiment)

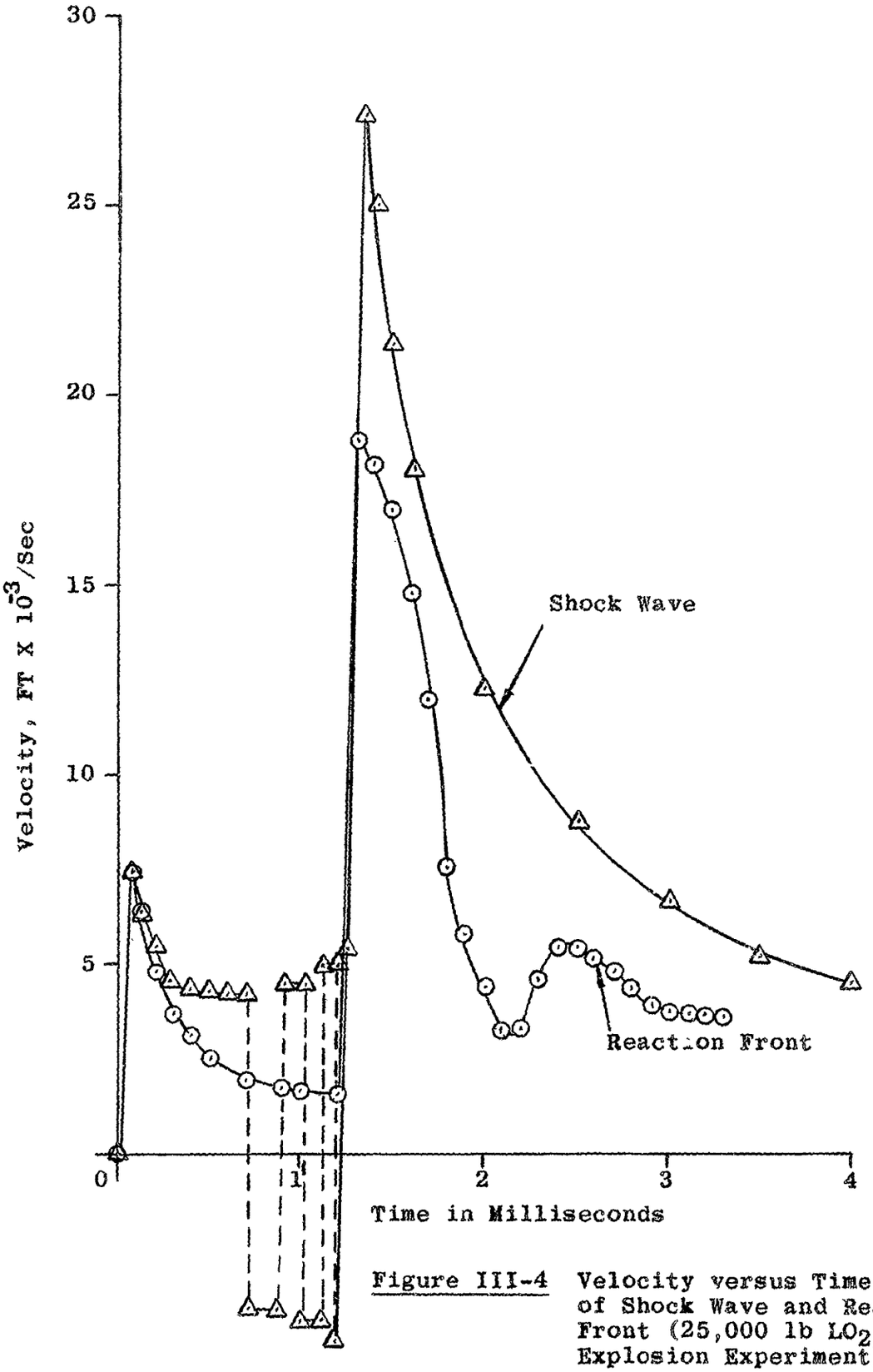

Figure III-4 Velocity versus Time of Shock Wave and Reaction Front (25,000 lb LO_2/RP-1 Explosion Experiment)

almost simultaneously from the tank with jumps in velocity due to the decrease in density of the carrier medium and sudden loss of confinement.

The shock wave or front reaches a velocity of about 27,000 ft/sec but is attenuated within a very few feet. The reaction front reaches a velocity of about 19,000 ft/sec also being attenuated rapidly, forming the fireball and then the combustion products cloud.

Fig. III-2 shows the distance from the point of ignition versus time. Fig. III-4 gives the velocity versus time showing how fast the velocity changes occur and Fig. III-3 shows the velocity variation versus distance from the point of ignition indicating that the most severe conditions occur very near the exploding missile.

Fig. 8 of Appendix C shows the fireball and the combustion products cloud volume as a function of time for both of these 25,000 lb liquid propellant explosion experiments.

The Figures show clearly the shock wave getting ahead of the reaction front inside the tank configuration, then waiting through energy transfer and reflection for the reaction front so that they break through the tank wall, which by this time is moving outward, essentially together. After separating, the pulsations of the reaction front or fireball are clearly shown in the velocity versus time presentation and later in the fireball volume versus time or distance presentation.

200 lb Liquid Propellant Cold-Flow and Explosion Experiment

The 200 lb liquid propellant cold-flow and explosion experiment was carried out to first determine the similarity between the mixing function obtained by real propellants and the simulated liquids used in the laboratory experiments. This similarity was established as shown in Part II

As a bonus the final mixture was ignited with two explosion bolts so as to give information on reaction front, shock front, fireball and combustion products cloud characteristics.

The thermocouple grid installation was identical to the one of experiment No. 282 only smaller in size. Half of the high speed cameras were operated during and after firing of the ram just in case auto-ignition should occur. This was not expected, since the probability for this event was very low, and it did not happen. The rest of the high speed cameras were started shortly before the controlled initiation with two explosion bolts.

The results from this test are presented in Fig. III-5, III-6, and III-7. They are very similar to the 25,000 lb explosion experiment results, with the velocities of both shock wave and reaction front about the same as in the larger test but with the velocities outside the tank configuration somewhat lower. Again the reflections were observed but not as clearly since the distances and times were much smaller and the resulting resolution capability not as good. Similar pulsations of the reaction front or fireball can again be seen.

Fig. III-8 gives the fireball and combustion products cloud volume as a function of time corresponding to the information presented for the 25,000 lb experiments.

Closure

It is believed that this investigation has added a number of new facts to the knowledge of liquid propellant explosions, has actually presented measurements inside an exploding liquid propellant missile and interpreted the recorded data in terms of meaningful parameters.

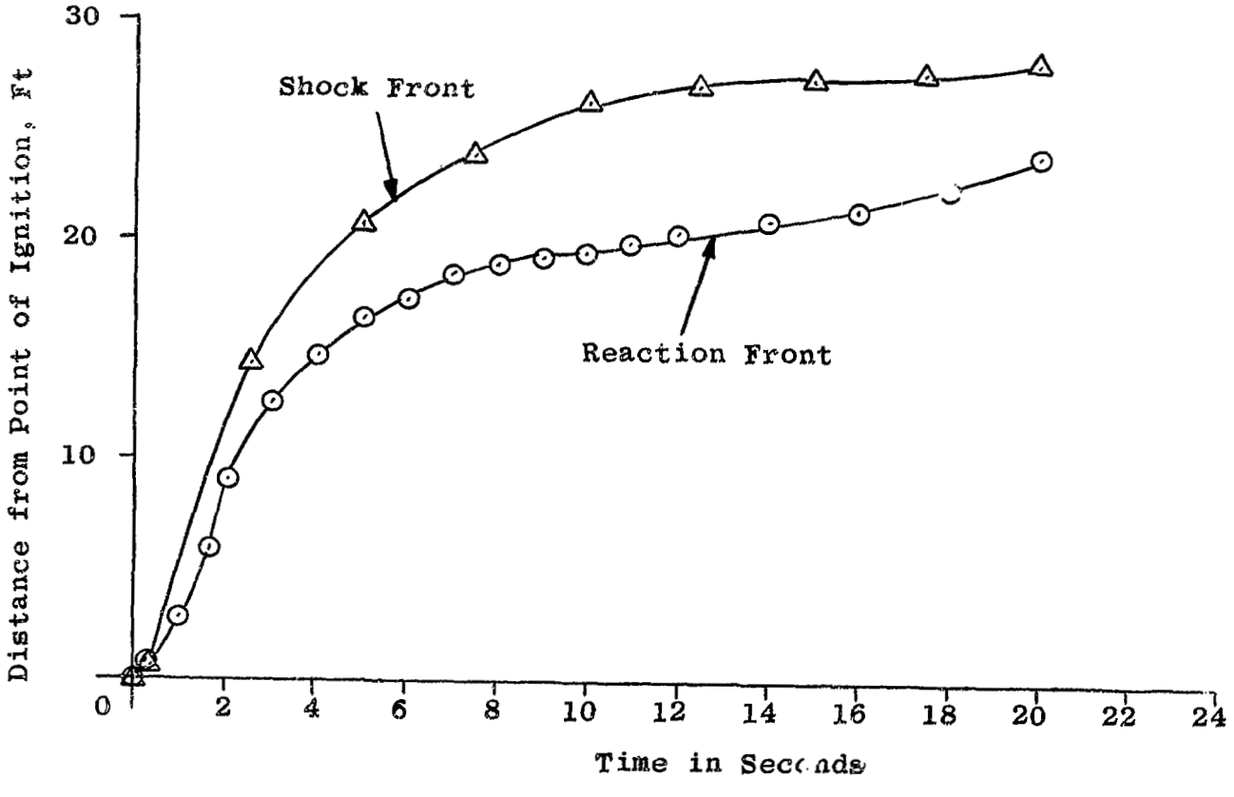

Figure III-5 Distance versus Time of Shock Wave and Reaction Front (200 lb Cold Flow and Explosion Experiment)

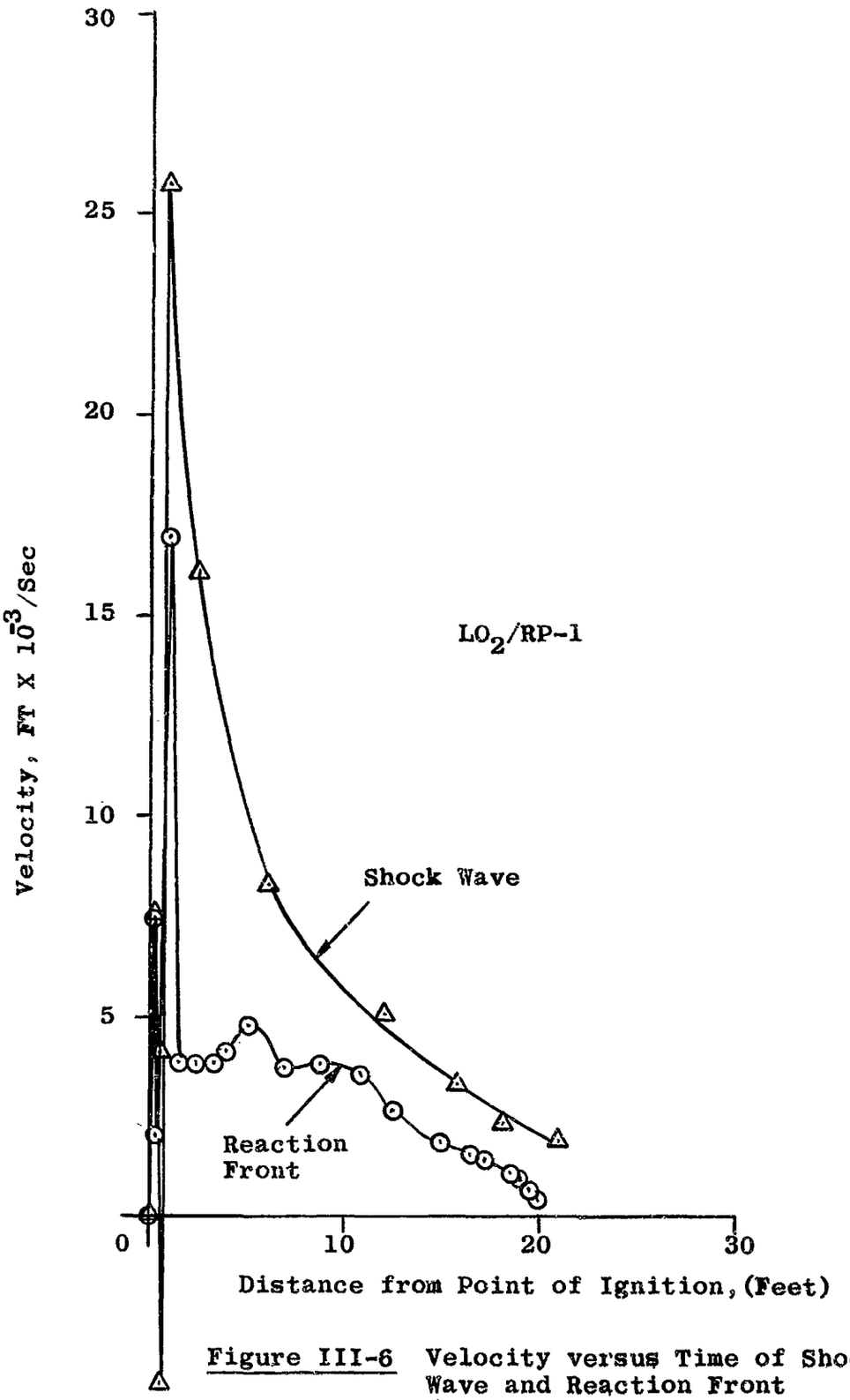

Figure III-6 Velocity versus Time of Shock Wave and Reaction Front (200 lb Cold Flow and Explosion Experiment)

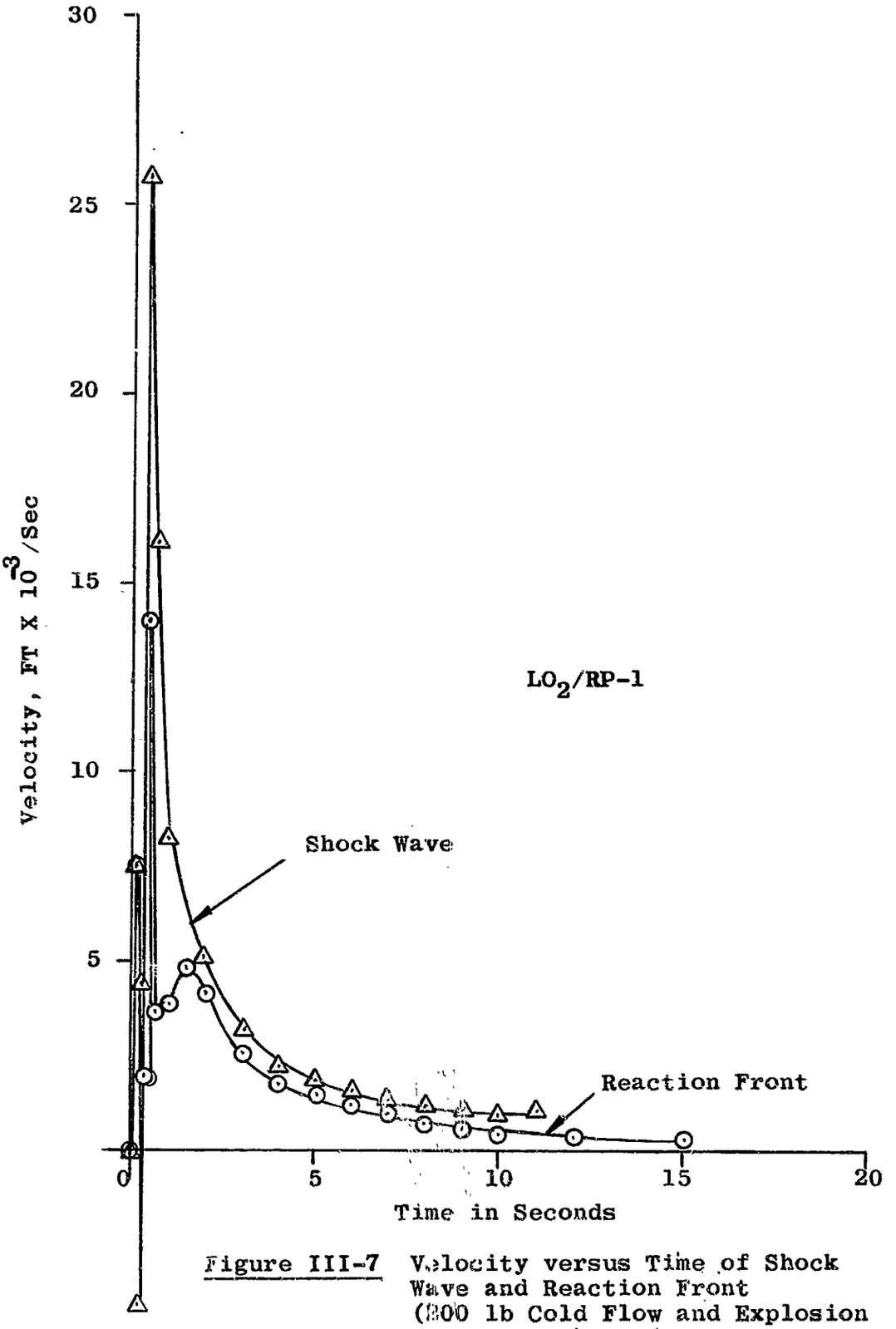

Figure III-7 Velocity versus Time of Shock Wave and Reaction Front (200 lb Cold Flow and Explosion Experiment)

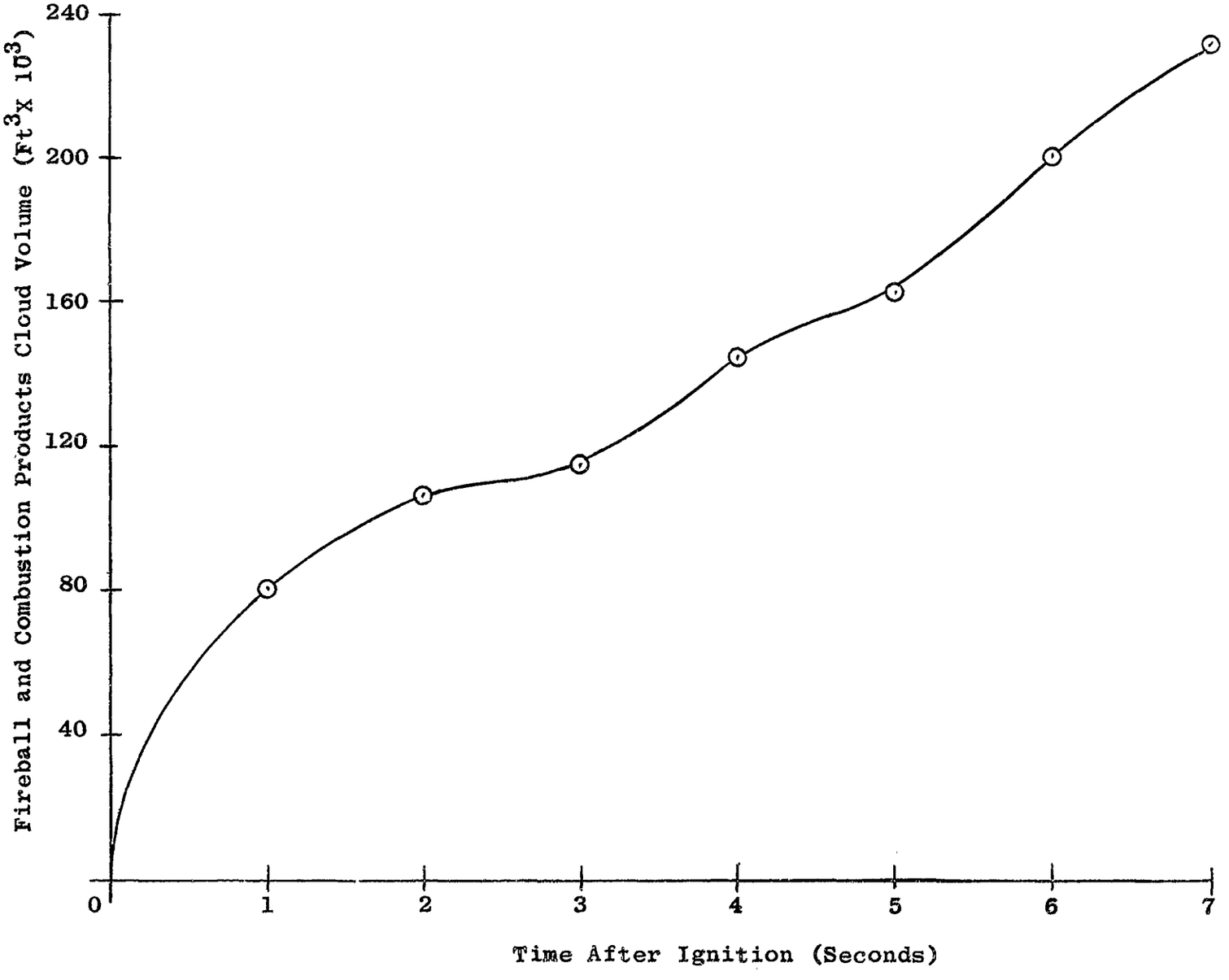

Figure III-8 Fireball and Combustion Products Cloud as a Function of Time (200 lb Cold Flow and Explosion Experiment)

Like always more knowledge opens up more questions and f rther investigation is desirable especially near the wall of the tanks both inside and out to gain information on exactly what goes on in this critical region III of the fireball hypothesis.

Having obtained information for the characteristics of a particular type of bulkhead failure by methods developed by this investigation other types of failures and propellants can be investigated. The method of investigation has proved itself and the tools for such investigation are now available.

From the present work it seems that the reaction front and shock front characteristics are a factor of the propellants involved, modified by scale.

Having described a number of the characteristics of liquid propellant explosions from initiation of failure to the formation of a combustion products cloud it remains to take a closer look at this cloud.

The composition of tne combustion products cloud may become of importance when toxic propellants are used so that the hazards by such clouds to populations and plant life can be assessed.

The analysis of this last remainder and a computerized method for finding the combustion products cloud composition will be presented in Part IV, the last part of this report.

Part IV

Fireball and Post-Fireball Combustion Products Cloud History and Composition

Introduction

After the detonation has occurred the behavior of the fireball from the explosion which is formed and then gradually changes into a combustion products cloud is of importance. How large a fireball is formed, what is its temperature and what are the pressures inside? To be able to obtain this information the knowledge of how the fireball comes about, how it cools and then changes into a combustion products cloud is essential. Thus, its behavior is really one of the last groups of phenomena or processes in a series.

So for this phase of the work the knowledge of the fireball and combustion products cloud, volume-time, pressure-time and temperature-time histories have been assumed known and then the composition of the combustion phenomena has been determined. The composition of the fireball and of the combustion products cloud are important as well as their interaction with the atmosphere, especially when toxic materials such as Flourine are used in the propellants.

The volume-time, pressure-time, and temperature-time histories of the explosion from liquid propellants were chosen as input since they may be determined theoretically [20,21] or may be measured in experiments thus giving a check on the theoretically determined information, with its statistical variations, etc.

For this investigation the best information available at this time has been used as input and t' ' rather elaborate computer programs have been used in obtaining the desired results[22]. Homogeneity of the fireball

and of the combustion products cloud have been assumed in all calculations and this seems to be a reasonably good basis since the turbulence of the reaction processes is great enough to tend to mix the different products well.

With the volume-time, pressure-time, and temperature-time history available, the mathematical equations controlling these processes were set up and then computer solutions worked out to give the desired results.

Only a portion of all the information which was generated by this analysis is reported here but it seems ample to show the method of approach and the kind of results which can be obtained.

The fuel-oxidizer combination chosen here as examples for this investigation were ones which are used and some which may become important in the future development of liquid propellant rockets. they are:

LH_2/LO_2

RP-1/LO_2

LH_2/LF_2

RP-1/LF_2

LH_2/RP-1/LO_2

LH_2/LO_2 + 1% F
+ 5% F
+ 10% F

RP-1/LO_2 + 1% F
+ 5% F
+ 10% F

LH_2/RP-1/LO_2 + 1% F
+ 5% F
+ 10% F

For the above combinations of fuel and oxidizer, assuming a quantity of propellants of about 100,000 lbs, the results which are all normalized are presented as follows:

1. Fuel consumption versus time
2. Volume of entrained air versus time
3. Partial Pressures (of combustion products) versus time
   Partial volumes (of combustion products) versus time
4. Partial weights (of combustion products) versus time

Both the input information as well as the results are given in graphical form since it is believed that this method of presentation will give the maximum amount of information in the minimum amount of space.

It might be mentioned that the method and computer program developed are rather general and by no means restricted to the above fuel-oxidizer combination.

Theory of Approach

Equilibrium Composition of Chemical Reactions of Liquid Propellants Taking Place in the Atmosphere.

The purpose of this phase of the research program is to theoretically determine the amounts of product gases formed, as a function of time, as the result of a reaction involving liquid propellants and entrained air. This type of reaction is continuous since all of the available fuel does not react immediately and furthermore the resulting fireball (which grows with time as more fuel reacts) continually entrains air. Given the initial amounts of fuel and oxidant as well as the volume - time history of the fireball (theoretically determined or as observed from high speed films), equilibrium compositions can be determined.

The equilibrium composition for the system of n products of reaction is determined by the simultaneous solution of n+1 equations consisting of the equations of mass balance, pressure balance and the dissociation equations involving equilibrium constants.

Assuming a constant pressure process as well as an instantaneous reaction time and making use of either theoretically obtained or experimentally determined pressure-time and temperature-time histories of the fireball, a solution is found such that the total theoretical volume of the products of reaction is made identically equal to the total experimental volume by adjusting the fuel burning rate and/or adjusting the amount of entrained air. As a first approximation, it is further assumed that no air entrainment exists until all of the available fuel is burned.

To efficiently meet these demands, a computer program has been developed. The program is general but limited here to the following reactants: liquid hydrogen, kerosene (RP-1), liquid oxygen, liquid fluorine, and air. Fifteen products of reaction were considered.

The equations and method of solution follows.

Controlling Equations

Symbol	Description	Reactant
A_1	moles of LH_2	A_1H_2
A_2	moles of RP-1	$A_2C_xH_{2x}$
A_3	moles of LO_2	A_3O_2
A_4	moles of LF_2	A_4F_2
A_5	moles of air	$\frac{A_5}{4.79}(O_2 + 3.79\ N_2)$

The reactants can then be written as:

$$(A_1 + A_2X)\ H_2 + (A_3 + 0.209A_5)\ O_2 + A_4F_2 + 0.792A_5N_2 + A_2XC$$

Consider the following products of reaction; such that the right hand side of the equilibrium equation is

$$\frac{N}{P}\ (p_1H_2O + p_2CO_2 + p_3H_2 + p_4N_2 + p_5F_2 + p_6O_2 + p_7HF + p_8CO$$

$$+ p_9NO + p_{10}OH + p_{11}H + p_{12}N + p_{13}F + p_{14}C + p_{15}O)$$

where,

N = total number of moles of products of reaction

P = total pressure

p_i = partial pressure of ith product

The unknowns are $p_i (i = 1, \ldots 15)$, N. Hence 16 equations are necessary for a solution. The balance equations are:

(a) Pressure Balance

$$p = \Sigma p_i = 0$$

(b) Hydrogen Balance

$$2(A_1 + A_2X) - \frac{N}{P}\ (2p_1 + 2p_3 + p_7 + p_{10} + p_{11}) = 0$$

(c) Oxygen Balance

$$2(A_3 + 0.209A_5) - \frac{N}{P}\ (p_1 + 2p_2 + 2p_6 + p_8 + p_9 + p_{10} + p_{15}) = 0$$

(d) Nitrogen Balance

$$1.584\ A_5 - \frac{N}{P}(2p_4 + p_9 + p_{12}) = 0$$

(e) Carbon Balance

$$A_2X - \frac{N}{P}(p_2 + p_8 + p_{14}) = 0$$

(f) Fluorine Balance

$$2A_4 - \frac{N}{P}(2p_5 + p_7 + p_{13}) = 0$$

The above 6 equations can be reduced to 5 equations by eliminating $\frac{N}{P}$. Since we will be dealing with hydrogen (either LH_2 and/or RP-1), $\frac{N}{P}$ can be eliminated by dividing the 2nd equation into the last 4 equations. The 5 equations are:

$$P - p_1 - p_2 - \ldots\ldots - p_{15} = 0 \qquad (1)$$

$$(2Y_1 - Y_2)\,p_1 - 2Y_2p_2 + 2Y_1p_3 - 2Y_2p_6 + Y_1p_7 - Y_2p_8 - Y_2p_9$$

$$+ (Y_1 - Y_2)\,p_{10} + Y_1p_{11} - Y_2p_{15} = 0 \qquad (2)$$

$$2Y_3p_1 + 2Y_3p_3 - 2Y_2p_4 + Y_3p_7 - Y_2p_9 + Y_3p_{10} + Y_3p_{11} - Y_2p12 = 0 \qquad (3)$$

$$2Y_4p_1 - Y_2p_2 + 2Y_4p_3 + Y_4p_7 - Y_2p_8 + Y_4p_{10} + Y_4p_{11} - Y_2p_{14} = 0 \qquad (4)$$

$$2Y_5p_1 + 2Y_5p_3 - 2Y_2p_5 + (Y_5 - Y_2)p_7 + Y_5p_{10} + Y_5p_{11} - Y_2p_{13} = 0 \qquad (5)$$

where

$$Y_1 = 2(A_3 + 0.209A_5)$$

$$Y_2 = 2(A_1 + A_2X)$$

$$Y_3 = 1.584A_5$$

$$Y_4 = A_2X$$

$$Y_5 = 2A_4$$

The remaining 10 equations required for a solution are the dissociation equations. Tables of equilibrium coefficients are available(23) in terms of partial pressures rather than concentrations of the products of reaction. The appropriate equations are given below.

$2H + O \rightarrow H_2O$ such that $p_1 - K_1 p_{11}^2 p_{15} = 0$ (6)

$C + 2O \rightarrow CO_2$ such that $p_2 - K_2 p_{14} p_{15}^2 = 0$ (7)

$2H \rightarrow H_2$ such that $p_3 - K_3 p_{11}^2 = 0$ (8)

$2N \rightarrow N_2$ such that $p_4 - K_4 p_{12}^2 = 0$ (9)

$2F \rightarrow F_2$ such that $p_5 - K_5 p_{13}^2 = 0$ (10)

$2O \rightarrow O_2$ such that $p_6 - K_6 p_{15}^2 = 0$ (11)

$H + F \rightarrow HF$ such that $p_7 - K_7 p_{11} p_{13} = 0$ (12)

$C + O \rightarrow CO$ such that $p_8 - K_8 p_{14} p_{15} = 0$ (13)

$$N + O \rightarrow NO \quad \text{such that } p_9 - K_9 p_{12} p_{15} = 0 \tag{14}$$

$$O + H \rightarrow OH \quad \text{such that } p_{10} - K_{10} p_{11} p_{15} = 0 \tag{15}$$

The equilibrium coefficients K_i vary systematically with the temperature of the reaction. It is assumed that the products of reaction calculated at a particular temperature and pressure, are formed instantaneously. Hence, one need only solve the above 15 equations for given values of P, T, and the amounts of reactants, to arrive at the equilibrium composition.

Solution of These Equations

Since the dissociation equations are non-linear, there exists no direct solution. The Newton-Raphson method is used to obtain a "trial and error" solution.

(1) Initially, estimates of $p_i (i = 1, \ldots 15)$ are taken and each of the 15 equations is expanded in a Taylor's series about the estimated point, p_i.

(2) Corrections to p_i are then found (Δp_i) and the new estimates of p_i, given by $p_i + \Delta p_i$, are used in place of the initial estimates in (1).

(3) The procedure is repeated until Δp_i becomes negligible.

Consider a solution to two non-linear equations; $f(x,y) = 0$, $g(x,y) = 0$. Let the initial estimate of the required solution (x,y) be the point (x_1,y_1). Expanding f, g in a Taylor's series about the point (x_1,y_1), then

$$f(x,y) = 0 = f(x_1,y_1) + \frac{\partial f}{\partial x}(x_1,y_1) + \frac{\partial f}{\partial y}(x_1,y_1) \cdot (y - y_1) + \ldots\ldots$$

$$g(x,y) = 0 = g(x_1,y_1) + \frac{\partial g}{\partial x}(x_1,y_1) \cdot (x-x_1) + \frac{\partial g}{\partial y}(x_1,y_1) \cdot (y-y_1) + \ldots\ldots$$

or

$$\Delta f = \frac{\partial f}{\partial x} \cdot \Delta x + \frac{\partial f}{\partial y} \cdot \Delta y + \ldots$$

$$\Delta g = \frac{\partial g}{\partial x} \cdot \Delta x + \frac{\partial g}{\partial y} \cdot \Delta y + \ldots$$

where

$$\Delta f = f(x,y) - f(x_1,y_1) = - f(x_1,y_1)$$

$$\Delta g = g(x,y) - g(x_1,y_1) = - g(x_1,y_1)$$

and

$$\Delta x = x-x_1$$

$$\Delta y = y-y_1$$

Hence the non-linear equations have been transformed into linear correction equations of the form

$$f(x_1,y_1) + f_x \cdot \Delta x + f_y \cdot \Delta y = 0$$

$$g(x_1,y_1) + g_x \cdot \Delta x + g_y \cdot \Delta y = 0$$

where $f_x = \frac{\partial f}{\partial x}$, $f_y = \frac{\partial f}{\partial y}$, etc., and the derivatives of second order and higher have been neglected.

The equations are solved for Δx, Δy and new estimates are given by $x_1 + \Delta x$, $y_1 + \Delta y$. The procedure is repeated until the desired accuracy is obtained.

The full procedure can best be demonstrated with an example.

Example

Consider a solution to

$$f(x,y) = x^2y + y^2 + 3 = 0$$

$$g(x,y) = x^3 - 2xy^2 + 4y = 0$$

then

$$f_x = 2xy$$

$$f_y = x^2 + 2y$$

$$g_x = 3x^2 - 2y^2$$

$$g_y = -4xy + 4 = 4(1 - xy)$$

Let $x_1 = 1$, $y_1 = -1$, be the initial estimates.

Then substituting into the linear correction equations

$$3 - 2\Delta x - \Delta y = 0$$

$$-5 + \Delta x + 8\Delta y = 0$$

the solution to the above equations is

$$\Delta x = 38/30 \cong 1.3$$

$$\Delta y = 7/15 \cong 0.5$$

The new estimates of x, y are given by x_2, y_2 where

$$x_2 = x_1 + \Delta x = 2.3$$

$$y_2 = y_1 + \Delta y = -0.5$$

Substituting into the linear correction equations, then

$$0.6 - 2.5\,\Delta x + 4.3\,\Delta y = 0$$

$$9 + 15.4\Delta x + 10\,\Delta y = 0$$

The solution to the above equations is

$$\Delta x \cong -0.4$$

$$\Delta y \cong -0.3$$

The new estimates for x, y become

$$x_2 + \Delta x = 1.9$$

$$y_2 + \Delta y = -0.8 \qquad \text{etc.}$$

The correct solution is (2, -1).

For more than 2 unknowns, the linear correction equations take the form

$$f(x,y,z,...) + f_x \cdot \Delta x + f_y \cdot \Delta y + f_z \cdot \Delta z + ... = 0$$

$$g(x,y,z,...) + g_x \cdot \Delta x + g_y \cdot \Delta y + g_z \cdot \Delta z + ... = 0$$

$$h(x,y,z,...) + h_x \cdot \Delta x + h_y \cdot \Delta y + h_z \cdot \Delta z + ... = 0$$

$$i(x,y,z,...) + ... = 0$$

$$j(x,y,z,...) + ...$$

etc.

where the subscripted variable, f_x for example, represents the partial derivative of $f(x,y,z,...)$ with respect to x.

Denoting equations (1) to (15) by B_i ($i = 1, ..., 15$); the correction equations are given by

$$B_1 + A_{1,1} \cdot \Delta p_1 + A_{1,2} \cdot \Delta p_2 + ... + A_{1,15} \cdot \Delta p_{15} = 0$$

.....

.....

$$B_{15} + A_{15,1} \cdot \Delta p_1 + A_{15,2} \cdot \Delta p_2 + ... + A_{15,15} \cdot \Delta p_{15} = 0$$

where $A_{i,j}$ is the partial derivative of B_i with respect to p_j. For example, $A_{7,14}$ is the partial derivative of equation (7), i.e. B_7, with respect to p_{14}. The equations are solved for Δp_i ($i = 1$ to 15) by first assuming initial estimates of p_i. Subsequent estimates of p_i are given by $p_i + \Delta p_i$ and the procedure is repeated until Δp_i approaches zero.

The coefficients of the correction equations ($A_{i,j}$) are denoted by matrix A and the constants B_i are denoted by the vector, -B. Hence, in matrix notation, the set of linear correction equations is given by

$$B = A \cdot \Delta p$$

and its solution is given by

$$\Delta p = A^{-1}B$$

where A^{-1} is the inverse matrix.

Outline for the Fortran IV Computer Program

The program is presently designed to handle nine sets of values of pressure, temperature and volume for a given propellant mixture. That is, equilibrium coefficients are incorporated into the program for values of temperature between 3000 K and 1400 K in 200 degree increments.

Input Data

The following information is required:

(a) Weights of reactants, i.e., the total amount of fuel and oxidizer available.

(b) Yield

(c) Temperature of reaction

(d) Pressure at which reaction occurs

(e) Volume of products of reaction

Assumptions

The following assumptions are implied:

(a) Constant pressure process

(b) Instantaneous reaction time

(c) No air entrainment until all of the available propellants are used up.

Procedure

For each data point (i.e. for a given value of P, T, and V) the program determines the partial pressures of the products of reaction such that the theoretical volume of the product gases is identical to the given input volume.

For the first data point, however, since no value of volume is available, the yield is used to determine the initial amounts of propellant burned and the partial pressures are then determined.

For subsequent data points, the fuel burning rate is continually adjusted and partial pressures are calculated in turn so that finally the resultant theoretical volume becomes identical to the given (theoretically determined or experimentally evaluated) volume.

This latter procedure is repeated for subsequent data points until all of the available fuel is used up. From then on, air is added as a reactant combined with all of the available fuel in order to satisfy the "identical volume" condition.

The program also converts the resultant partial pressures into the following:

1. Pound Moles
2. Pressure-Ratios, Mole-Ratios, Volume-Ratios
3. Pound Weights
4. Weight-Ratios

The fuel burning rate, the amount of entrained air, and the theoretical volume for each data point are also determined.

Subroutine Invert

The subroutine solves the set of linear equations

$$\Delta p = A^{-1}B$$

The input data card is

CALL INVERT (A, NA, NAD, B, NB, NBD, DETERM, IERROR)

where A = matrix of order NA

B = vector having NB=1 constant vector

NAD = row dimension of A in main program

NBD = row dimension of B in main program

DETERM = dummy

IERROR = dummy

The output consists of A^{-1} placed in A, Δp placed in B, and the determinant of A placed in DETERM. IERROR is an error signal equal to 0 for successful inversion; equal to -1 for overflow, equal to +1 if no inverse is obtainable.

The maximum size of A can be 100 x 100.

Symbols Used in Main Program

Subscripted Variables

A - coefficients appearing in the correction equations

B - constant appearing in the correction equations

C - equilibrium constants

P - partial pressure

PR - partial pressure-ratio, mole-ratio, volume-ratio

PT - total pressure

T - temperature

TNT - partial moles

V - volume

WMOL - molecular weight

WT - partial weight

WTR - partial weight-ratio

Floating Point Variables

F^2 - weight of liquid fluorine available

H^2 - weight of liquid hydrogen available

O^2 - weight of liquid oxygen available

RP1 - weight of liquid RP-1 available

RNAIR - mole-ratio of entrained air

RWAIR - weight-ratio of entrained air

TN - total theoretical moles of products of reaction

TNE - total experimental moles of products of reaction

TVOL - total theoretical volume of products of reaction

WAIR - weight of entrained air

X - number of carbon atoms in the RP-1 molecule, C_XH_{2X}

YIELD - percentage of fuel burned at time "zero"

The fixed point variable, MA, is the number of experimental runs with combinations of LH_2, RP-1, LO_2 and LF_2.

The Fortran IV program follows with an example of the output data for one of the nine data points using LH_2/RP-1/LO_2/LF_2 and entrained air.

Input Information

Many different quantities could have been chosen for the input information based upon which the desired fireball composition and atmospheric chemistry could be calculated.

For this investigation the

Volume-time history

Pressure-time history

Temperature-time history

were taken as the principal input information.

The reason for this choice was that another phase of this over-all program deals with the theoretical determination of these functions and most of all that it is possible to measure the above quantities and thus verify any theoretical results by actual field experimentation. This latter fact seems to be of extreme importance if theories are developed since without experimental verification they are of little use and certainly not much credence can be given to them.

Other factors such as fuel burning rates, etc. were selected by others[20,21] but the investigators of this project do not see how such quantities could be verified experimentally and therefore would remain assumptions throughout the work.

As mentioned above much work is being done on the determination of the volume-time, pressure-time, and temperature-time histories of the explosion phenomena from a theoretical point of view. Rather than wait for the results from this separate investigation and because of contract commitments it was decided to present the methods of obtaining the fireball and combustion cloud composition from such input data as mentioned above and for the present combine both theory and experimental information to obtain the most plausible functions at this time.

A brief description of how the volume-time, pressure-time, and temperature-time functions have been determined for this report follows:

Volume-Time History of Fireball and Combustion Products Cloud from Liquid Propellant Explosions

The volume of combustion products produced by liquid propellant explosions transgresses a number of stages with time, changing in shape from one typical configuration into another. These stages can be observed in the high speed film records of such explosions and can be, in part at least, analyzed mathematically or theoretically. These major stages are:

1. Hemisphere
2. Truncated Sphere
3. Sphere
4. Pinched Sphere
5. Toroid

The above 5 stages are distinct and can be observed in at least the larger explosions.

Stage 1. Hemisphere

This stage is the earliest one which can be observed and is of relatively short duration. It involves a very rapid growth of the combustion products both along the ground and up into the atmosphere so that the shape can best be approximated by a hemisphere. The size of this initial hemisphere depends upon the yield of the liquid propellant explosion, the very rapid combination of the fuel and oxidizer so as to form detonation and shock waves. The larger the yield the larger the initial hemispherical fireball.

Stage 2. Truncated Sphere

Following the very rapid formation of the hemispherical fireball from liquid propellant explosions the hot combustion products begin to rise. This upward motion and the convection currents due to the bouyant forces undercut the rising mass thus forming a truncated sphere, in contact with the ground at the flat base.

As the center of the mass rises the fireball changes more and more from the original hemisphere into a sphere, the shape which is attained when the combustion products become essentially tangent to the ground.

This stage in the development is referred to as "Lift Off," at which most of the fuel seems to have been consumed[20,21].

Stage 3. Sphere

Having attained essentially a spherical configuration at "Lift Off" the combustion products continue to rise as a rather turbulent, well mixing sphere which however gradually changes shape from the almost perfect sphere into the first slightly pinched and then rather pronounced pinched sphere.

Stage 4. Pinched Sphere

The change from the spherical configuration to the pinched sphere is rather gradual and then as the indentations become larger and larger, the appearance of the sphere is lost. A cross-section by a vertical plane through the center would give the appearance of a "Bar Bell."

As this process continues the indentations will eventually touch, forming a toroid.

Stage 5. Toroid

From the time the toroid is formed the initial contact point of the indentation becomes a hole with the general configuration of a ring or doughnut.

As this toroid grows in diameter the size of the hole increases but the volume now at this stage of development increases relatively slowly.

Finally this well defined configuration diffuses into the atmosphere losing its resemblance to any characteristic shape and being controlled to a great extent by the prevailing atmospheric conditions.

Each of these stages as described above and schematically shown in Fig. IV-1, takes a longer and larger part on the time scale. Stage 1 may occur in fractions of a second while the last stage will be a matter of minutes.

Utilizing this 5 stage concept for the purpose of analysis a volume versus time curve can be obtained, either theoretically by the use of restricting assumptions or by the actual analysis of high speed film records of liquid propellant explosions.

The variation is greatest in stage 1 which is controlled by the yield while the statistical differences are rather small (but somewhat dependent upon atmospheric conditions) as long as the same quantities of propellants are involved and it is assumed that essentially all the propellants take part in the formation of the fireball and cloud[20,21].

Fig. IV-2 shows the volume versus time curve for the S-IV PYRO experiment. The yield as reported was about 4 1/2% which is in agreement with the predictions of reference (1).

FIGURE IV-1-. TYPICAL DEVELOPMENTAL CONFIGURATION STAGES OF LIQUID PROPELLANT EXPLOSIONS

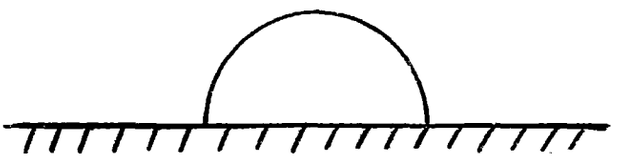

STAGE 1-. HEMISPHERE

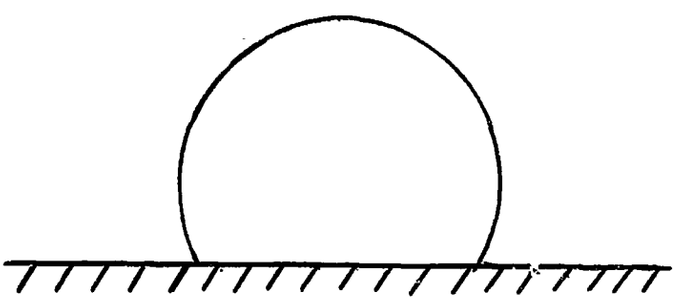

STAGE 2-. TRUNCATED SPHERE

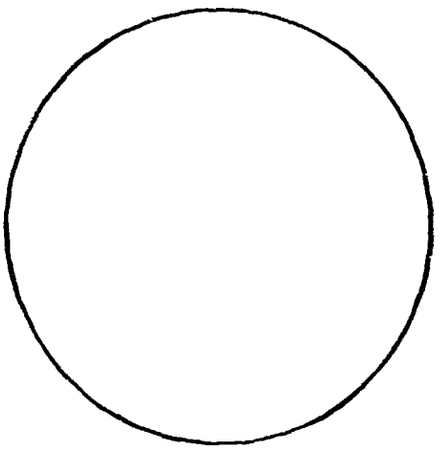

STAGE 3-. SPHERE

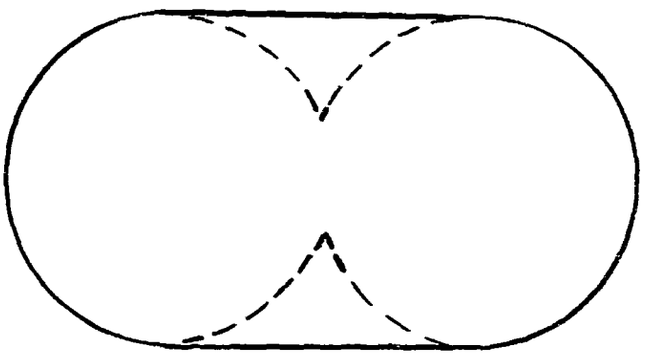

STAGE 4-. PINCHED SPHERE

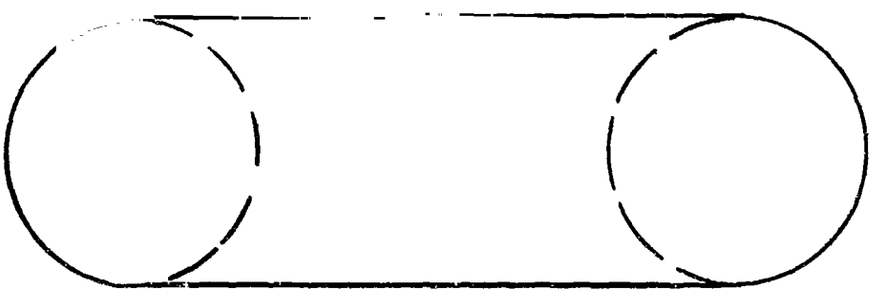

STAGE 5-. TOROID

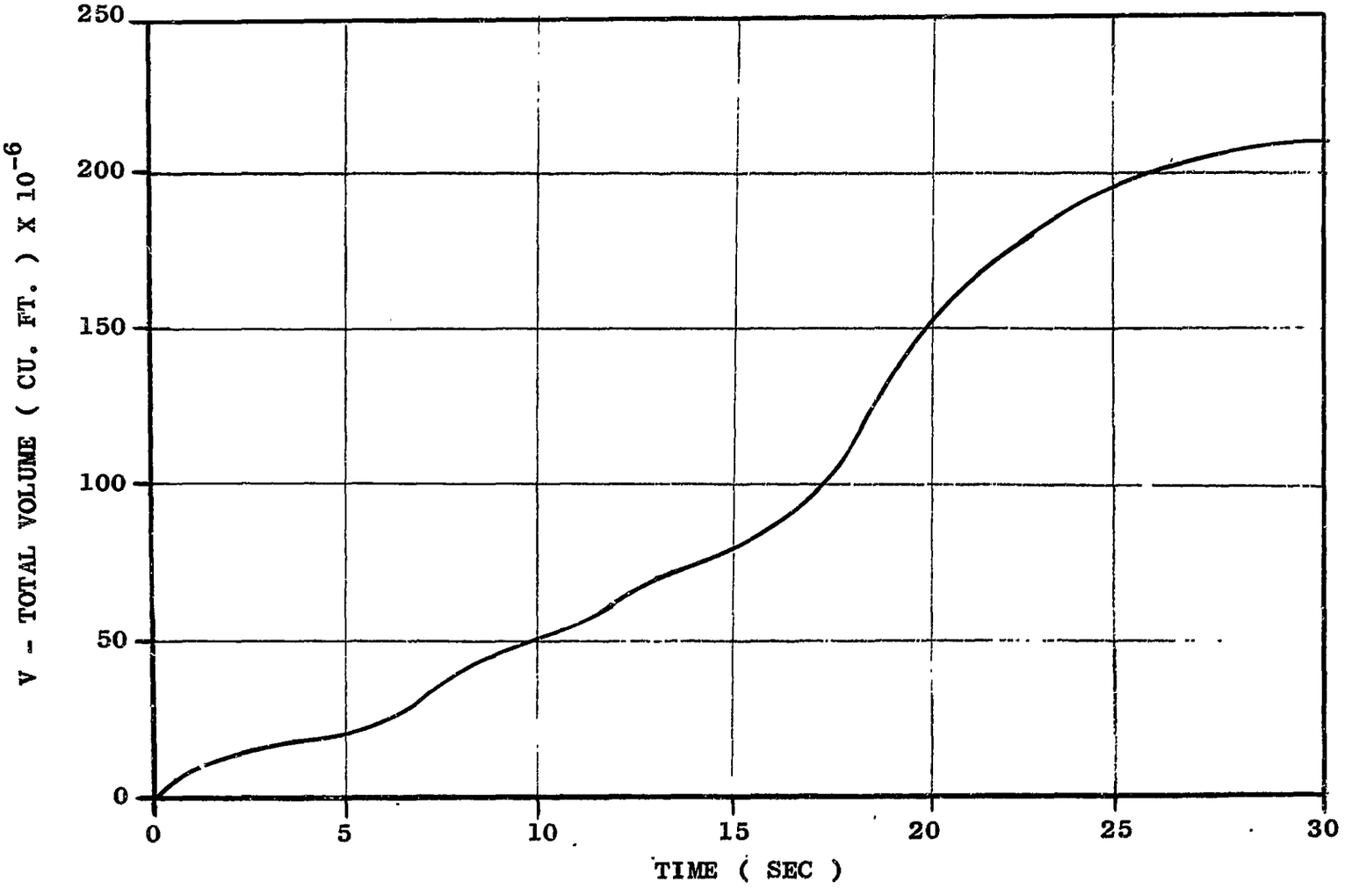

FIGURE IV-2-. TYPICAL VOLUME-TIME FUNCTION FOR LIQUID PROPELLANT EXPLOSION PRODUCTS (YIELD = 4.5 PERCENT)

Similar volume versus time curves have been developed for the various fuel oxidizer combinations considered and reported upon here.

Pressure-Time History of Fireball and Combustion Products Cloud from Liquid Propellant Explosions

The pressure-time history as presented here and as used as input data for the determination of the composition of both the fireball and the combustion products cloud was determined partially from preliminary theoretical considerations[16] and partially from the analysis of field data obtained by the liquid propellant explosion program of project PYRO[22].

The theoretical analysis was necessary for the early time processes since no experimental data is available and the results were then checked and agreed with experimental results in the later stages.

In general it might be said that the pressure immediately after ignition rises very rapidly to very high values inside the missile due to the confinement of the propellants and the tanks, reaching a maximum some where as the reaction front progresses toward the boundary of the missile configuration. After this maximum is reached the pressure falls very rapidly to almost atmospheric conditions.

From the time of "Lift-Off' of the fireball which occurs at essentially atmospheric pressure[24] the pressure drops very slowly due to the rise of the explosion products and the effect on atmospheric pressure due to altitude.

The pressure-time history presented here for approximately 100,000 lbs of propellants was used for all the propellants reported upon here.

Analysis of the sparse experimental information of liquid propellant explosion experiments seems to support this general pressure-time history. The yield produced by the explosion will change the early values of the pressure. Again for the analysis here a yield of 4 1/2% was taken based upon the most likely value as given in reference (2).

The actual curve used here is presented in Fig. IV-3. If better information is to be used an experimental program could be instituted to actually measure these pressures, an important reason for this choice of input information is because it allows theoretical determination and experimental verification.

Temperature-Time History of Fireball and Combustion Products Cloud from Liquid Propellant Explosions

The third and last principal input information needed for the determination of the composition of the fireball and combustion products cloud including air entrainment and atmospheric interaction is the temperature-time relationship.

Again theoretical considerations and the available rough experimental observations of fireball temperatures and variations with time indicate that the initial temperature is close to the maximum obtainable by the particular propellants involved. Then, at low yields at least, since only a small part of the propellants take part in the initial stages of the fireball formation the reaction of the remaining fuel and oxidizer, both in the propellants as well as the atmosphere, make the temperature drop with temperature in an almost linear manner. This is observed in theoretical work[20,21] and seems to be closely approximated by the available experimental information[22].

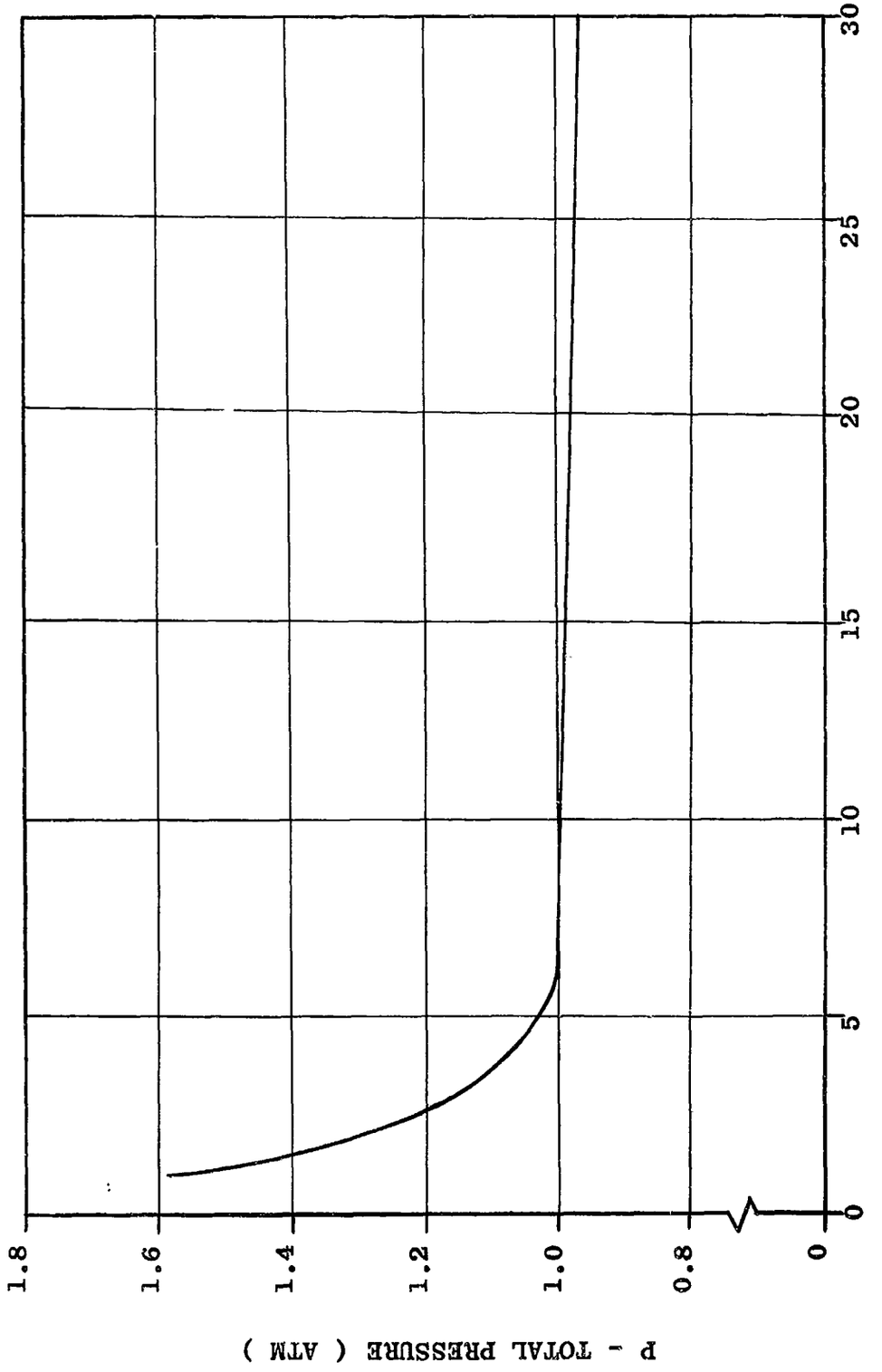

FIGURE IV-3- . TYPICAL PRESSURE-TIME FUNCTION FOR LIQUID PROPELLANT EXPLOSION PRODUCTS (YIELD = 4.5 PERCENT)

This linear decrease of the temperature with time continues until the incandescence of the fireball ends often referred to as the "duration" which can be approximated as shown in (24).

For the purpose of analysis here it was assumed that the actual variation can be closely approximated by further linear decreases changing the slope to a value 1/2 the previous one for each subsequent "duration" time interval.

By this method a curve representing the temperature-time history of the liquid propellant explosion is obtained which from both theoretical and the available sparse experimental observations seems to approximate the actual conditions. This again is taken here for low yield (4 1/2% in this case) liquid propellant explosions.

Again it is believed that an experimental program can be designed, if desired, to obtain this temperature-time history for various cases and verify or modify the presently used information, which is presented in Fig. IV-4 and again was used for all the fuel-oxidizer combinations analyzed and reported upon here.

It should be mentioned again that the volume-time, pressure-time, and temperature-time histories were selected as the principal input data because it is felt by these investigators that this information which can be generated with appropriate assumptions theoretically, can be verified experimentally. In addition these volume-time, pressure-time, and temperature-time histories are of great interest to other investigators for various reasons. A number of groups are presently engaged in trying to measure pressures and temperatures within fireballs and of combustion products clouds produced by liquid propellant explosions.

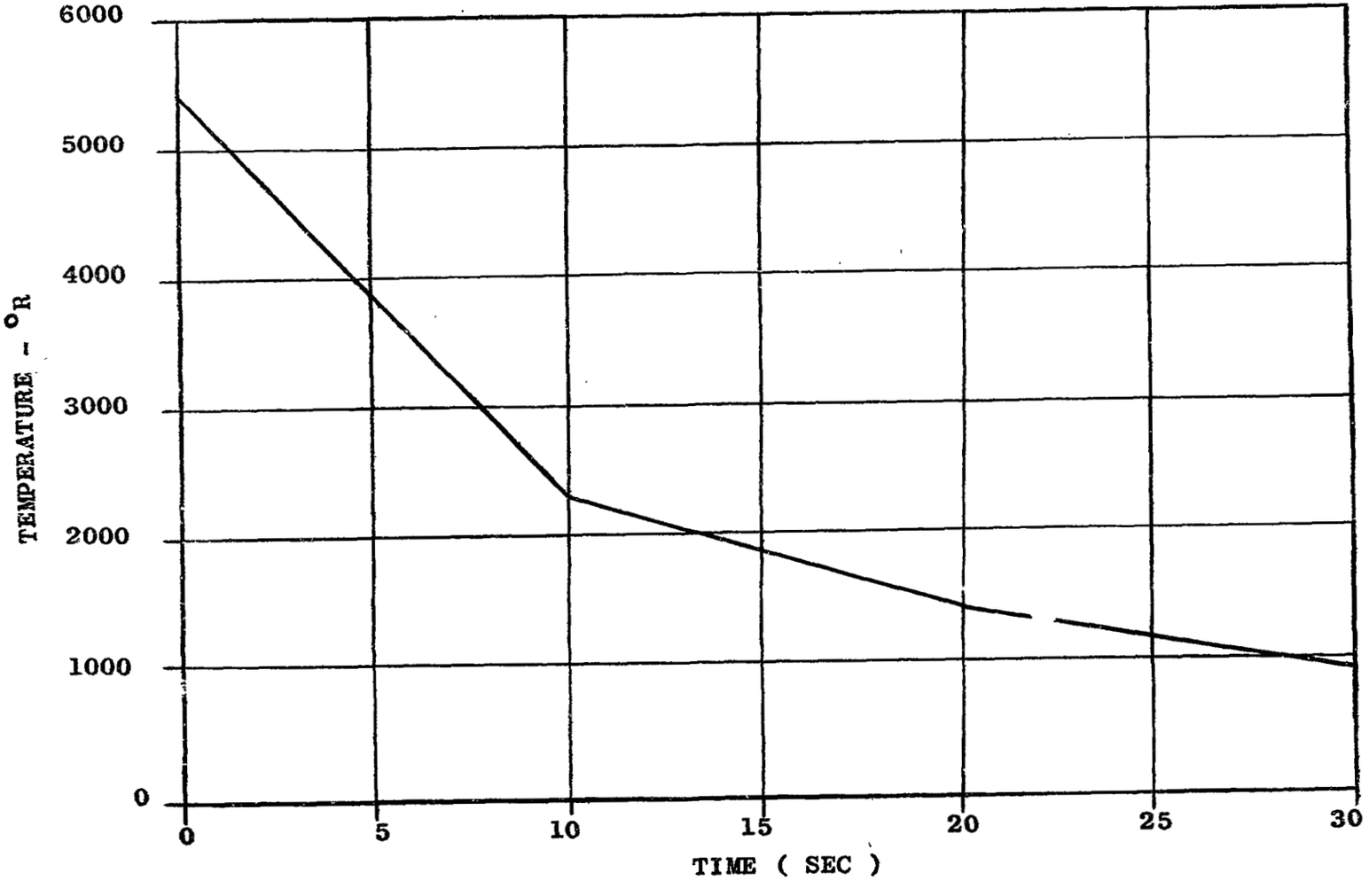

FIGURE IV-4 . TYPICAL TEMPERATURE-TIME FUNCTION FOR LIQUID PROPELLANT EXPLOSION PRODUCTS (YIELD = 4.5 PERCENT)

It should also again be emphasized that in this investigation homogeneity of the fireball as well as of the combustion products cloud was assumed. These assumptions seem to be reasonably well satisfied because of the tremendous turbulence observed within the fireball which tends to produce thorough mixing within a relatively short time.

In addition to the principal input information, the volume-time, pressure-time, and temperature-time functions it is necessary to know

4. The Type of Propellants
5. Propellant Composition
6. Propellant Quantities
7. Yield

4, 5, and 6 are easily obtainable as original data, while 7 is selected to obtain the results for this particular value of yield, a value which may again be dictated by theoretical considerations.

Type of Propellants

The type of propellants selected for this presentation are combinations of fuel and oxidizers which are presently used in liquid propelled rocket systems or combinations which may become important in the future development of these rockets.

The method however used is perfectly general and any propellant type and combinations could be analyzed in the same manner.

The types selected for this presentation are:

LH_2/LO_2

RP-1/LO_2

LH_2/LF_2

$RP\text{-}1/LF_2$

$LH_2/RP\text{-}1/LO_2$

LH_2/LO_2 + 1% F
+ 5% F
+ 10% F

$RP\text{-}1/LO_2$ + 1% F
+ 5% F
+ 10% F

$LH_2/RP\text{-}1/LO_2$ + 1% F
+ 5% F
+ 10% F

Propellant Composition

The propellant type was outlined above with the composition of fuel to oxidizer chosen as follows:

LH_2/LO_2	1 : 5 by weight
$RP\text{-}1/LO_2$	1 : 2.25 by weight
LH_2/LF_2	
$RP\text{-}1/LF_2$	
$LH_2/RP\text{-}1/LO_2$	1 : 2.6 : 5.86 by weight

In the combinations with Fluorine traces the weight ratios of the main constituents were the same as given above.

The chemical composition of the RP-1 was taken as $C_{11.6}\ H_{23.2}$ which was obtained from reference (25).

Propellant Quantities

The propellant quantities were taken as 100,000 lbs in all cases. This allowed the standardization of the pressure-time and temperature-time histories for the present analysis, since it seems that the quantity of propellants used has the major effect on the time axis of pressure and temperature.

Yield

The yield, the energy release as a fraction of the theoretical maximum, for these calculations and analyses was taken as 4 1/2% which .rom previous theoretical invest·gations (2) and from experimental observations (2, 22) seems to come close to the statistica.'y most probable value.

Again it might be mentioned that other values could be taken just as well without changing the method of analysis. The resulting compositions of the fireball and explosion products cloud would, however, be different.

With the input information as described above a number of cases were analyzed and many quantities calculated. Rather elaborate computer programs were developed for this purpose and the main program will be presented in the appendix.

The results which seem to be most pertinent to this investigation are presented in the following pages, mostly in graphical form.

Results Obtainable

Utilizing the data information as discussed above and the calculation and analyzing procedures outlined earlier many important quantities can be calculated.

Because of space limitations only the ones most pertinent to this investigation will be presented here. They are only a small fraction of all the quantities calculated but even though they form about 70 graphs many of them with a number of individual curves on them.

As mentioned earlier the same pressure-time, and temperature-time history was used for all the propellant combinations presented here, but individual volume-time histories for each type of propellant had to be calculated.

Then through a rather large iterative computer program such quantities as partial moles, partial pressures, partial volumes, partial weights, volume of air entrained, weight of air entrained, unburned fuel present, etc., were calculated.

Some of these quantities were then normalized and a few of them were presented here graphically as a function of time. They are

a. Fuel and oxidizer consumption wgt. (Normalized)
b. Volume of entrained air (Normalized)
c. Partial pressures (Normalized)
d. Partial volumes (Normalized)
e. Partial weights (Normalized)

These results and the manner of presentation, it is believed, give a good picture of the composition and its time variation of the fireball and the combustion products cloud for 14 different propellant combinations.

It is believed that the graphs are self-explanatory and the characteristics of the different fuel-oxidizer combinations can easily be compared.

The Fluorine tracer quantities added seem to have a hypergolic effect upon the cryogenic propellants to render the prediction of the most probable ignition and delay times and thus yield more certain.

Presentation of Selected Results

LH_2/LO_2

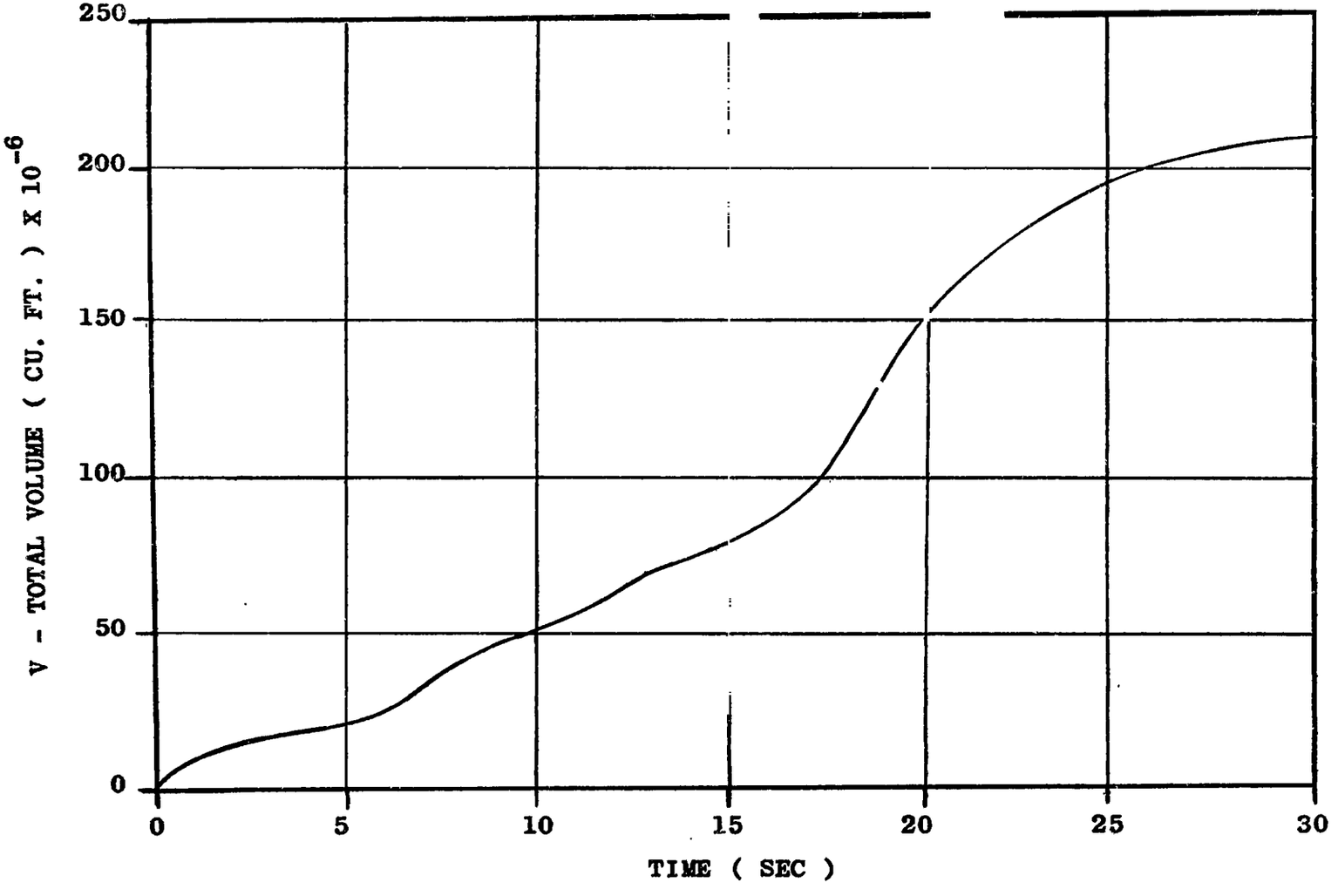

FIGURE IV-5 -. VOLUME-TIME FUNCTION FOR LH_2/ LO_2 LIQUID PROPELLANT EXPLOSION PRODUCTS (YIELD = 4.5 PERCENT)

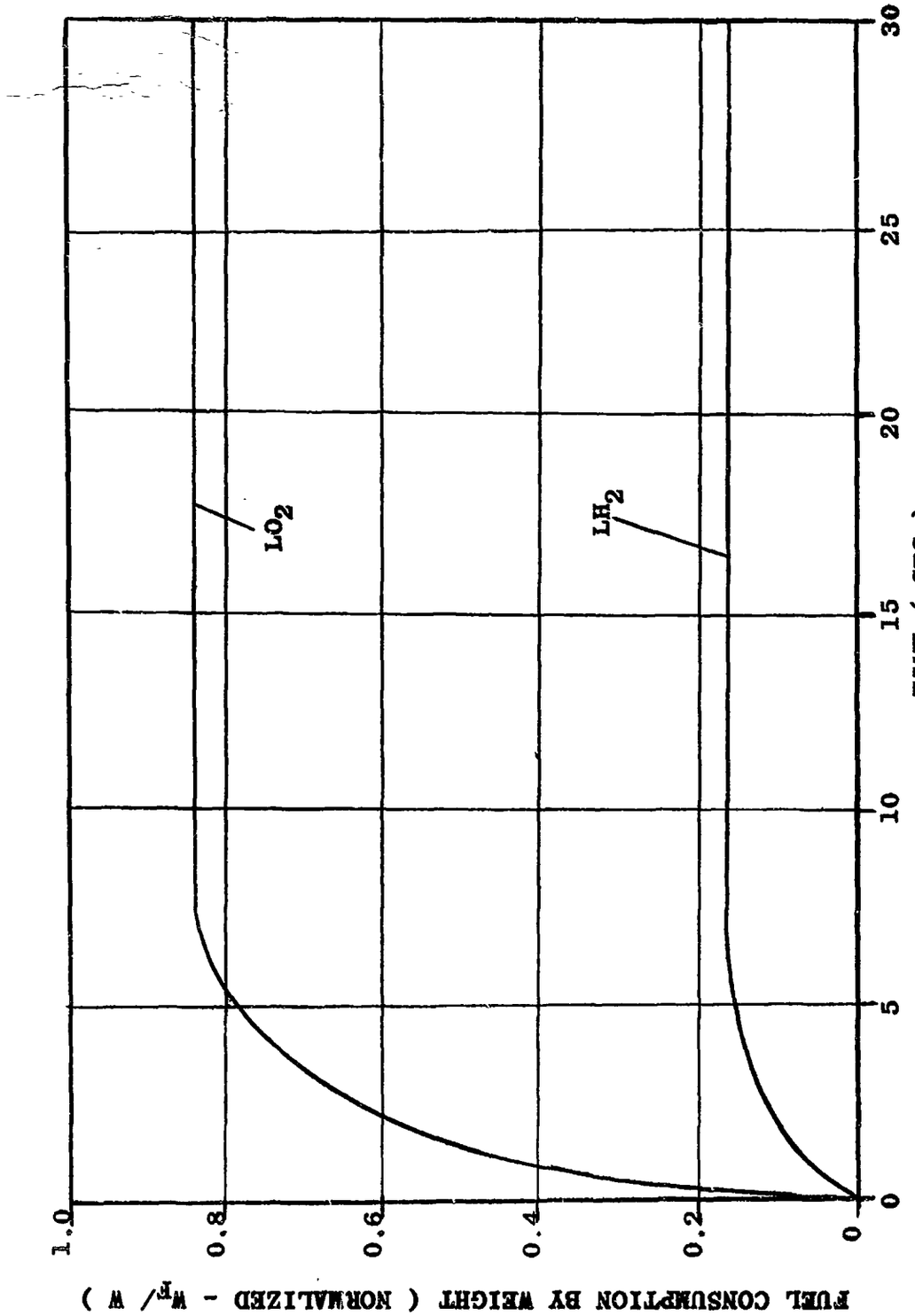

FIGURE IV-6- FUEL CONSUMPTION FOR LH_2/ LO_2 LIQUID PROPELLANT EXPLOSION (YIELD = 4.5 PERCENT)

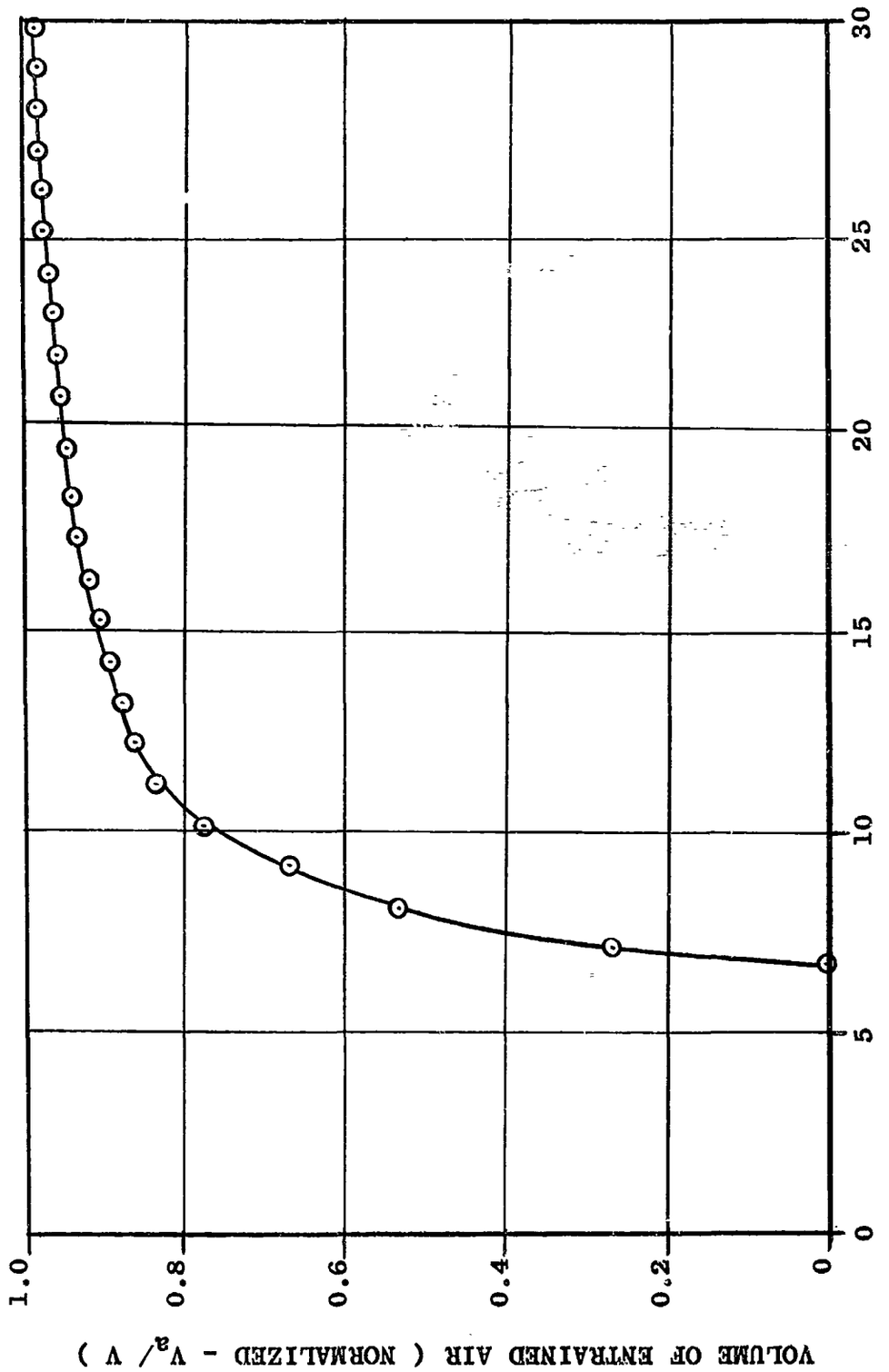

FIGURE IV-7 - VOLUME OF ENTRAINED AIR FOR LH_2/LO_2 LIQUID PROPELLANT EXPLOSION (YIELD = 4.5 PERCENT)

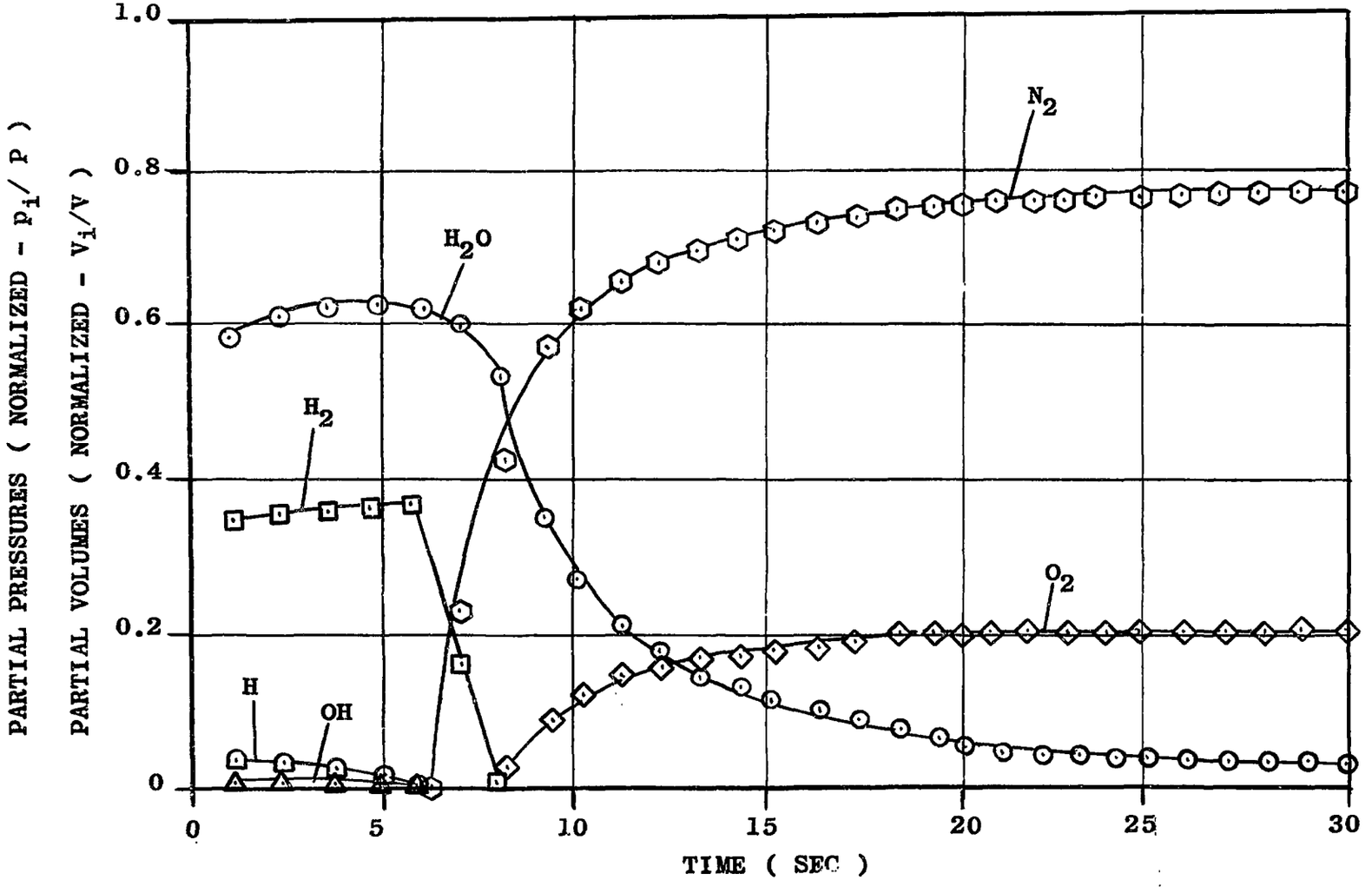

FIGURE IV-8. PARTIAL PRESSURES AND PARTIAL VOLUMES FOR LH_2/LO_2 LIQUID PROPELLANT EXPLOSION PRODUCTS (YIELD = 4.5 PERCENT)

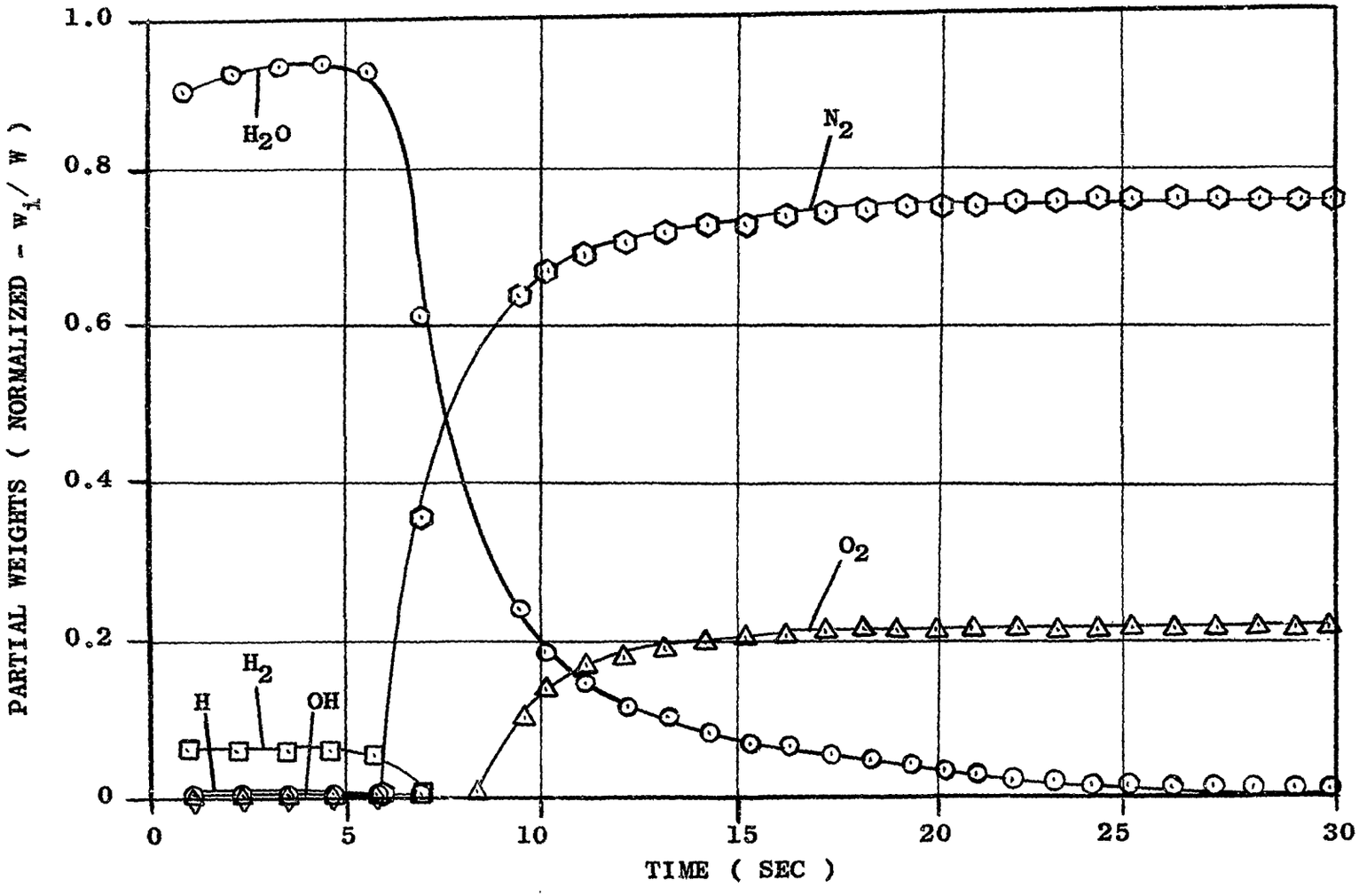

FIGURE IV-9-. WEIGHT COMPOSITION OF THE COMBUSTION PRODUCTS FROM LH_2/ LO_2 LIQUID PROPELLANT EXPLOSION (YIELD = 4.5 PERCENT)

$RP\text{-}1/LO_2$

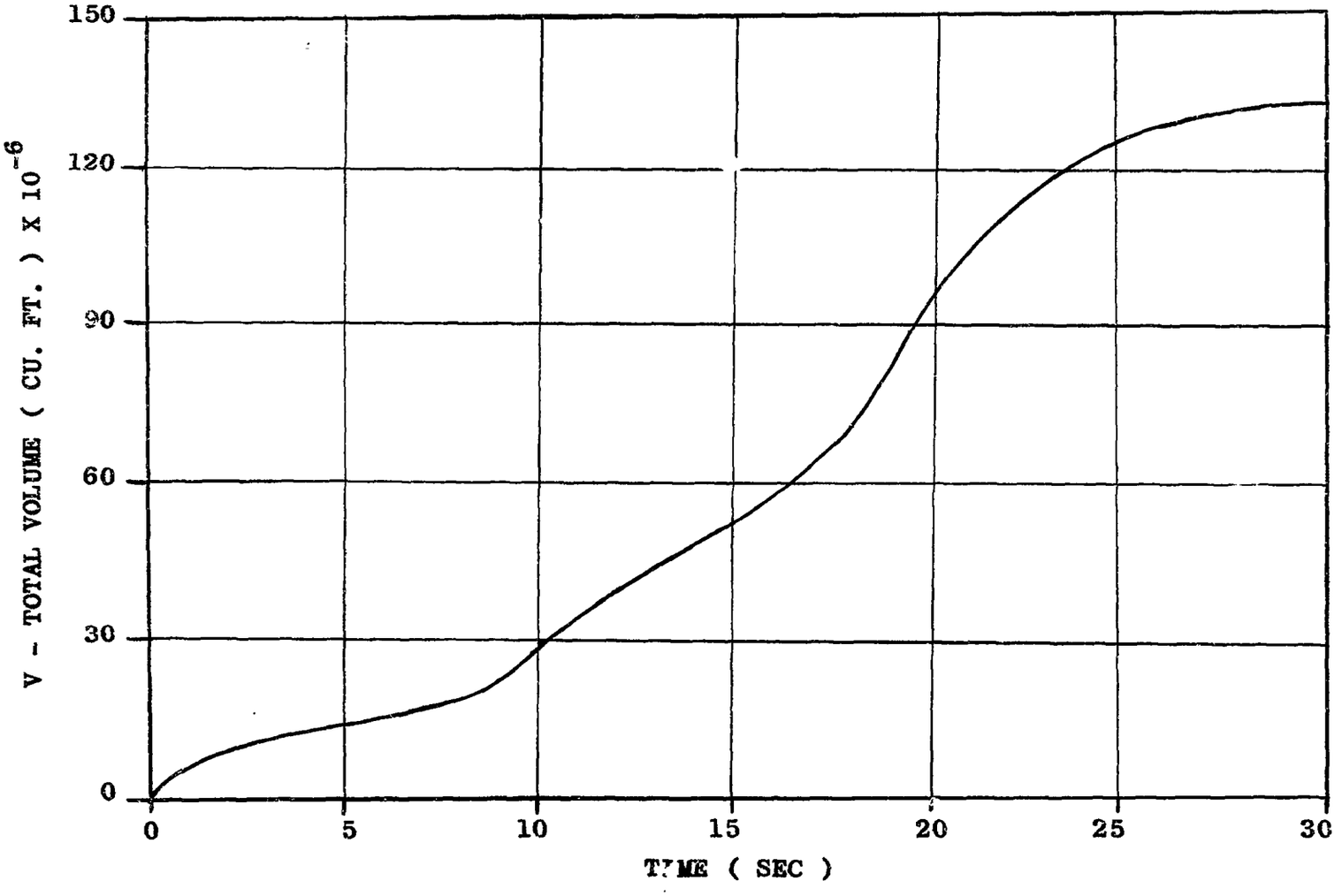

FIGURE IV-10-. VOLUME-TIME FUNCTION FOR RP-1/LO_2 LIQUID PROPELLANT EXPLOSION PRODUCTS (YIELD = 4.5 PERCENT)

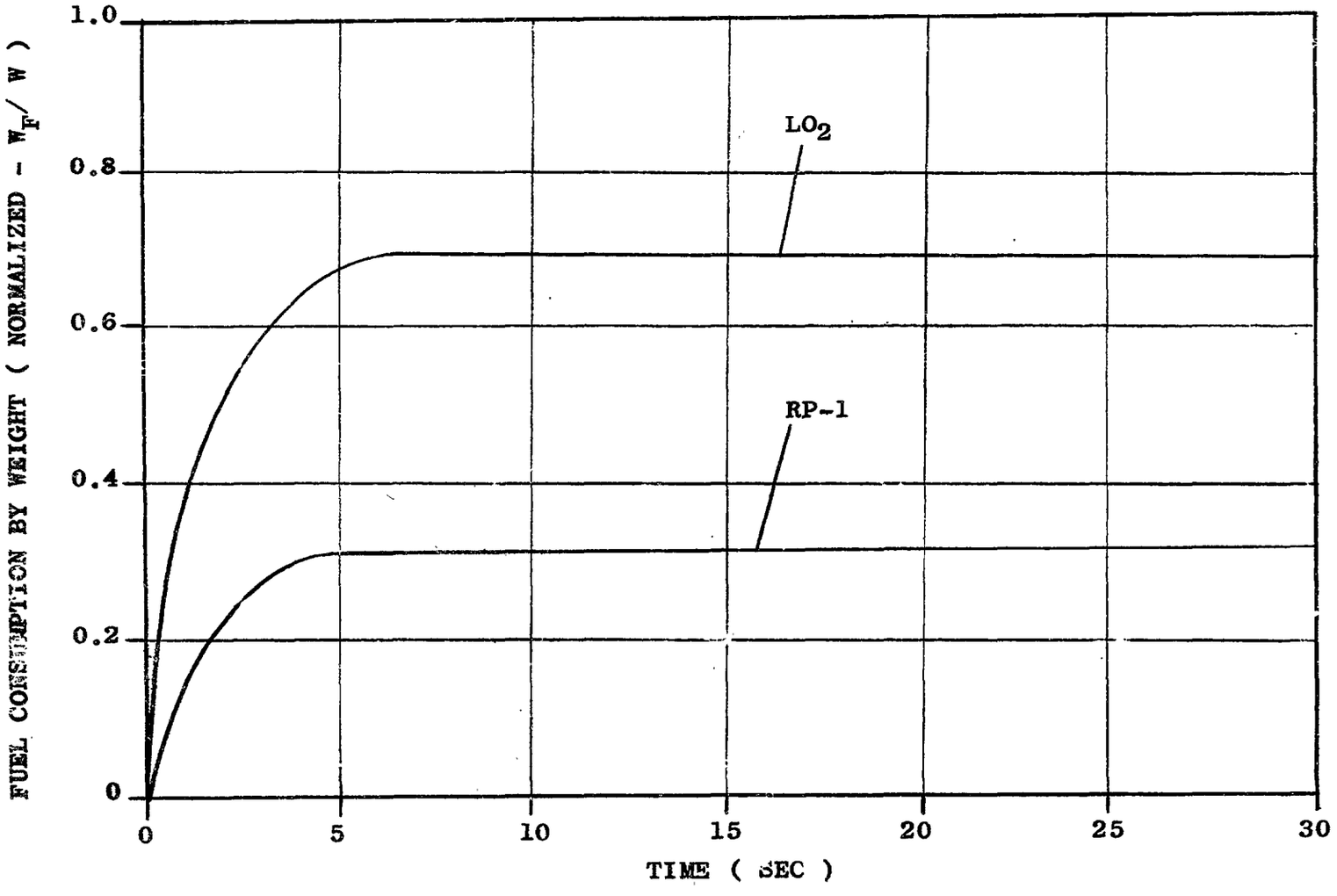

FIGURE IV-11-. FUEL CONSUMPTION FOR RP-1/LO_2 LIQUID PROPELLANT EXPLOSION (YIELD = 4.5 PERCENT)

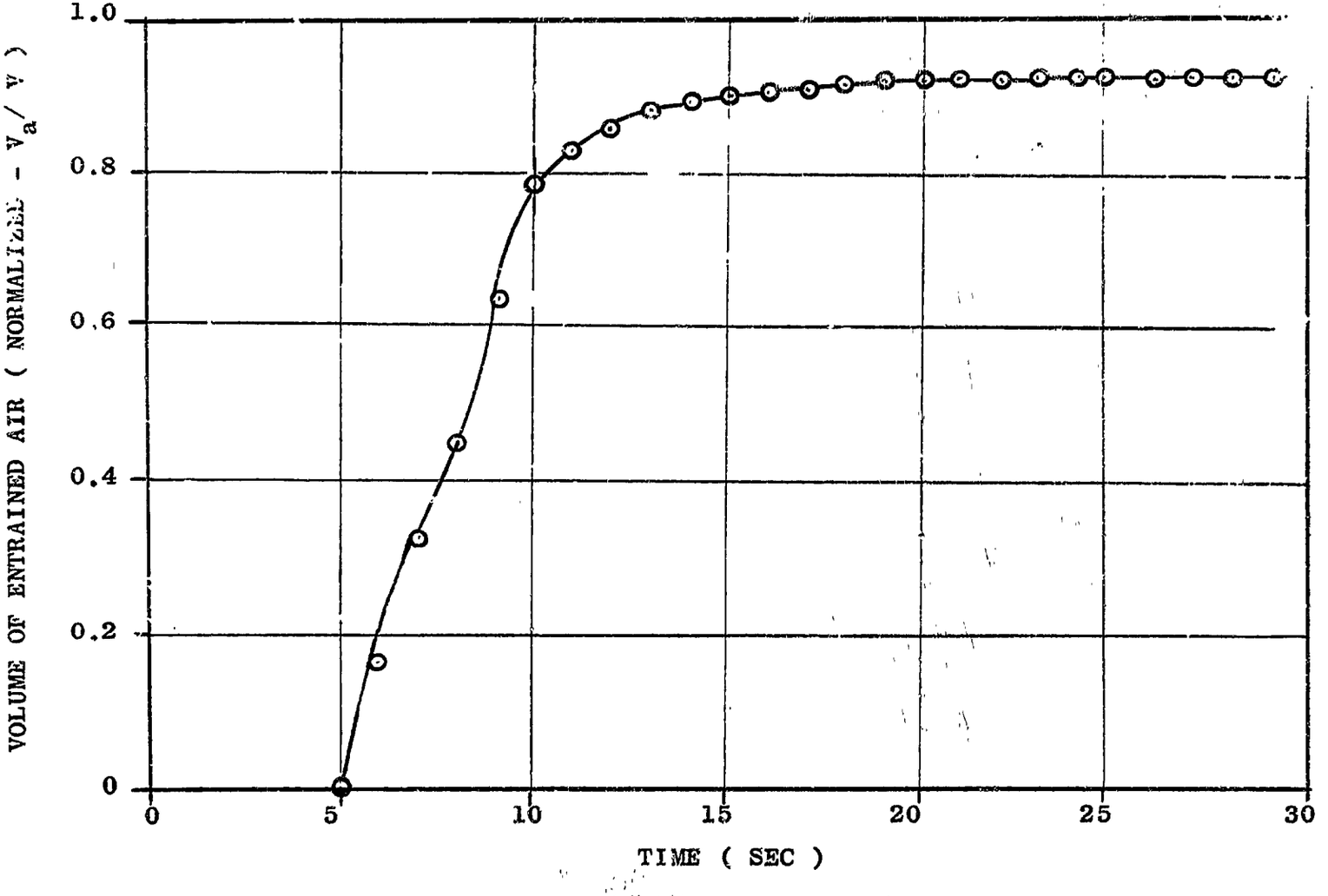

FIGURE IV-13. VOLUME OF ENTRAINED AIR FOR RP-1/ LO_2 LIQUID PROPELLANT EXPLOSION (YIELD = 4.5 PERCENT)

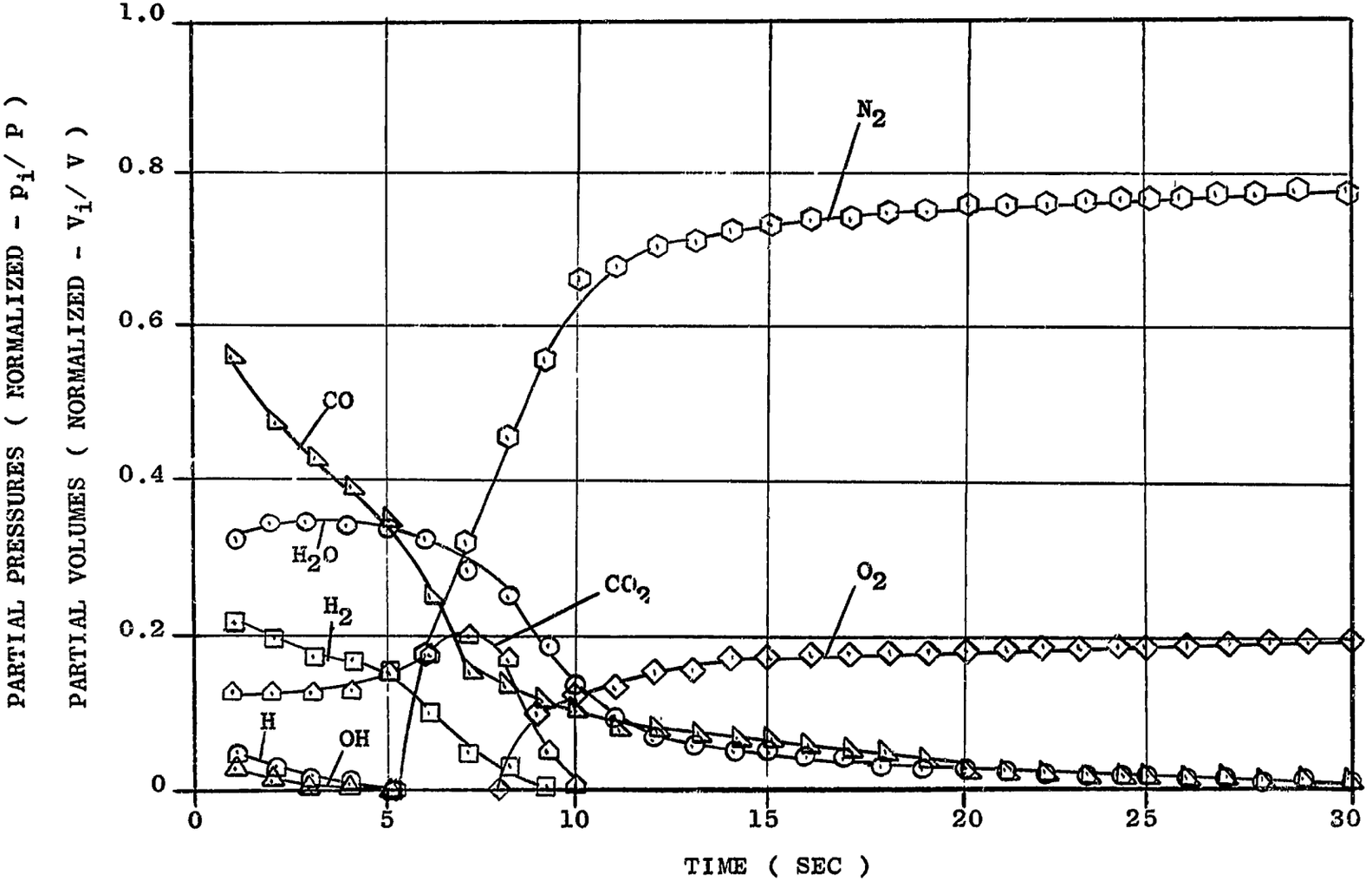

FIGURE IV-13-. PARTIAL PRESSURES AND PARTIAL VOLUMES FOR RP-1/ LO_2 LIQUID PROPELLANT EXPLOSION PRODUCTS (YIELD = 4.5 PERCENT)

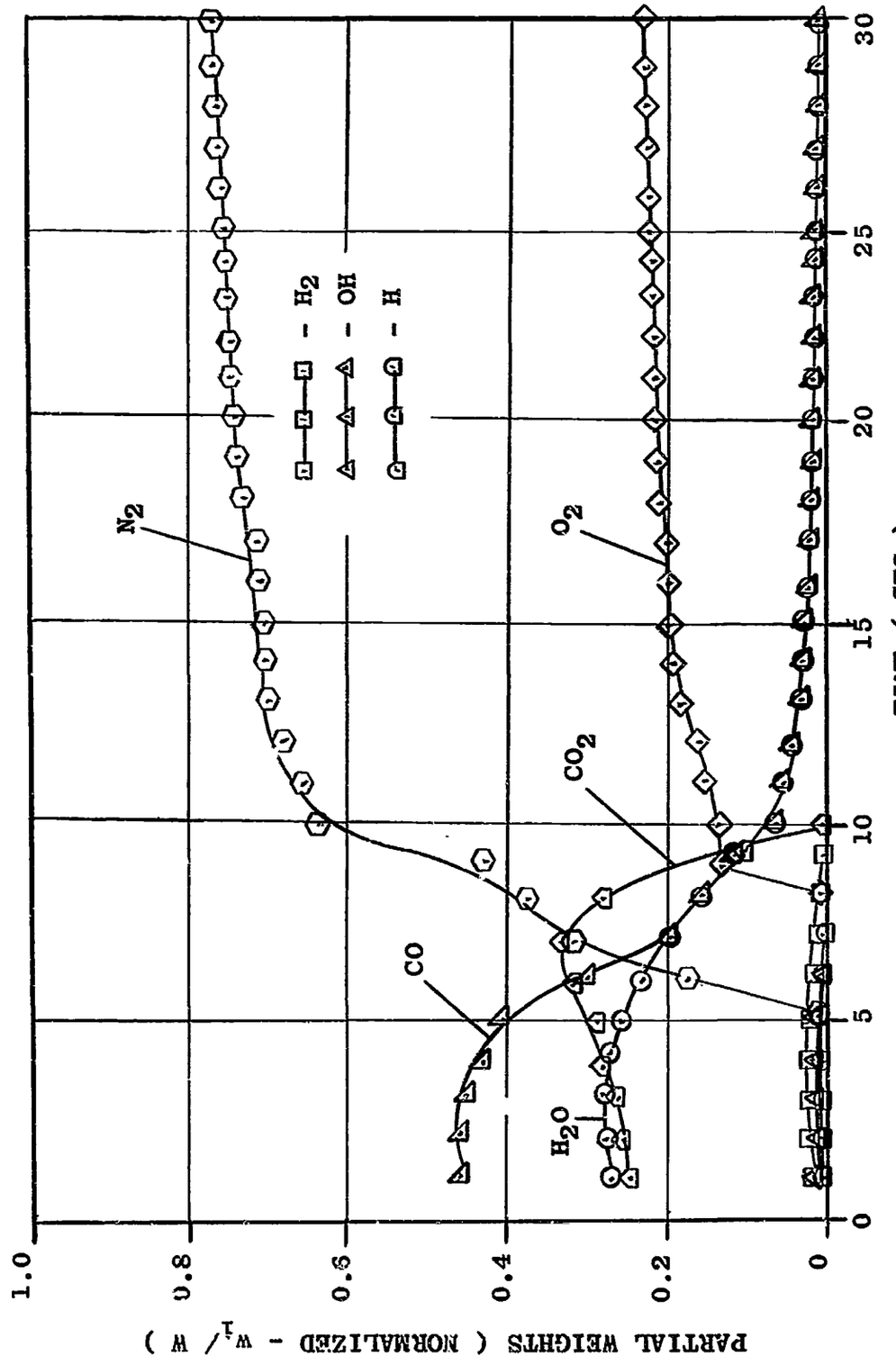

Figure IV-14-. WEIGHT COMPOSITION OF THE COMBUSTION PRODUCTS FROM RP-1/ LO_2 LIQUID PROPELLANT EXPLOSION (YIELD = 4.5 PERCENT)

LH_2/LF_2

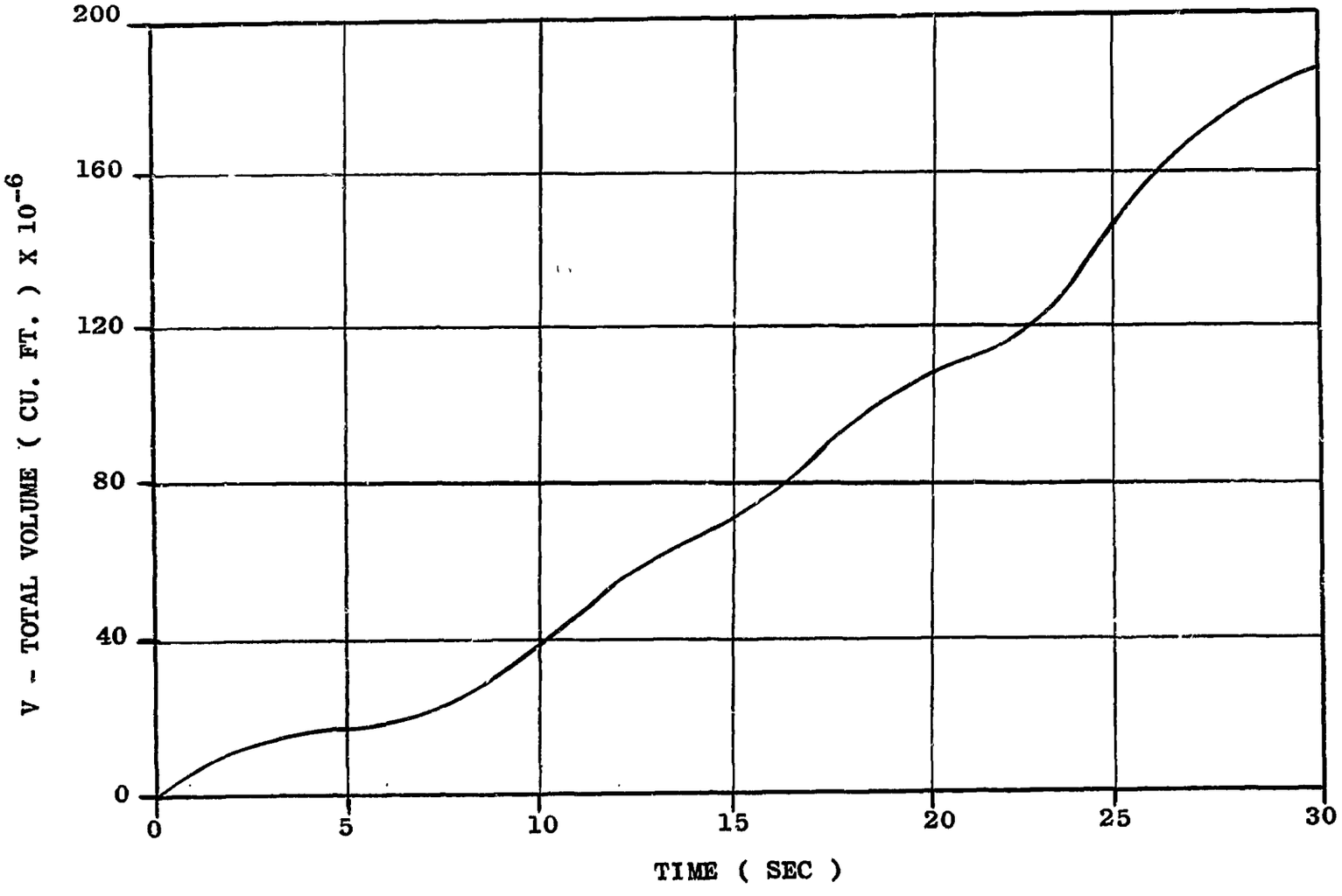

FIGURE IV-15-. VOLUME-TIME FUNCTION FOR LH_2/LF_2 LIQUID PROPELLANT EXPLOSION PRODUCTS (YIELD = 4.5 PERCENT)

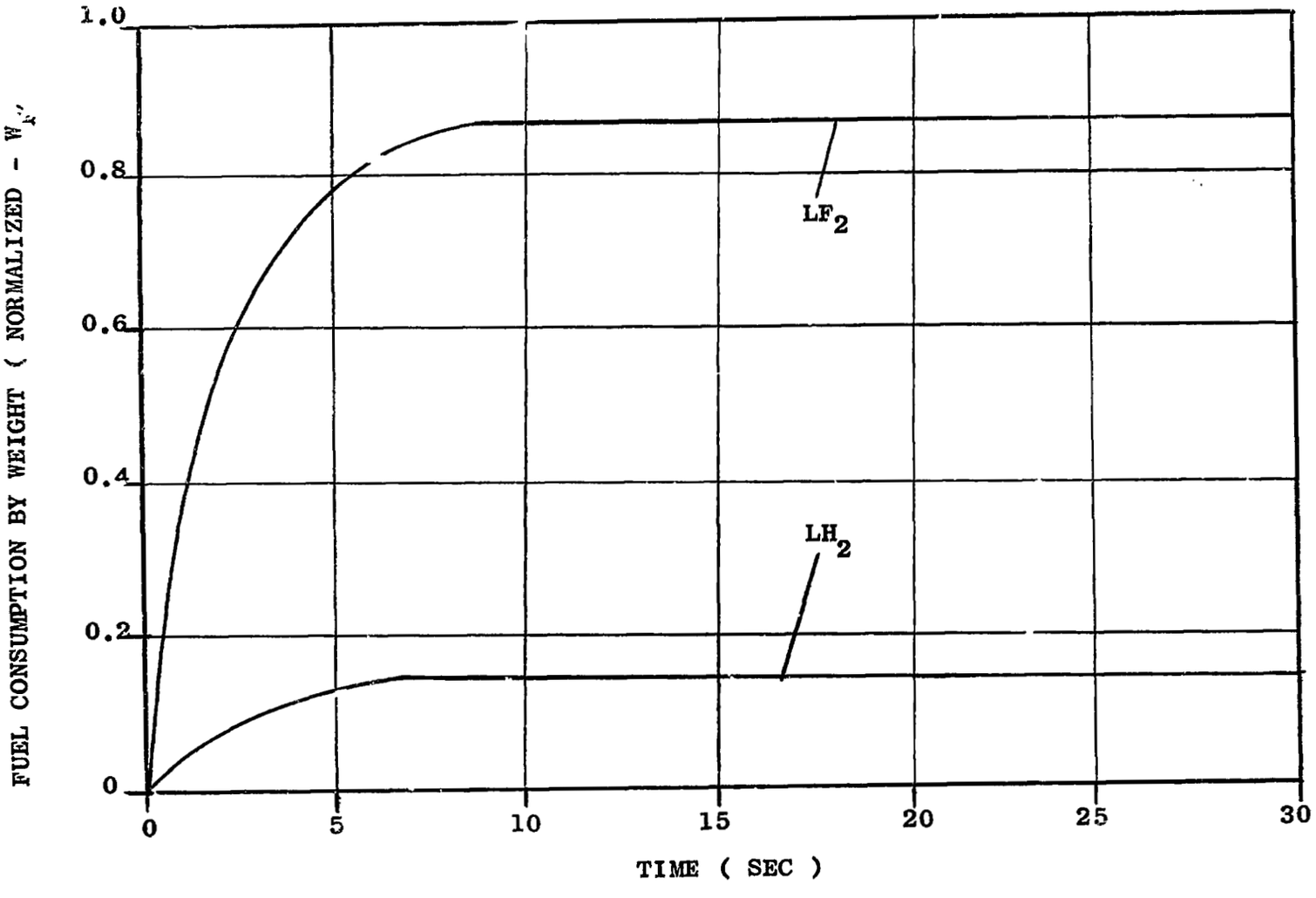

FIGURE IV-16-. FUEL CONSUMPTION FOR LH_2/LF_2 LIQUID PROPELLANT EXPLOSION (YIELD = 4.5 PERCENT)

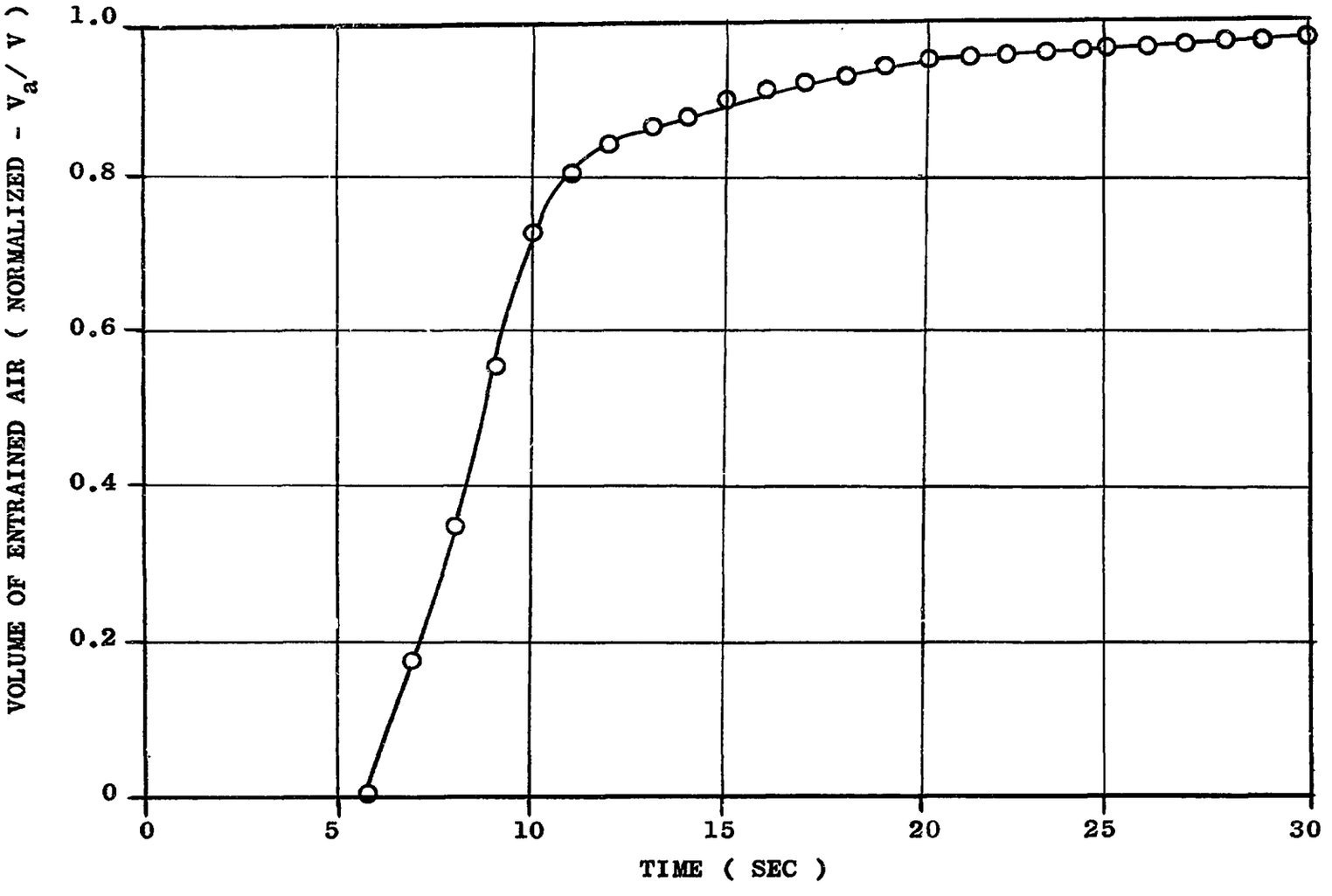

FIGURE IV-17-. VOLUME OF ENTRAINED AIR FOR LH_2/LF_2 LIQUID PROPELLANT EXPLOSION (YIELD = 4.5 PERCENT)

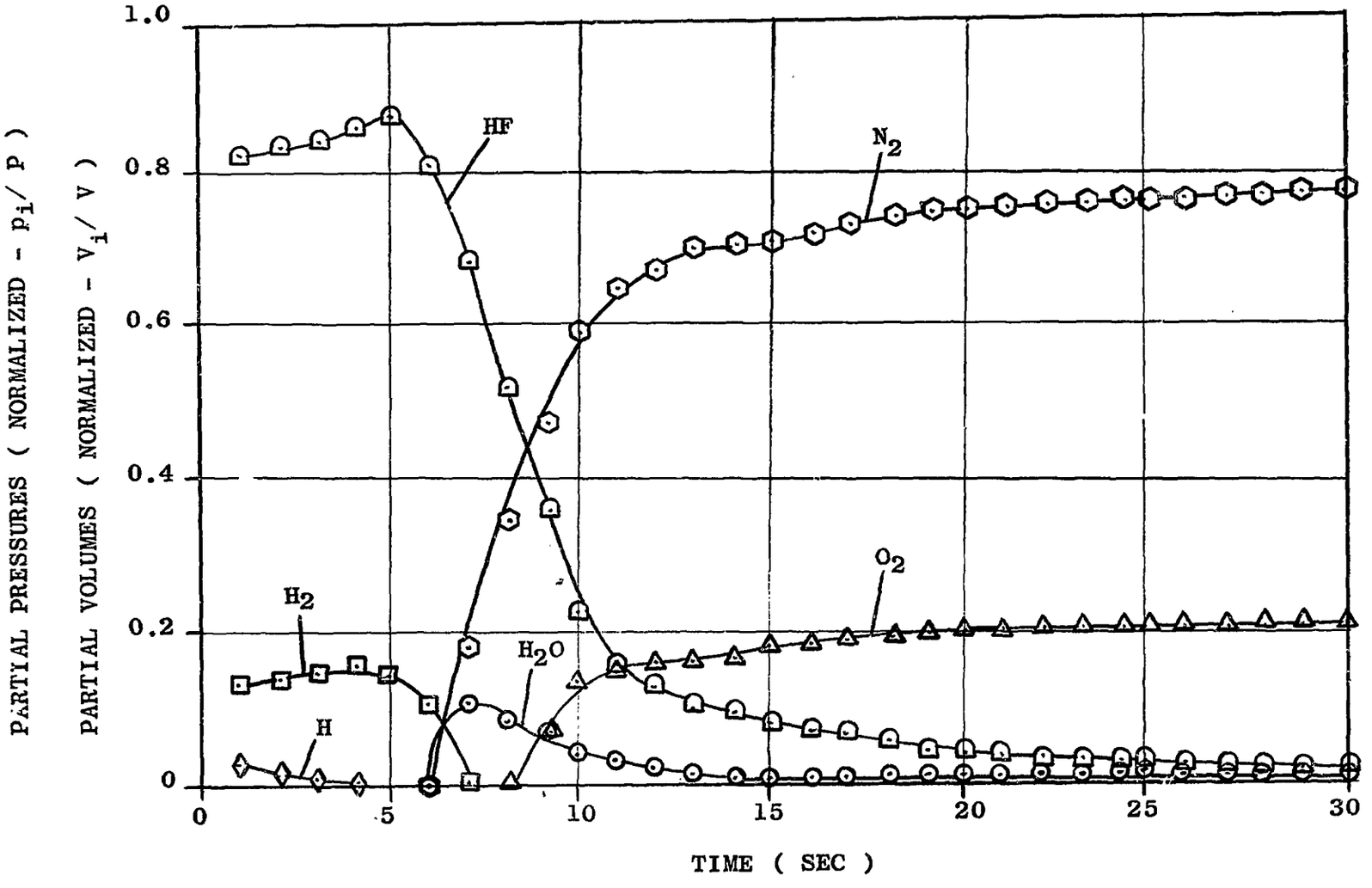

FIGURE IV-18-. PARTIAL PRESSURES AND PARTIAL VOLUMES FOR LH_2/LF_2 LIQUID PROPELLANT EXPLOSION PRODUCTS (YIELD = 4.5 PERCENT)

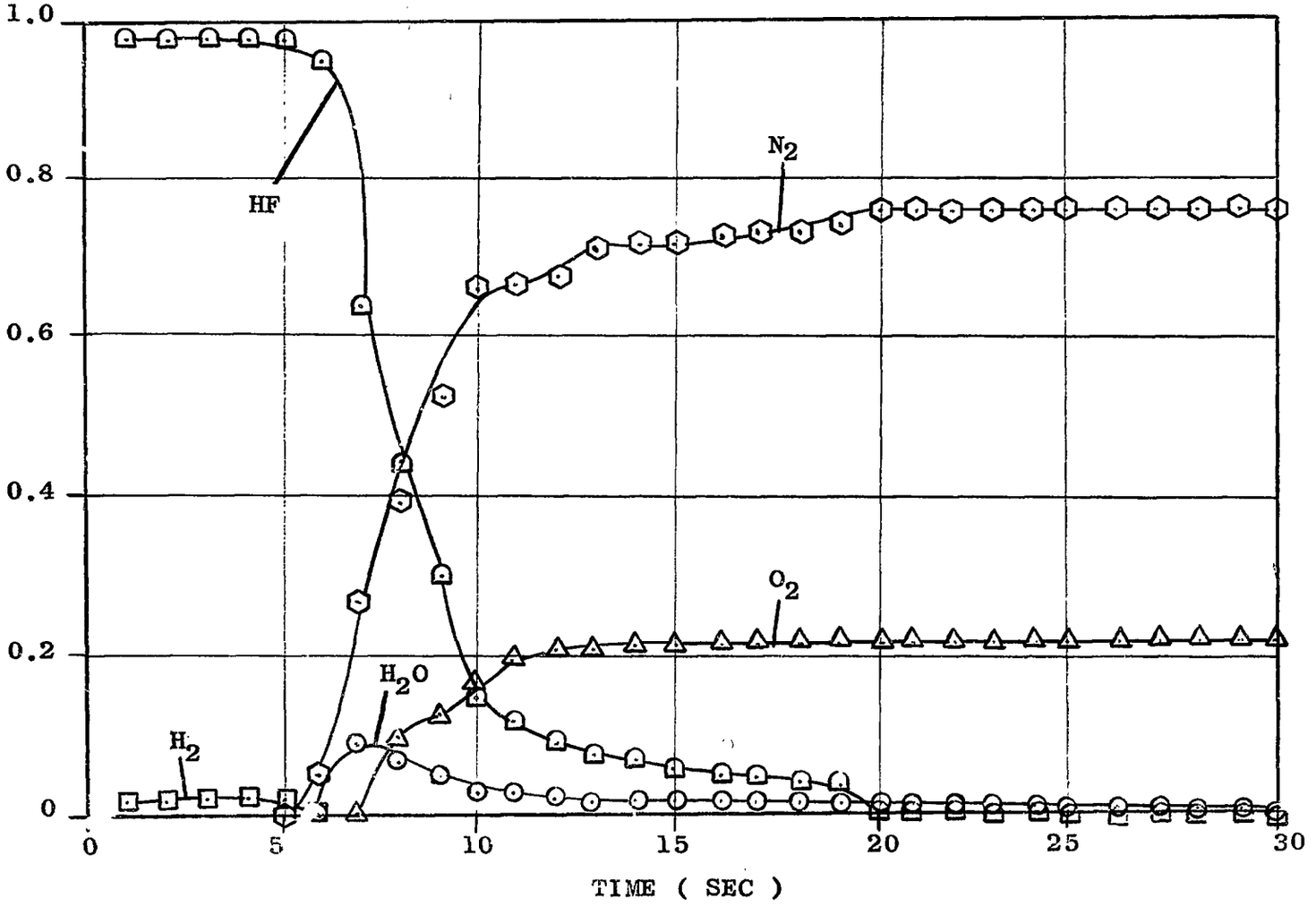

FIGURE IV-19-. WEIGHT COMPOSITION OF THE COMBUSTION PRODUCTS FROM LH_2/ LF_2 LIQUID PROPELLANT EXPLOSION (YIELD = 4.5 PERCENT)

$RP\text{-}1/LF_2$

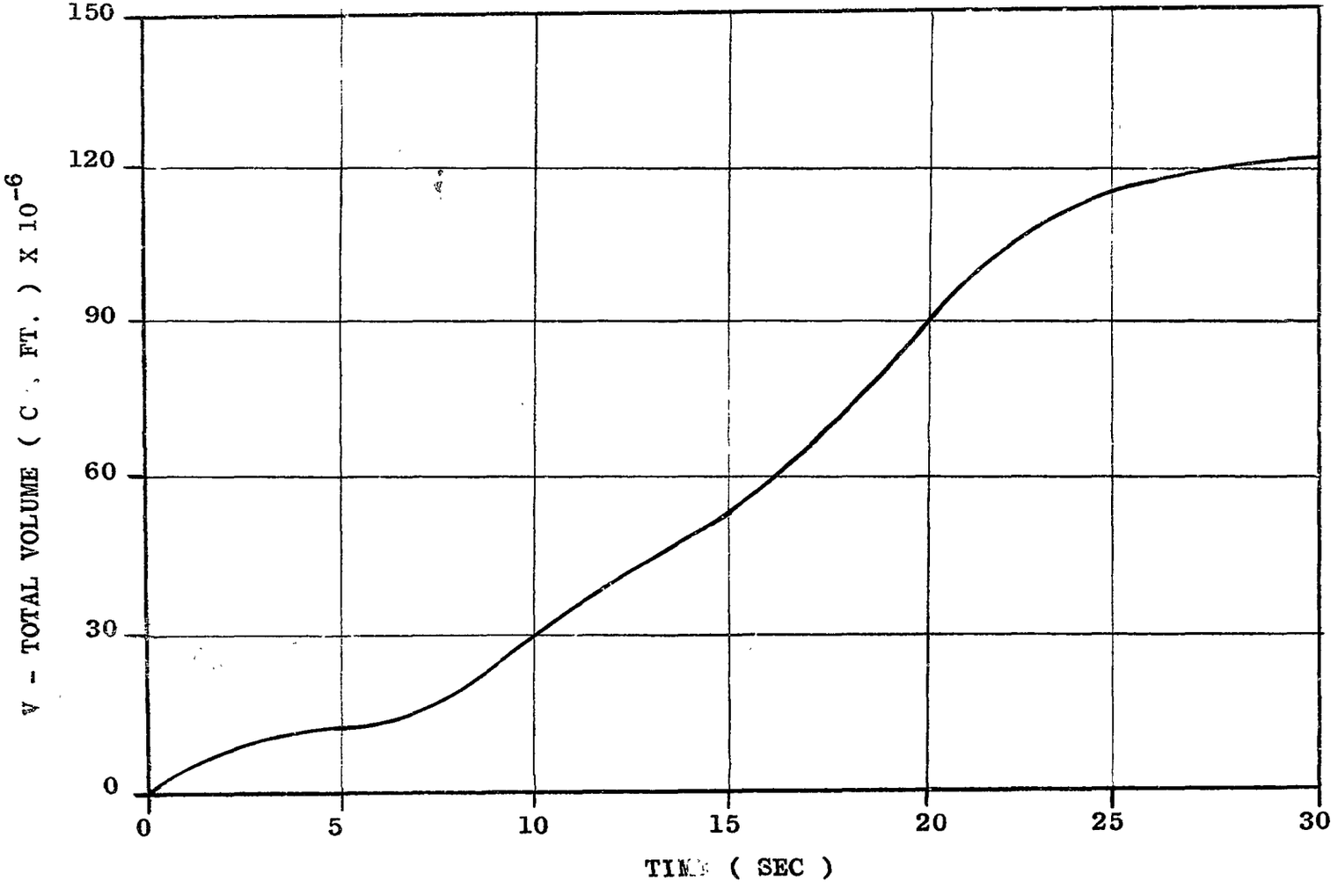

FIGURE IV-20-. VOLUME-TIME FUNCTION FOR RP-1/LF_2 LIQUID PROPELLANT EXPLOSION PRODUCTS (YIELD = 4.5 PERCENT)

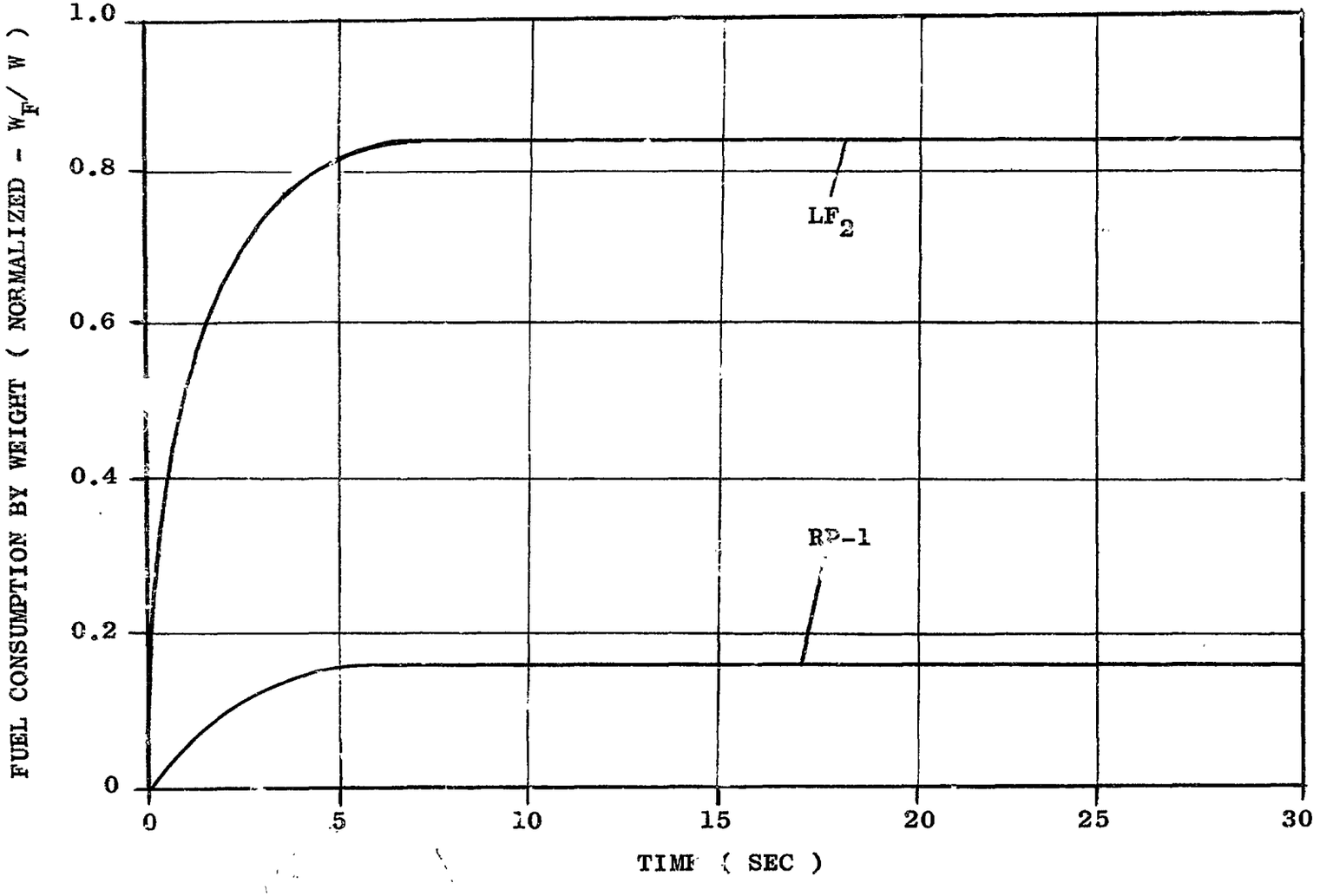

FIGURE IV-21-. FUEL CONSUMPTION FOR RP-1/LF_2 LIQUID PROPELLANT EXPLOSION (YIELD = 4.5 PERCENT)

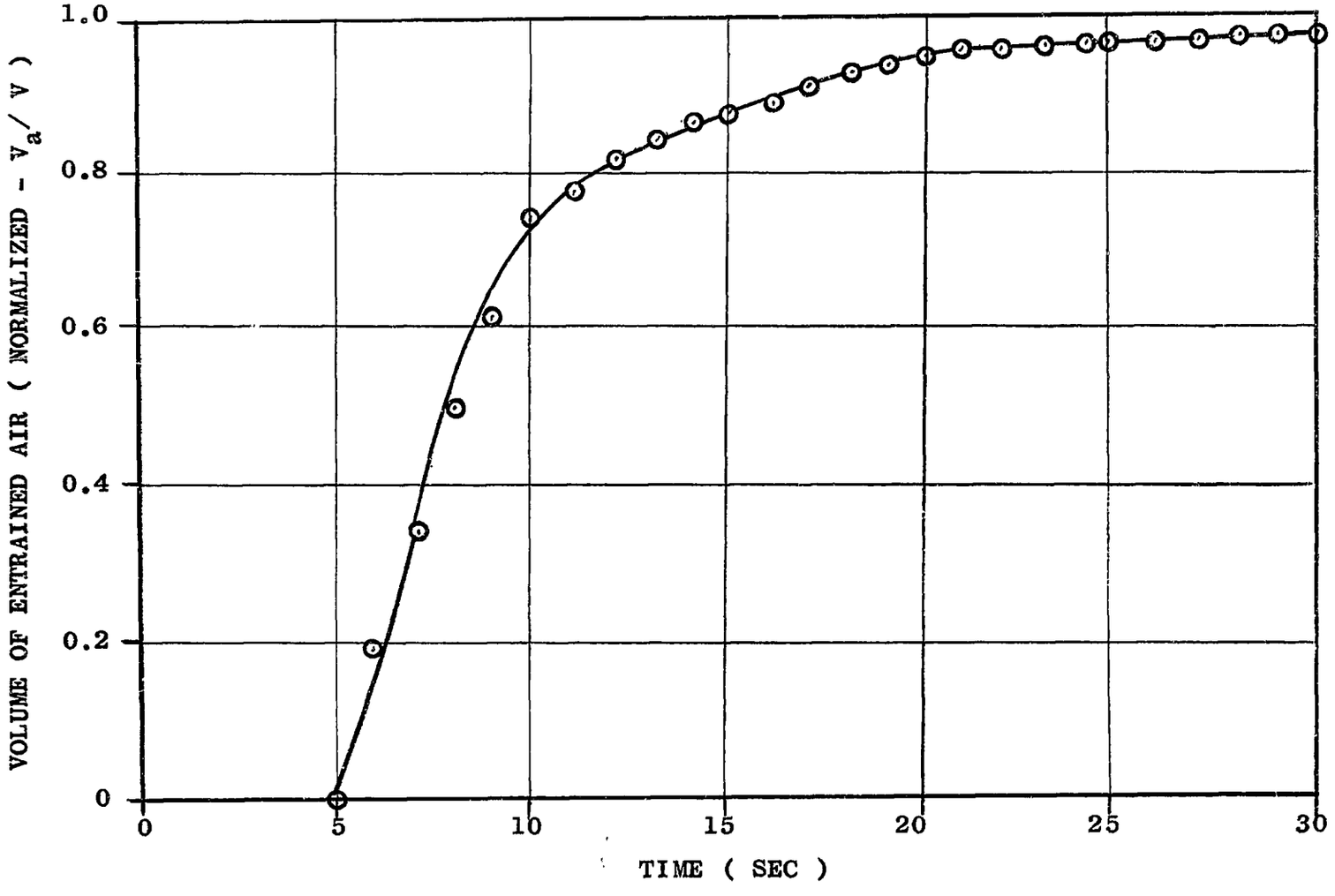

FIGURE IV-22-. VOLUME OF ENTRAINED AIR FOR RP-1/LF_2 LIQUID PROPELLANT EXPLOSION (YIELD = 4.5 PERCENT)

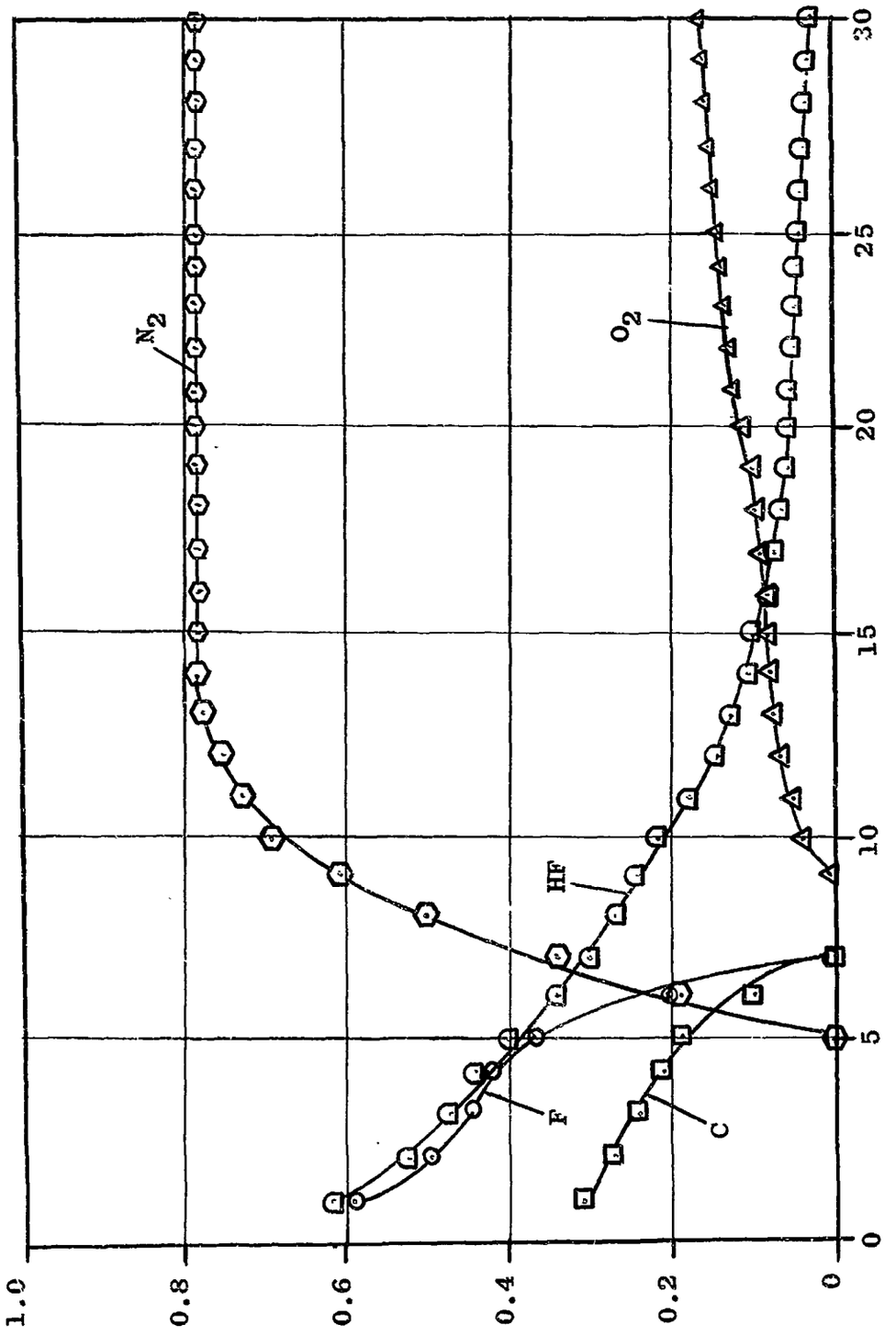

FIGURE IV-23-. PARTIAL PRESSURES AND PARTIAL VOLUMES FOR RP-1/LF_2 LIQUID PROPELLANT EXPLOSION PRODUCTS (YIELD = 4.5 PERCENT)

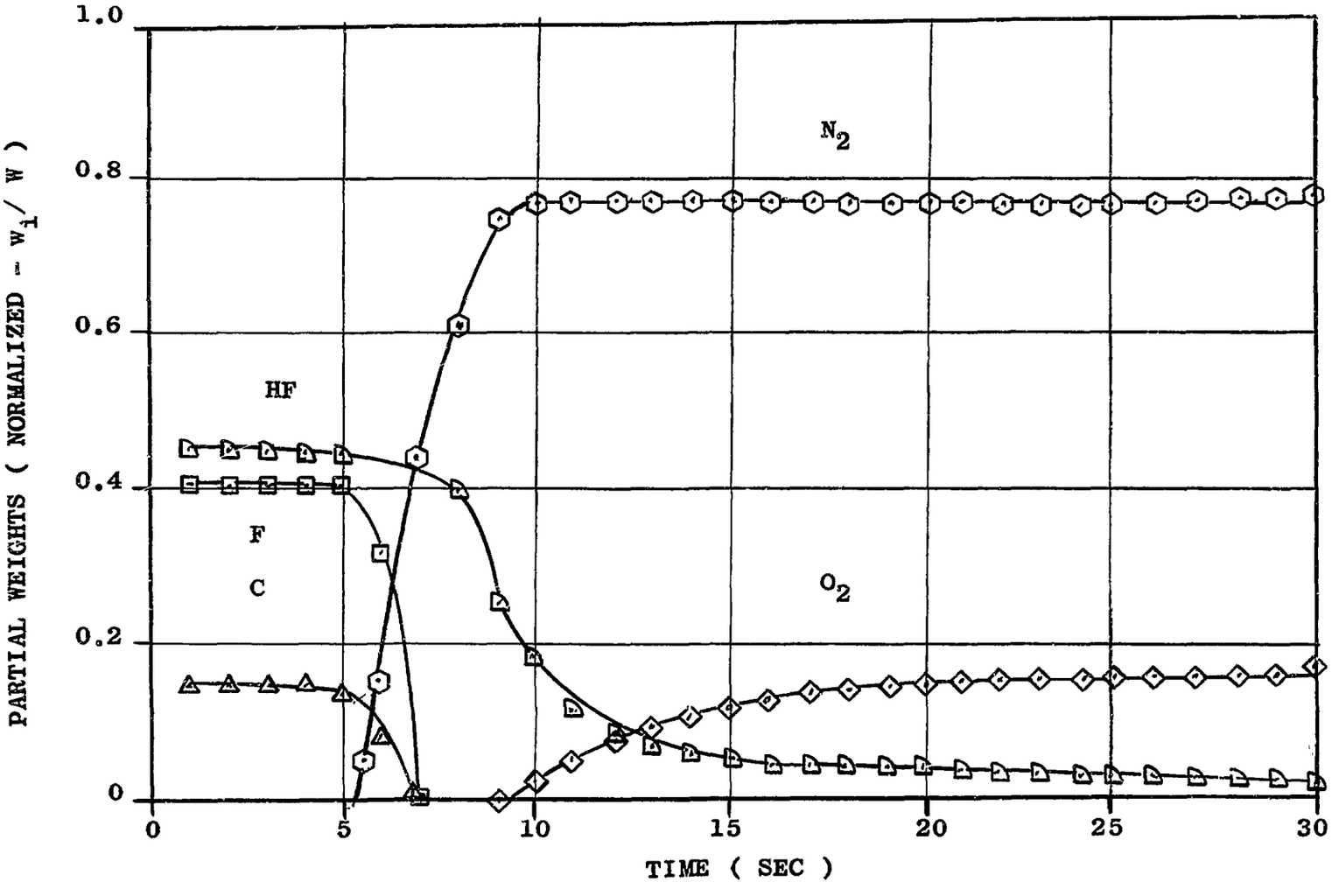

FIGURE IV-24-. WEIGHT COMPOSITION OF THE COMBUSTION PRODUCTS FROM RP-1/LF_2 LIQUID PROPELLANT EXPLOSION (YIELD = 4.5 PERCENT)

$LH_2/RP\text{-}1/LO_2$

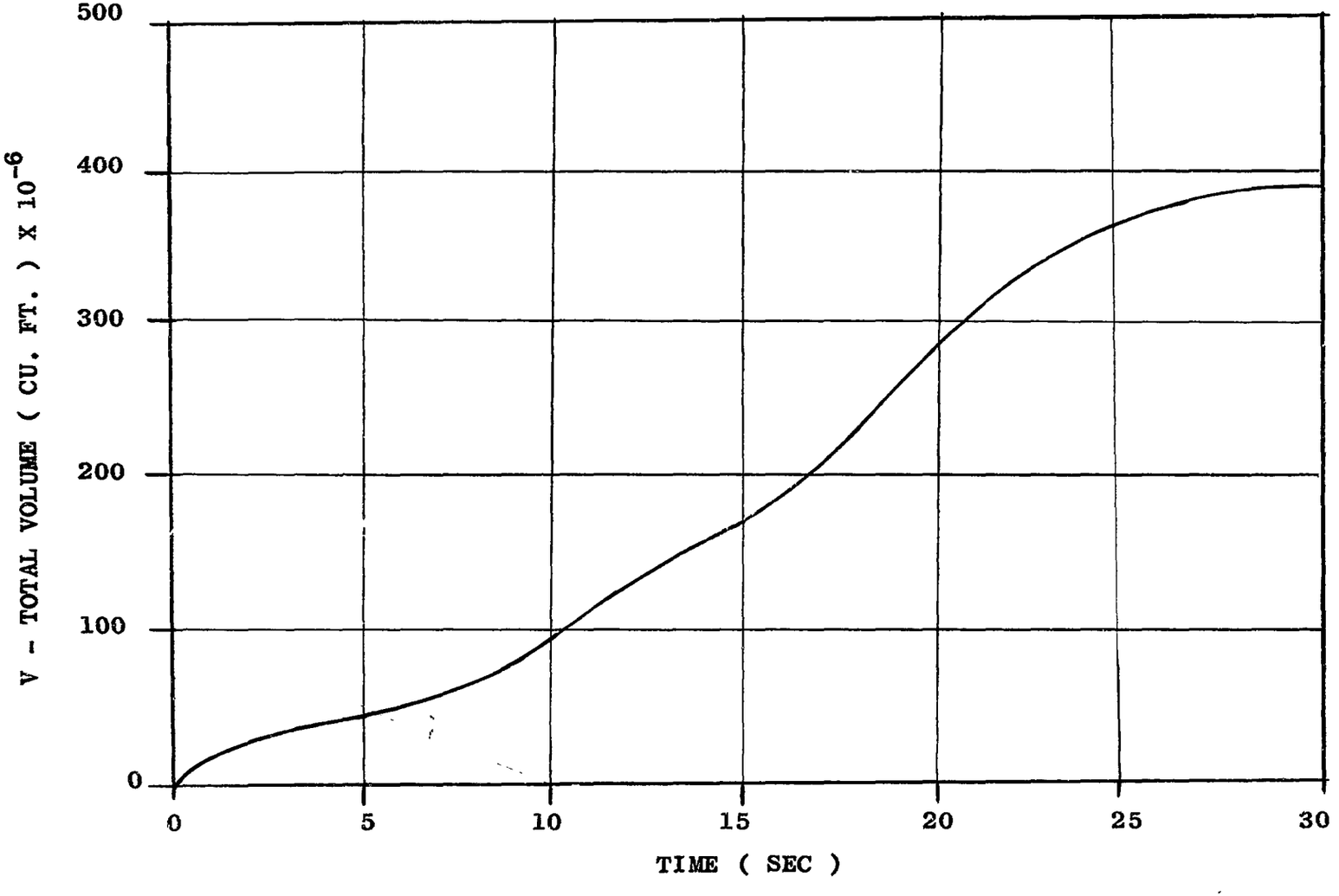

FIGURE IV-25-. VOLUME-TIME FUNCTION FOR LH_2/ RP-1/ LO_2 LIQUID PROPELLANT EXPLOSION PRODUCTS (YIELD = 4.5 PERCENT)

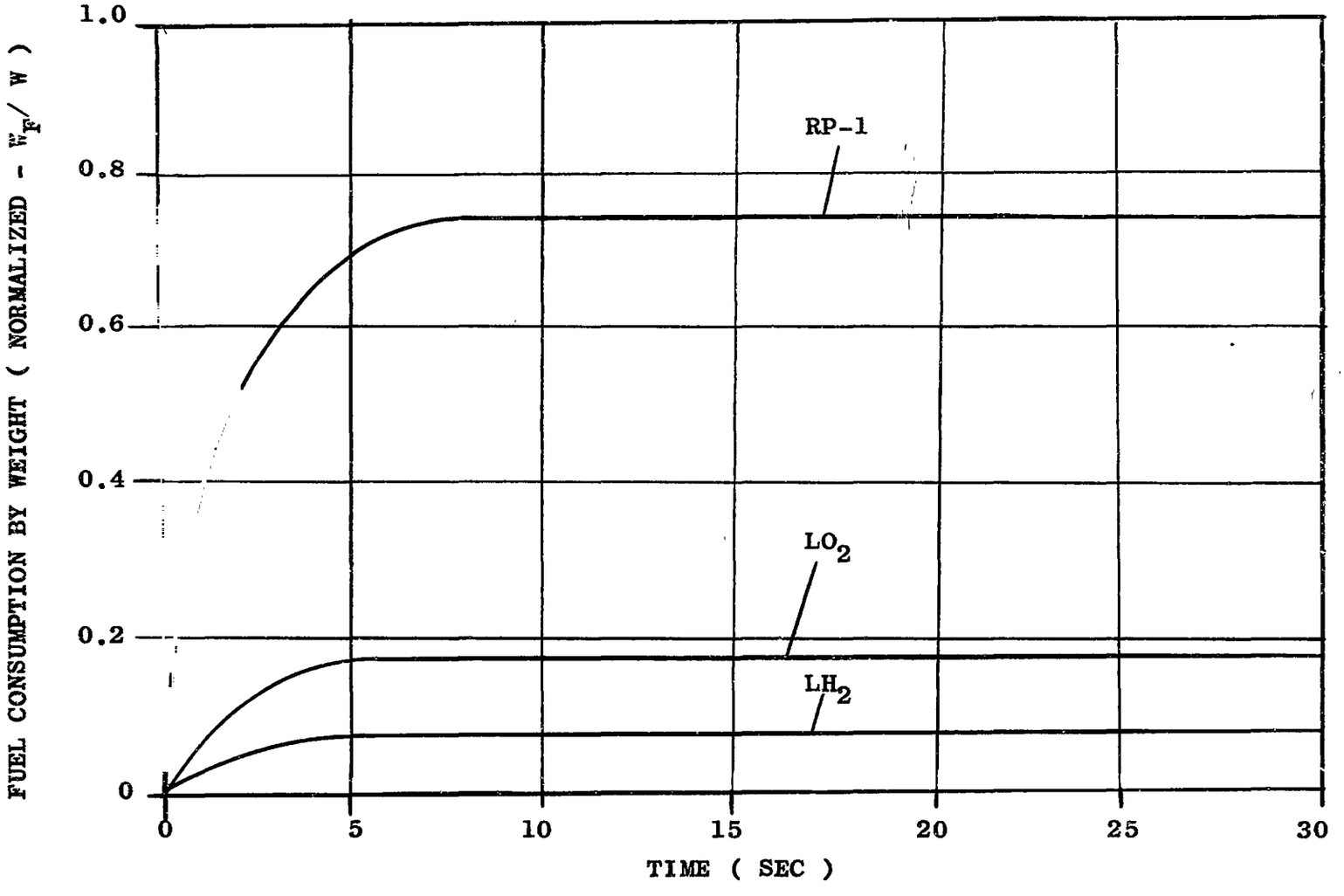

FIGURE IV-26-. FUEL CONSUMPTION FOR LH_2/ RP-1/ LO_2 LIQUID PROPELLANT EXPLOSION (YIELD = 4.5 PERCENT)

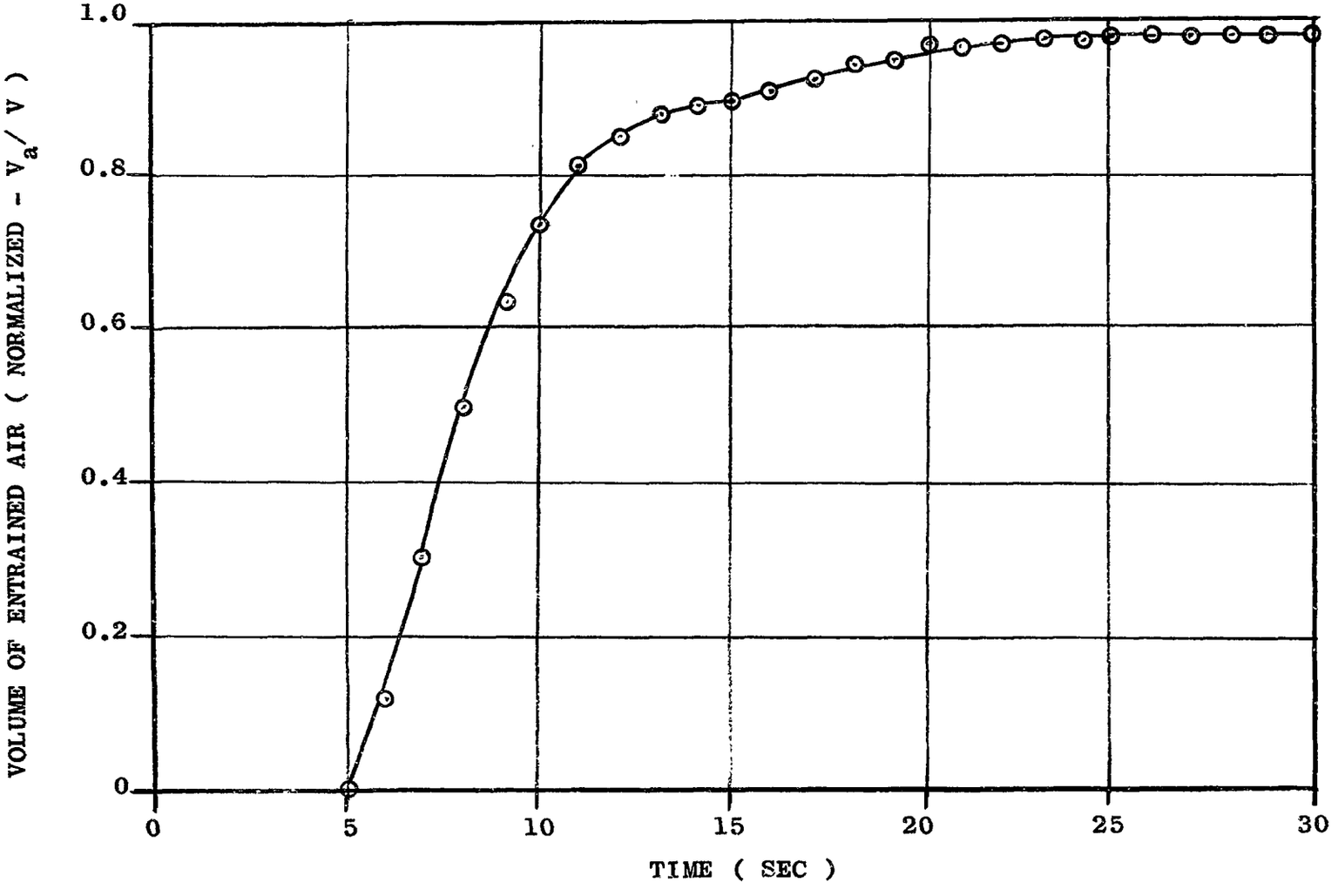

FIGURE IV-27-. VOLUME OF ENTRAINED AIR FOR $LH_2/RP\text{-}1/LO_2$ LIQUID PROPELLANT EXPLOSION (YIELD = 4.5 PERCENT)

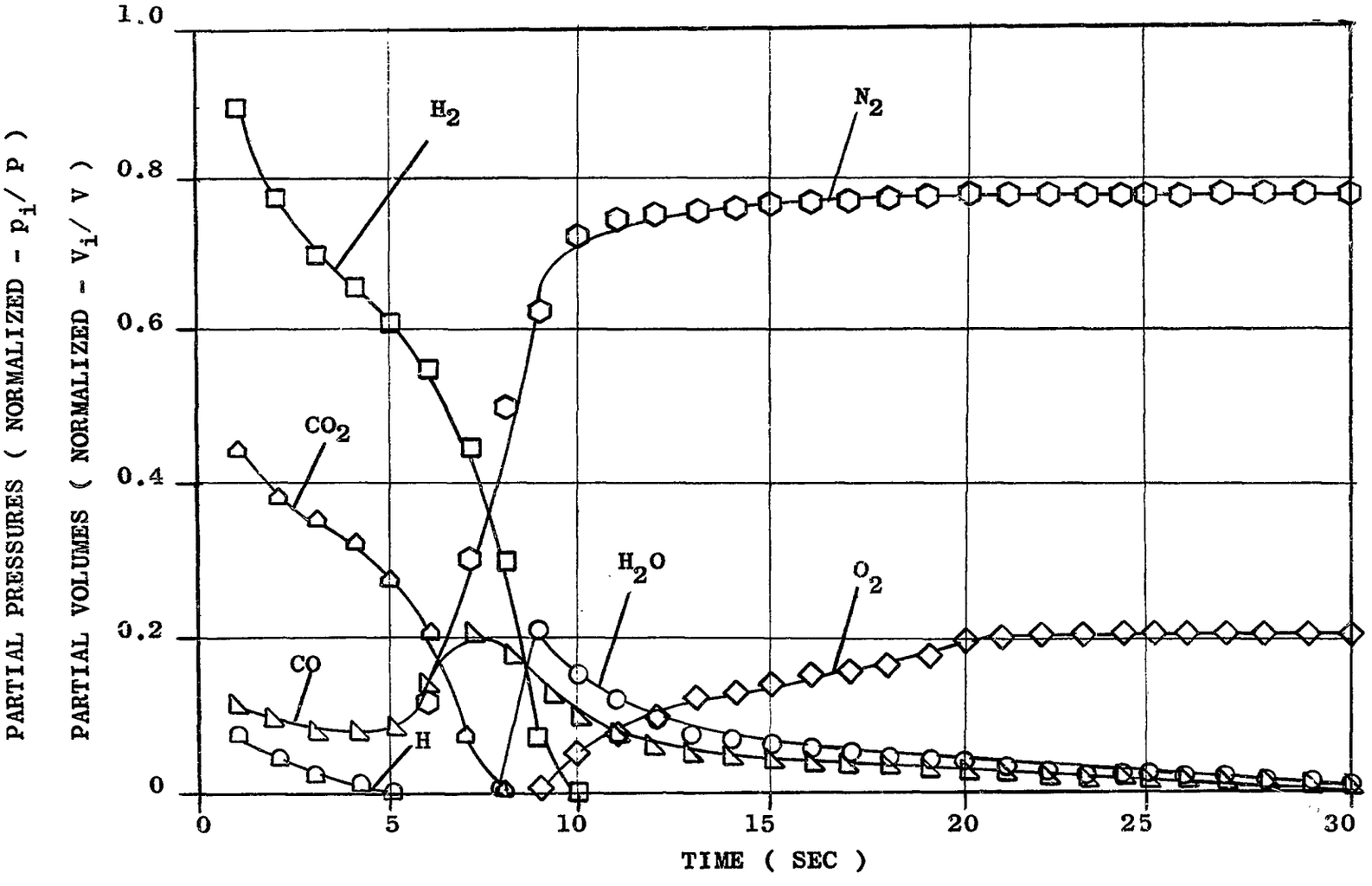

FIGURE IV-28-. PARTIAL PRESSURES AND PARTIAL VOLUMES FOR LH_2/ RP-1/ LO_2 LIQUID PROPELLANT EXPLOSION PRODUCTS (YIELD = 4.5 PERCENT)

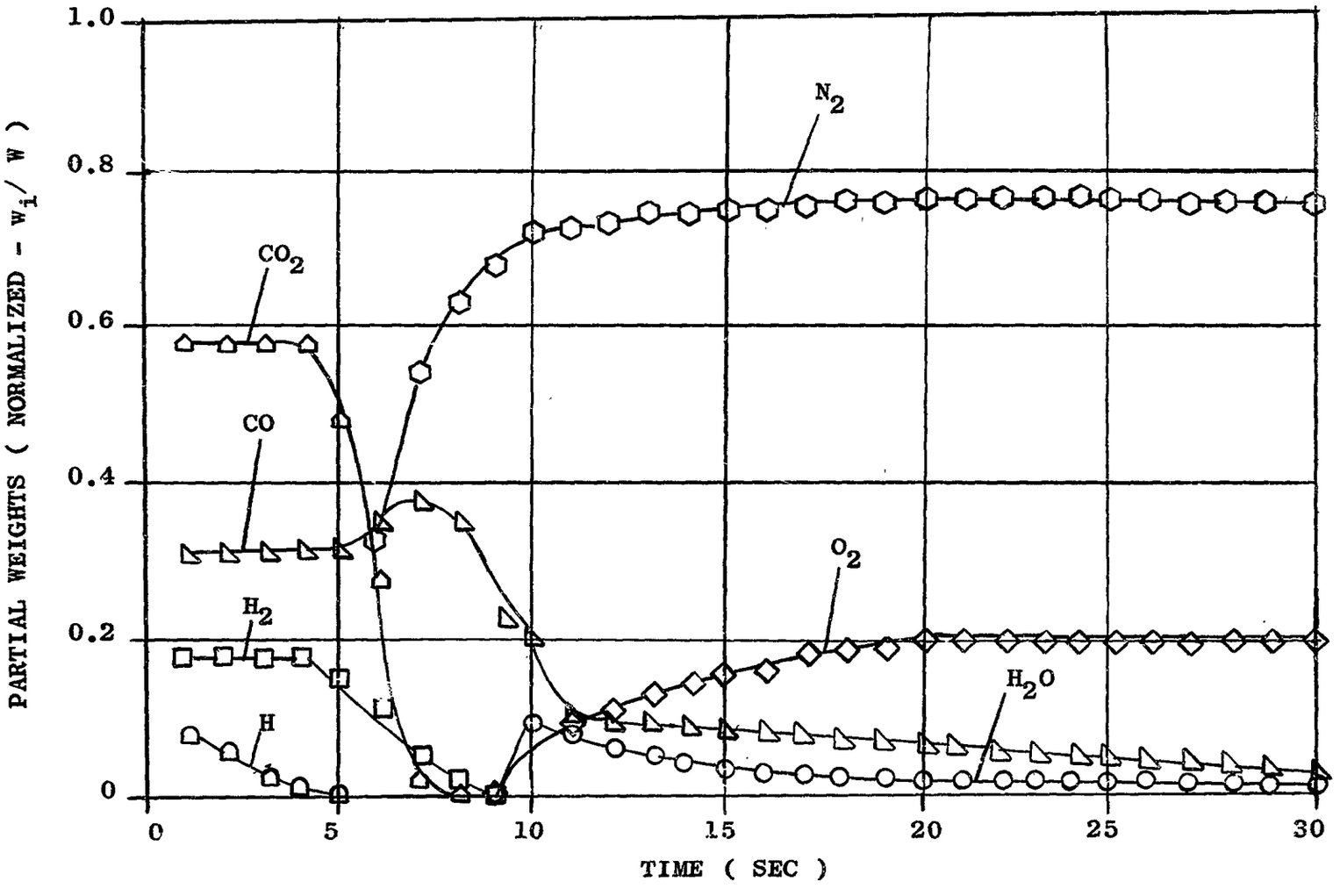

FIGURE IV-29-. WEIGHT COMPOSITION OF THE COMBUSTION PRODUCTS FROM LH_2/ RP-1/ LO_2 LIQUID PROPELLANT EXPLOSION (YIELD = 4.5 PERCENT)

LH_2/LO_2 + 1% F

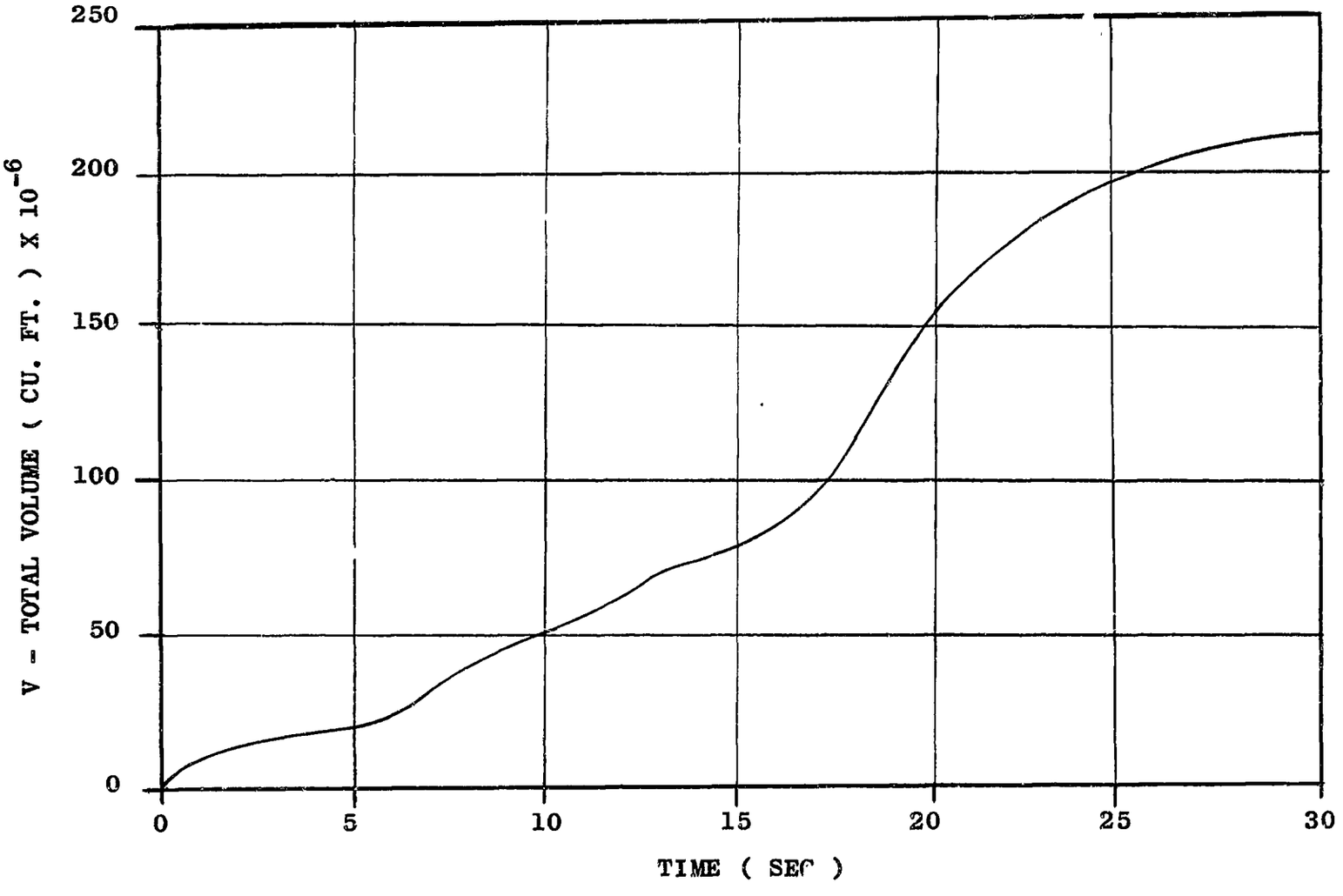

FIGURE IV-30-. VOLUME-TIME FUNCTION FOR LH_2/ LO_2+ 1% F LIQUID PROPELLANT EXPLOSION PRODUCTS (YIELD = 4.5 PERCENT)

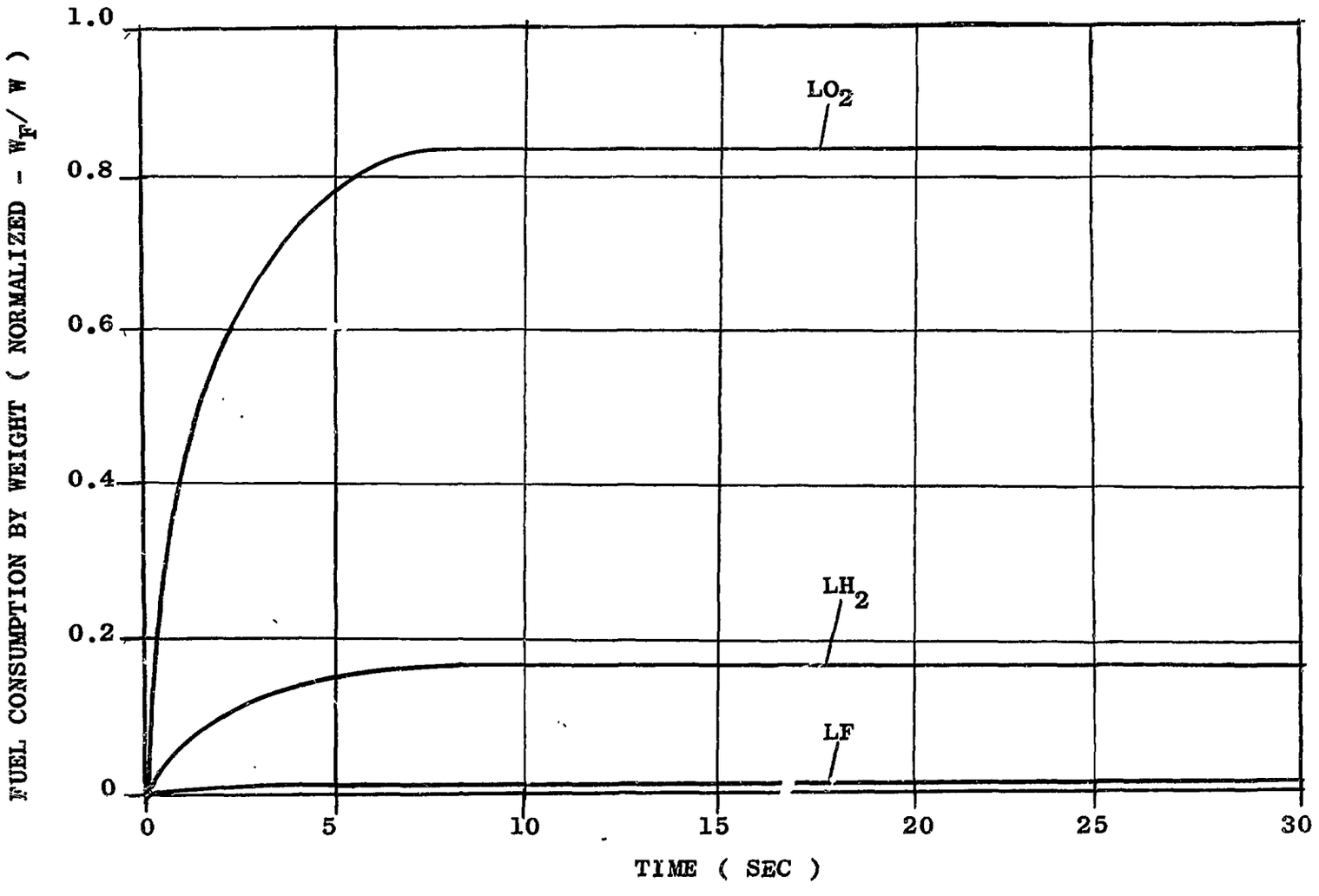

FIGURE IV-31-. FUEL CONSUMPTION FOR LH_2/LO_2+ 1% F LIQUID PROPELLANT EXPLOSION (YIELD = 4.5 PERCENT)

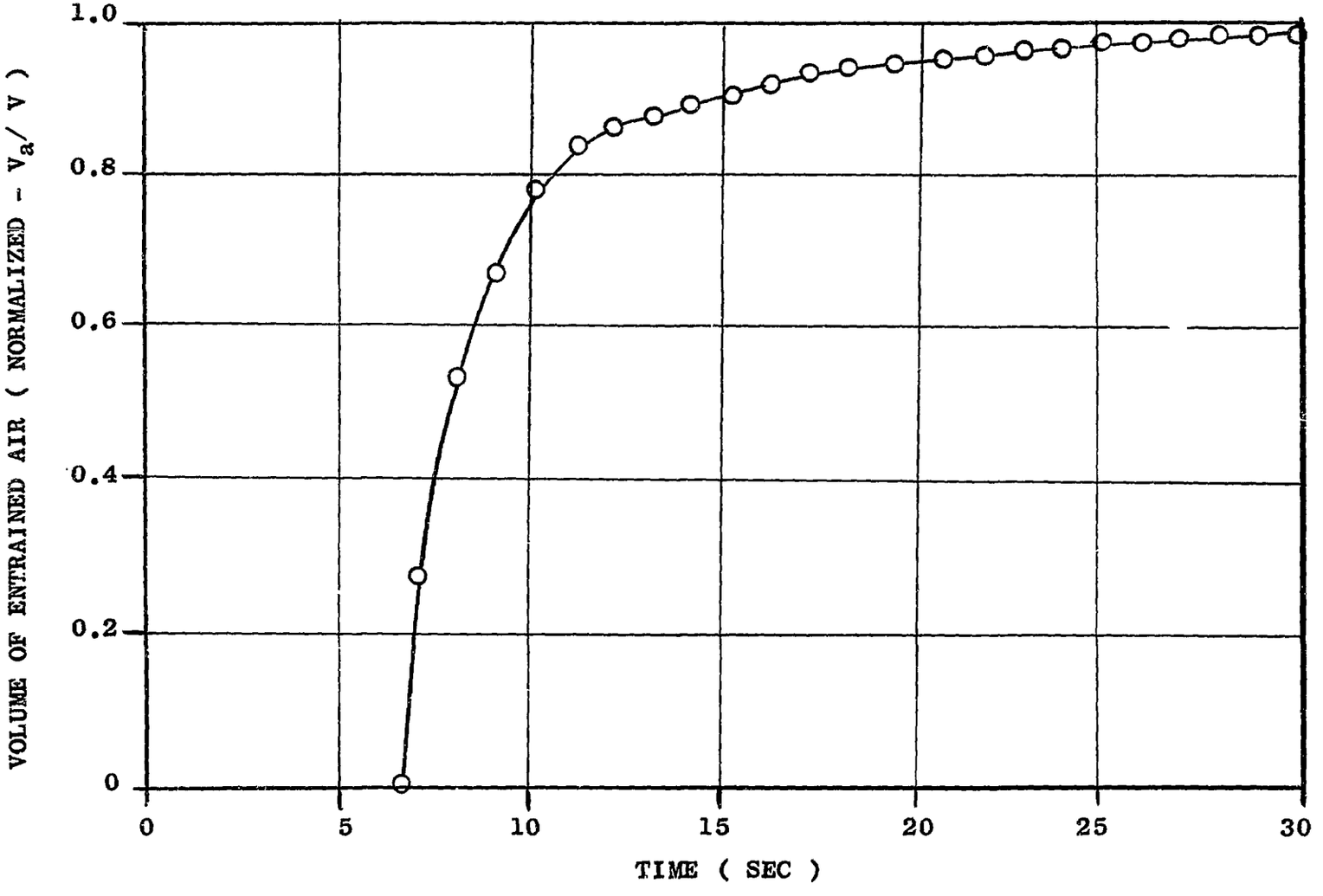

FIGURE IV-32-. VOLUME OF ENTRAINED AIR FOR LH_2/ LO_2 + 1% F LIQUID PROPELLANT EXPLOSION (YIELD = 4.5 PERCENT)

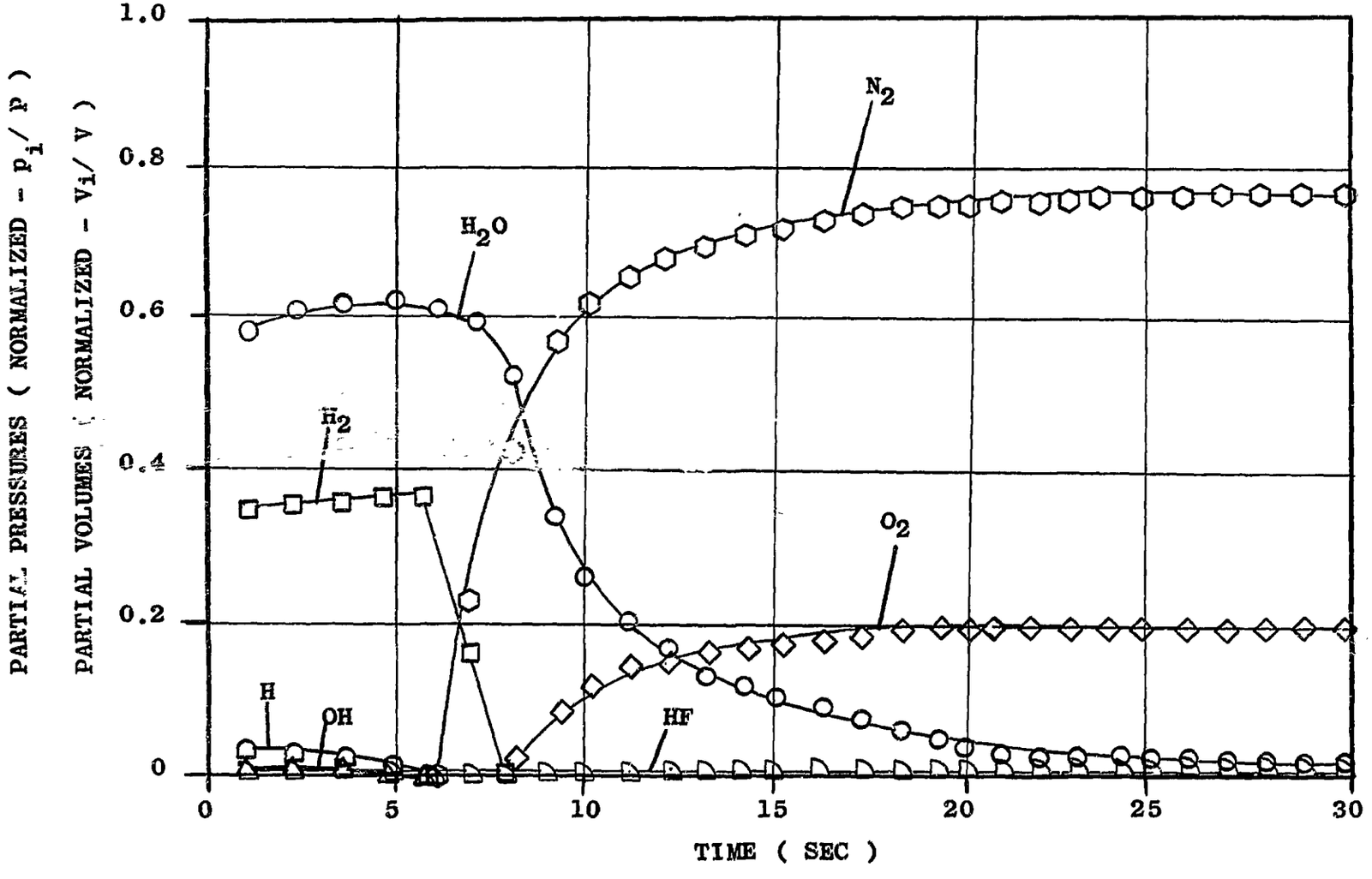

FIGURE IV-33-. PARTIAL PRESSURES AND PARTIAL VOLUMES FOR LH_2/LO_2 + 1% F LIQUID PROPELLANT EXPLOSION PRODUCTS (YIELD = 4.5 PERCENT)

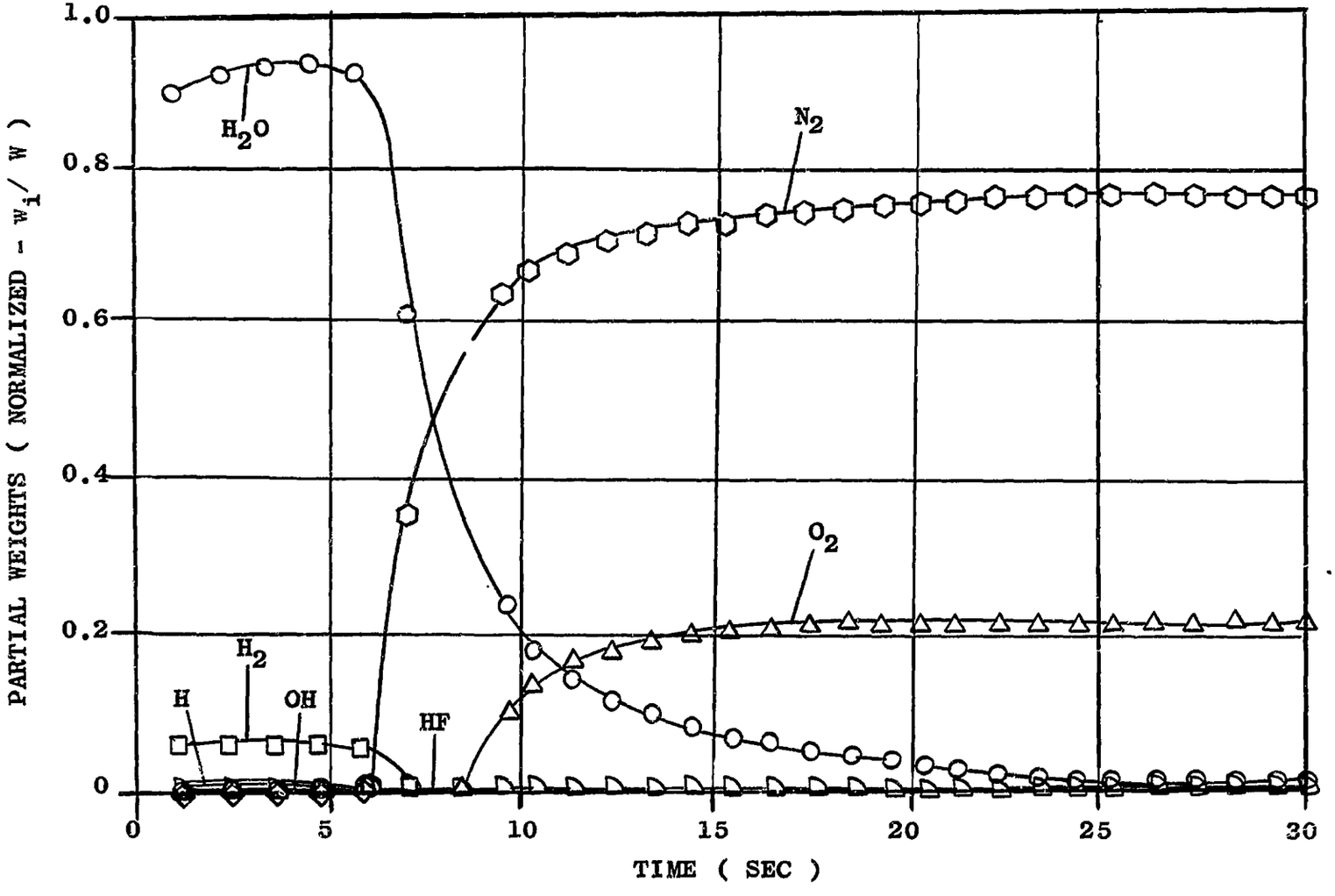

FIGURE IV-34. WEIGHT COMPOSITION OF THE COMBUSTION PRODUCTS FROM LH_2 / LO_2 + 1%F LIQUID PROPELLANT EXPLOSION (YIELD = 4.5 PERCENT)

LH_2/LO_2 + 5% F

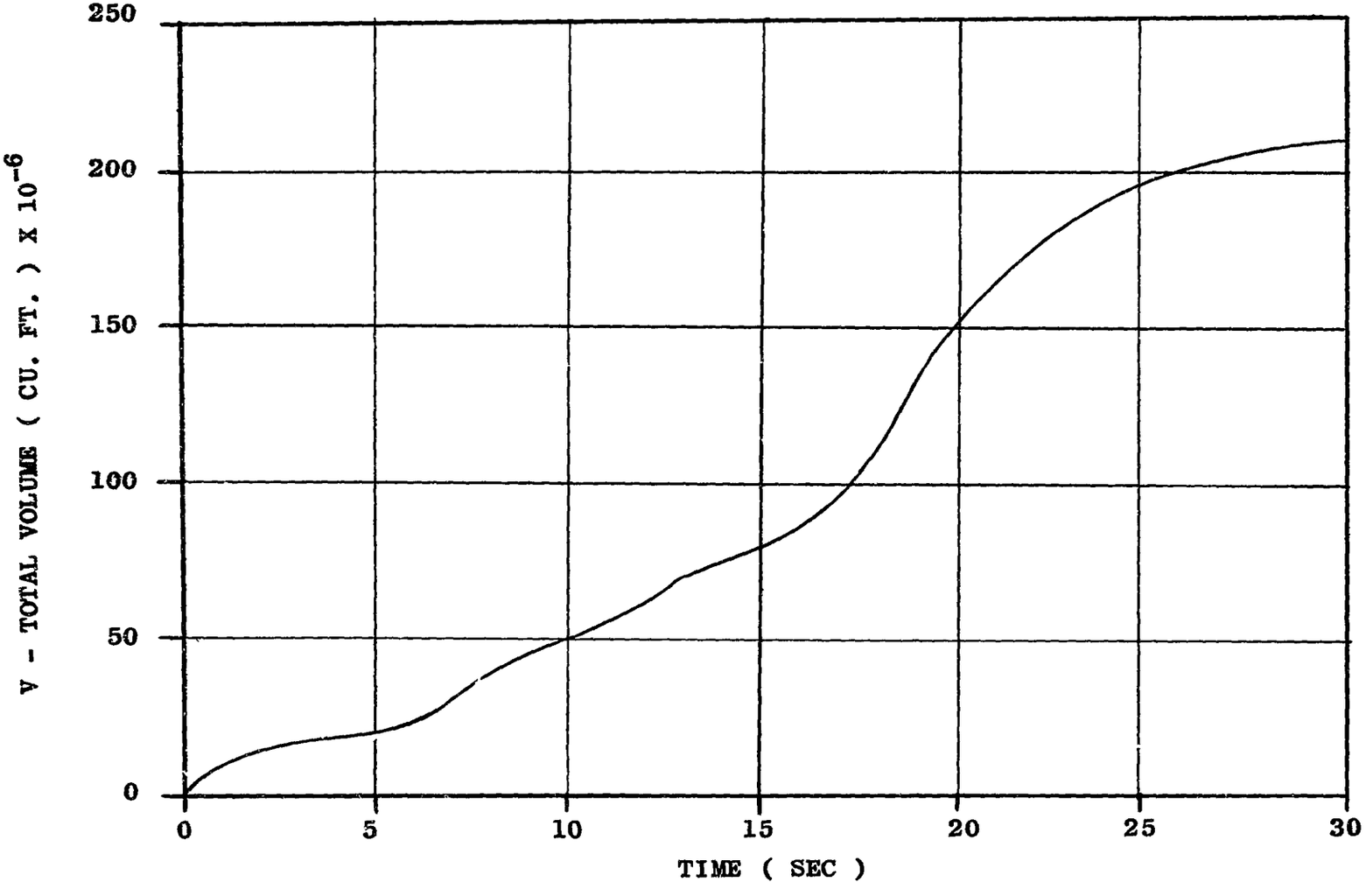

FIGURE IV-35-. VOLUME-TIME FUNCTION FOR LH_2/ LO_2 + 5% F LIQUID PROPELLANT EXPLOSION PRODUCTS (YIELD = 4.5 PERCENT)

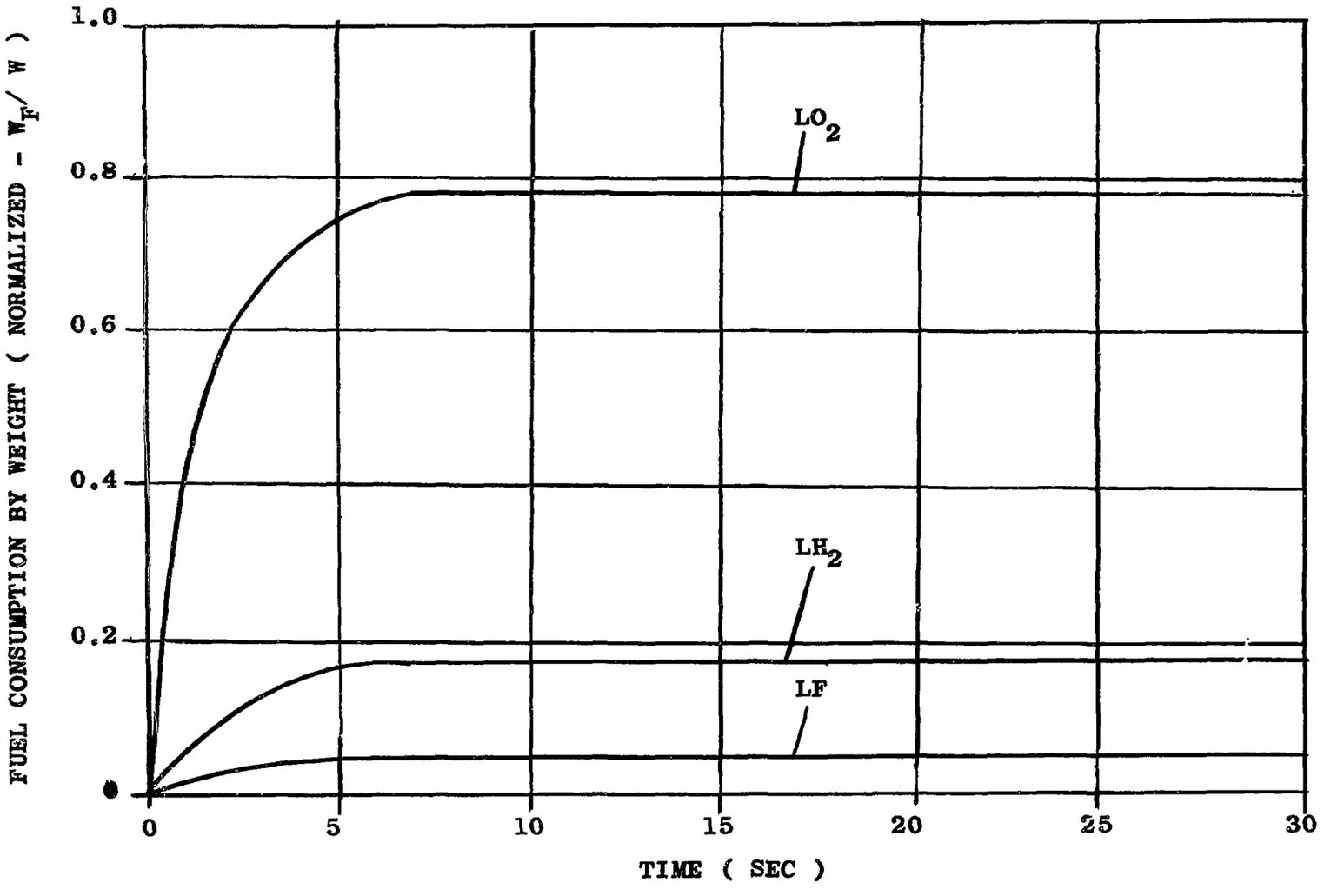

FIGURE IV-36-. FUEL CONSUMPTION FOR LH_2/LO_2 + 5% F LIQUID PROPELLANT EXPLOSION (YIELD = 4.5 PERCENT)

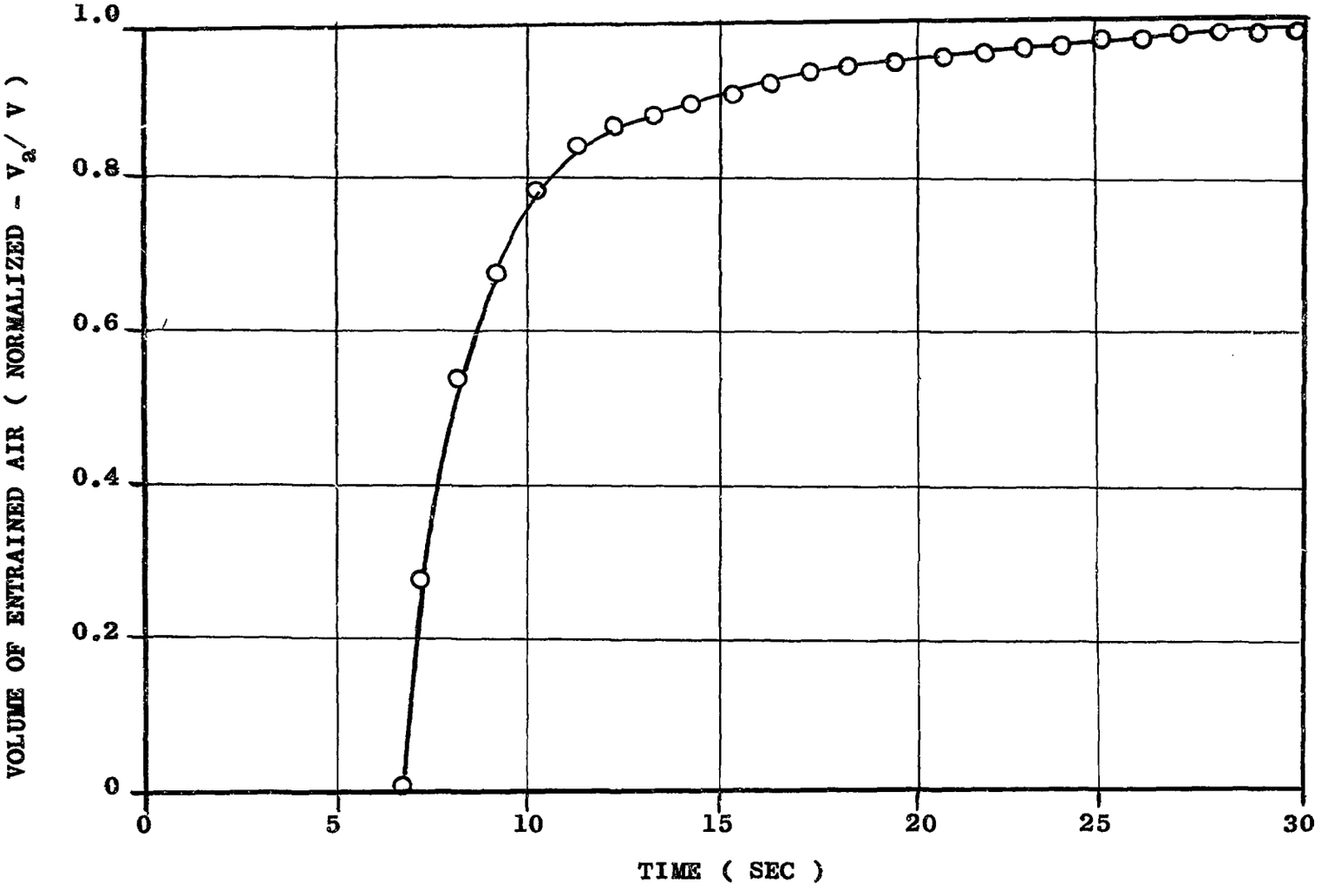

FIGURE IV-37-. VOLUME OF ENTRAINED AIR FOR LH_2/LO_2 + 5% F LIQUID PROPELLANT EXPLOSION (YIELD = 4.5 PERCENT)

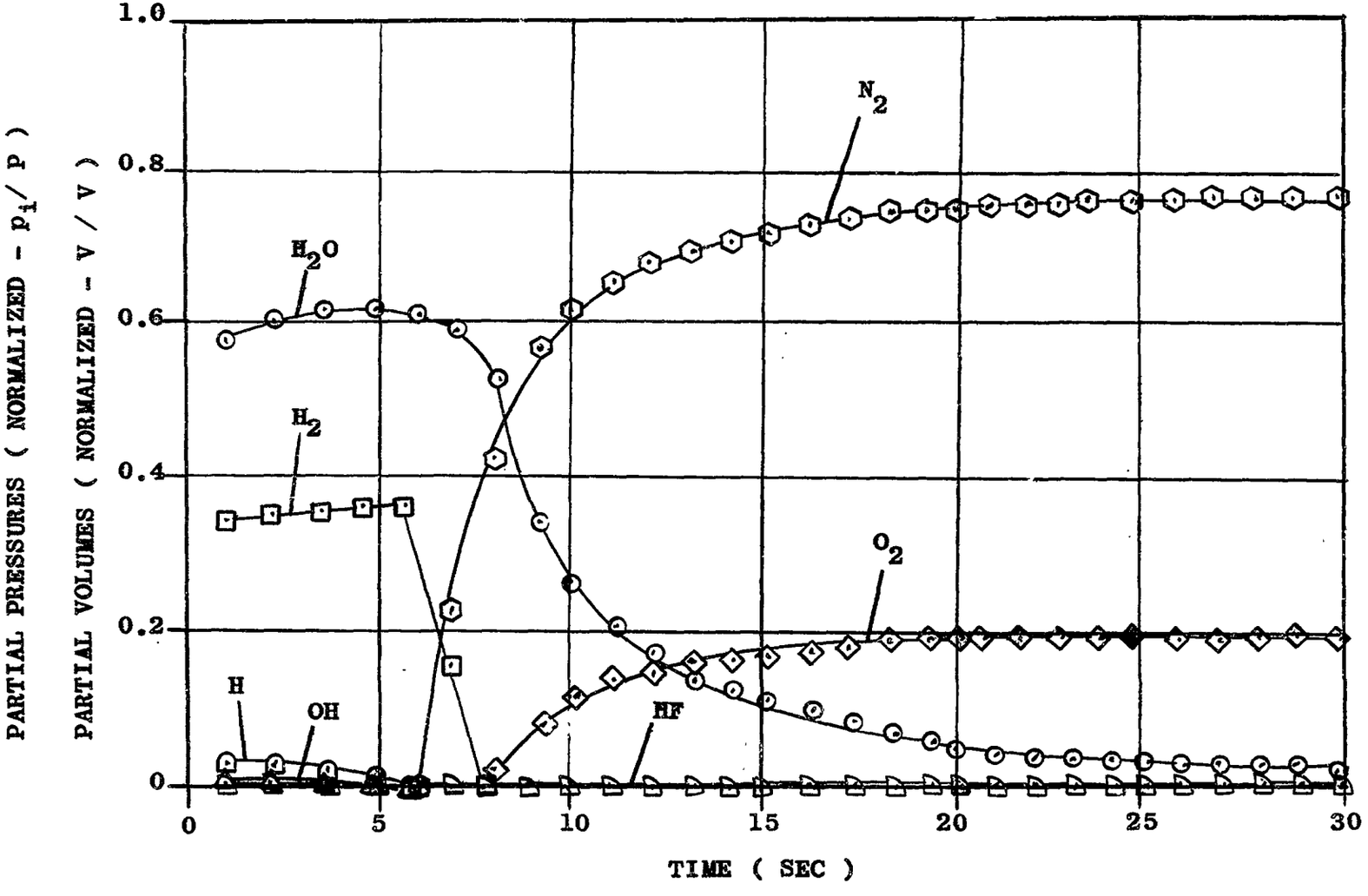

FIGURE IV-38-. PARTIAL PRESSURES AND PARTIAL VOLUMES FOR LH_2/ LO_2 + 5% F LIQUID PROPELLANT EXPLOSION PRODUCTS (YIELD = 4.5 PERCENT)

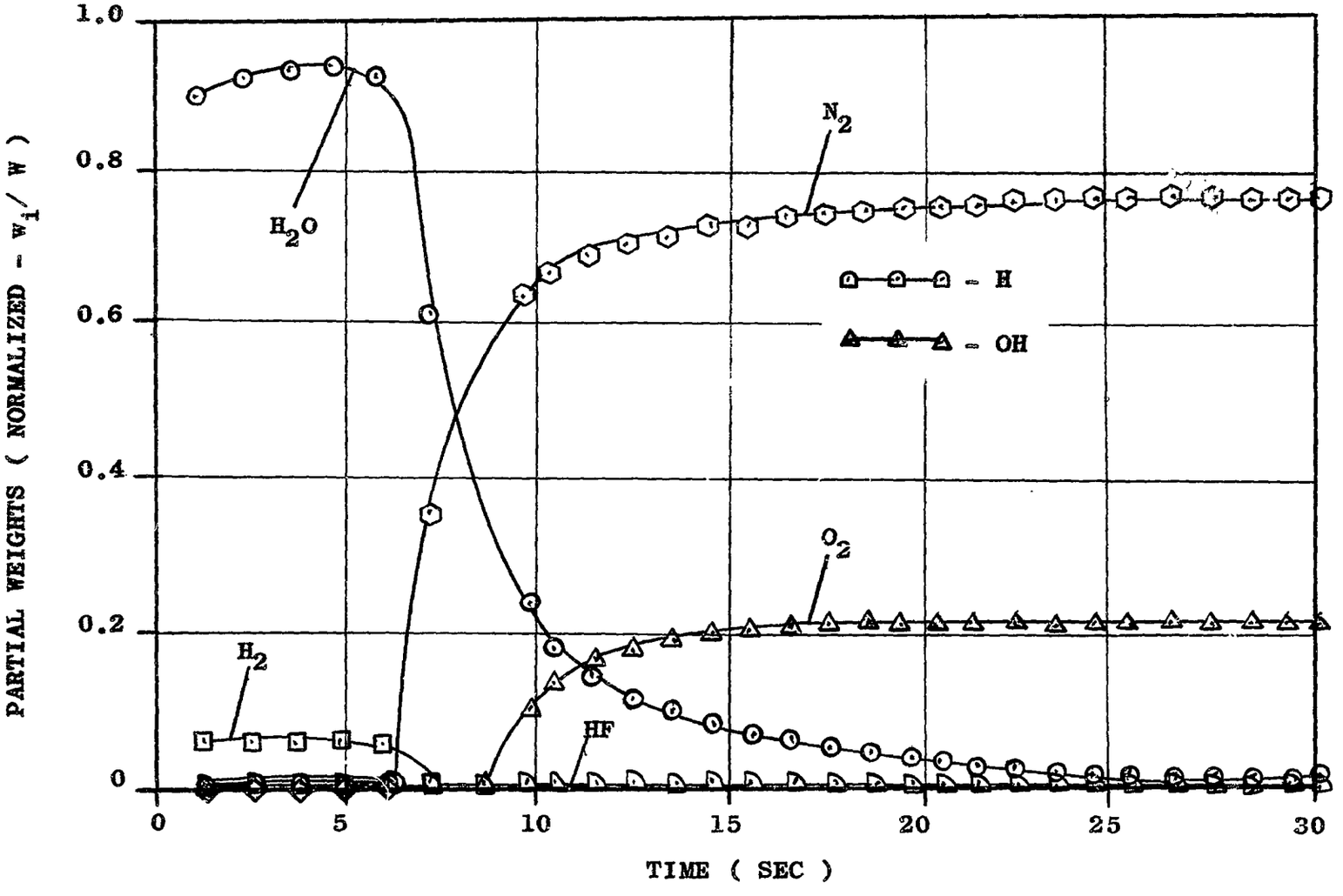

FIGURE IV-39-. WEIGHT COMPOSITION OF THE COMBUSTION PRODUCTS FROM LH_2 / LO_2 + 5% F LIQUID PROPELLANT EXPLOSION (YIELD = 4.5 PERCENT)

LH_2/LO_2 + 10% F

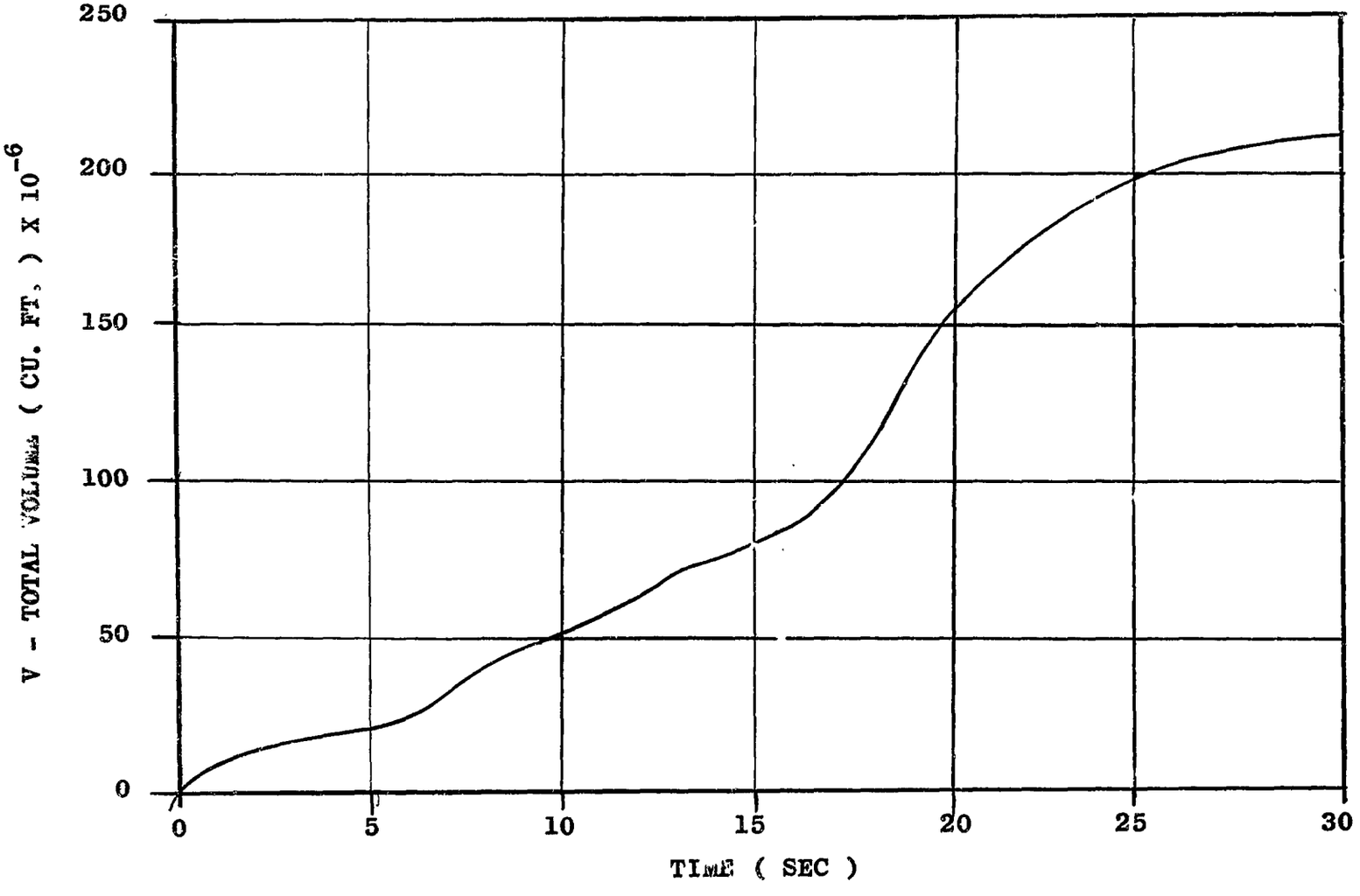

FIGURE IV-40-. VOLUME-TIME FUNCTION FOR LH_2/ LO_2 + 10% F LIQUID PROPELLANT EXPLOSION PRODUCTS (YIELD = 4.5 PERCENT)

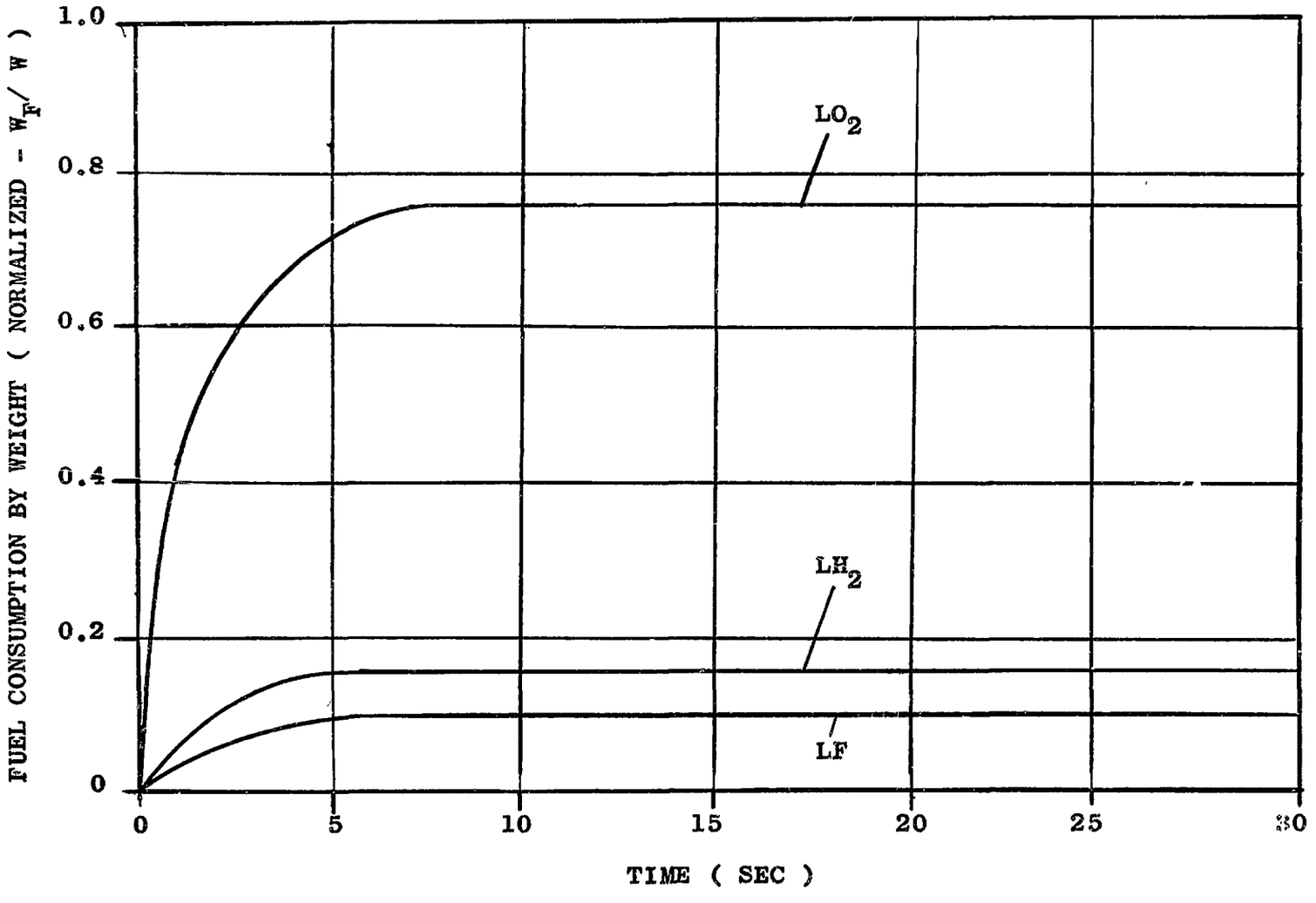

FIGURE IV-41-. FUEL CONSUMPTION FOR LH_2/ LO_2 + 10% F LIQUID PROPELLANT EXPLOSION (YIELD = 4.5 PERCENT)

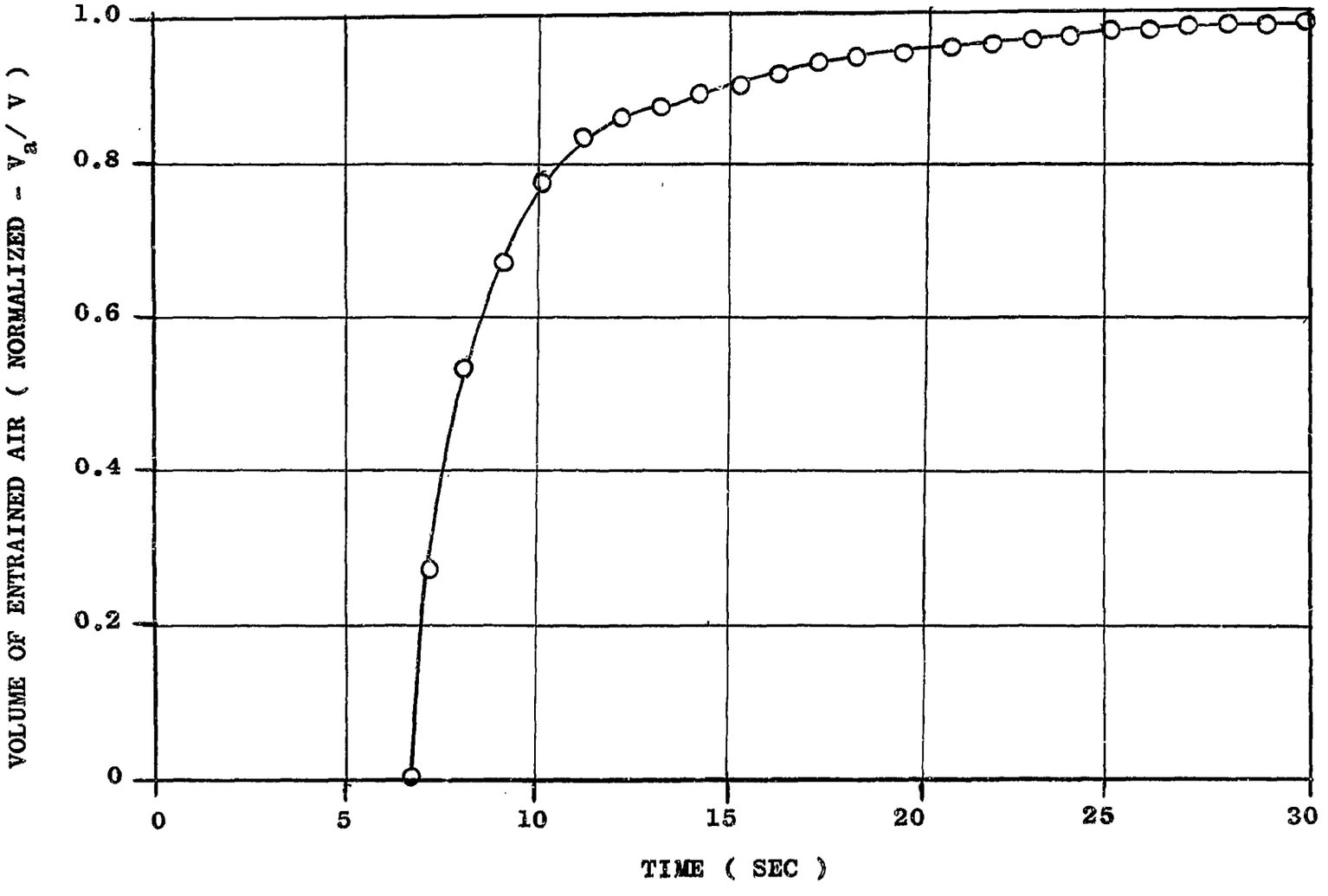

FIGURE IV-42-. VOLUME OF ENTRAINED AIR FOR LH_2/ LO_2 + 10% F LIQUID PROPELLANT EXPLOSION (YIELD = 4.5 PERCENT)

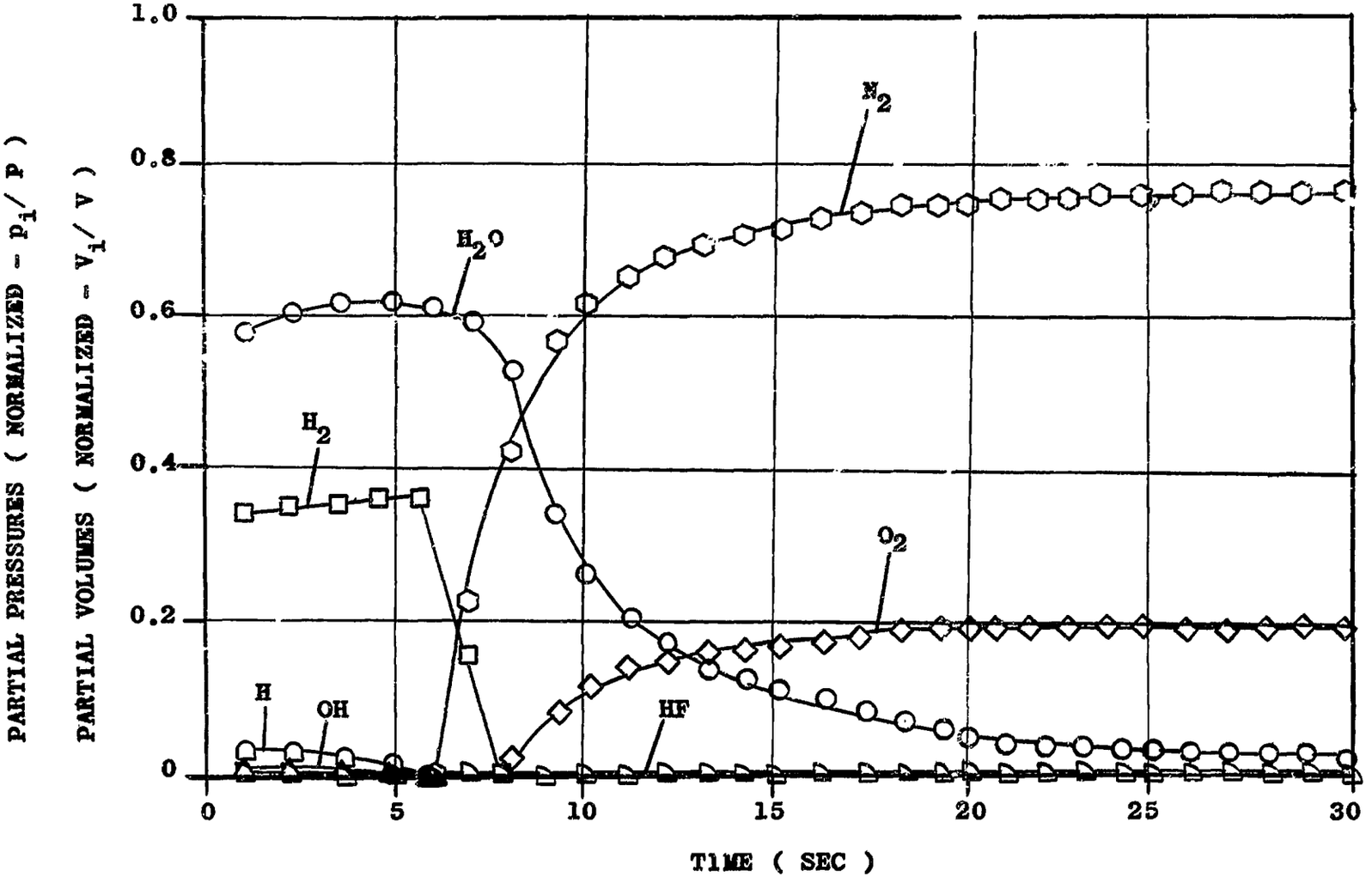

FIGURE IV-43-. PARTIAL PRESSURES AND PARTIAL VOLUMES FOR LH_2/ LO_2 + 10% F LIQUID PROPELLANT EXPLOSION PRODUCTS (YIELD = 4.5 PERCENT)

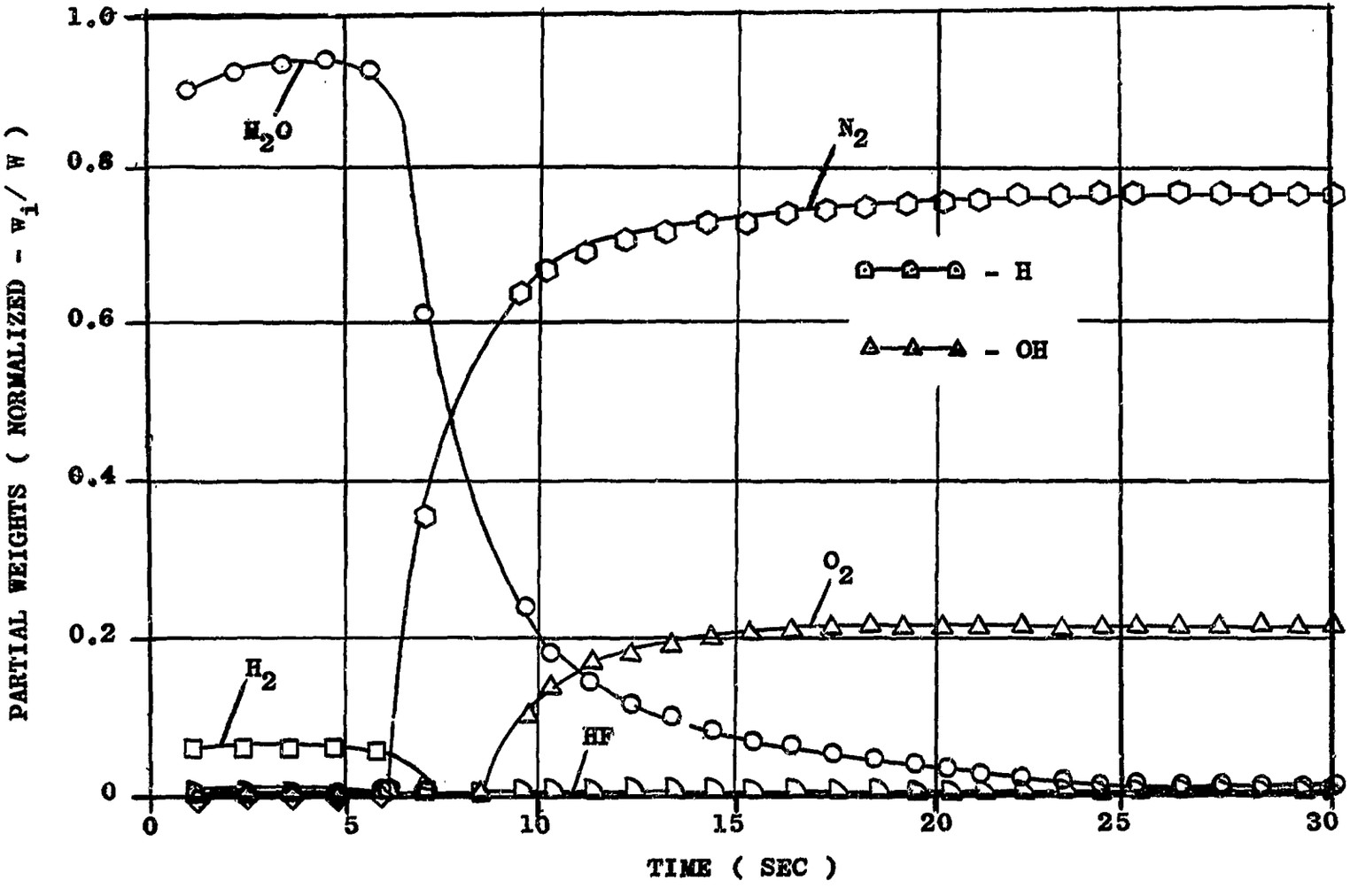

FIGURE IV-44-. WEIGHT COMPOSITION OF THE COMBUSTION PRODUCTS FROM LH_2/ LO_2 + 10% F LIQUID PROPELLANT EXPLOSION (YIELD = 4.5 PERCENT)

$RP\text{-}1/LO_2$ + 1% F

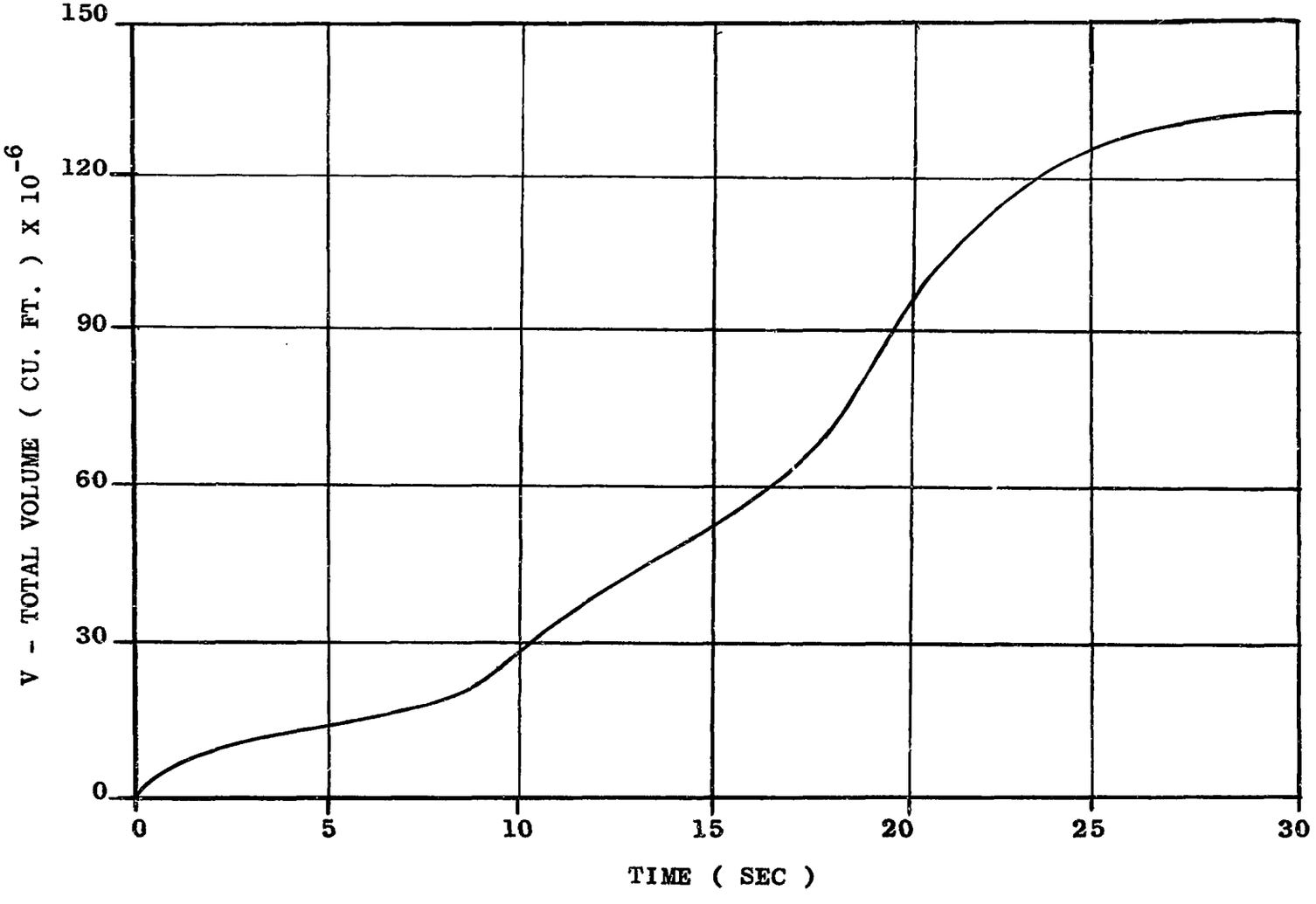

FIGURE IV-45-. VOLUME-TIME FUNCTION FOR RP-1/ LO_2 + 1% F LIQUID PROPELLANT EXPLOSION PRODUCTS (YIELD = 4.5 PERCENT)

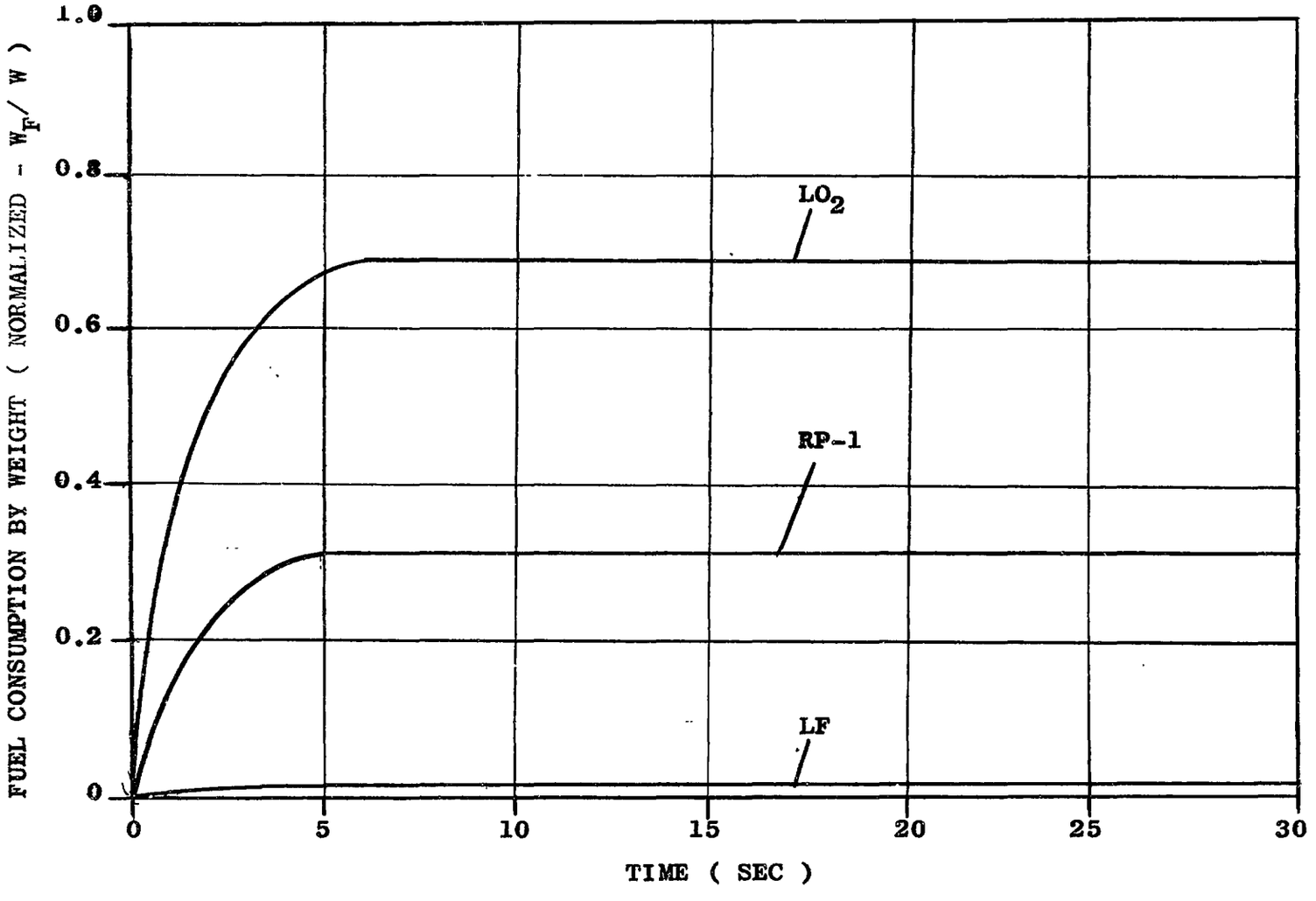

FIGURE IV-46-. FUEL CONSUMPTION FOR RP-1/ LO_2 + 1% F LIQUID PROPELLANT EXPLOSION (YIELD = 4.5 PERCENT)

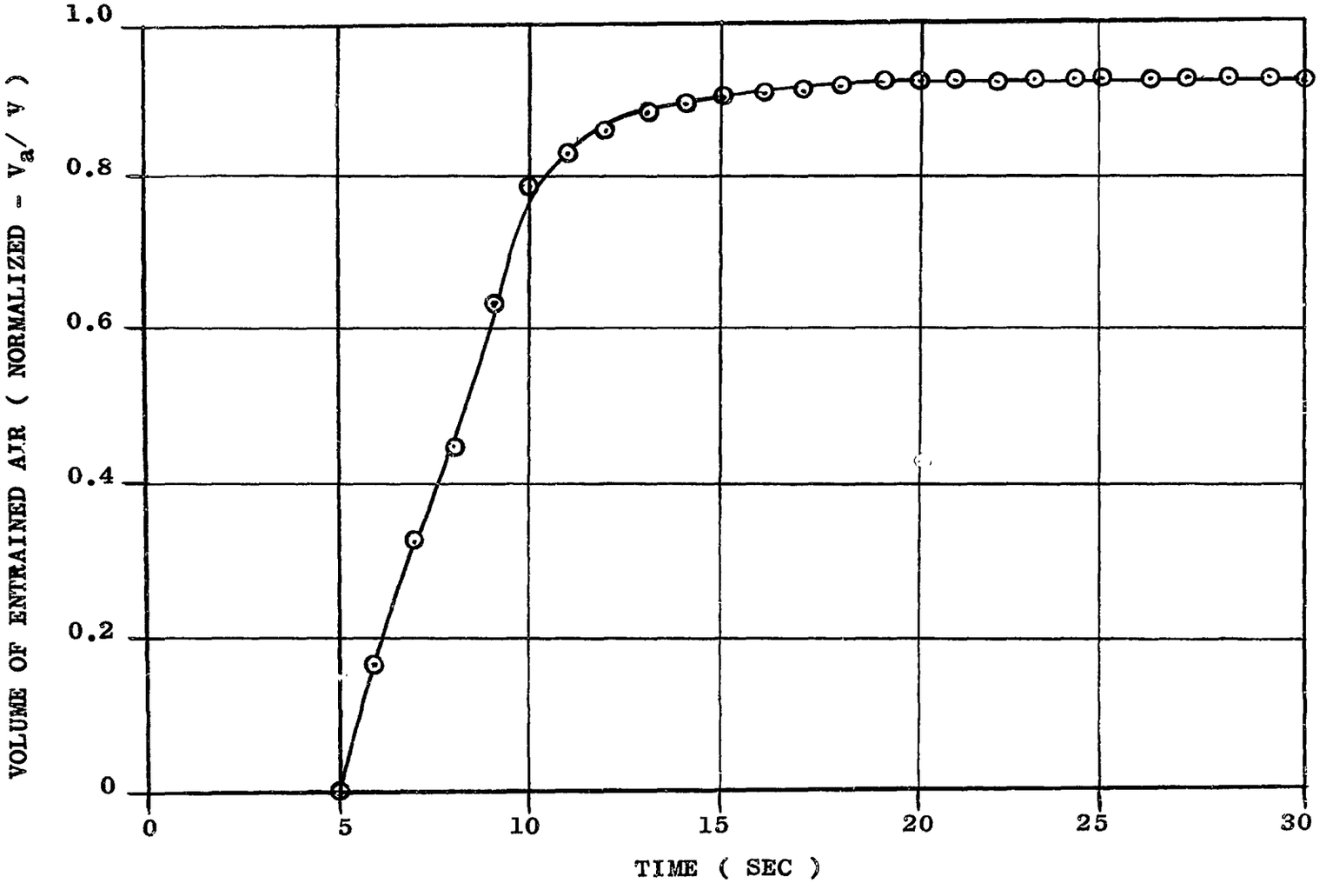

FIGURE IV-47-. VOLUME OF ENTRAINED AIR FOR RP-1/LO_2 + 1% F LIQUID PROPELLANT EXPLOSION (YIELD = 4.5 PERCENT)

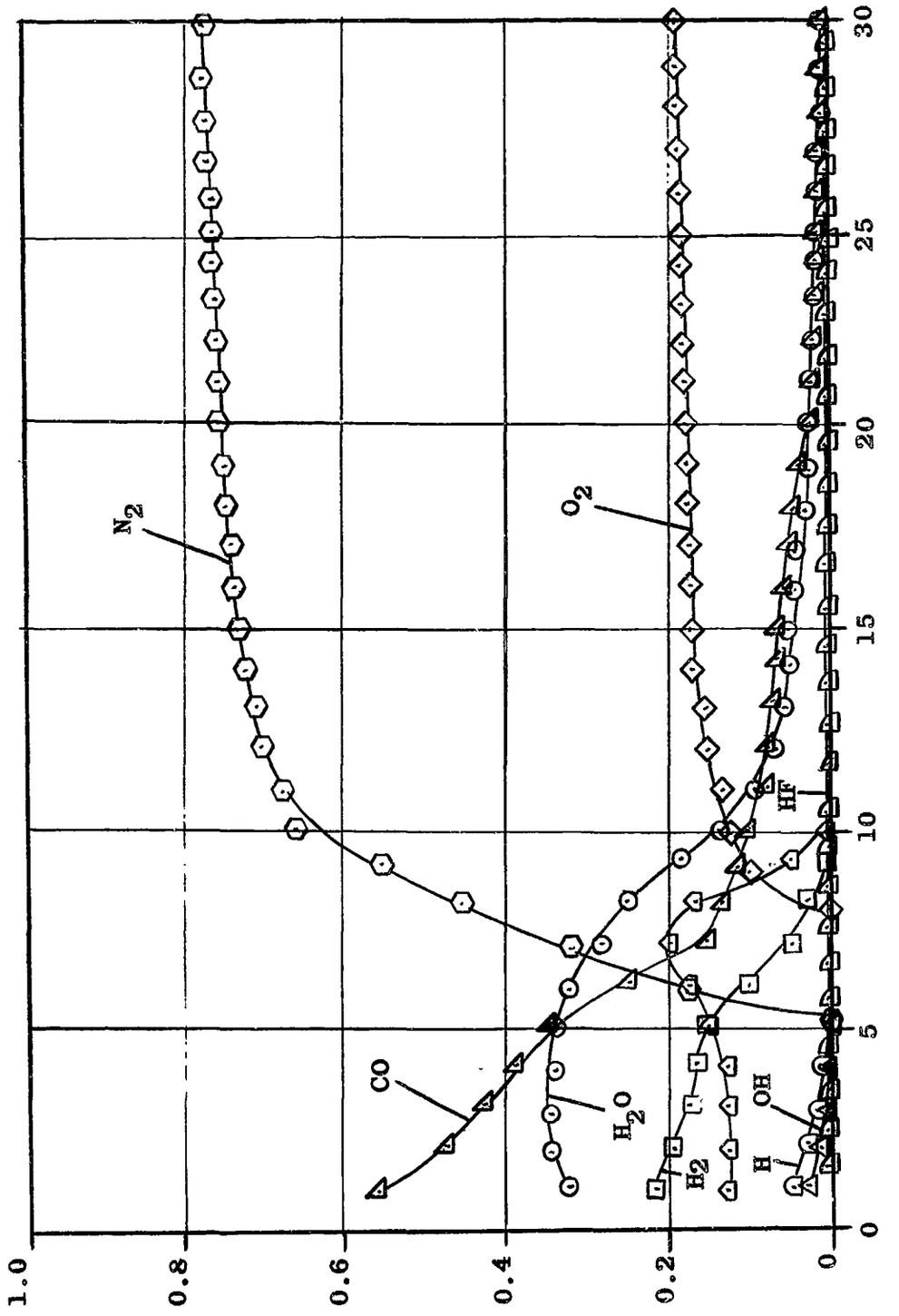

FIGURE IV-48. PARTIAL PRESSURES AND PARTIAL VOLUMES FOR RP-1/ LO_2 + 1% F
LIQUID PROPELLANT EXPLOSION PRODUCTS (YIELD = 4.5 PERCENT)

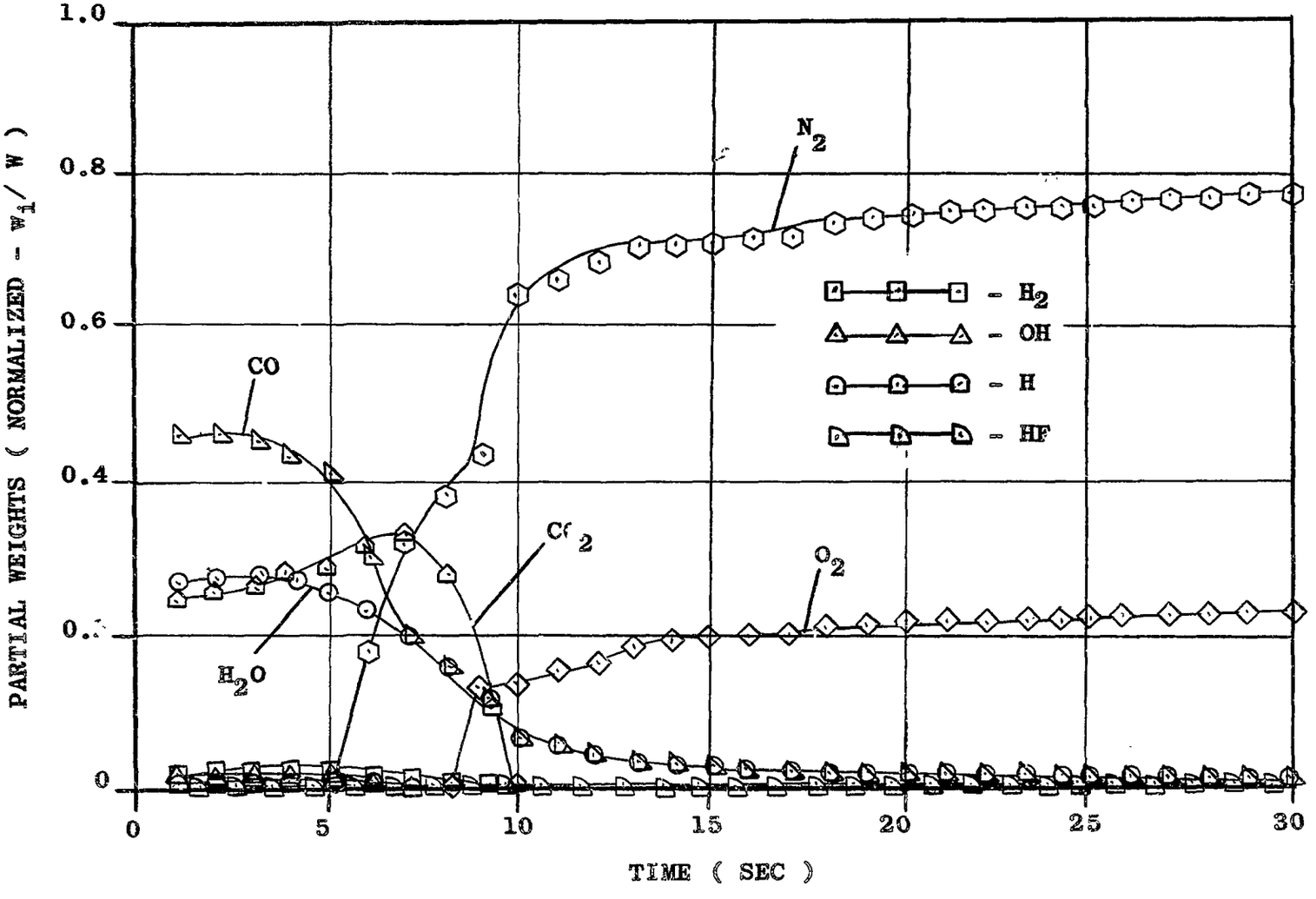

FIGURE IV-49-. WEIGHT COMPOSITION OF THE COMBUSTION PRODUCTS FROM RP-1/ LO_2 + 1% F LIQUID PROPELLANT EXPLOSION (YIELD = 4.5 PERCENT)

RP-1/LO_2 + 5% F

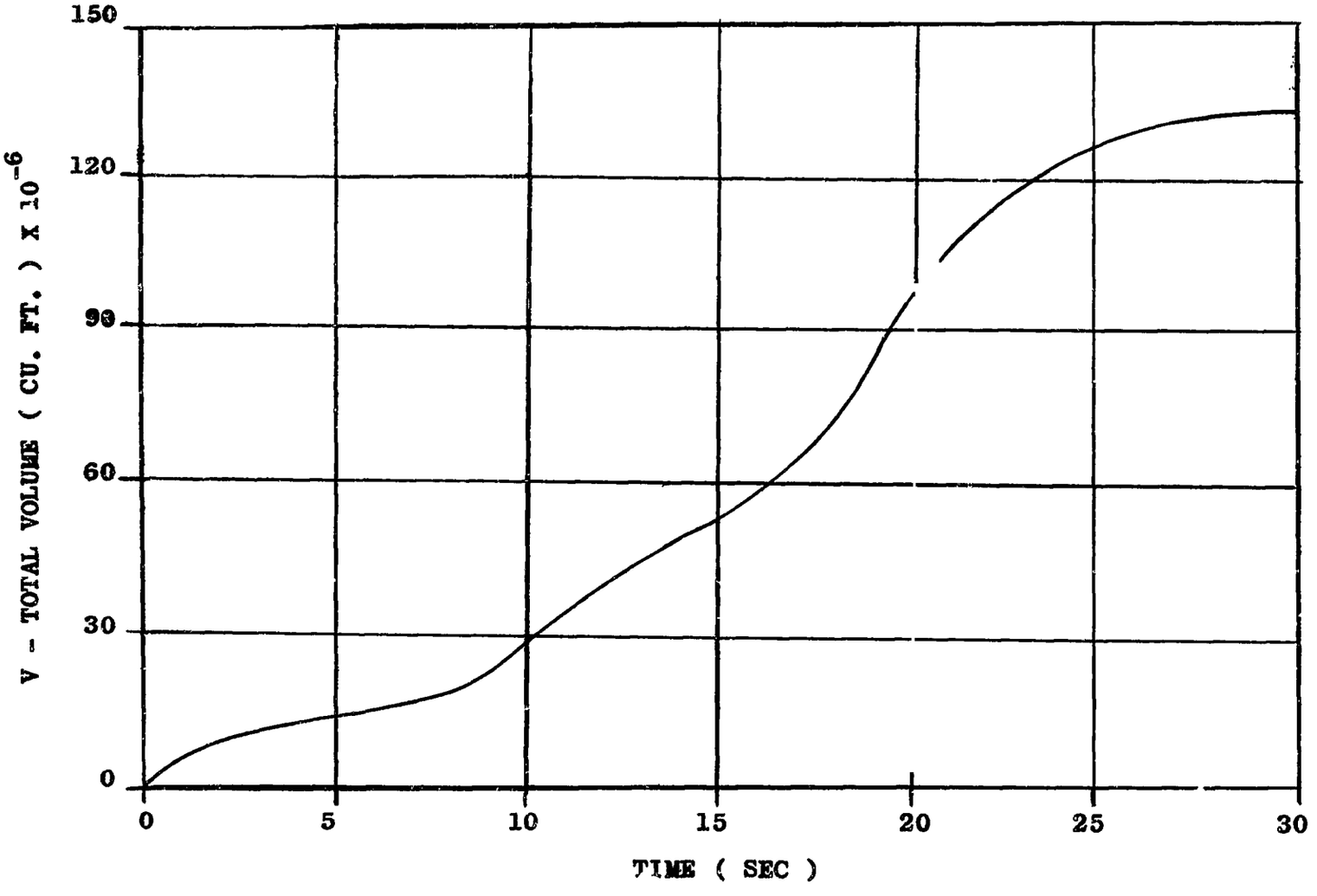

FIGURE IV-50-. VOLUME-TIME FUNCTION FOR RP-1/ LO_2 + 5% F LIQUID PROPELLANT EXPLOSION PRODUCTS (YIELD = 4.5 PERCENT)

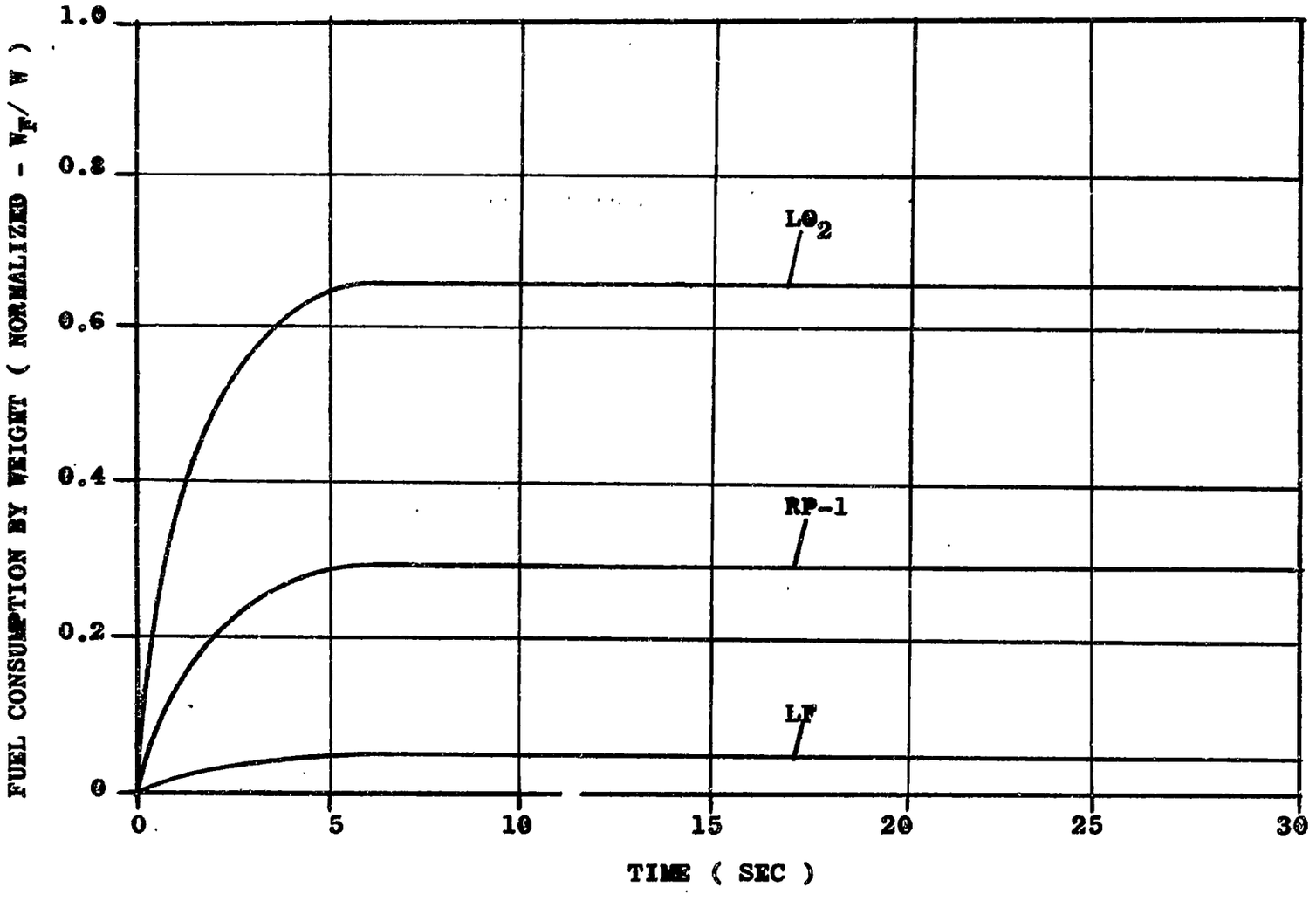

FIGURE IV-51-. FUEL CONSUMPTION FOR RP-1/ LO_2 + 5% F LIQUID PROPELLANT EXPLOSION (YIELD = 4.5 PERCENT)

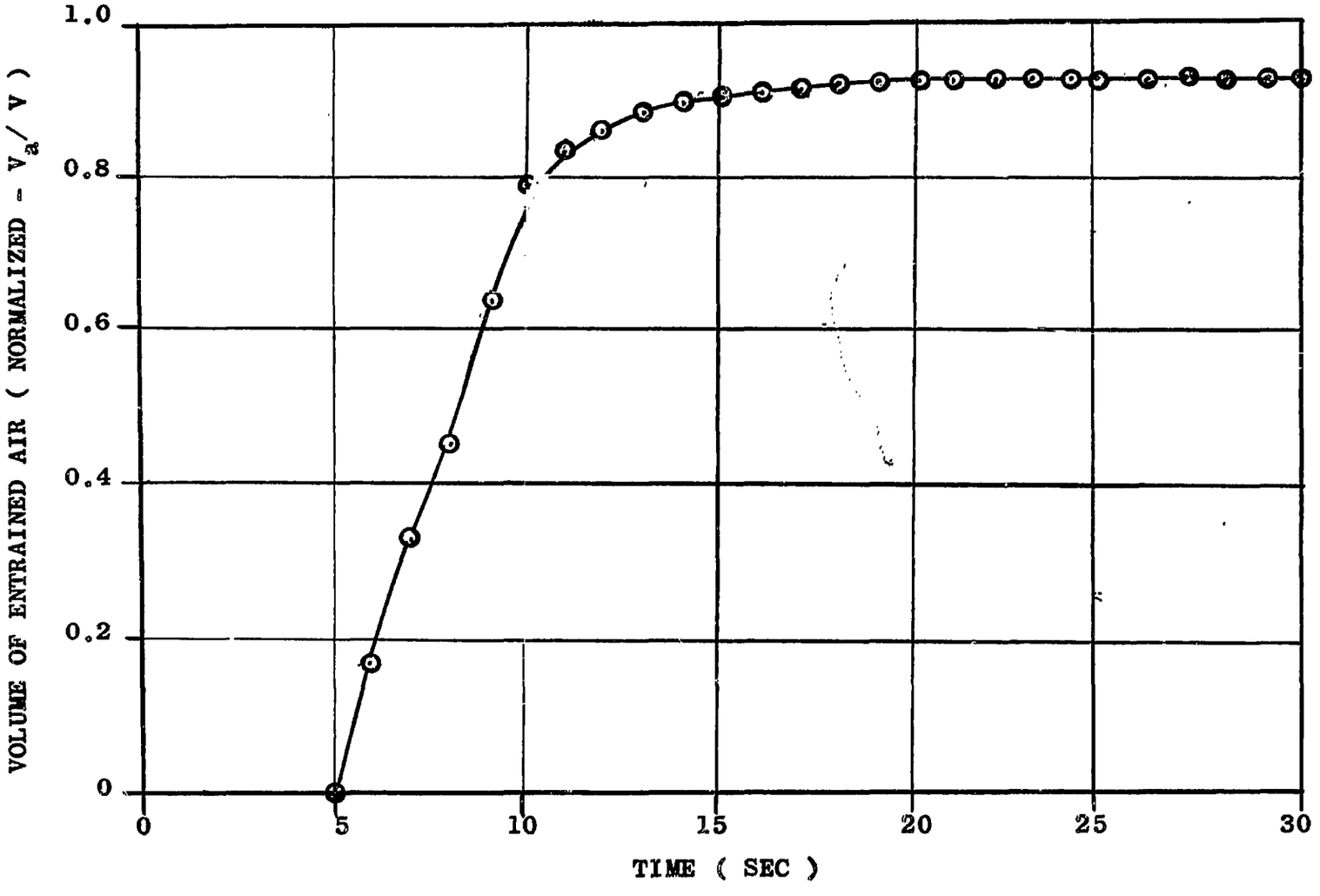

FIGURE IV-52-. VOLUME OF ENTRAINED AIR FOR RP-1/LO_2 + 5% F LIQUID PROPELLANT EXPLOSION (YIELD = 4.5 PERCENT)

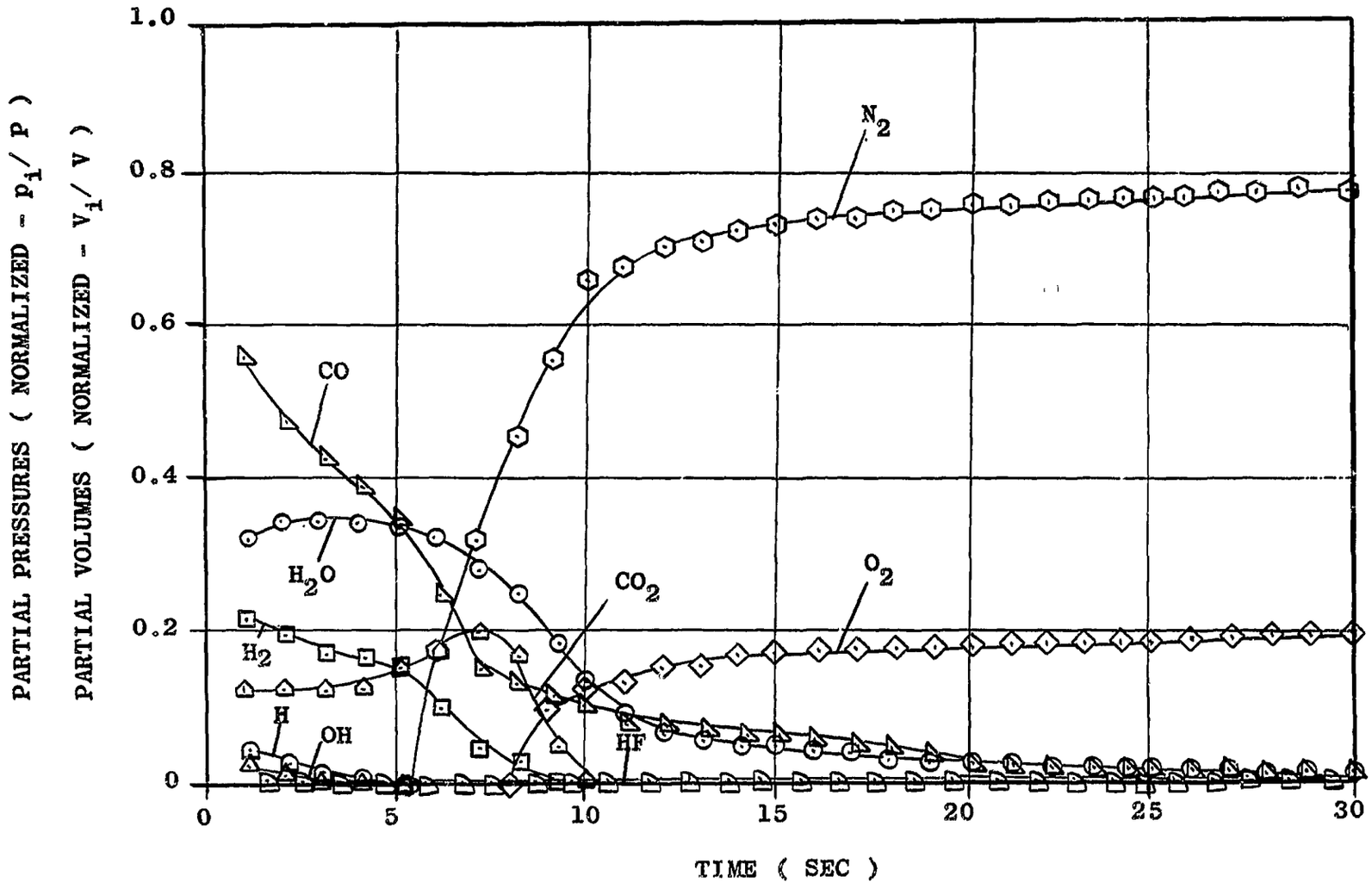

FIGURE IV-53. PARTIAL PRESSURES AND PARTIAL VOLUMES FOR RP-1/ LO_2 + 5% F LIQUID PROPELLANT EXPLOSION PRODUCTS (YIELD = 4.5 PERCENT)

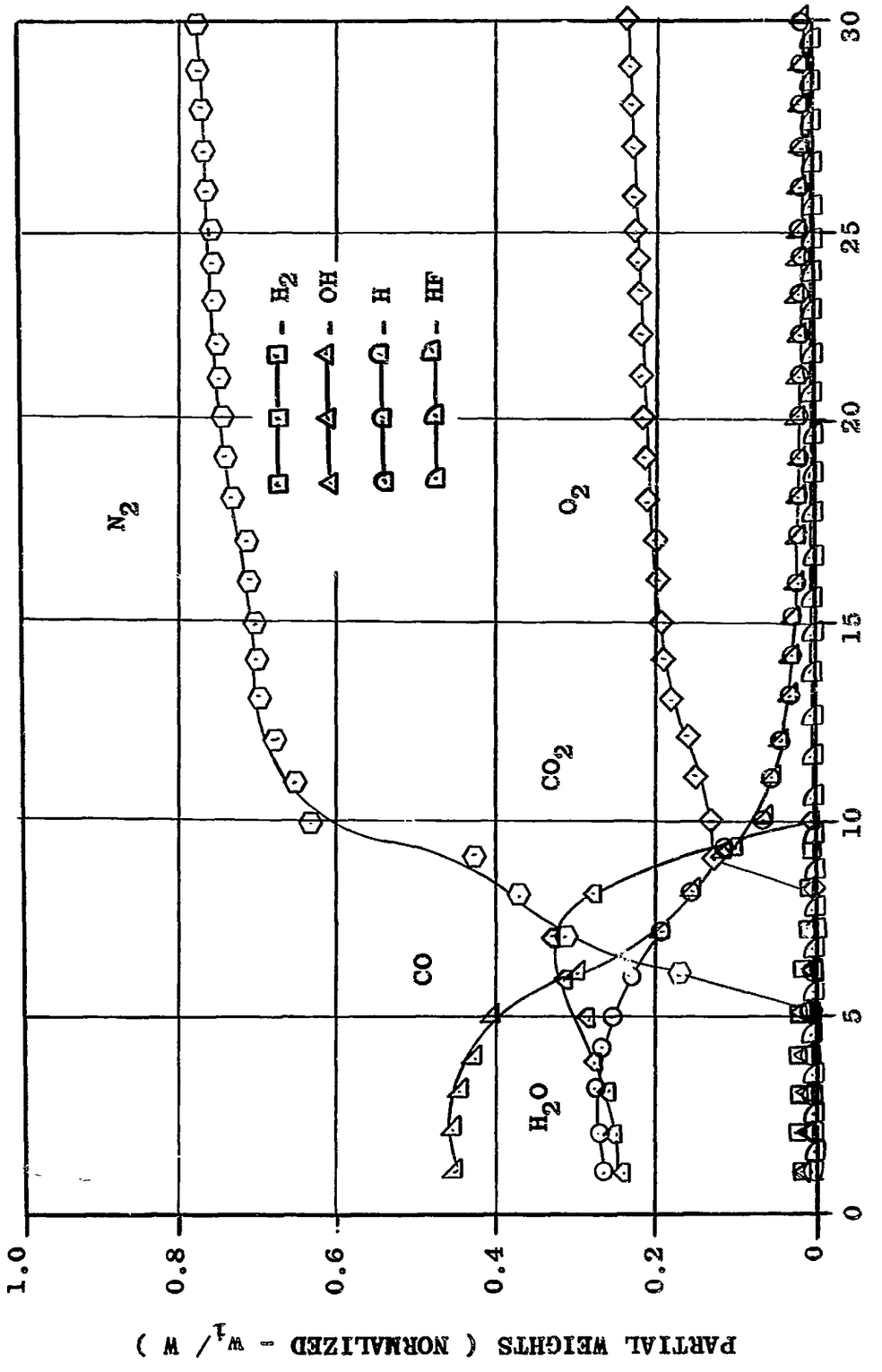

FIGURE IV-54 - WEIGHT COMPOSITION OF THE COMBUSTION PRODUCTS FROM RP-1/LO_2+ 5%F LIQUID PROPELLANT EXPLOSION (YIELD = 4.5 PERCENT)

$RP\text{-}1/LO_2$ + 10% F

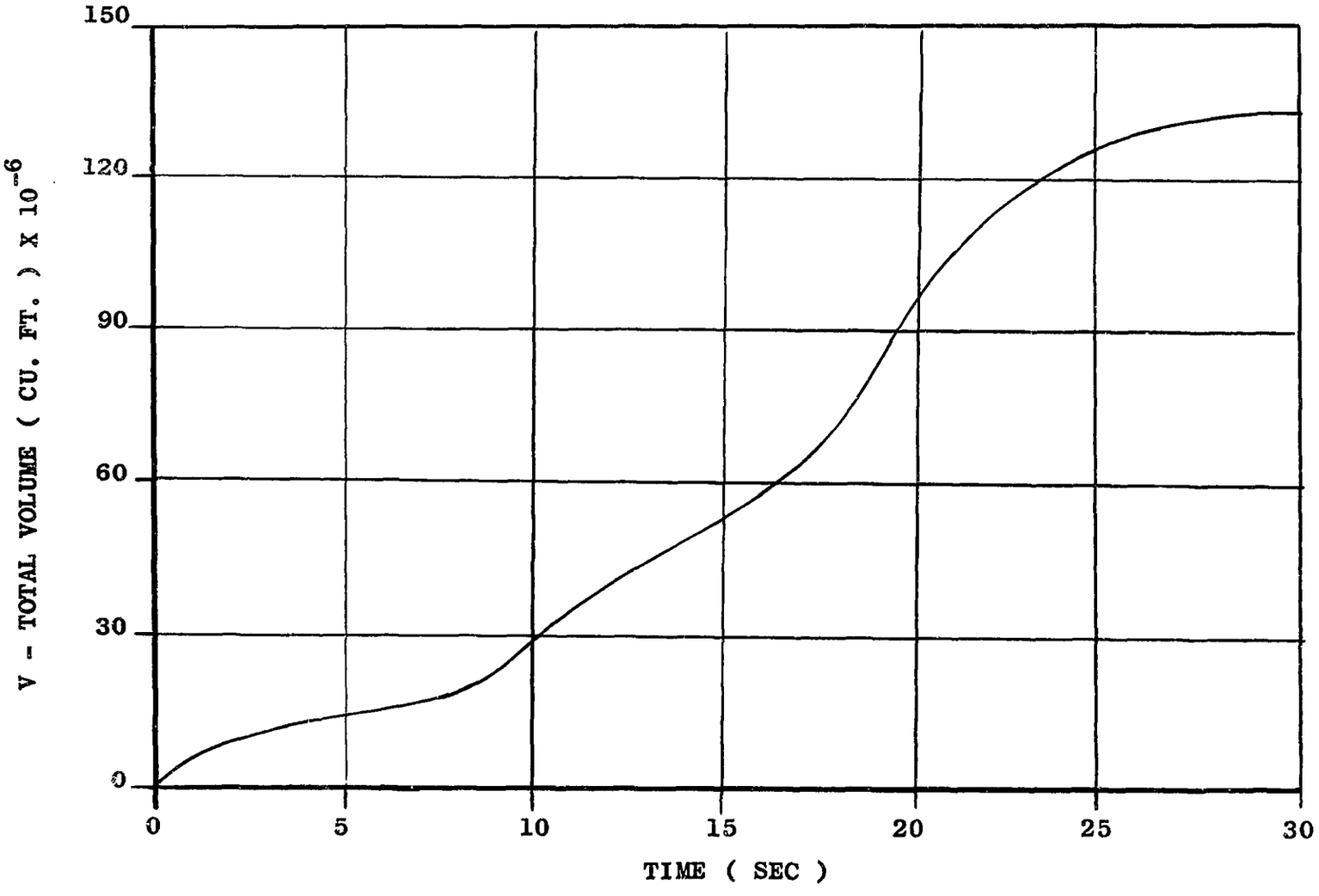

FIGURE IV-55-. VOLUME-TIME FUNCTION FOR RP-1/LO_2 + 10% F LIQUID PROPELLANT EXPLOSION PRODUCTS (YIELD = 4.5 PERCENT)

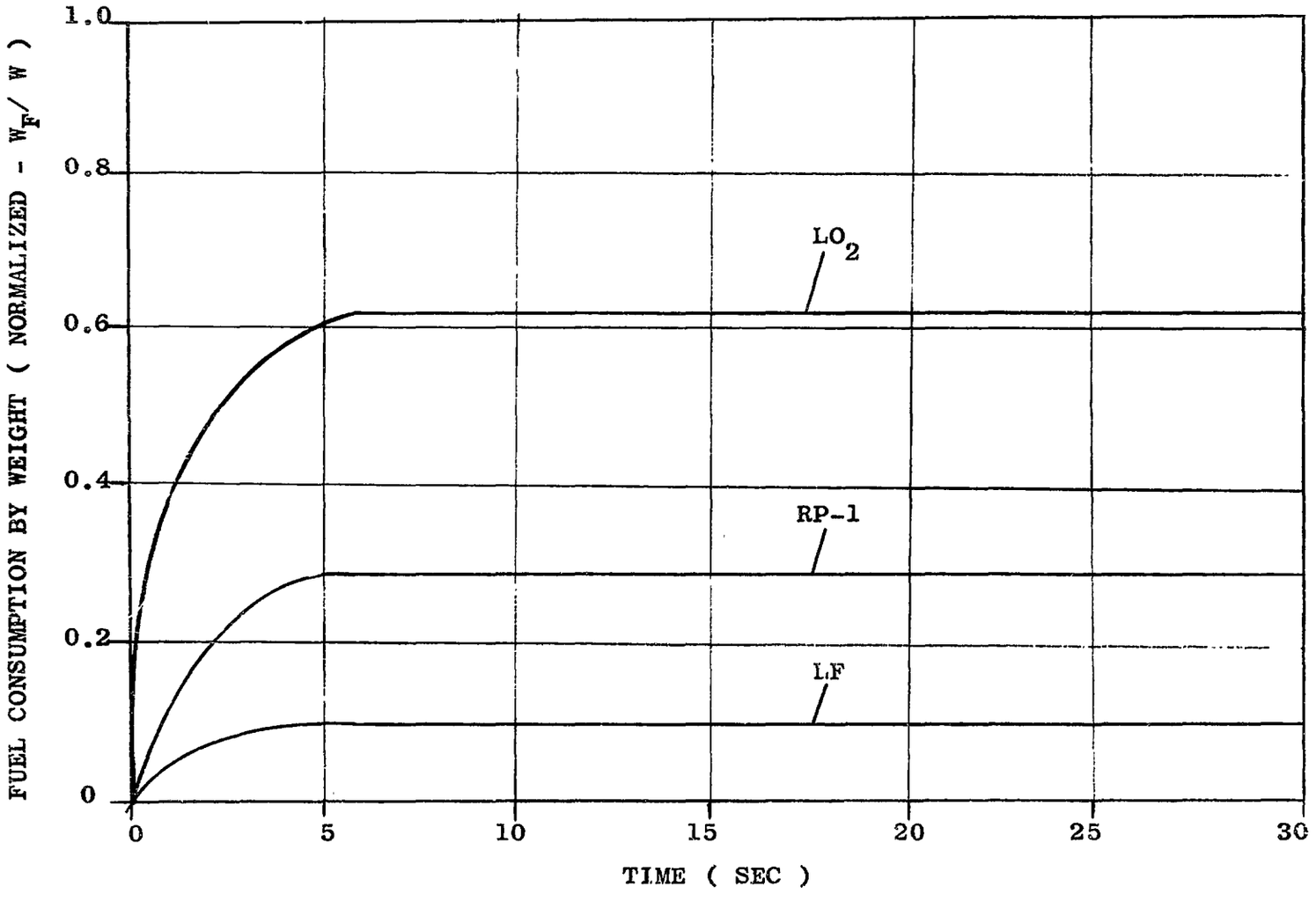

FIGURE IV-56-. FUEL CONSUMPTION FOR RP-1/LO_2 + 10% F LIQUID PROPELLANT EXPLOSION (YIELD = 4.5 PERCENT)

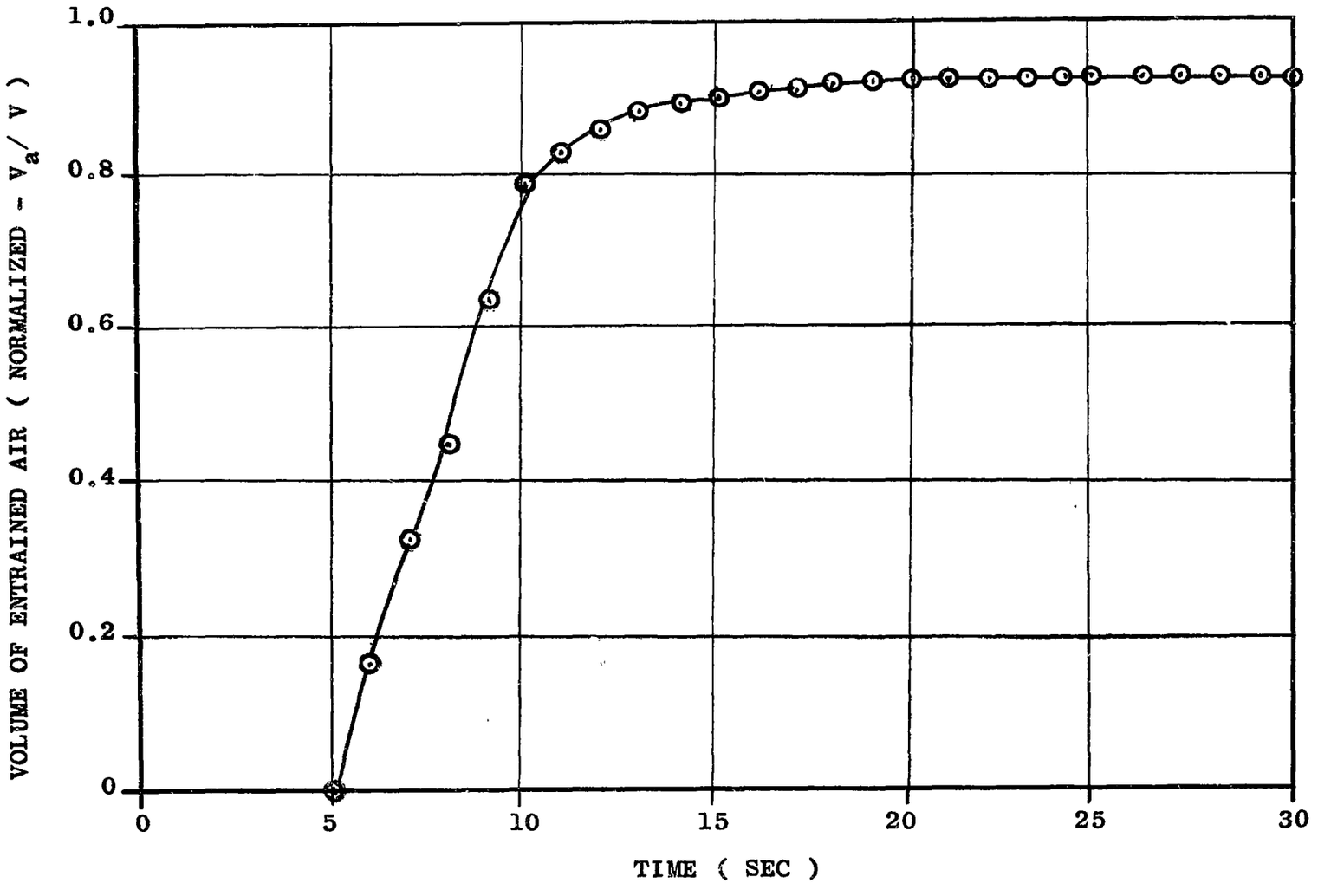

FIGURE IV-57-. VOLUME OF ENTRAINED AIR FOR RP-1/LO_2 + 10% F LIQUID PROPELLANT EXPLOSION (YIELD = 4.5 PERCENT)

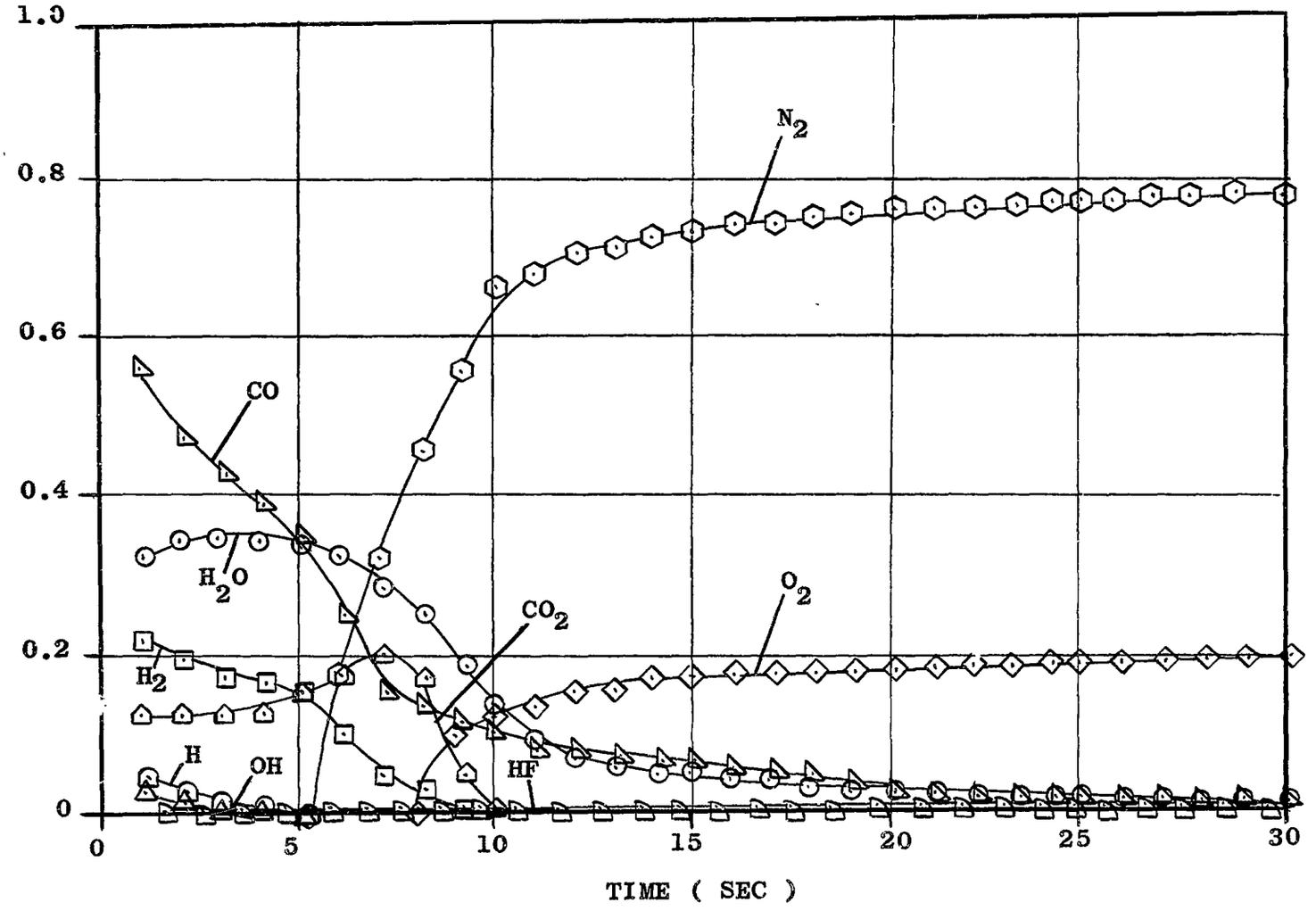

FIGURE IV-58-. PARTIAL PRESSURES AND PARTIAL VOLUMES FOR RP-1/LO_2 + 10% F LIQUID PROPELLANT EXPLOSION PRODUCTS (YIELD = 4.5 PERCENT)

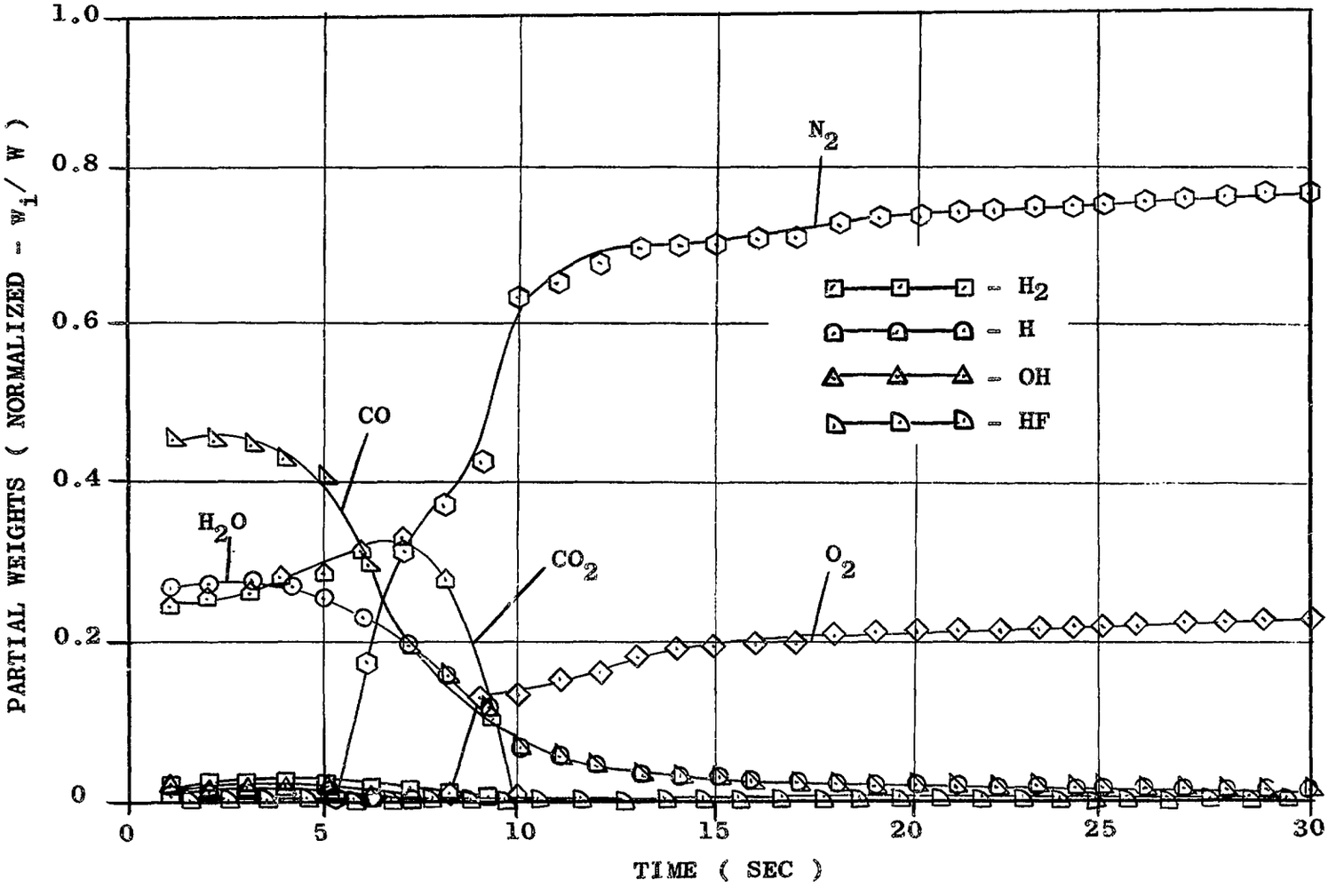

FIGURE IV-59. WEIGHT COMPOSITION OF THE COMBUSTION PRODUCTS FROM RP-1/LO_2+ 10% F LIQUID PROPELLANT EXPLOSION (YIELD = 4.5 PERCENT)

$LH_2/RP\text{-}1/LO_2$ + 1% F

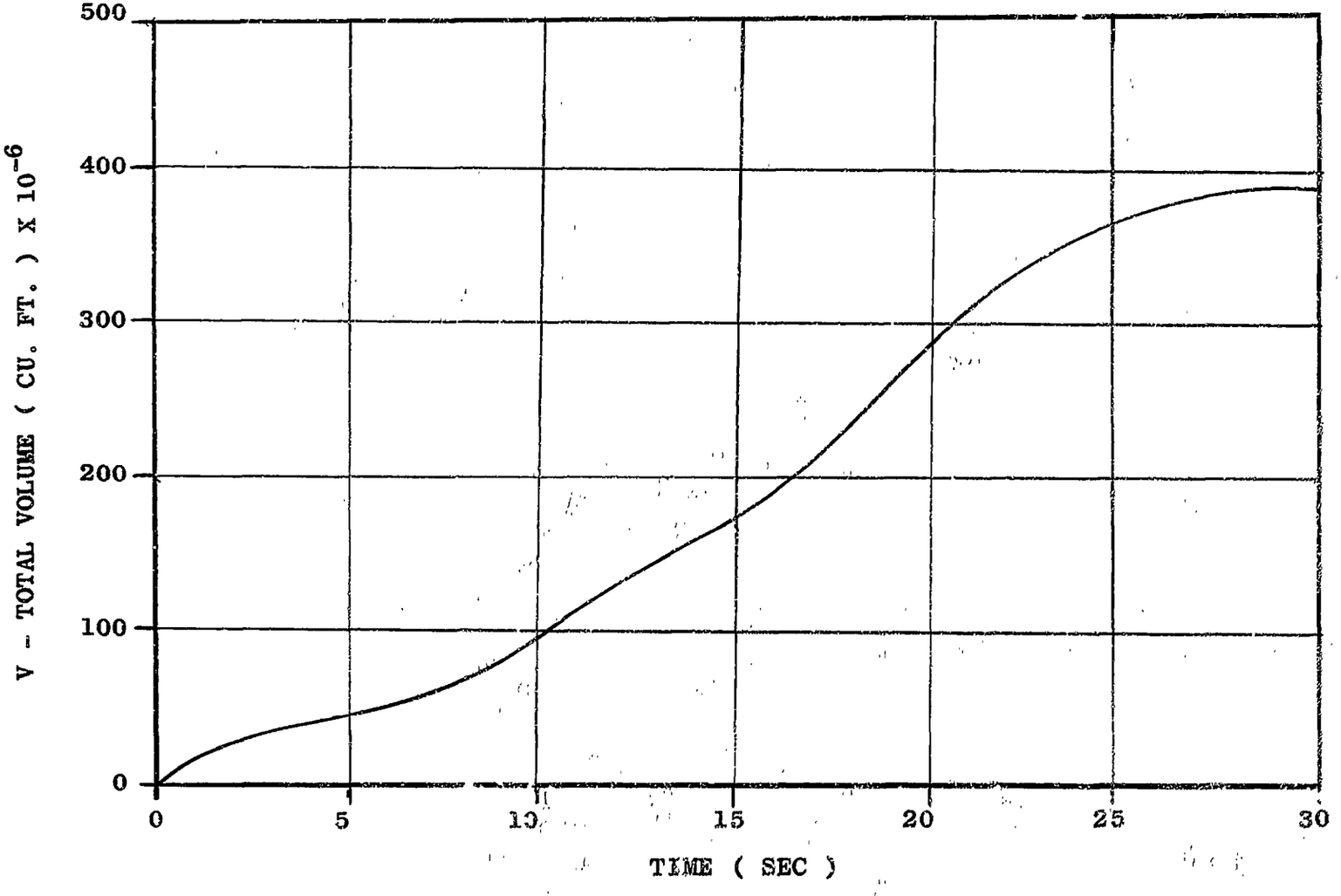

FIGURE IV-60-. VOLUME-TIME FUNCTION FOR $LH_2/RP\text{-}1/LO_2$ + 1% F LIQUID PROPELLANT EXPLOSION PRODUCTS (YIELD = 4.5 PERCENT)

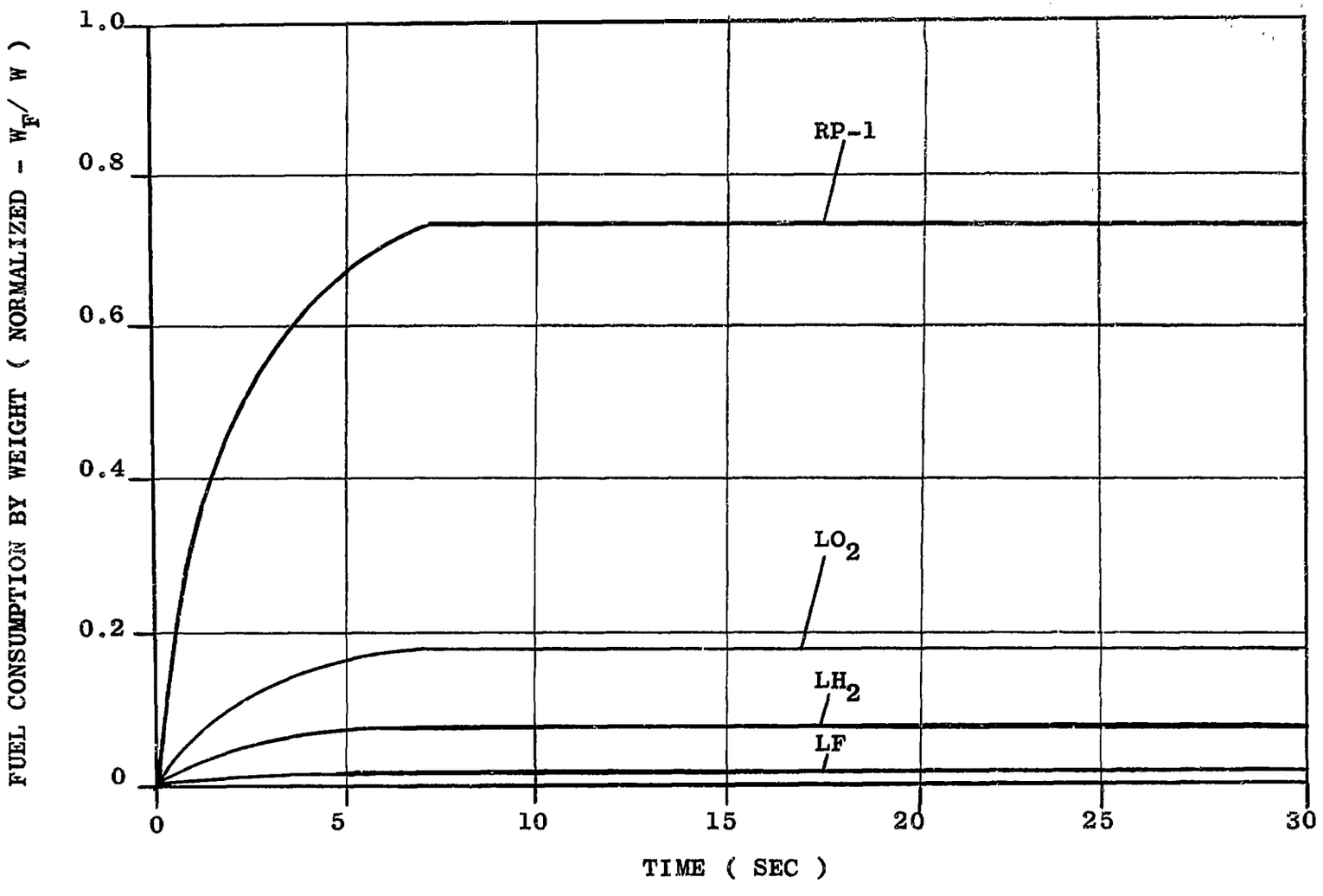

FIGURE IV-61-. FUEL CONSUMPTION FOR $LH_2/RP\text{-}1/LO_2$ + 1% F LIQUID PROPELLANT EXPLOSION (YIELD = 4.5 PERCENT)

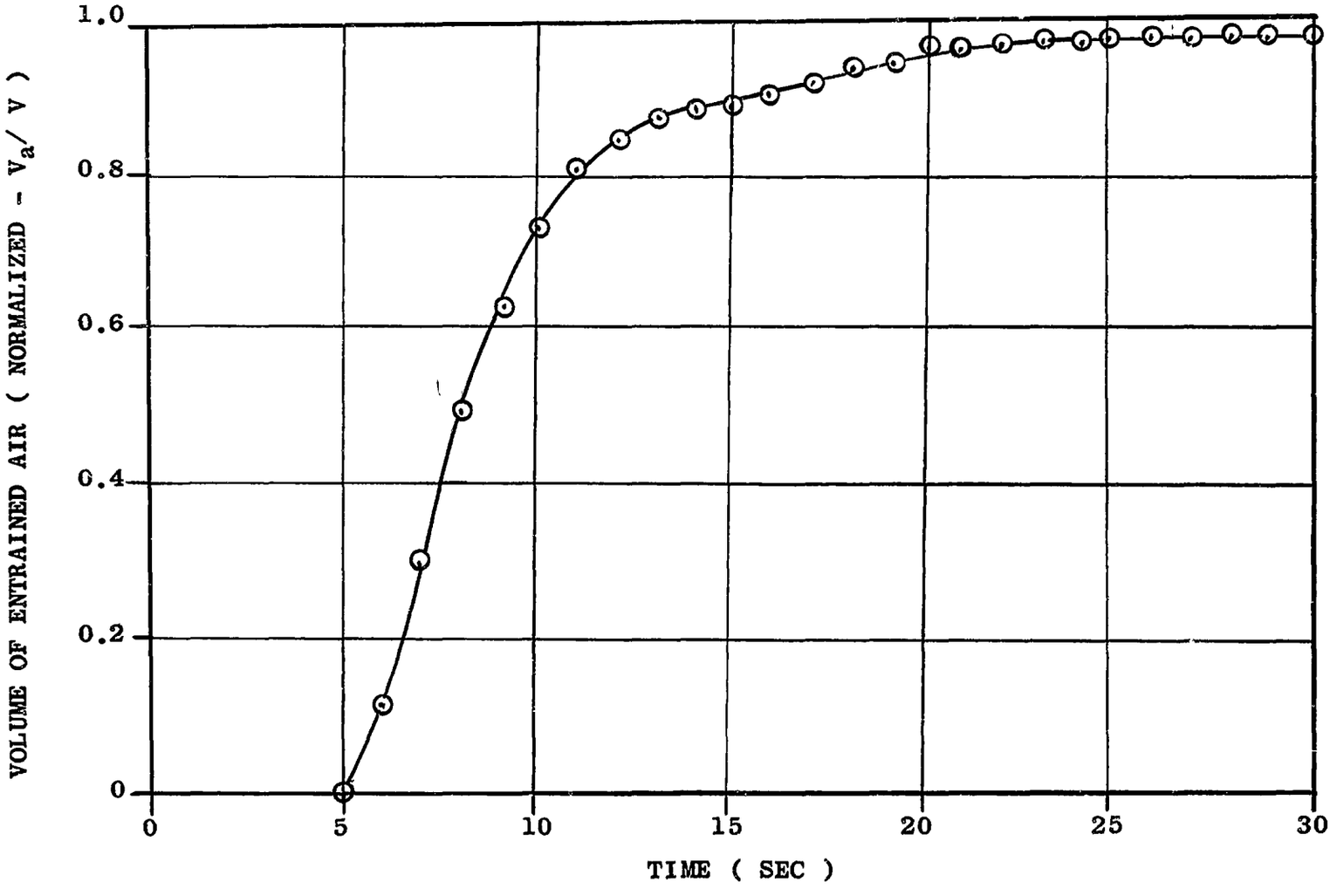

FIGURE IV-62-. VOLUME OF ENTRAINED AIR FOR $LH_2/RP\text{-}1/LO_2$ + 1% F LIQUID PROPELLANT EXPLOSION (YIELD = 4.5 PERCENT)

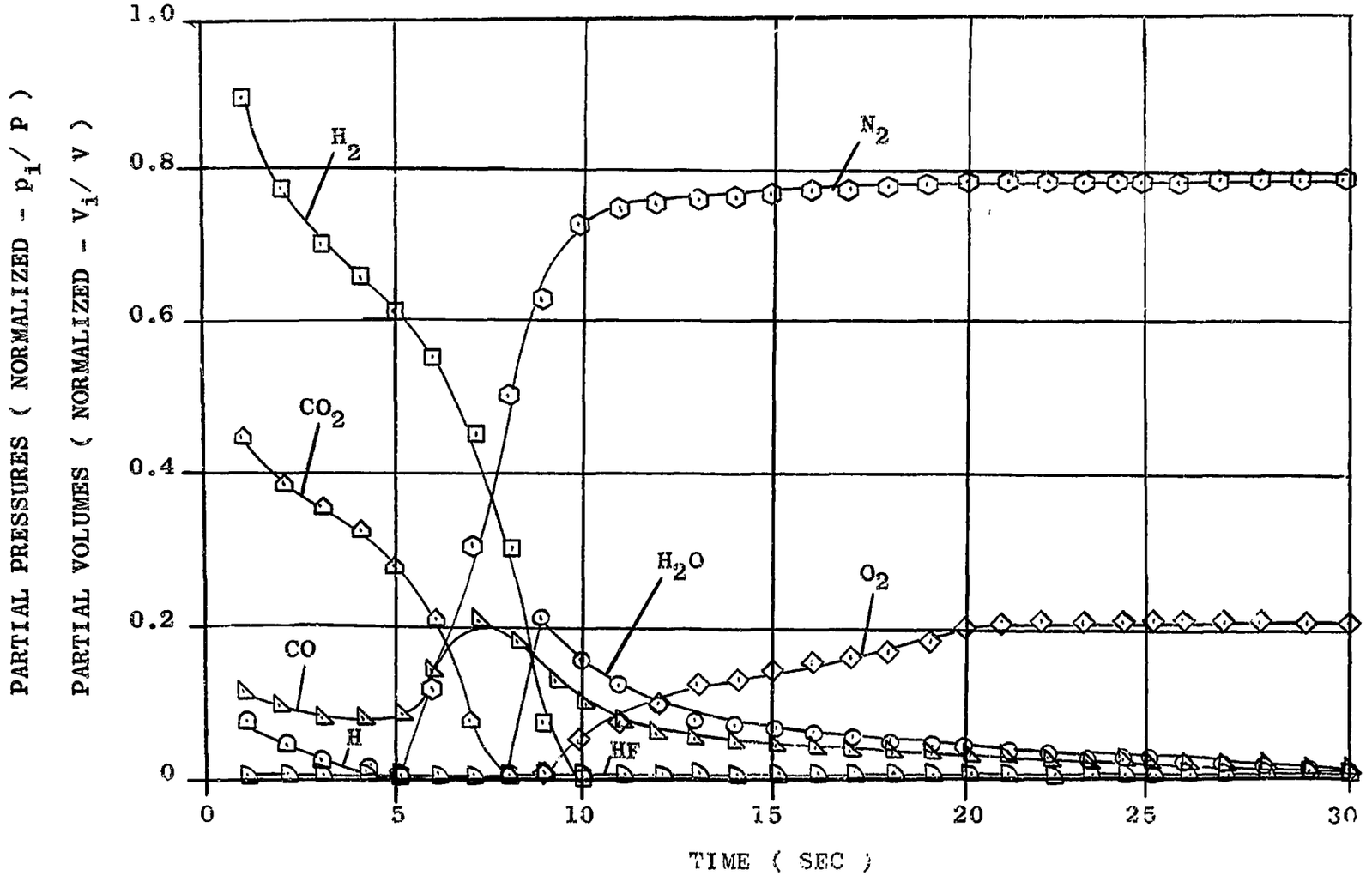

FIGURE IV-63. PARTIAL PRESSURES AND PARTIAL VOLUMES FOR LH_2/RP-1/LO_2 + 1% F LIQUID PROPELLANT EXPLOSION PRODUCTS (YIELD = 4.5 PERCENT)

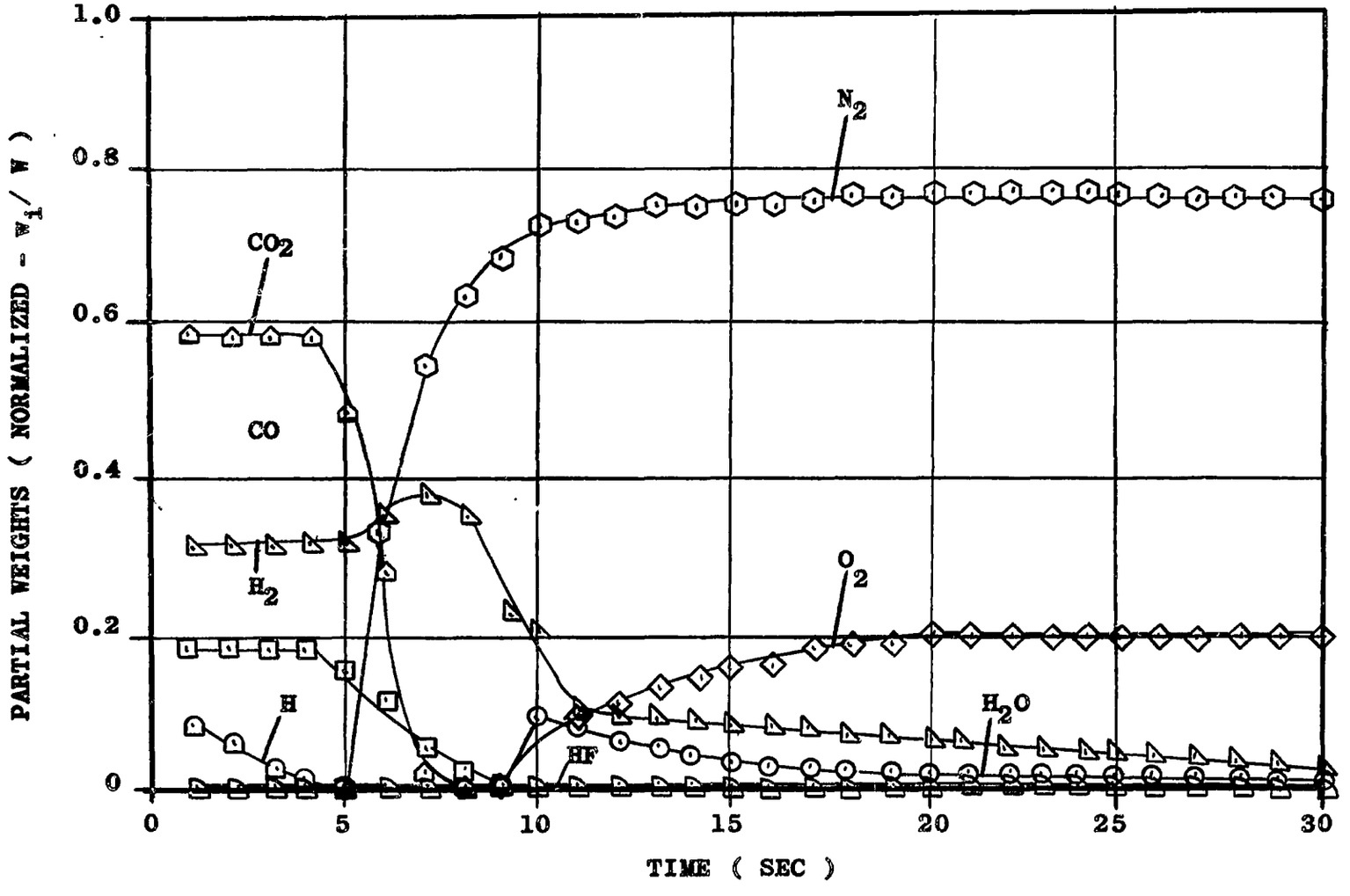

FIGURE IV-64-. WEIGHT COMPOSITION OF THE COMBUSTION PRODUCTS FROM $LH_2/RP\text{-}1/LO_2$+ 1% F LIQUID PROPELLANT EXPLOSION (YIELD = 4.5 PERCENT)

$LH_2/RP\text{-}1/LO_2$ + 5% F

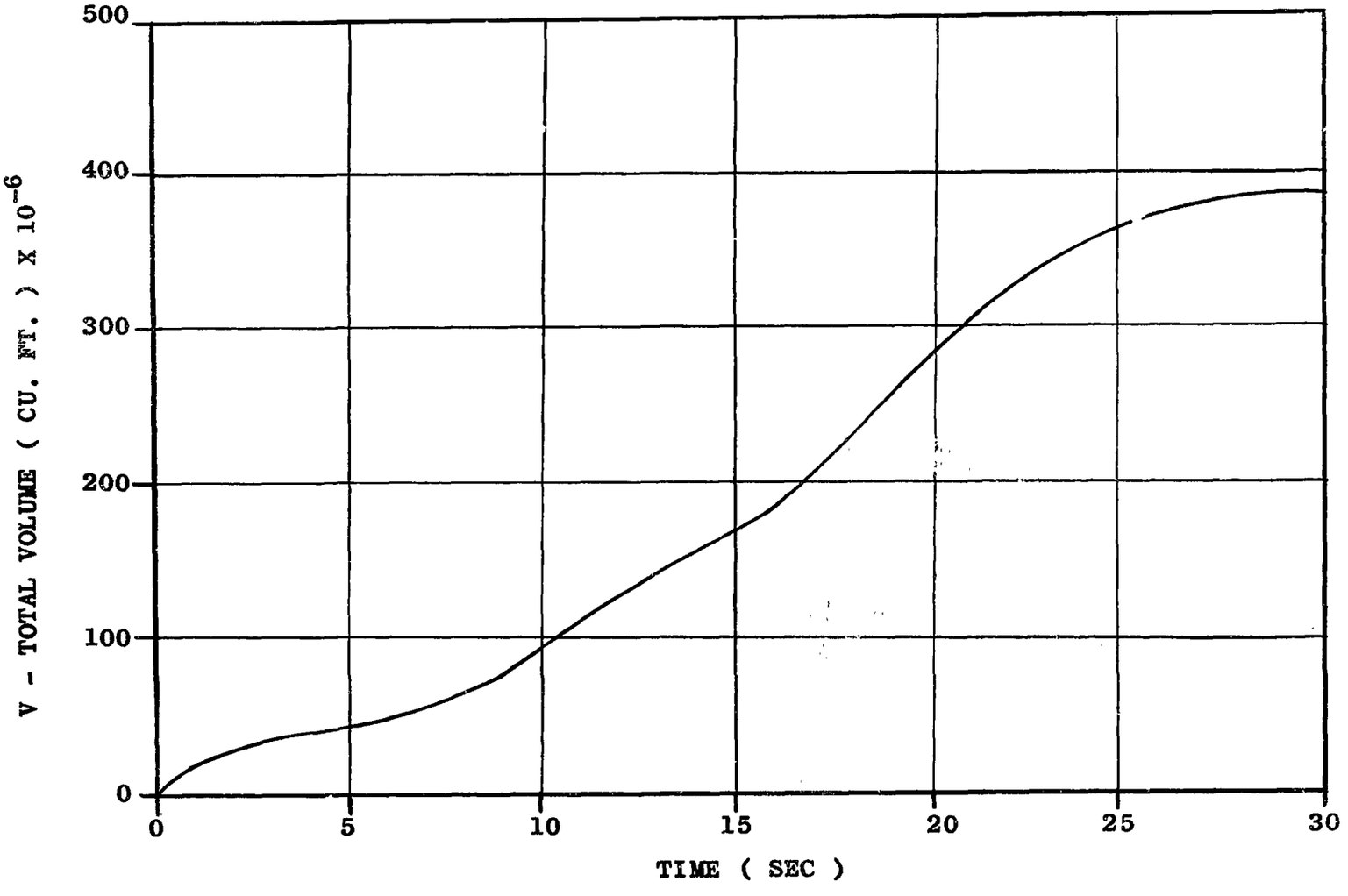

FIGURE IV-65-. VOLUME-TIME FUNCTION FOR $LH_2/RP\text{-}1/LO_2$ + 5% F LIQUID PROPELLANT EXPLOSION PRODUCTS (YIELD = 4.5 PERCENT)

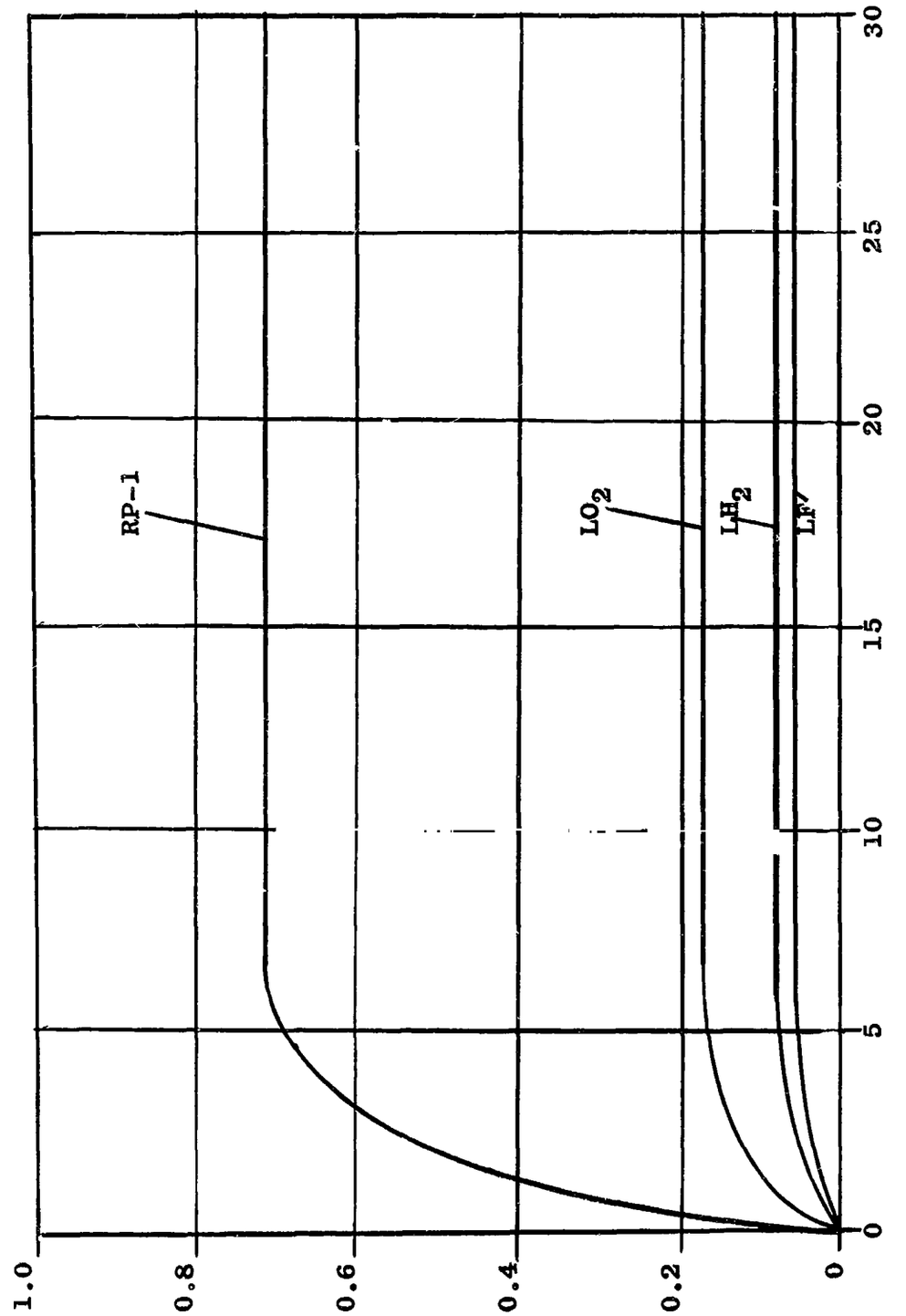

FIGURE IV-66-. FUEL CONSUMPTION FOR LH_2/RP-1/LO_2 + 5% F LIQUID PROPELLANT EXPLOSION (YIELD = 4.5 PERCENT)

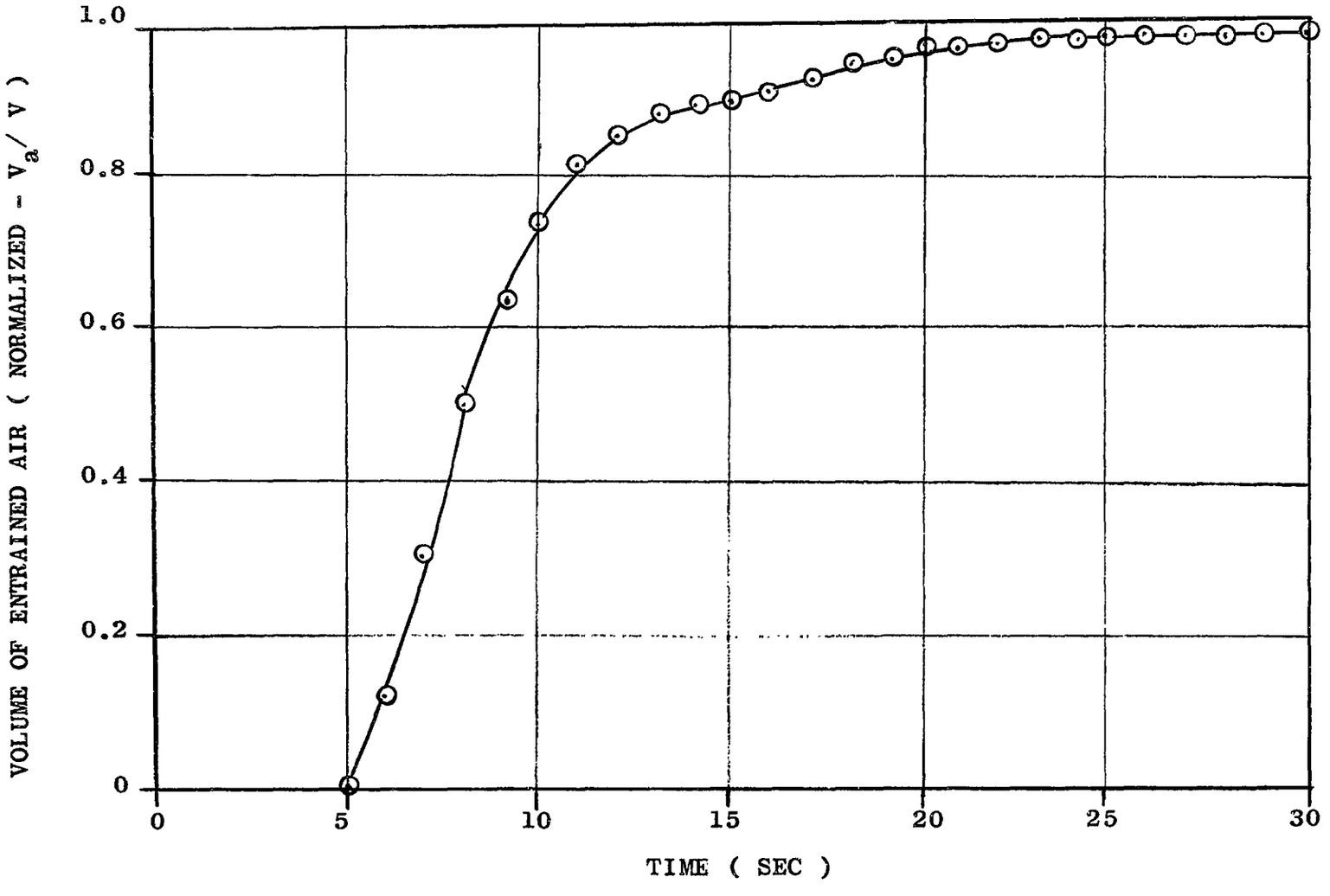

FIGURE IV-67-. VOLUME OF ENTRAINED AIR FOR $LH_2/RP\text{-}1/LO_2$ + 5% F LIQUID PROPELLANT EXPLOSION (YIELD = 4.5 PERCENT)

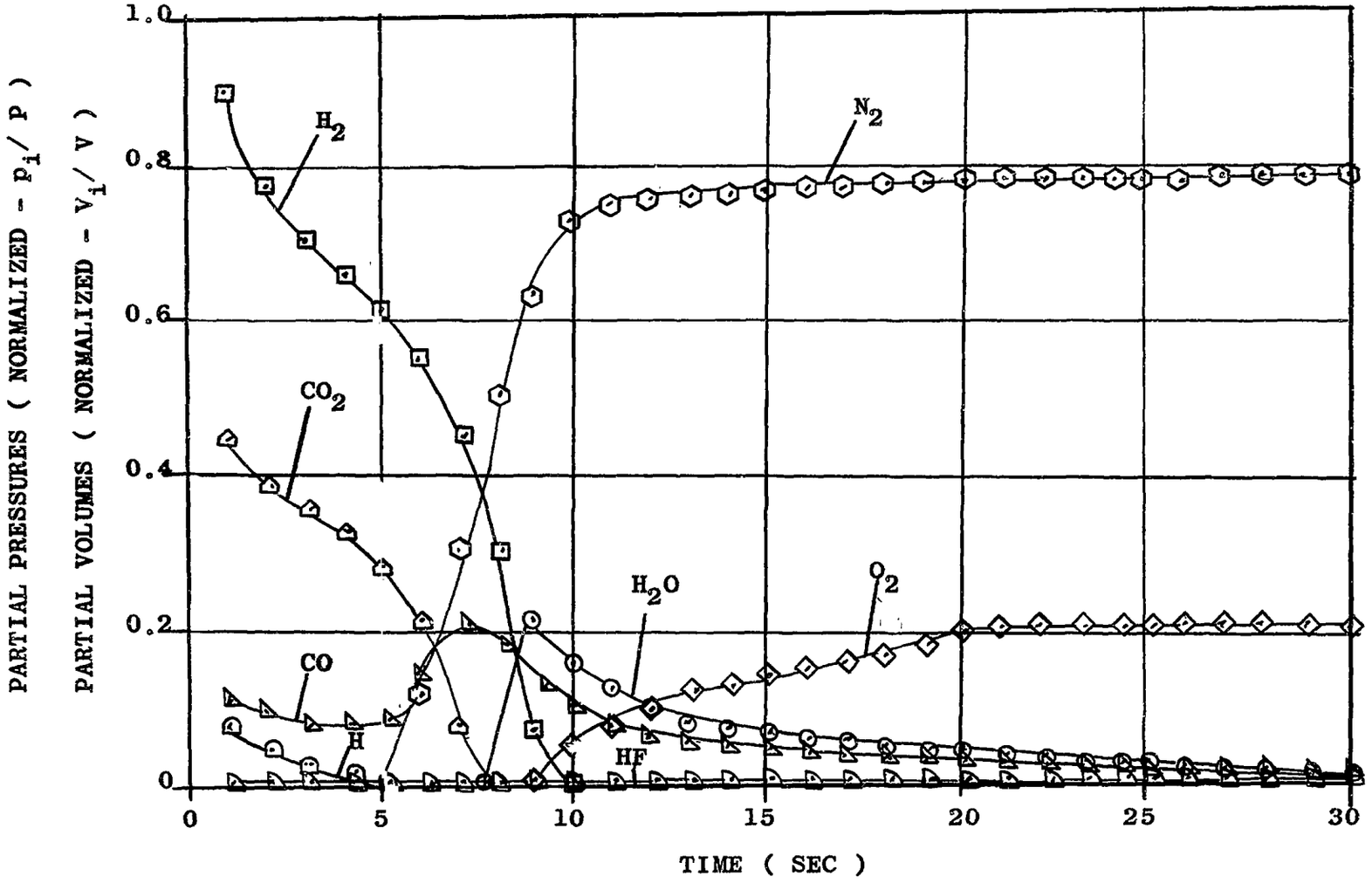

FIGURE IV-68-. PARTIAL PRESSURES AND PARTIAL VOLUMES FOR LH_2/RP-1/LO_2 + 5% F LIQUID PROPELLANT EXPLOSION PRODUCTS (YIELD = 4.5 PERCENT)

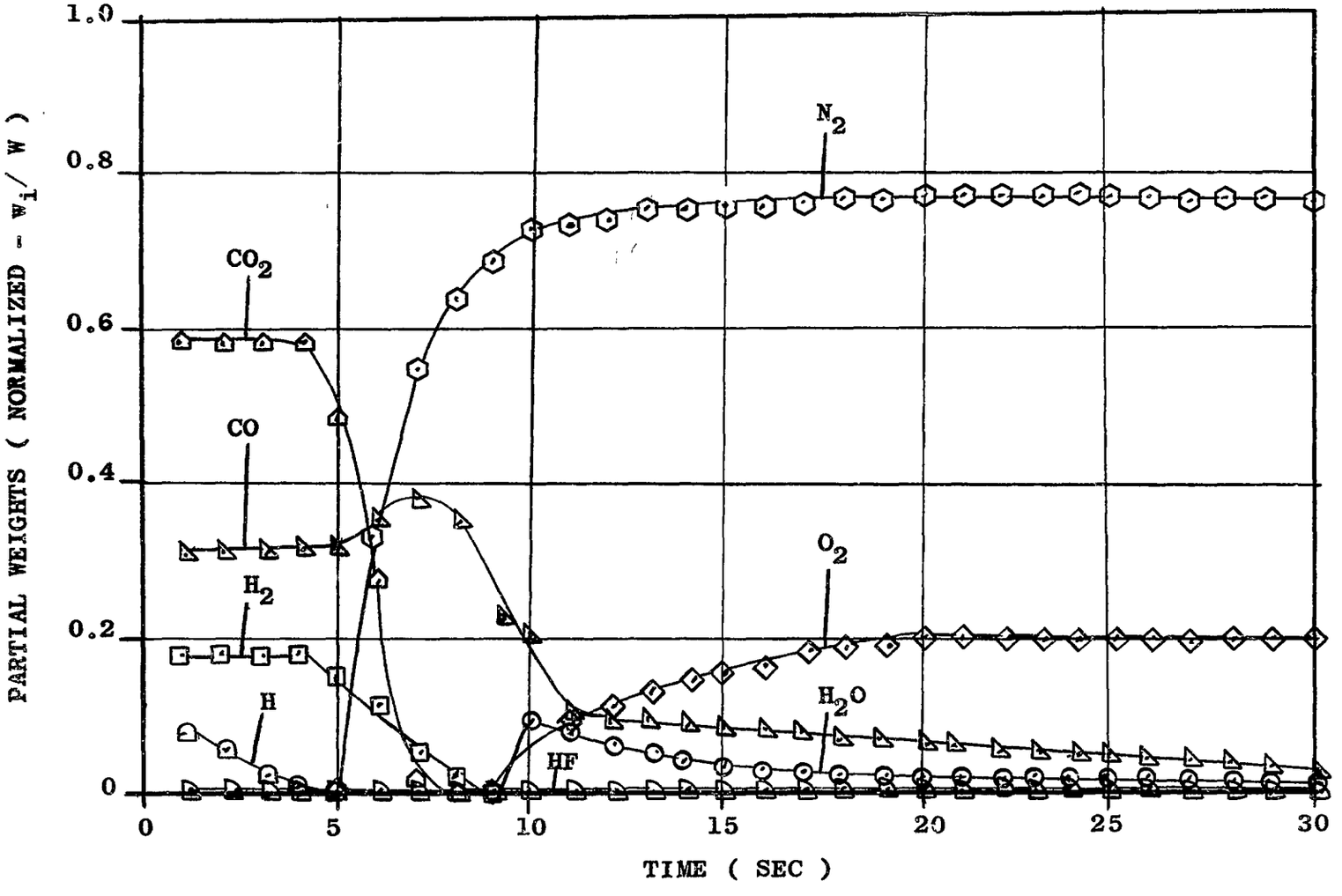

FIGURE IV-69-. WEIGHT COMPOSITION OF THE COMBUSTION PRODUCTS FROM LH_2/RP-1/LO_2+ 5%F LIQUID PROPELLANT EXPLOSION (YIELD = 4.5 PERCENT)

$LH_2/RP\text{-}i/LO_2$ + 10% F

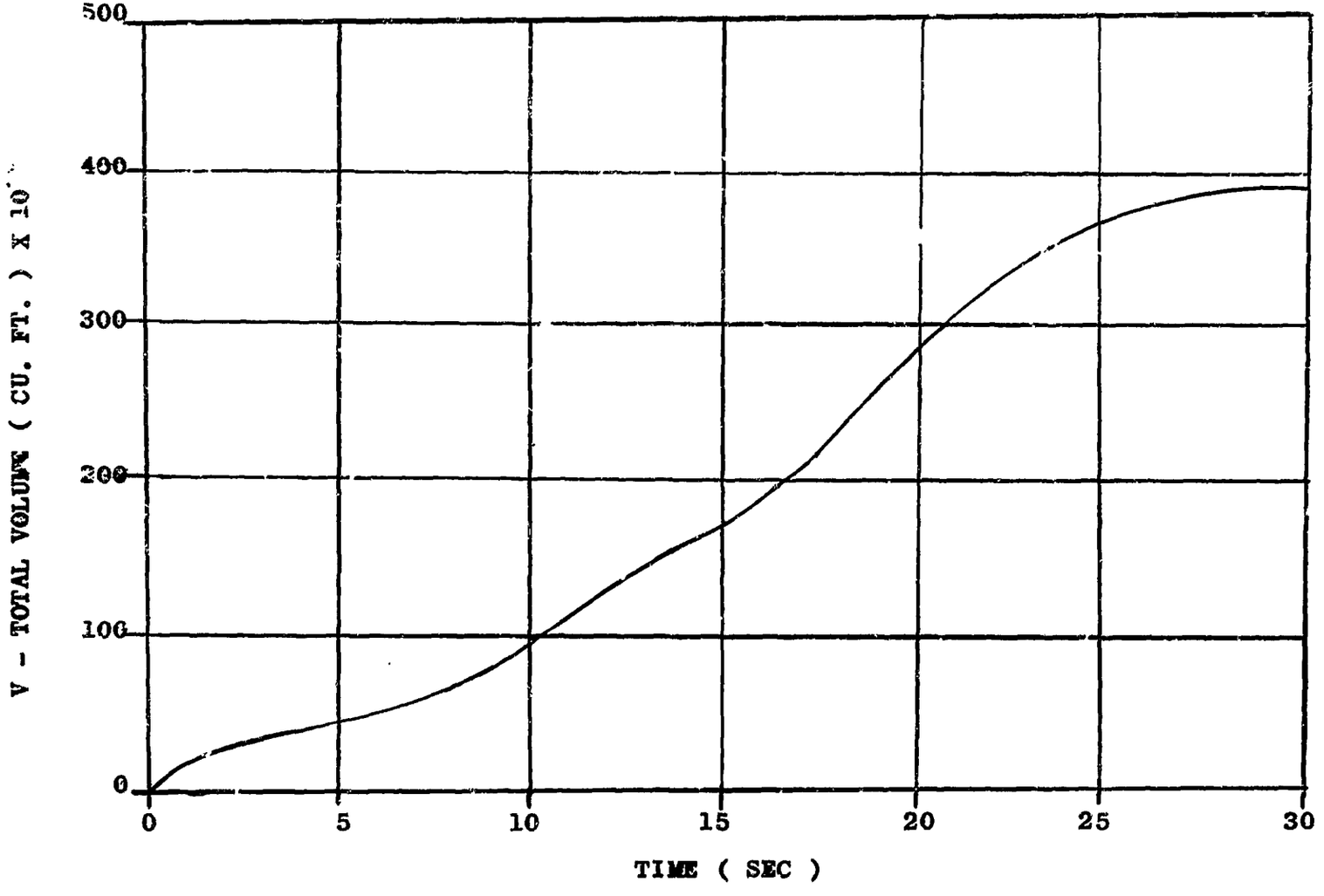

FIGURE IV-70. VOLUME-TIME FUNCTION FOR $LH_2/RP\text{-}1/LO_2$ + 10% F LIQUID PROPELLANT EXPLOSION PRODUCTS (YIELD = 4.5 PERCENT)

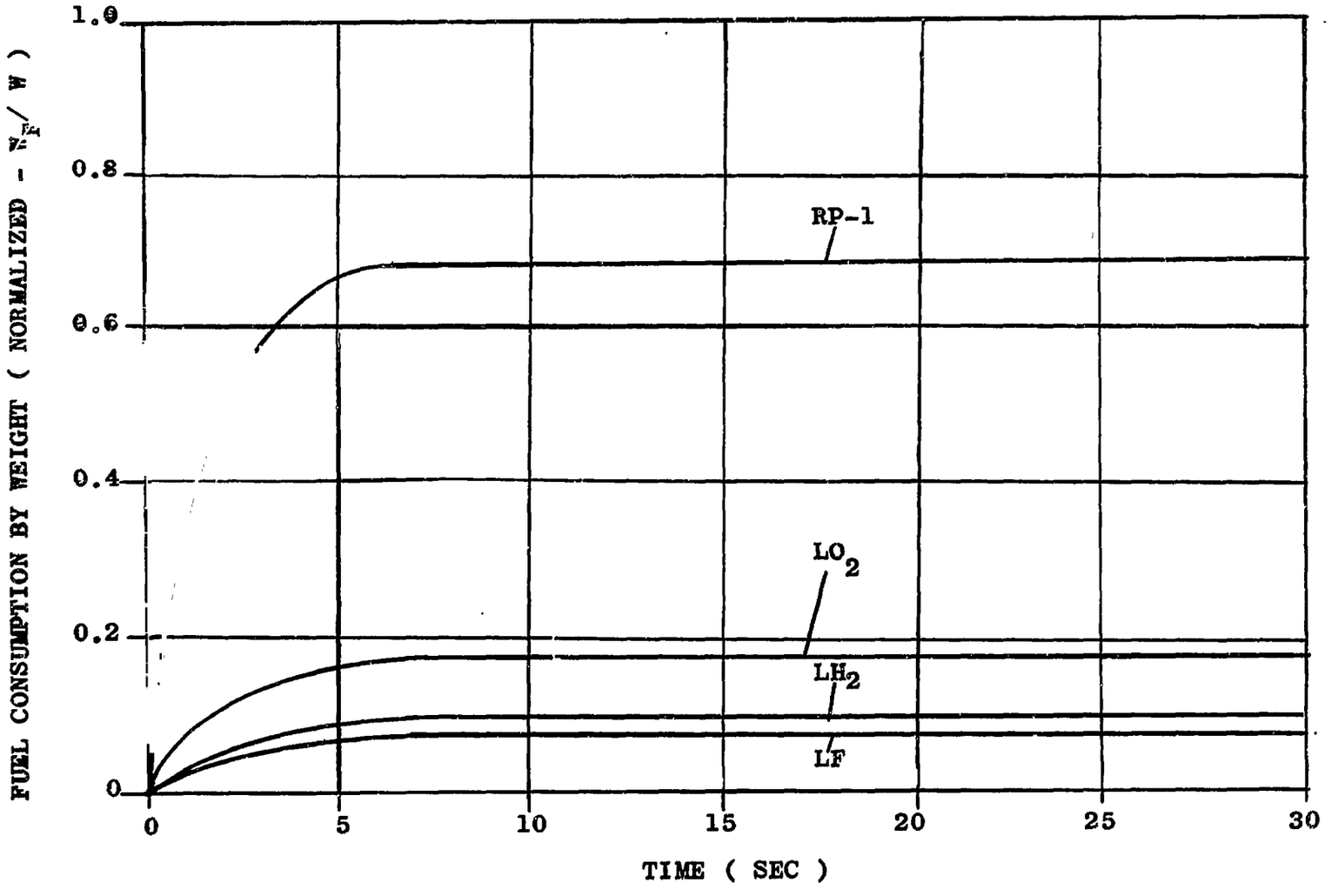

FIGURE IV-71-. FUEL CONSUMPTION FOR LH_2/RP-1/LO_2 + 10% F LIQUID PROPELLANT EXPLOSION (YIELD = 4.5 PERCENT)

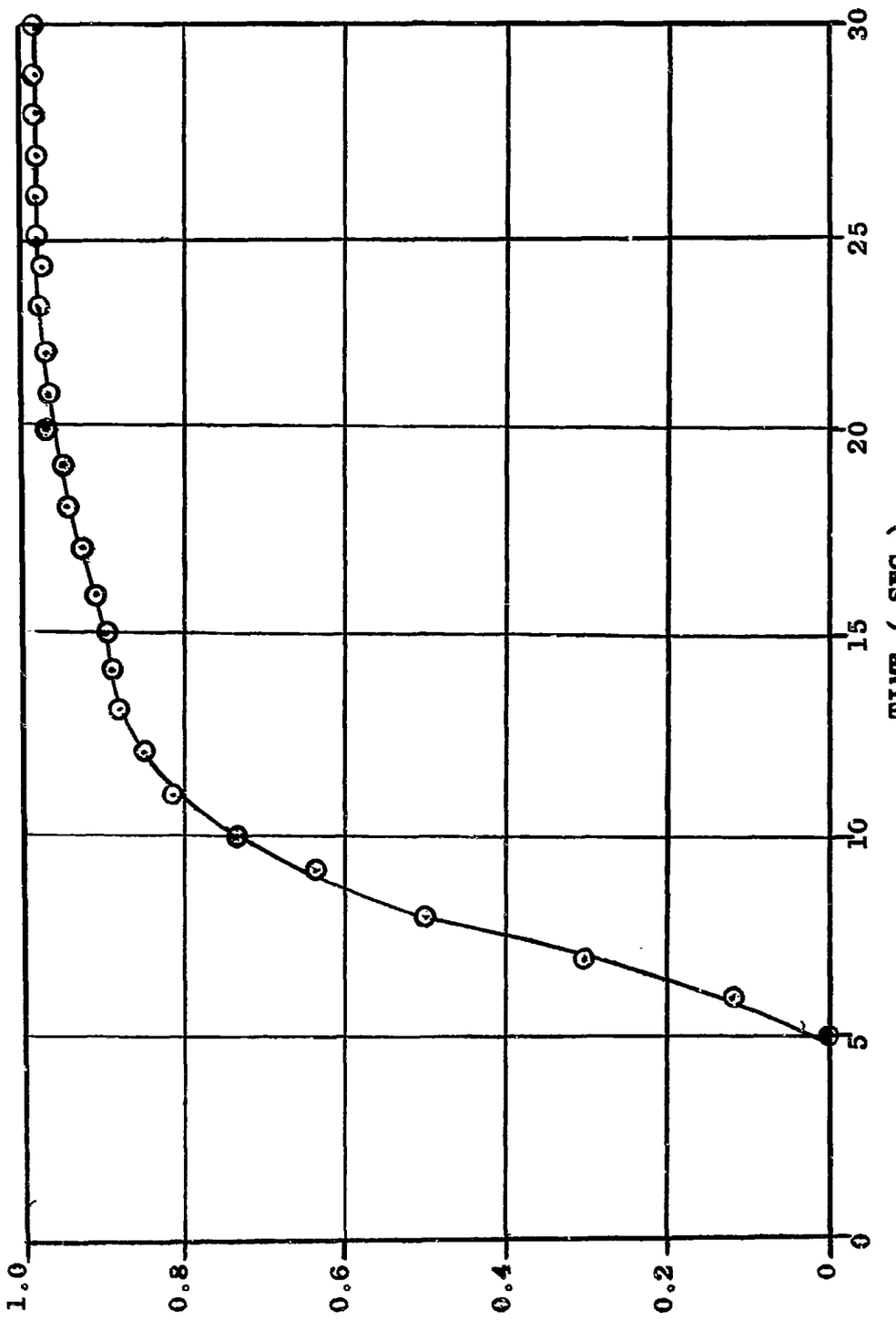

FIGURE IV-72-. VOLUME OF ENTRAINED AIR FOR LH_2/RP-1/LO_2 + 10% F LIQUID PROPELLANT EXPLOSION (YIELD = 4.5 PERCENT)

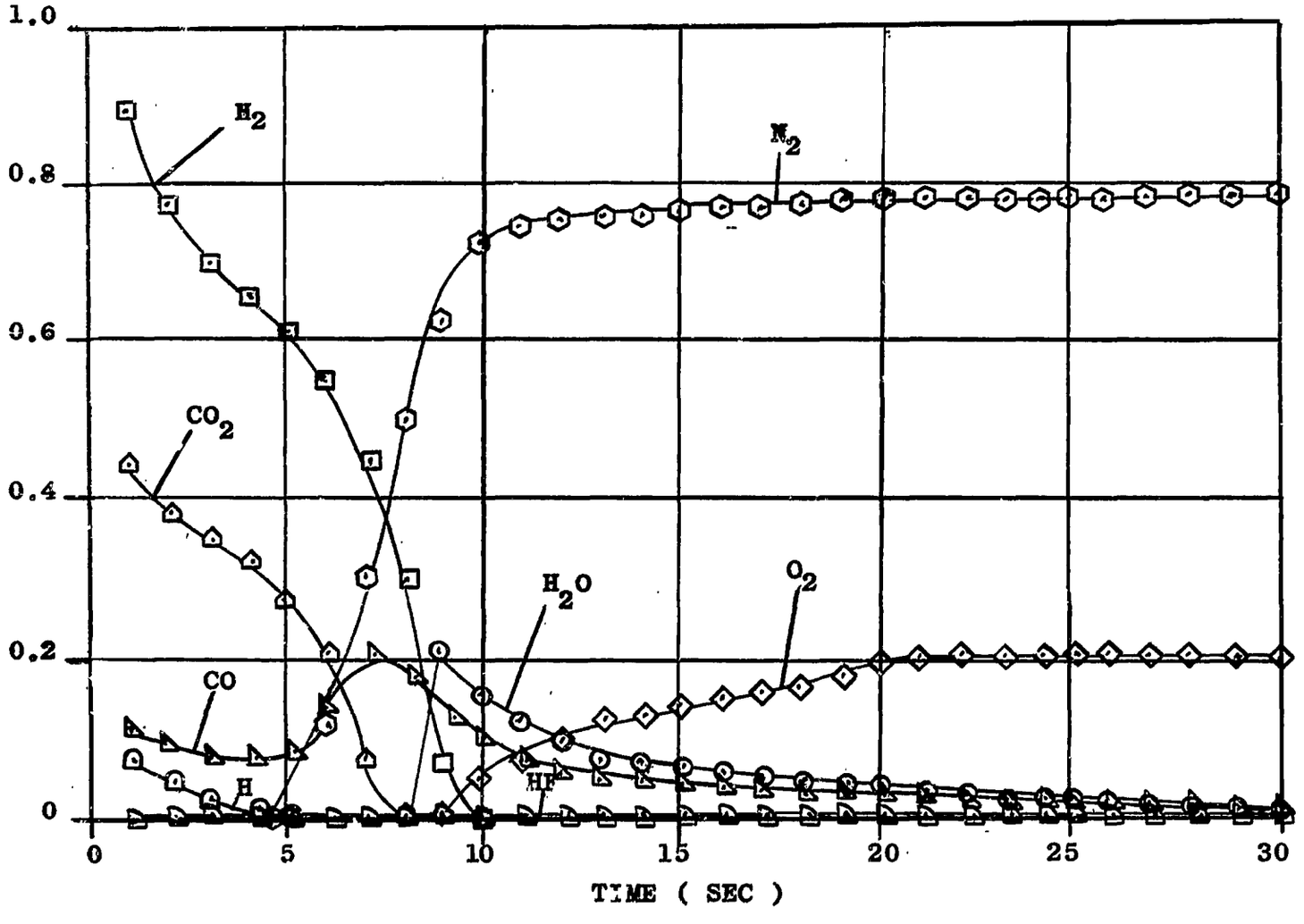

FIGURE IV-73-. PARTIAL PRESSURES AND PARTIAL VOLUMES FOR LH_2/RP-1/LO_2 + 10%F LIQUID PROPELLANT EXPLOSION PRODUCTS (YIELD = 4.5 PERCENT)

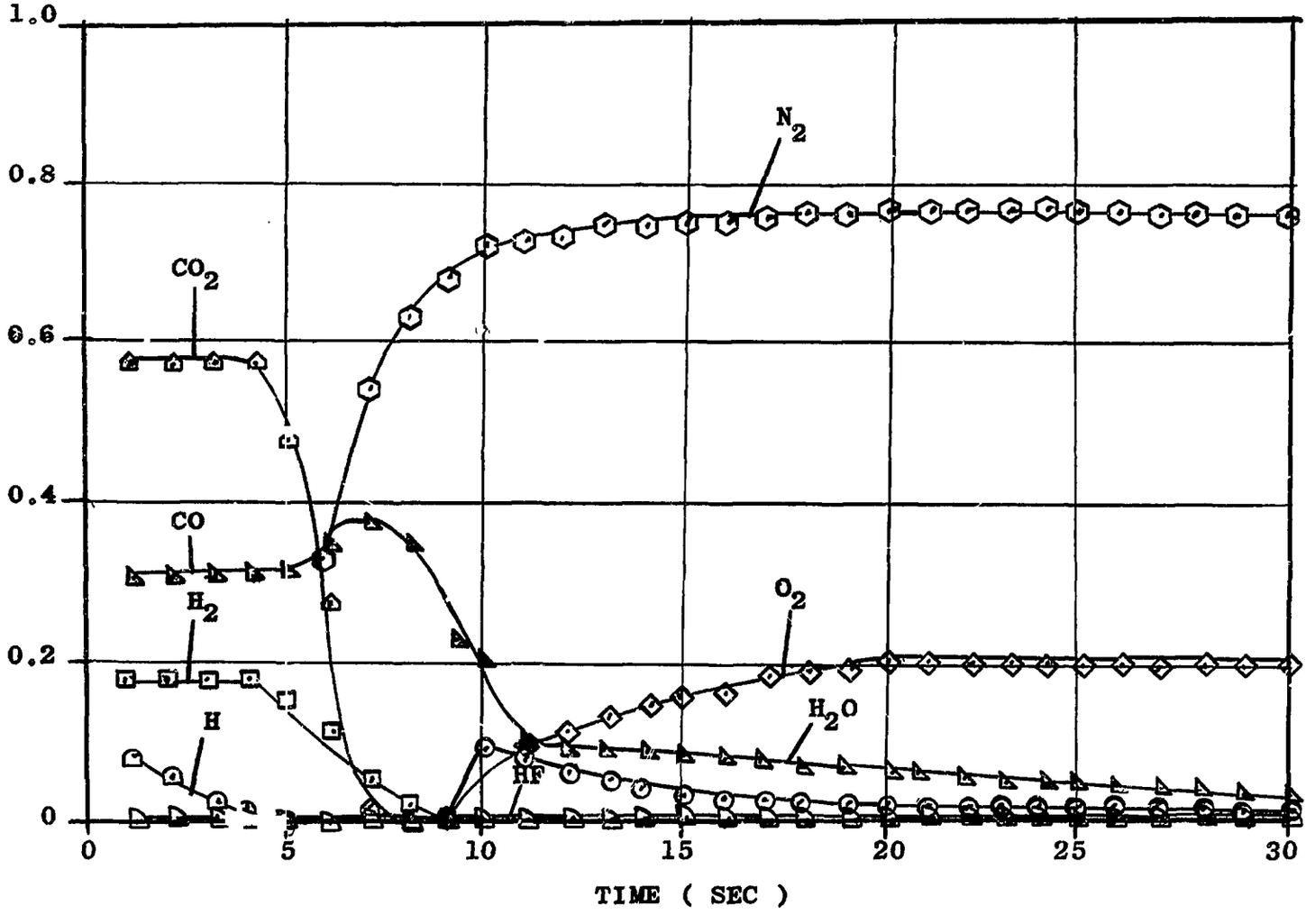

FIGURE IV-74-. WEIGHT COMPOSITION OF THE COMBUSTION PRODUCTS FROM LH_2/RP-1/LO_2+ 10%F LIQUID PROPELLANT EXPLOSION (YIELD = 4.5 PERCENT)

Computer Programs

I Reaction Products

```
* 148218    STEWART            *060* REACTION PRODUCTS
$IBJOB          GO
$IBFTC MAIN     NODECK
      DIMENSION A(15,15),B(15),T(9),C(10,9),PT(15),P(15),PR(15),V(9)
      DIMENSION WT(15),WMOL(15),WTR(15),TNT(15)
      READ(5,102) X, MA
      READ(5,105) (T(J),J=1,9)
      READ(5,110)(PT(J),J=1,9)
      READ(5,106) ((C(I,J),J=1,9),I=1,10)
      READ (5,99) (WMOL(J), J=1,8)
      READ (5,99) (WMOL(J), J=9,15)
      DO 7 I=1,10
      DO 7 J=1,9
      IF(C(I,J)-88.03/2.3)31,32,32
   32 C(I,J)=88./2.31
   31 CONTINUE
    7 C(I,J)=10.**C(I,J)
      READ (5,100) YIELD
      DO 10 K,J=1,MA
      READ (5,103) (V(J), J=1,5)
      READ (5,103) (V(J), J=6,9)
      READ (5,101) H2, RP1, O2, F2
      B1=H2/2.016
      B2 =RP1/(14.026*X)
      B3=O2/32.
      B4=F2/38.
      A1=YIELD*B1
      A2=YIELD*B2
      A3=YIELD*B3
      A4=YIELD*B4
      IF(A1)300,300,301
  300 A1=.01
  301 IF(A2)302,302,303
  302 A2=.01
  303 IF(A3)304,304,305
  304 A3=.01
  305 IF(A4)306,306,307
  306 A4=.01
  307 A5=.01
      DO 222 I=1,15
  222 P(I)=PT(1)/15.
      DO 10 J=1,9
      TNE=PT(J)*V(J)/(T(J)*1.314)
      WRITE (6,220)
      WRITE (6,130) H2
      WRITE (6,131) RP1
      WRITE (6,132) O2
      WRITE (6,133) F2
      WRITE (6,134)
      WRITE (6,135) T(J)
      WRITE (6,136) PT(J)
      WRITE (6,137) V(J)
      IF(J-1)600,600,601
  600 WRITE(6,237)YIELD
  601 WRITE (6,138)
      WRITE (6,139)
      WRITE (6,140)
      WRITE (6,141)
      WRITE (6,142)
      KL=0
    8 KL=KL+1
```

```
      Y1=2.*(A3+0.209*A5)
      Y2=2.*(A1+A2*X)
      Y3=1.584*A5
      Y4=A2*X
      Y5=2.*A4
      DO 1I=1,15
      DO 1K=1,15
    1 A(I,K)=0.0
      DO 2I=1,15
    2 A(1,I)=-1.0
      DO 3K=6,15
      I=K-5
    3 A(K,I)=1.0
      A(2,1)= 2.0*Y1-Y2
      A(2,2)= -2.0*Y2
      A(2,3)= 2.0*Y1
      A(2,6)= -2.0*Y2
      A(2,7)=Y1
      A(2,8)=-Y2
      A(2,9)=-Y2
      A(2,10)= Y1-Y2
      A(2,11)= Y1
      A(2,15)= -Y2
      A(3,1)= 2.0*Y3
      A(3,3)= 2.0*Y3
      A(3,4)= -2.0*Y2
      A(3,7)= Y3
      A(3,9)=-Y2
      A(3,10)= Y3
      A(3,11)= Y3
      A(3,12)= -Y2
      A(4,1)=2.*Y4
      A(4,2)=-Y2
      A(4,3)=2.*Y4
      A(4,7)=Y4
      A(4,8)=-Y2
      A(4,10)= Y4
      A(4,11)= Y4
      A(4,14)= -Y2
      A(5,1)=2.*Y5
      A(5,3)=2.*Y5
      A(5,5)=-2.*Y2
      A(5,7)=Y5-Y2
      A(5,10)= Y5
      A(5,11)= Y5
      A(5,13)= -Y2
      A(6,11)= -2.0*C(1,J)*P(11)*P(15)
      A(6,15)= -C(1,J)*P(11)**2
      A(7,14)= -C(2,J)*P(15)**2
      A(7,15)= -2.0*C(2,J)*P(14)*P(15)
      A(8,11)= -2.0*C(3,J)*P(11)
      A(9,12)= -2.0*C(4,J)*P(12)
      A(10,13)= -2.0*C(5,J)*P(13)
      A(11,15)= -2.0*C(6,J)*P(15)
      A(12,11) = -C(7,J)*P(13)
      A(12,13) = -C(7,J)*P(11)
      A(13,14) = -C(8,J)*P(15)
      A(13,15) = -C(8,J)*P(14)
      A(14,12) = -C(9,J)*P(15)
      A(14,15) = -C(9,J)*P(12)
      A(15,11)=-C(10,J)*P(15)
```

```
      A(15,15) = -C(10,J)*P(11)
      SUM = 0.
      DO 4I=1,15
    4 SUM=SUM+P(I)
      B(1)=PT(J)-SUM
      B(2)=(2.*Y1-Y2)*P(1)-2.*Y2*P(2)+2.*Y1*P(3)-2.*Y2*P(6)+Y1*P(7)
     1 -Y2*P(8)-Y2*P(9)+(Y1-Y2)*P(10)+Y1*P(11)-Y2*P(15)
      B(3)=2.*Y3*P(1)+2.*Y3*P(3)-2.*Y2*P(4)+Y3*P(7)-Y2*P(9)+Y3*P(10)+
     1Y3*P(11)-Y2*P(12)
      B(4)=2.*Y4*P(1)-Y2*P(2)+2.*Y4*P(3)+Y4*P(7)-Y2*P(8)+Y4*P(10)+Y4
     1 *P(11)-Y2*P(14)
      B(5)=2.*Y5*P(1)+2.*Y5*P(3)-2.*Y2*P(5)+(Y5-Y2)*P(7)+Y5*P(10)+Y5*P(1
     11)-Y2*P(13)
      B(6)=P(1)-C(1,J)*P(11)**2*P(15)
      B(7)=P(2)-C(2,J)*P(14)*P(15)**2
      B(8)=P(3)-C(3,J)*P(11)**2
      B(9)=P(4)-C(4,J)*P(12)**2
      B(10)=P(5)-C(5,J)*P(13)**2
      B(11)=P(6)-C(6,J)*P(15)**2
      B(12)=P(7)-C(7,J)*P(11)*P(13)
      B(13)=P(8)-C(8,J)*P(14)*P(15)
      B(14)=P(9)-C(9,J)*P(12)*P(15)
      B(15)=P(10)-C(10,J)*P(11)*P(15)
      DO 55I=1,15
   55 B(I)=-B(I)
      CALL INVERT(A,15,15,B,1,15,DETERM,IERROR)
      DO 6 I=1,15
      P(I)=P(I)+B(I)
      IF(P(I)) 41,6,6
   41 P(I)=0.0
    6 CONTINUE
      SUM1=0.
      DO 30 I= 1,15
   30 SUM1=SUM1+ABS(B(I))
      IF(SUM1-.0005)51,51,8
   51 TN=PT(J)*Y2/(2.*P(1)+2.*P(3)+P(7)+P(10)+P(11))
      TNR=TNE/TN
      IF(KL-150)25,25,50
   25 IF(V(J))50,50,49
   49 IF(ABS(TNR-1.)-.001)50,50,27
   27 IF(A1-0.01) 52,52,53
   53 A1=A1*TNR
      IF(B1-A1) 70,70,52
   70  A1= B1
   52 IF(A2-0.01) 54,54,95
   95 A2=A2*TNR
      IF(B2-A2)71,71,54
   71 A2=B2
   54 IF(A3-0.01) 56,56,57
   57 A3=A3*TNR
      IF (B3-A3) 72,72,56
   72 A3=B3
   56 IF( A4-0.01) 58,58,59
   59 A4=A4*TNR
      IF (B4-A4) 73,73,58
   73 A4=P
   58 IF (B1-A1) 75,75,79
   75 IF(B2-A2 ) 76,76,79
   76 IF (B3-A3) 77,77,79
   77 IF(B4-A4) 78,78,79
   78 IF(A5-.01)80,80,88
```

```
 80 A5=TNE-TN
    GO TO 79
 88 A5=A5*TNR
 79 CONTINUE
 74 GO TO 8
 50 WRITE(6,104) RL
    WRITE(6,111)
    WRITE(6,112) (P(I), I=1,5)
    WRITE(6,112) (P(I), I=6,10)
    WRITE(6,112) (P(I), I=11,15)
    DO 214 I=1,15
    PR(I)=P(I)/PT(J)
    TNT(I)=PR(I)*TN
214 WT(I)=TNT(I)*WMOL(I)
    WRITE(6,113)
    WRITE( 6,114) (TNT(I), I=1,5)
    WRITE (6,114) (TNT(I), I=6,10)
    WRITE (6,114) (TNT(I), I=11,15)
    WRITE(6,115)
    WRITE(6,112) (PR(I), I=1,5)
    WRITE(6,112) (PR(I), I=6,10)
    WRITE(6,112) (PR(I), I=11,15)
    WPROD=0.0
    DO 117 I=1,15
117  WPROD=WPROD+WT(I)
    DO 118 I=1,15
118 WTR(I)=WT(I)/WPROD
    WRITE(6,116)
    WRITE(6,119) (WT(I), I=1,5)
    WRITE (6,119)(WT(I), I=6,10)
    WRITE(6,119) (WT(I), I=11,15)
    WRITE(6,120)
    WRITE(6,212) ( WTR(I), I=1,5)
    WRITE (6,212) (WTR(I), I=6,10)
    WRITE (6,212) (WTR(I), I=11,15)
    WRITE(6,121)
    C1=A1*2.016
     C2=A2*(14.026*X)
    C3=A3*32.
    C4=A4*38.
    WRITE(6,122) C1
    WRITE(6,123) C2
    WRITE (6,124) C3
    WRITE(6,125) C4
    WRITE( 6,126)
    WRITE(6,127) A5
    WAIR=A5*28.966
    WRITE(6,128) WAIR
    RNA.   A5/TN
    RWAIR=WAIR/WPROD
    WRITE(6,129) RNAIR
    WRITE(6,230) RWAIR
    WRITE(6,161) TN
    TVOL=TN*T(J)*1.314/PT(J)
    WRITE(6,143) TVOL
 10 CONTINUE
10  FORMAT(F5.1,I3)
10  FORMAT(9F6.0)
110 FORMAT(9F6.2)
106 FORMAT(9F8.4)
103 FORMAT(5F12.0)
```

```
   99 FORMAT(8F7.3)
  100 FORMAT( F7.4)
  101 FORMAT(4F10.2)
  220 FORMAT(/////,8X,28HAMOUNT OF PROPELLANT,POUNDS  )
  130 FORMAT(12X,4HLH2=F10.2)
  131 FORMAT(12X,5HRP-1=F10.2)
  132 FORMAT(12X,4HLO2=F10.2)
  133 FORMAT(12X,4HLF2=F10.2)
  134 FORMAT(//,8X,34HEXPERIMENTAL VALUES OF T,P,V       )
  135 FORMAT(/,12X,16HDEGREES KELVIN =F7.1)
  136 FORMAT(12X,12HATMOSPHERES=F6.1)
  137 FORMAT(12X,11HCUBIC FEET=F12.0)
  237 FORMAT(12X,6HYIELD=F7.4)
  138 FORMAT(//,13X,20HTHEORETICAL RESULTS )
  139 FORMAT(/,8X,39HIDENTIFICATION OF PRODUCTS OF REACTION )
  140 FORMAT(/,8X,3HH2O,5X,3HCO2,5X,2HH2,6X,2HN2,6X,2HF2)
  141 FORMAT(8X,2HC2,6X,2HHF,6X,2HCO,6X,2HNO,6X,2HOH)
  142 FORMAT(8X,1HH,7X,1HN,7X,1HF,7X,1HC,7X,1HO)
  104 FORMAT(8X,I3,20H ITERATIONS REQUIRED)
  111 FORMAT(/,19X,17HPARTIAL PRESSURES)
  112 FORMAT(8X,5(F7.3,1X))
  113 FORMAT(/,32X,11HPOUND MOLES)
  114 FORMAT(5X,5(F12.2,1X))
  115 FORMAT(/,14X,27HPRESSURE,MOLE,VOLUME RATIOS )
  116 FORMAT(/,32X,13HPOUND WEIGHTS)
  119 FORMAT(5X,5( F12.0,1X))
  120 FORMAT(/,19X,13HWEIGHT RATIOS)
  212 FORMAT(8X,5F7.4)
  121 FORMAT(/,8X,19HBURNING RATE,POUNDS)
  122 FORMAT(9X,4HLH2=F12.0)
  123 FORMAT(9X,5HRP-1=F12.0)
  124 FORMAT(9X,4HLO2=F12.0)
  125 FORMAT(9X,4HLF2=F12.0)
  126 FORMAT(/,8X,23HAMOUNT OF ENTRAINED AIR)
  127 FORMAT(8X,6HMOLES=F12.0)
  128 FORMAT(8X,7HPOUNDS=F12.0)
  129 FORMAT(8X,27HPRESSURE,MOLE,VOLUME RATIO=F8.3)
  230 FORMAT(8X,13HWEIGHT RATIO=F7.4)
  161 FORMAT(/,8X,30HTOTAL THEORETICAL POUND MOLES=F12.0)
  143 FORMAT(/,8X,19HTHEORETICAL VOLUME=F12.0)
      RETURN
      END
$DATA
 11.6  3
 3000. 2800. 2600. 2400. 2200. 2000. 1800. 1600. 1400.
 31.7   1.52  1.25  1.12  1.05  1.    1.    1.    1.
  3.8617  5.0661  6.4532  8.0683  9.9730 12.2533 15.0332 18.4983 22.9395
 13.0585 15.0772 17.4062 20.1232 23.3337 27.1855 31.8923 37.7738 45.3324
  1.6064  2.1772  2.8344  3.5994  4.5010  5.5798  6.8941  8.5311 10.6275
  5.7261  6.6404  7.6640  8.9216 10.3703 12.1063 14.2247 16.8684 20.2614
 -3.9111 -3.7015 -3.4608 -3.1816 -2.8534 -2.4618 -1.9859 -1.3945  -.6388
  1.8415  2.6756  3.2066  4.0586  5.0643  6.2695  7.7403  9.5756 11.9307
  3.6997  4.4307  5.2726  6.2528  7.4086  8.7922 10.4788 12.5810 15.2752
 11.6713 13.0338 14.6045 16.4352 18.5966 21.1878 24.3515 28.3020 33.375
  2.8677  3.5299  4.2927  5.1811  6.2293  7.4848  9.0165 10.9274 13.3789
  1.7434  2.2979  2.9363  3.6792  4.5549  5.6027  6.8793  8.4697 10.5267
 18.016 44.01   2.016 28.016 38.    32.    20.008 28.01
 30.008 17.008  1.008 14.008 19.    12.01  16.
  .045
         0.   12000000.   17500000.   20000000.   21000000.
  21000000.   25500000.   34000000.   44500000.
```

```
16700.00       0.00   83300.00    5000.00
        0.    6500000.    9500000.    11300000.    12000000.
 13000000.    15000000.   18500000.   23000000.
    0.00   30800.00   69200.00    5000.00
        0.    21000000.   29000000.   34500000.    38000000.
 40000000     47000000.   60000000.   76000000.
 7000.00    75300.00   17700.00    5000.00
```

NDFILE

II Subroutine Invert

```
      SUBROUTINE INVERT (A,NA1,NAD1,B,NB1,NBD1,DETERM,IERROR)
      DIMENSION INDEX(100) , B1(100) , A(1) , B(1)                      609
      EQUIVALENCE (B1,INDEX)                                            609
C                 INITIALIZE                                            609
    1 CALL OVERFL (INDEX)                                               609
   10 NA = NA1                                                          609
      NAD = NAD1                                                        609
      NB = NB1                                                          609
      NBD = NBD1                                                        609
      DET = 1.0                                                         609
      IERROR = 0                                                        609
      DO 20 I = 1,NA                                                    609
   20 INDEX(I) = -1                                                     609
      DO 130 I = 1,NA                                                   609
C                 SEARCH FOR PIVOTAL ELEMENT                            609
      PIVOT = 0.0                                                       609
      IJ =  0                                                           609
      DO 60 J = 1,NA                                                    609
      IF(INDEX(J)) 30,250,60                                            609
   30 DO 55 II = 1,NA                                                   609
      IF(INDEX(II)) 40,250,55                                           609
   40 IJ1 = IJ + II                                                     609
      IF(ABS (PIVOT) - ABS (A(IJ1))) 50,55,55                           609
   50 IROW = II                                                         609
      JCOL = J                                                          609
      PIVOT = A(IJ1)                                                    609
   55 CONTINUE                                                          609
   60 IJ = IJ + NAD                                                     609
      IF(PIVOT) 65,250,65                                               609
   65 INDEX(JCOL) =IABS (INDEX(JCOL))                                   609
C                 INTERCHANGE ROWS TO PUT PIVOTAL ELEMENT ON DIAGONAL   609
      IF(IROW - JCOL) 70,90,70                                          609
   70 DET = -DET                                                        609
      IJ = IROW                                                         609
      IJ1 = JCOL                                                        609
      DO 80 J = 1,NA                                                    609
      SAVE = A(IJ)                                                      609
      A(IJ) = A(IJ1)                                                    609
      A(IJ1) = SAVE                                                     609
      IJ = IJ + NAD                                                     609
   80 IJ1 = IJ1 + NAD                                                   609
   90 INDEX(I) = INDEX(I) * (1000 * IROW + JCOL)                        609
      DET = DET * PIVOT                                                 609
C                 DIVIDE PIVOTAL ROW BY PIVOTAL ELEMENT                 609
      IJ = JCOL + (JCOL - 1) * NAD                                      609
      A(IJ) = 1.0                                                       609
      IJ = JCOL                                                         609
      DO 100 J = 1,NA                                                   609
      A(IJ) = A(IJ) / PIVOT                                             609
  100 IJ = IJ + NAD                                                     609
C                 REDUCE NON-PIVOTAL ROWS                               609
      IJ = (JCOL - 1) * NAD                                             609
      DO 130 II = 1,NA                                                  609
      IJ = IJ + 1                                                       609
      IF(II - JCOL) 110,130,110                                         609
  110 SAVE = A(IJ)                                                      609
      A(IJ) = 0.0                                                       609
      IJ2 = JCOL                                                        609
      IJ1 = II                                                          609
      DO 120 J = 1,NA                                                   609
      A(IJ1) = A(IJ1) - A(IJ2) * SAVE                                   609
```

```
      IJ1 = IJ1 + NAD                                                   609
  120 IJ2 = IJ2 + NAD                                                   609
  130 CONTINUE                                                          609
      DETERM = DET                                                      609
C                 INTERCHANGE COLUMNS                                   609
      DO 160 K = 1,NA                                                   609
      J = NA + 1 - K                                                    609
      IROW = INDEX(J) / 1000                                            609
      JCOL = INDEX(J) - IROW * 1000                                     609
      IF(JCOL - IROW) 140,160,140                                       609
  140 IJ = (IROW - 1) *NAD                                              609
      IJ1 = (JCOL - 1) *NAD                                             609
      DO 150 I = 1,NA                                                   609
      IJ = IJ + 1                                                       609
      IJ1 = IJ1 + 1                                                     609
      SAVE = A(IJ)                                                      609
      A(IJ) = A(IJ1)                                                    609
  150 A(IJ1) = SAVE                                                     609
  160 CONTINUE                                                          609
C                 A INVERSE IS NOW STORED IN A                          609
C                 FIND SOLUTION VECTORS FOR ALL CONSTANT VECTORS INPUT  609
      IF(NB) 210,210,170                                                609
  170 IJ1 = 0                                                           609
      DO 200 K = 1,NB                                                   609
      DO 180 I = 1,NA                                                   609
      BI(I) = 0.0                                                       609
      IJ = I                                                            609
      DO 180 J = 1,NA                                                   609
      IJ2 = IJ1 + J                                                     609
      BI(I) = BI(I) + A(IJ) * B(IJ2)                                    609
  180 IJ = IJ + NAD                                                     609
      DO 190 I = 1,NA                                                   609
      IJ2 = IJ1 + I                                                     609
  190 B(IJ2) = BI(I)                                                    609
  200 IJ1 = IJ1 + NBD                                                   609
C                 SOLUTION VECTORS NOW IN B                             609
C                 CHECK FOR OVERFLOW CONDITION AND SET ERROR SIGNAL     609
  210 CALL OVERFL(INDEX)                                                609
      IF (INDEX-1)230,230,240                                           609
  230 IERROR = -1                                                       609
  240 RETURN                                                            609
C                 IF CONTROL REACHES 250, MATRIX IS SINGULAR OR A MACHINE 609
C                 ERROR HAS OCCURED                                     609
  250 IERROR = 1                                                        609
      GO TO 240                                                         609
      END                                                               609
```

III Sample Data Output

SAMPLE DATA OUTPUT

```
        AMOUNT OF PROPELLANT, POUNDS
           LH2    =  7000.00
           RP-1   =  75300.00
           LO2    =  17700.00
           LF2    =  5000.00
        EXPERIMENTAL VALUES OF T, P, V
        DEGREES KELVIN  =  1800.0
        ATMOSPHERES     =  1.0
        CUBIC FEET      =  47000000.

                THEORETICAL RESULTS
     IDENTIFICATION OF PRODUCTS OF REACTION
H2O         CO2         H2          N2          F2
O2          HF          CO          NO          OH
H           N           F           C           O
      47 ITERATIONS REQUIRED FOR SOLUTION
                PARTIAL PRESSURES
0.000       0.000       0.439       0.278       0.
0.          0.013       0.202       0.000       0.000
0.000       0.000       0.000       0.068       0.000
                POUND MOLES
0.00        0.00        8706.90     5512.21     0.
0.          263.16      4015.47     0.00        0.00
4.70        0.00        0.00        1353.13     0.00
          PRESSURE, MOLE, VOLUME RATIOS
0.000       0.000       0.439       0.278       0.
0.          0.013       0.202       0.000       0.000
0.000       0.000       0.000       0.068       0.000
                POUND WEIGHTS
0.          0.          17553.      154430.     0.
0.          5265.       112473.     0.          0.
5.          0.          0.          16251.      0.
                WEIGHT RATIOS
0.0000      0.0000      0.0574      0.5047      0.
0.          0.0172      0.3676      0.0000      0.0000
0.0000      0.0000      0.0000      0.0531      0.0000
            BURNING RATE, POUNDS
               LH2   =  7000.
               RP-1  =  75300.
               LO2   =  17700.
               LF2   =  5000.
            AMOUNT OF ENTRAINED AIR
               MOLES  =  6960.

               POUNDS =  201599.
               PRESSURE, MOLE, VOLUME RATIO = 0.351
               WEIGHT RATIO = 0.6589

               TOTAL THEORETICAL POUND MOLES = 19856.

               THEORETICAL VOLUME = 46962371.
```

Appendix

ENGINEERING PROGRESS
at the
UNIVERSITY OF FLORIDA

Vol. XX, No. 3 March, 1966

TECHNICAL PAPER SERIES

No. 346: A Mathematical Model for Defining Explosive Yield and Mixing Probabilities of Liquid Propellants

By E. A. FARBER

No. 347: A Systematic Approach for the Analytical Analysis and Prediction of the Yield from Liquid Propellant Explosions

By E. A. FARBER and J. H. DEESE

Reprinted from "The Challenge of Space," *Proceedings of the Third Space Congress,* March 7-10, 1966, Cocoa Beach, Florida. Sponsored by the Canaveral Council of Technical Societies.

Published monthly by the

FLORIDA ENGINEERING AND INDUSTRIAL EXPERIMENT STATION

COLLEGE OF ENGINEERING • UNIVERSITY OF FLORIDA • GAINESVILLE

Entered as second-class matter at the Post Office at Gainesville, Florida

A MATHEMATICAL MODEL FOR DEFINING EXPLOSIVE YIELD AND MIXING PROBABILITIES OF LIQUID PROPELLANTS

by

E. A. Farber*

ABSTRACT

This paper describes how a mathematical model can be constructed to fit theoretical or experimental data on yield and spill of liquid propellants. It shows how these primary quantities can be separated, how probability distributions can be found for each, and how probability confidence regions and confidence limits can be established.

The fundamental function of this very general mathematical model, based upon four independent parameters, and the characteristics of the resulting probability surface are discussed in detail.

The mathematical model, programmed for an IBM 709 computer, is applied to some spill test data of liquid propellants for which the necessary information is available and then, with a minimum number of assumptions, to missile failure yield estimates.

INTRODUCTION

The yield from liquid propellant explosions as a result of missile failures is of extreme importance in assessing the hazards to astronauts, launch support personnel, launch support facilities and surrounding structures.

To prepare against the effects from such liquid propellant explosions, methods must be found by which the most probable expected yield can be predicted.

Unfortunately many of the physical phenomena involved in producing the yield are little understood, making the prediction of the expected yield difficult and complex.

---

*Professor and Research Professor of Mechanical Engineering, University of Florida.

One approach to this problem for the prediction of the over-all effects by means of a mathematical model is suggested in this paper. The mathematical model developed here allows for a well-balanced procedure of theoretical and experimental investigations, with the theory guiding the experimentation which in turn modifies the theory.

The mathematical model suggested in this paper is very general in nature, being able to satisfy a wide range of either theoretical information or experimental data and has the required statistical characteristics to make it possible to separate the yield and spill functions, giving probability distributions, confidence limits, confidence regions, and so forth.

With this model it is then possible to extract a maximum amount of information from extremely sparse data and to guide future experimental programs. This procedure furthermore allows the conducting of small-scale, relatively inexpensive experiments to define the model and to reduce the large-scale, expensive experiments to very few in number. The large-scale tests serve as check points to validate or modify the model.

In this manner it is possible to develop a valid scaling law for liquid propellant explosions through a well-planned program, with theory guiding the experimental procedure, and to do this in the shortest possible time and at minimum cost.

THEORY OF APPROACH

The basis of the development of the mathematical model is the fundamental characteristic of the sparse experimental data giving information on the yield and spill of liquid propellants. Work is under way to extend this data by developing theoretical yield-spill relationships.

With the above information it is possible, as is shown in this paper, to develop a very general mathematical model which can express presently available data and is flexible enough to incorporate future information as it becomes available. It also satisfies the statistical requirements providing for valid estimating procedures of the parameters involved, and allows the separation of the individual characteristics of the yield function and the spill function. The model may be referred to as a modified Dirichlet bivariate surface.

THE YIELD AND SPILL FUNCTIONS

The primary quantities used in formulating the mathematical model are the yield function and the spill function.

The yield function is preferably defined as the fraction of maximum theoretical yield potential of the on-board liquid propellants (also utilizing the oxygen of the atmosphere, where applicable). It can also be expressed in therms of TNT equivalency, presently a common method of reporting the data.

The spill function is the fraction of the total on-board propellants which are spilled, or actually mixed, at the time of reaction between fuel and oxidizer. In either case it is a time dependent variable different for each missile configuration and mode of failure.

In the formulation of the model it is assumed that the relationship between the yield function and the spill function is available. Information of this type can be found in literature, but only in very small quantity, representing liquid propellant spill tests. Preliminary investigations are now under way to extend these data both theoretically and experimentally, and the indications are that the resulting yield functions and spill functions will have lower values in most cases than those reported in literature based upon tests which were designed to give a high degree of mixing.

THE MATHEMATICAL MODEL

With the relationship between the yield function (y) and the spill function (x) established either theoretically or by experiment, the model can be formulated, resulting in a statistical function which is capable of incorporating the above x-y relationship, and is able to provide for valid estimating procedures of the parameters involved. Details of the development of this mathematical model are given in the references [1, 7]; only the high points are presented here.

The relationship between the yield function and the spill function can be expressed in terms of three parameters d, b, and c as shown in equation (1).

$$y = \frac{b}{b + c} x^d \tag{1}$$

From this a statistical function can be developed capable of incorporating physical information over a rather wide range, and which satisfies the theoretical requirements for statistical analysis. It is a modified Dirichlet bivariate surface having four parameters a, b, c, and d, making it extremely flexible. This statistical surface is expressed mathematically as equation (2).

$$f(x, y) = \frac{d\Gamma\,(a + b + c)}{\Gamma(a)\,\Gamma(b)\,\Gamma(c)} x^{d-1}(1 - x^d)^{a-1}\, y^{b-1}\, (x^d - y)^{c-1} \tag{2}$$

where Γ is the Gamma function. The only restrictions on this function are that

$$y > 0, \quad x > 0, \quad y \leq x^d, \quad d \neq 0$$

To fully define the above function for a specific class of information it is necessary to evaluate the parameters a, b, c, and d on the basis of the particular yield function — spill function relationship describing the physical phenomena.

Evaluation of the Parameters a, b, c, and d

To evaluate the parameters a, b, c, and d for the modified Dirichlet bivariate surface the following statistical estimating procedure is used.

Defining

$$u_i = 1 - x_i^d \tag{3a}$$

$$v_i = \frac{y_i}{x_i^d} \tag{3b}$$

four simultaneous estimation equations can be written for the four parameters a, b, c, and d.[1]

$$\overline{\ln v} = \psi(b) - \psi(b+c) \tag{4a}$$

$$\ln \bar{v} = \ln(b) - \ln(b+c) \tag{4b}$$

$$\overline{\ln u} = \psi(a) - \psi(a+b+c) \tag{4c}$$

$$\ln \bar{u} = \ln(a) - \ln(a+b+c) \tag{4d}$$

Where a bar over an expression indicates the average value of all available values

ln indicates the natural logarithm (base e)

ψ is Euler's Digamma Function

The mathematical model is now ready to be applied to theoretical information or experimental data. Evaluation of the parameters a, b, c, and d gives the model its characteristic configuration, and analysis of the resulting statistical surface produces a wealth of new information.

CHARACTERISTICS OF THE MATHEMATICAL MODEL

The parameters a, b, c, and d give the mathematical model, expressed by the function of equation (2) its characteristics, which can be brought out by proper mathematical analysis. Some of the most significant ones with regard to this investigation are the

A. Probability Distribution of the Yield, P_y
B. Probability Distribution for the Spill, P_x
C. Confidence Regions for the Yield and Spill
D. Confidence Limits for the Yield Function
E. Confidence Limits for the Spill Function

A detailed discussion of how these characteristics can be extracted from the above mathematical model follows.

A. Probability Distribution for the Yield, P_y

To obtain the probability distribution for the yield function it is necessary to determine the ordinate of the probability distribution for each value of y.

This ordinate for a particular value of y is represented by the area of the cross-section of the mathematical model at this value of y and perpendicular to the x-y plane. This area can be obtained graphically, or by integration requiring a large-scale computer.

The integral representing the probability ordinate is

$$P_y(y) = \int_{y\frac{1}{d}}^{1} f(x, y)\, dx \tag{5}$$

The lower limit of equation (5) is the value at which f(x, y) becomes positive for the chosen value of y. The function f(x, y) is given in equation (2).

B. Probability Distribution for the Spill, P_x

To obtain the probability distribution for the spill function the procedure is the same as in the above paragraph except that the variables x and y are interchanged so as to obtain the integral

$$P_x(x) = \int_{0}^{x^d} f(x, y)\, dy \tag{6}$$

Here the upper limit is the value of y at which f(x, y) becomes negative for a chosen value of x.

C. Confidence Regions for Yield and Spill

To obtain probability regions for spill (x) and yield (y) it is necessary to determine the volume under the probability surface, and then divide this volume into slabs of desired subvolumes.

In this manner regions are obtained representing the intersections of planes, parallel to the x-y plane, which define the subvolumes, with the statistical surface. These intersections projected as regions simulate contour lines on a topographical map representing the various elevations.

The above analysis can be made by building a physical model of the mathematical function (using clay, putty, wood, and so forth) and by determining the total

volume and subvolumes by submersion into liquid; it can also be done by double integration, again necessitating a large-scale computer to solve integrals like

$$V_{x,y} = \int_0^1 \int_0^{x^d} f(x, y)\, dy\, dx \qquad (7)$$

for the total volume and with different limits for the subvolumes. The limits of the integrals have to give the required subvolumes to include the desired percentages of x and y surface values.

D. Confidence Limits for the Yield

To obtain confidence limits for the yield function it is necessary to work with fractional areas under the yield probability distribution.

The peak of this curve represents the statistically most probable value. The fraction of the total area under the probability distribution lying between two values of y represents the fraction of all y values in this interval. If the highest statistically expected yield is desired with a confidence, let us say of 95 per cent, then the value of y has to be found for which 95 per cent of the area under the probability distribution curves lies to the left of it. Many other questions of this type can be answered in this manner.

E. Confidence Limits for the Spill

The same information regarding the spill probabilities can be obtained as were described above for the yield. The procedure is the same except that the spill probability distribution curve is used in this case.

Information, in addition to the above, can be extracted from the mathematical model by sectioning it and subsectioning it physically or mathematically in various ways.

The calculation procedures A through E were computerized[1] and quantitive results are presented as examples for

I. The Mathematical Model Applied to Available Experimental Data

II. The Mathematical Model Applied to Available Experimental Data and Missile Failure Yield Estimates

III. The Mathematical Model Applied to Available Missile Failure Yield Estimates

A comparison of the results, obtained by the mathematical model defined here by a minimum of data, from these three examples and the actual observations, will give better insight into the workings and characteristics discussed above. With more representative, and better, data this mathematical model could be defined

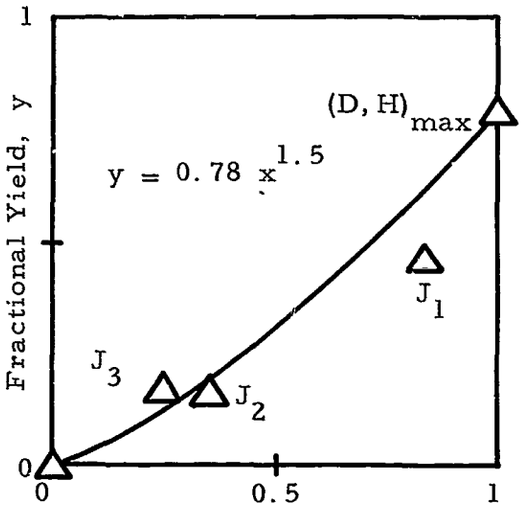

Fig. 1 Yield Function - Spill Function Relationship

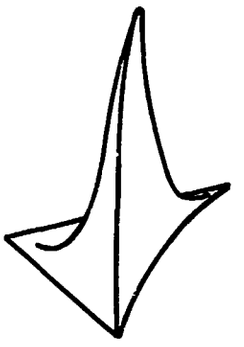

Fig. 2 Mathematical Model Represented by a Statistical Surface (Shark Fin)

with greater statistical confidence, and the reliability of the numerical results presented increased.

I. THE MATHEMATICAL MODEL APPLIED TO AVAILABLE EXPERIMENTAL DATA

In this section the mathematical model, which was developed as described above, is applied to test results which contain the necessary information to make this application possible. These are the results presented in Table I. They may or may not be representative of actual missile failures, but they certainly exhibit fundamental characteristics of liquid propellant explosions.

TABLE I

Experimental Data of Liquid Propellant Explosions[2]

1.	$(D,H)_{max}$ Test Series	y = 0.78	x = 1.00
2.	J_1 Test	0.47	0.846
3.	J_2 Test	0.165	0.348
4.	J_3 Test	0.186	0.252

This very sparse experimental data is presented in Figure 1 graphically. Applying standard curve fitting procedures the x-y functional relationship is obtained as also shown in this figure.

The estimating procedure, as outlined above, using equations (3a) through (4d) results in numerical values for the parameters a, b, c, and d. These values are $a = 3.1$, $b = 4.0$, $c = 1.1$, $d = 1.5$

The values of the parameters substituted into equation (2) define the mathematical model as controlled by the input as shown. The resulting function becomes a three-dimensional configuration as seen in Figure 2. It has steep sides and a flat body, best described as simulating a "Shark Fin."

Analysis of this surface gives much information about the original data, which were used in describing this surface, which could not have been obtained in any other way.

Evaluation of equation (5), using the above values for the parameters a, b, c, and d results in the yield probability distribution shown in Figure I-1. Closer inspection of this distribution indicates that the most probable yield value for these experiments, as predicted by the model, is about 0.43, and analysis to obtain confidence limits indicates that, for instance, 95 per cent of all yield values fall statistically below 0.8. From this yield probability distribution, other confidence limits can be obtained as desired.

Evaluation of equation (6) results in the probability distribution for the spill function. It is graphically presented in Figure I-2. Using the same analysis procedures as above, the most probable spill value, as predicted by the model, is

The Mathematical Model, $a = 3.1$, $b = 4.0$, $c = 1.1$, $d = 1.5$

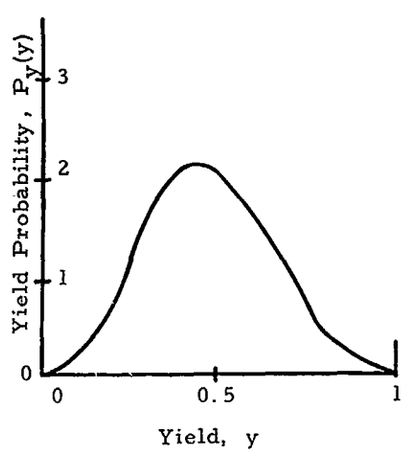

Fig. I-1
Probability Distribution
for the Yield Function
(Experimental Results)

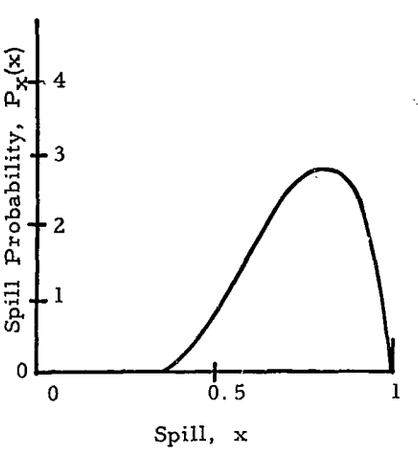

Fig. I-2
Probability Distribution
for the Spill Function
(Experimental Results)

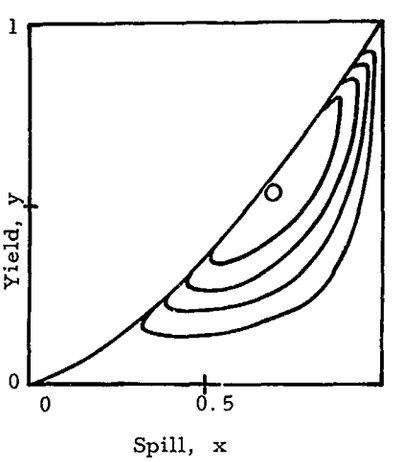

Fig. I-3
Yield - Spill
Probability Regions
(Experimental Results)

about 0.8, and 95 per cent of all spill values lie below a spill value of 0.94. Again other confidence regions can be obtained as desired.

Confidence regions for both yield and spill can be obtained from the model by solving integrals of the type of equation (7) for the total volume and the required subvolumes with the results as shown in Figure I-3. In this figure, all x-y values fall into an approximate triangular region bounded by points (0, 0), (0, 1), and (1, 1); 95 per cent of all x-y values fall into the next smaller region; 80 per cent into the next smaller region, 70 and 50. The peak point of the surface is also indicated.

Other relationships and information could be obtained by sectioning the mathematical model in different ways.

II. THE MATHEMATICAL MODEL APPLIED TO AVAILABLE EXPERIMENTAL DATA AND MISSILE FAILURE YIELD ESTIMATES

The mathematical model is next applied to both the available experimental data and actual missile failure yield estimates. Unfortunately no actual missile failures have been instrumented thus far to provide the required information. For this reason a basic assumption had to be made before the missile failure information could be used. This assumption is that the relationship between the quantity of propellants mixed and the resulting yield is a fundamental characteristic of liquid propellant explosions. Preliminary investigations now under way seem to support this assumption.

The results presented in this section are based upon the data presented in Table I, the estimates of Table II, and the above stated basic assumption.

TABLE II

Yield Estimates and Data of Missile Failures[3, 4, 5, 6]

5.	Atlas 9-C	y = 0.18	
6.	Atlas 48-D	0.08	
7.	Atlas	0.06	
8.	Titan 1	~ 0.02	
9.	Titan 1	~ 0.01	
10.	Atlas	0.0088	
11.	Centaur	0.029	Quad. 0.089, 0.017 0.007, 0.003
12.	Jupiter #9 (Impact)	0.11	
13.	S-IV Failure	1	
14.	S-IV Test (Pyro)	0.03 - 0.06	

Evaluating the parameters a, b, c, and d for the new input information in the same manner as for Section I gives

$$a = 21, \qquad b = 4.0, \qquad c = 1.1, \qquad d = 1.5$$

Comparing the new values with those obtained in Section I shows that only the value for parameter a changed, the others remained the same. Again more and better data would determine these parameters with greater accuracy defining the mathematical model with greater statistical reliability.

The results for the above numerical set of parameter values are presented graphically in Figure II-1, the yield probability distribution; Figure II-2, the spill probability distribution; and Figure II-3, the confidence regions for yield and spill.

From these results the most probable yield value as predicted by the model is now about 0.13 with 95 per cent of all yield values falling below a yield value of about 0.29.

The most probable spill value as predicted by this model is about 0.32 with 95 per cent of all spill values falling below about 0.48.

The yield-spill confidence regions are much smaller than before, as can be seen by comparing Figures I-3 and II-3, and are much closer to the origin. Again the regions containing 100, 85, 70, 50 and 30 per cent of all x and y values are shown.

The Mathematical Model, a = 21, b = 4.0, c = 1.1, d = 1.5

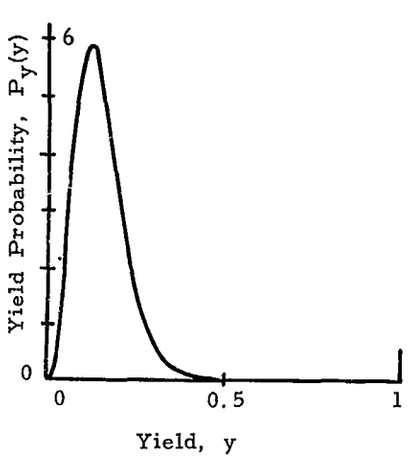

Fig. II-1
Probability Distribution for the Yield Function (Experimental Results and Missile Failures)

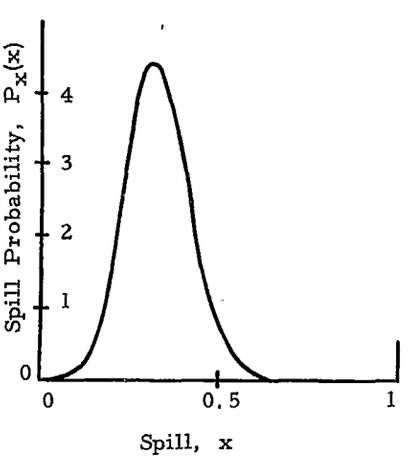

Fig. II-2
Probability Distribution for the Spill Function (Experimental Results and Missile Failures)

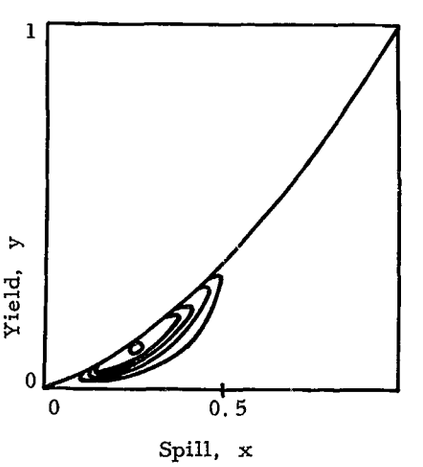

Fig. II-3
Yield - Spill Probability Regions (Experimental Results and Missile Failures)

The Mathematical Model, a = 70, b = 4.0, c = 1.1, d = 1.5

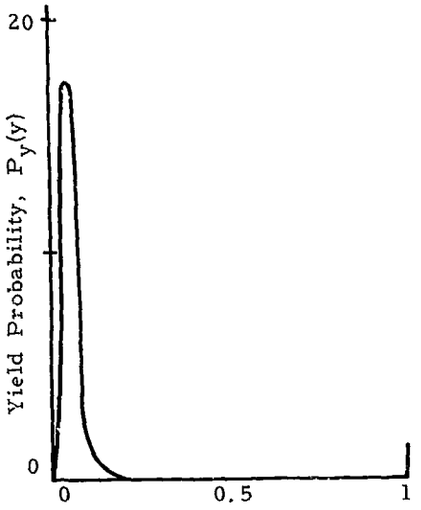

Fig. III-1
Probability Distribution
for the Field Function
(Missile Failures)

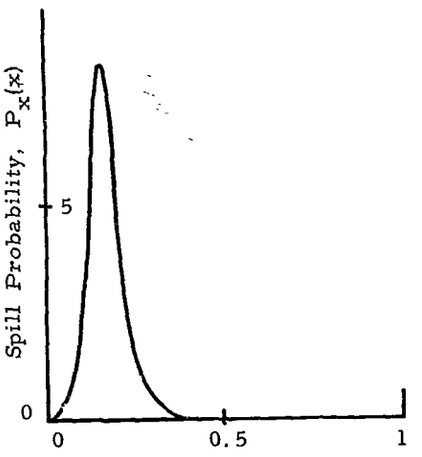

Fig. III-2
Probability Distribution
for the Spill Function
(Missile Failures)

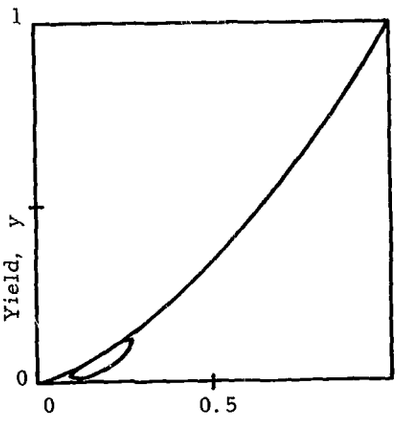

Fig. III-3
Yield - Spill
Probability Regions
(Missile Failures)

III. THE MATHEMATICAL MODEL APPLIED TO AVAILABLE MISSILE FAILURE YIELD ESTIMATES

Applying the mathematical model as developed above to the data shown in Table II and the assumption made in Section II, the parameters take on the following values: a = 70, b = 4.0, c = 1.1, d = 1.5

The statistical surface described by these new parameter values produces, when analyzed, the results presented in Figure III-1, the yield probability distribution; Figure III-2, the spill probability distribution; and Figure III-3, the confidence regions for yield and spill.

This analysis shows the most probable yield value, as predicted by this model, centers around a value of about 0.04 with 95 per cent of the yield values falling below about 0.11.

The most probable spill function value, as predicted by this model, is about 0.16 with 95 per cent of all spill values falling below about 0.27.

The yield-spill confidence regions are now getting quite small and so only the 100 and 80 per cent regions are shown. The peak point of the statistical surface has now moved rather close to the origin.

A POSSIBLE SCALING LAW AS SUGGESTED BY THE MATHEMATICAL MODEL

Closer scrutiny of the numerical results presented here shows that for the information used, only parameter a changed between Sections I, II, and III.

One of the major differences underlying the data of these sections is the quantity of propellants involved.

This fact, and that the parameter a was the only thing that had to be changed to redefine the model to make it applicable to the various sections, suggests that its variation with quantity of propellants involved may constitute the basis for a "Scaling Law."

Expressing the parameter a as a function of the scale (s)

$$a = F(s) \tag{8}$$

which is an exponential relationship for the data and estimates presented here, and substituting this relationship into equation (2) gives the mathematical model described in terms of the scale (s) and the previous parameters b, c, and d.

Analysis of the mathematical model as described by equations (2) and (8) give the required scaling law for liquid propellant explosions.

CLOSURE

From the work discussed and presented in this paper it is seen how a mathematical model can be constructed based upon the general characteristics of theoretical and experimental results of liquid propellant explosions, how this model can be applied to experimental results and the wealth of information which can be obtained in this manner.

The mathematical model developed and used here is very general in nature containing four controlling parameters and can therefore satisfy a wide range of data. It is not overly sensitive to changes in these parameters.

To demonstrate how this model can be used it was applied to the very sparse experimental data available and with a basic assumption, that the yield-spill relationship is a fundamental characteristic of liquid propellant explosions, to actual missile failure yield estimates.

The quantitative results predicted by this analysis such as probability distributions, confidence regions, confidence limits, and so on, should be considered preliminary since the model used here was defined by very little data even though the obtained results are in general agreement with the limited actual experience.

The results obtained from the mathematical analysis of the model seem to suggest the parameter a as a "scaling factor" allowing the prediction of the characteristics of liquid propellant explosions as a function of scale, or quantities of propellants involved.

The reliability of the model should be improved for prediction purposes by better theoretical information and better experimental results, which describe and define the model more precisely by giving better values to the parameters.

In conclusion, it may be well to say again that the mathematical model presented here, and others like it can help in guiding future experimental programs, indicating what information is needed and where, and in reducing the cost of these programs by reducing the number of expensive tests necessary. Furthermore the approach through a mathematical model may well indicate the most direct route to follow to obtain a valid scaling law for yield prediction for liquid propellant explosions.

ACKNOWLEDGEMENTS

It is with sincere appreciation that the writer expresses his indebtedness to the National Aeronautics and Space Administration under whose sponsorship (part of contract NAS10-1255) this work was carried out; to the University of Florida; to Mr. J. H. Deese, Chief, Advanced Studies Office, KSC; to his colleagues, G. J. Schoessow, D. Van der Rayden, F. L. Schwartz, J. H. Brann, J. A. Wethington, T. M. Reed, J C. Reed, and to scientists at MFSC, MSC, NASA Headquarters in Washington, BRL and AFRPL.

BIBLIOGRAPHY

1. Farber, E. A., et al. "Feasibility Study to Explore the Explosive Effects of Liquid Propellants to Define the Mathematical Behavior of Physical Processes Involved," Final Report, Phase I, Contract No. NAS10-1255, University of Florida, February, 1965.

2. Arthur D. Little, Inc. "Summary Report on a Study of the Blast Effect of a Saturn Vehicle," February, 1962.

3. Information obtained from Lou Ullian, AFETR through informal correspondence and relayed by J. H. Deese.

4. Information obtained from J. H. Deese through informal correspondence.

5. Gayle, J. B. "Investigation of S-IV All Systems Vehicle Explosion," MSC, Huntsville, Alabama, NASA TM X-53039, April 27, 1964.

c. NASA/USAF Liquid Propellant Blast Hazards Program, Project Pyro Monthly Progress Report for Period Ending 31 July 1965, AF Rocket Propulsion Laboratory, Research and Technology Division, Edwards, California.

7. Edwards, J. W. Integral Calculus, MacMillan Co., London, 1896.

8. "Handbook of Mathematical Functions with Formulas, Graphs, and Mathematical Tables," U. S. Department of Commerce, NBS Applied Mathematics Series -55, 1964.

9. Deese, J. H. "A Correlation and Hypothesis of LH_2/LO_2/RP-1 Blast Data," Unpublished, January, 1963.

A SYSTEMATIC APPROACH FOR THE ANALYTICAL ANALYSIS AND PREDICTION OF THE YIELD FROM LIQUID PROPELLANT EXPLOSIONS

by

E. A. Farber* and J. H. Deese†

ABSTRACT

This paper presents a systematic approach by which the expected yield from liquid propellants can be predicted and furthermore gives an insight into the physical phenomena involved.

The yield potential and the mixing function can be determined allowing for the type of propellants, their relative proportions, the reaction rates between the components depending upon mixture composition, the heat transfer rates between the components and the propellants and the surroundings, the mode of failure and the resulting mixing characteristics, and the ignition and reaction delay times.

Combining the above information into seven charts as presented leads to a systematic analytical determination of the expected yield.

INTRODUCTION

In an effort to assess and minimize the hazards from liquid propellant explosions as a result of missile failures to astronauts, launch support personnel, launch facilities and surrounding structures it is of utmost importance to be able to predict the most probable expected yield.

An approach, considering the over-all characteristics of liquid propellant explosions, to predict the most probable yield, the most probable spill, probability distributions, confidence regions, confidence limits, and so forth, by means of a mathematical model was presented earlier [1, 2] by one of the authors of this paper. The method described there accomplished the ultimate goal of leading to a valid

---

*Professor and Research Professor of Mechanical Engineering, University of Florida.

†Chief, Facilities Technology Office, NASA-John F. Kennedy Space Center.

prediction procedure of yield, spill, and so forth, of liquid propellant explosions; it did not provide an insight into the physical phenomena producing this yield, spill, and so on.

The present paper suggests a more fundamental approach to this problem by considering the physical phenomena in detail which go into producing the most probable yield, spill, and so on. This approach therefore can, through understanding of the physical processes and phenomena, provide the information necessary to control these processes.

The approach presented here is referred to by the authors as the "Seven Chart Approach" since the procedure can be summarized in seven charts, constituting a complete, well planned program, outlining the necessary steps to be followed.

Furthermore, the "Seven Chart Approach" uses presently available information regarding these poorly understood phenomena producing the liquid propellant explosion yield; it points out where more theoretical and experimental work is needed, and what information it should provide. In this manner an ideal balance is obtained between theory guiding the experimental work and the results from the experiments modifying the theory. For these reasons this procedure is able to reach the desired goals along a most direct route in the shortest possible time and at a minimum cost.

Previous theoretical and experimental investigations [1,2,3,4,5], through their results, suggest that the actual phenomena producing the yield in liquid propellant explosions can be divided into groups which lend themselves to separate study, both theoretical and through small-scale experimentation.

For the purposes of the "Seven Chart Approach," suggested here for the prediction of the most probable yield, etc., for liquid propellant explosions, the problem is divided into three such groups of phenomena which can be studied separately but when combined allow the desired prediction. The groups revolve around

I. The Yield Potential Function

II. The Mixing Function

III. Delay and Detonation Times

and allow the incorporation of the basic characteristics of the particular propellants involved, of the missile design configuration, and of the mode of failure.

The yield potential function (I) is basically controlled by chemical kinetics, the mixing function (II) by the principles of hydrodynamics modified by heat trans-

fer, and the delay and detonation times (III) by characteristic functions for some propellants such as hypergolics or by random processes for others.

The separate studies can be combined by taking the yield potential, when expressed as a time function, and multiplying it by the mixing function to obtain the expected yield at any time after the start of the failure or after the mixing has begun. This mixing function will be different for different modes of failure and missile configurations.

The actual expected yield can be determined by superimposing the delay and detonation times upon the above obtained expected yield function, either as a fixed value where applicable or as a statistically most probable value with proper confidence limits. These delay and detonation times are characteristics of the propellants such as hypergolics, or cryogenics, modified by the propellant quantities, missile configuration, modes of failure, and so forth.

The total procedure can be summarized, with the seven charts supplying the necessary information, as the relationship

$$y = (y_p \cdot x)_{t^*}$$

where y expected yield at time t^*

y_p yield potential at time t^*

x mixing function at time t^*

t^* most probable detonation time

The development of the seven charts follows: conditions were assumed so that quantitative results could be calculated for cases which were investigated experimentally and for which results are reported in literature [4]. This gives more meaning to the procedure suggested and allows comparison of results obtained by the "Seven Chart Approach" with actual test results. The approach would be the same if other initial conditions, propellants or configurations were used.

I. THE YIELD POTENTIAL FUNCTION

The yield potential function for any propellants or combinations of them as a function of time can be obtained from theoretical considerations in four steps as follows:

1. Maximum Theoretical Energy Release (Chart 1)

The maximum amount of energy which can be released from any particular liquid propellant fuel-oxidizer mixture can be calculated employing the basic laws of chemical kinetics.

Figures 1A and 1B (in greater detail) show the results from such calculations for a three-component propellant mixture, $LO_2/LH_2/RP\text{-}1$.

The upper curve in these figures is the result of the three-component mixture $LO_2/LH_2/RP\text{-}1$, with the ratio of LH_2 to RP-1 held constant. In arriving at the numerical values it was assumed that all the LH_2 always reacts, and as much of the RP-1 as can be supplied with LO_2. Atmospheric oxygen could also be included if desired without any particular difficulty.

The lower curve is the result of a two-component mixture $LO_2/RP\text{-}1$, again presented here without atmospheric oxygen contribution. This curve is applicable to a two-component mixture or could be considered the condition after all the LH_2 of the three-component mixture has evaporated.

Thus any three-component $LO_2/LH_2/RP\text{-}1$ mixture will have its starting point on the upper curve and will, due to evaporation of both the LH_2 and the LO_2, follow a path from the upper curve to the lower curve toward the origin, this is if reaction does not occur somewhere along this path terminating this process. The actual path depends upon the changes in the relative quantities of each component present. Two such paths are shown in Figure 1A and in more detail in Figure 1B.

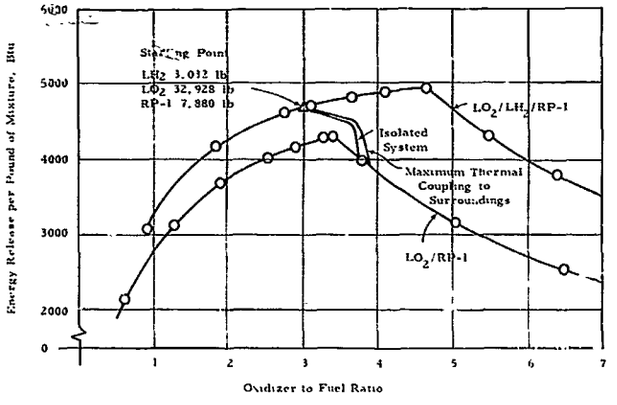

Figure 1A Maximum Amount of Energy Release for a Three Component Liquid Propellant Mixture

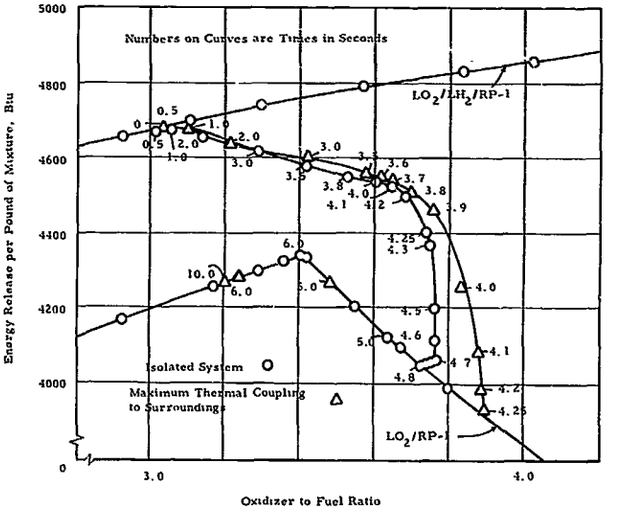

Figure 1B Maximum Amount of Energy Release for a Three Component Liquid Propellant Mixture

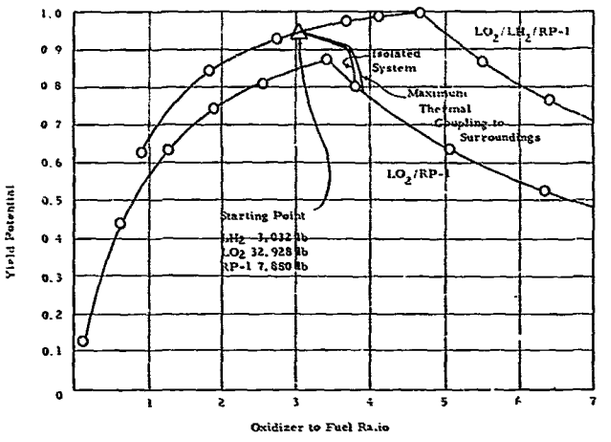

Figure 2 Yield Potential for a Three Component Liquid Propellant Mixture

How they are calculated will be explained later, but it might be mentioned at this time that they are for a mixture which was actually used in field experiments [4]. One path assumes that the system is thermally isolated from the surroundings and the other path assumes that maximum thermal interaction between the system and the surroundings occurs.

That the two paths are not as much different as might be expected indicates that the effect of the surroundings is minor.

2. Yield Potential as a Function of Oxidizer to Fuel Ratio (Chart 2)

The explosive yield of the liquid propellants will depend not only on the quantity of energy released, but also upon the rate at which this energy is released. Because of lack of information as to the variation in the reaction rates as a function of the propellant composition it was assumed for these calculations that the reaction rate remains essentially constant throughout the LO_2/fuel ratios under consideration here.

With this assumption, which can however be replaced by reaction rate information as soon as it becomes available, and the information of Figure 1, the yield potential can be calculated and normalized in terms of the theoretical maximum. The results are presented in Figure 2.

3. Mass-Fraction Time Relationship for LH_2 and LO_2 (Chart 3)

To be able to determine the actual paths as previously discussed and shown in Figures 1A, 1B, and 2 it is necessary to know the LH_2/LO_2 ratio and its variation. This is easiest obtained from calculations of the quantities of LH_2 and LO_2 present at any time.

The calculations are more or less standard, involving the principles of thermodynamics and heat transfer, but are very long and tedious. They involve simultaneous heat balance and heat transfer relationships with the proper heat transfer coefficients which allow, through step-by-step and iterated calculations, the estimation of the quantities of cryogenics vaporized, escaping, or again condensed in the mixture, the quantities of fuel and oxidizer frozen and portions remelted, and so forth. Some simplifying assumptions were made wherever it seemed advantageous in reducing the large amount of computations without appreciably affecting the results. Where quantities were encountered which had the same order of magnitude, but the opposite sign and were relatively small, they were sometimes cancelled against each other. These actions helped tremendously in reducing the scope of the necessary computations.

Contact area variations based upon mixing studies both at the University of Florida in connection with the study of explosive hazards of liquid propellants, and information found in literature, were used in the heat transfer equations together with the best available heat transfer coefficients to obtain the mass-fractions for LO_2 and LH_2.

The information needed and used, aside from that supplied by supporting studies at the University of Florida, are referenced in Table I but only the results from the actual calculations can be presented here because of the severe space limitations. The results are presented in Figures 3A and 3B.

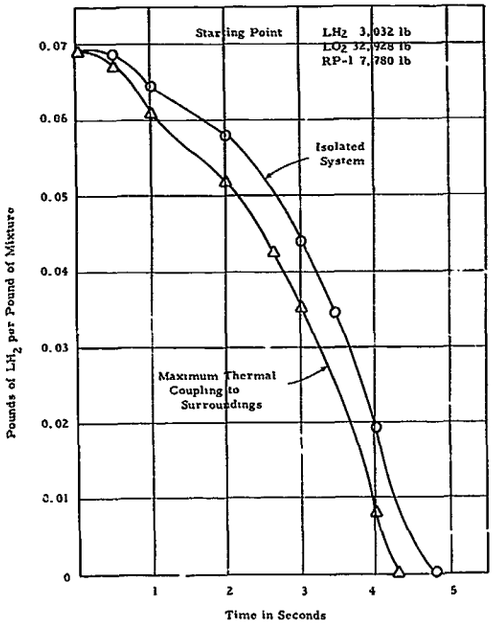

Figure 3A Amount of LH_2 Present at Time t

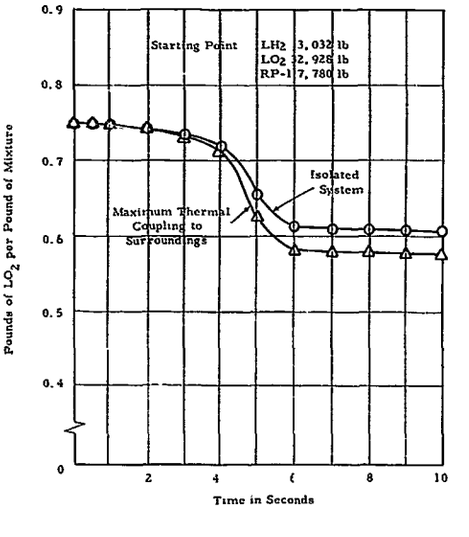

Figure 3B Amount of LO_2 Present at Time t

TABLE I

List of Literature References Used in Support of the Calculations for the Results Presented in Figures 1A through 3B

SUBJECT	REFERENCES
Average Chemical Formulas for Kerosene, RP-1	6, 16, 17, 19
Average Heat of Combustion for Kerosene	6, 7, 18
Heat of Combustion for Hydrogen	7
Propellant Proportion used in Heat Transfer Calculations	8
LAN/RP-1 Contact Area versus Time Data for LO_2/RP-1 Analogy	9
Film Coefficients for LAN/RP-1 Interface	9
Film Coefficients for LN_2/LH_2 Interface and LN_2/LH_2 Contact Area versus Time Data for LO_2/LH_2 Analogy	11
Latent Heat of Evaporation for H_2 and Specific Heat for GO_2	12
Specific Heat for L JP-1 to simulate RP-1	3
Latent Heat of Evaporation for O_2	12, 3
Latent Heat of Fusion for O_2	12
Approximation of Latent Heat of Fusion for RP-1	19
Approximation of Specific Heat of Solid Kerosene	13, 14, 15

4. Yield Potential — Time Relationship (Chart 4)

Since in the method for the calculation of the yield potential — oxidizer to fuel ratio relationship time t was the common variable used, it is easy to put a time scale right on the paths as shown (Figure 1B).

With these time scales right on the paths of Figure 2B, these curves can be replotted giving the yield potential versus time relationship as seen in Figure 4.

These curves represent the theoretical maximum yield which could be obtained at any time t from the above propellants due to the quantities of the constituents which are present at that time. One curve again represents the yield potential for the isolated system and the other for the system which has the maximum theoretical thermal interaction with the surroundings.

Since the curves of Figure 4 give the yield for propellants when perfectly mixed to produce maximum yield, these results must be modified by the mixing function, the actual amounts (fraction of the maximum amounts) which are mixed at any time t.

II. THE MIXING FUNCTION (Chart 5)

While the yield potential function as calculated above for a specific case established the actual quantities of the various constituents present and the maximum theoretical yield, if all these constituents are mixed most effectively, it does not give any information as to the actual degree of mixing of the constituents.

For example, at time 0 when the constituents just begin to mix, none of them are actually mixed and therefore an explosion could not be produced. Thus at time 0 the mixing function is 0 while the yield potential function is near its maximum. The product of the yield potential and the mixing function at time 0 gives the true or expected yield.

The mixing function is essentially a hydrodynamic function, however complicated by high rates of heat transfer. This makes the analytical approach difficult, and at least to start with, an experimental approach for determining this func-

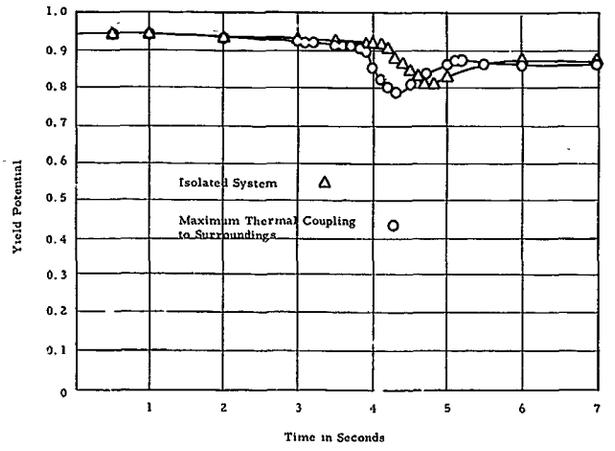

Figure 4 Yield Potential Plotted as Time Function

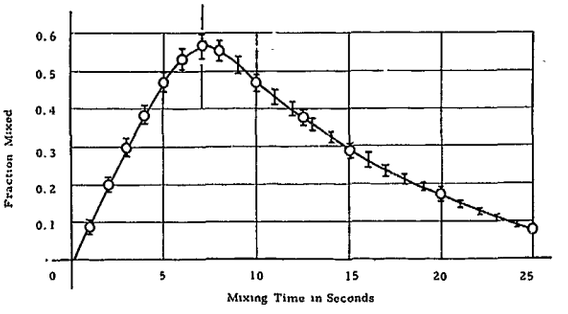

Figure 5 Mixing Function or Spill Function for Three Component Liquid Propellant Spill Tests

tion more promising. This is true especially since questionable assumptions are not involved.

Four methods have been developed in connection with the over-all systematic approach presented in this paper and to implement its execution. These four methods allow the detailed study of the mixing process and phenomena producing the mixing function of liquid propellants and have been used with great success. In preliminary studies, often applying two methods to the same experiment, these methods have independently produced results which are in excellent agreement.

The detailed description of these methods and the various methods of analysis and the results obtained by them are beyond the scope of this paper, but since they implement the approach suggested in this paper they are briefly mentioned. They are the

1. Film Analysis: A high speed photographic technique giving by use of mirrors a three-dimensional picture of the mixing process on the same film frame. Special analysis of these frames as to mixing profile, mixing volume, and turbulence factor allows the determination of contact area and degree of mixing.

2. Wax Cast Analysis: By use of hot wax and cold liquids the mixing process can be "frozen" at different stages of the mixing by varying the hot and cold temperatures. The "frozen" state of the mixing process can then be studied at leisure at any time later. These casts can be analyzed as to profile, outside area by projection or coating methods; they can be serially sectioned to give the total contact area, turbulence factors (total contact area over profile area), and so on.

3. Vibration Mixing Analysis: This method consists of mounting a particular configuration on a vibration table, simulating the various propellant components by particles of different color, size, density, shape, etc., and after removing partitions, partially or completely shaking the system. The components will mix and the degree of mixing can be periodically checked at desired locations. Evaporation or other losses can be simulated by removing programmed quantities or numbers of particles at desired locations and prescribed intervals.

4. Thermocouple Grid Analysis: This method of analysis employs a three-dimensional grid of fine thermocouples with each junction being monitored continuously. The traces give information regarding the mixing front, the degree of mixing at a particular point, the degree of turbulence at a point, the location of the point or points of ignition, the time delay from the start of mixing (or time of failure) to ignition, the propagation of the reaction front, the propagation of the shock front, the separation of the shock front from the reaction front, and so forth.

Results from the above methods can be correlated and compared easily by simultaneously applying the different methods of analysis to the same experiment. These methods provide information needed for the better understanding of the mixing phenomena of liquid propellants, they provide data as to the statistical reproducibility in seemingly identical experiments, the variations due to test configuration, and so on.

The Thermocouple Grid Analysis method is the most powerful since it directly relates the mixing phenomena and the yield obtained all in one and the same experiment. It is, however, considerably more expensive than the others. Instrumentation for high-speed monitoring of the individual junctions is expensive and the reduction of the data obtained time-consuming.

However, this Thermocouple Grid method is capable of taking measurements in liquid propellant mixtures from the start of failure up to and after ignition. If the grid is extended beyond the original boundaries of the propellant configuration, information can be obtained as to fireball growth rate, extent, temperature, shock wave strength, shock wave velocity, and so on.

Further and more detailed discussion of these four methods of analysis which can provide the mixing function-time relationship is left to another paper which includes the presentation of results obtained with these methods for a number of failure modes and configurations.

Only one of these result' is presented here corresponding to the series of spill experiments used as examples for comparison with the calculated numerical results. It is the mixing function presented in Figure 5, in this particular case obtained by method 3, the vibration mixing analysis. Since this method has no absolute time scale a number of runs were made adjusting the amplitude and frequency so that easily measurable changes were observed in reasonable time intervals (about 5 seconds). Since from theoretical considerations the maximum should occur at about 7 seconds this time was ascribed to the maximum point of the mixing curve. In this manner the absolute time scale was established.

The reproducibility of this curve as presented was within plus or minus 4 per cent. The reproducibility became better as the mixing violence increased. This fact was observed in all experiments whether simulated on the vibration table or with real liquids using the other methods.

III. DELAY AND DETONATION TIMES

Probably the least understood phenomena of the ones discussed in this paper are the ones controlling the delay and detonation times.

Both these quantities will be discussed in considerable detail in another paper where they are evaluated, and detonation times calculated, based upon a new hypothesis proposed and referred to in that paper as "Fireball Hypothesis."

In that paper delay time is defined as the time from the start of the failure to ignition, or the time from start of mixing to ignition, whichever is preferable.

The detonation time is the time from ignition until the reaction reaches the boundary of the original propellant configuration.

For the purpose of this presentation actually measured delay times from the experiments are taken and statistically analyzed so as to establish the most probable yield value as well as 95 per cent confidence limits. More data is needed to establish these quantities with greater reliability.

For the test used for comparison here the average delay plus detonation time is 3.3 seconds and the standard deviation for fixing confidence limits, 1.1 seconds.

1. Expected Yield Function — Time Relationship (Chart 6)

Having discussed the three groups of phenomena playing a roll in producing the yield of liquid propellant explosions, the results obtained in Sections I, II, and III can now be combined.

Taking the yield potential function calculated in Section I and presented in Figure 4 and the mixing function calculated in Section II and presented in Figure 5, and combining them by multiplying corresponding ordinates at time t, the expected yield function is obtained. This result is presented in Figure 6 which shows the yield which could be expected at any time t if detonation did occur at that time t. Only the curve for the isolated system is presented here but the other is obtained easily in the same manner. This expected yield function has a plus or minus 4 per cent variation in yield value due to this variation in the mixing function.

The expected yield function has a characteristic shape starting at zero increasing with a dip or double hump to a maximum value and then decreasing again. The dip or double hump is due to the initial proportions of the propellant components.

Figure 6 Expected Yield as a Time Function

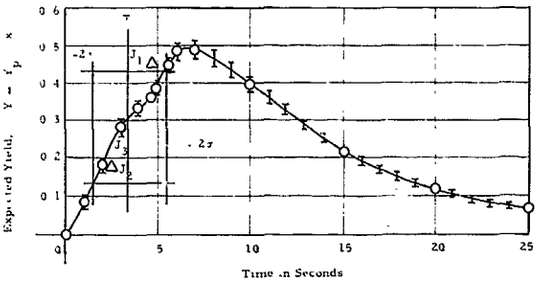

Figure 7 Expected Yield for Random Ignition and Detonation Showing the Upper and Lower Limits of the Statistical Confidence Regions for Liquid Propellant Spill Tests

The maximum is far from one since, with any appreciable quantity of liquid propellants, perfect mixing is almost impossible to achieve and furthermore, due to the time elapsed between the start of, and best, mixing the yield potential has fallen below one because of evaporation losses of the propellant components.

2. Expected Yield (Chart 7)

The last step in this series, to obtain the expected yield for liquid propellant explosions, is to superimpose the information of Section III upon the combined results of Sections I and II.

Figure 7 shows the result, the final step in this systematic approach, with the expected yield function on Figure 6 modified by the delay and detonation times fixing an interval within which, statistically, 95 per cent of all expected yield values should lie.

The highest value for the expected yield predicted for this test series, using 95 per cent confidence limits, should be about 0.45, the lowest 0.13. All values predicted by this approach should fall between 0 and 0.50.

CLOSURE

This paper suggested and presented a systematic approach referred to as the "Seven Chart Approach" for the prediction of expected yield for liquid propellant explosions. The "Seven Chart Approach" consists of seven steps expressible in seven charts:

1. Maximum Theoretical Energy Release
2. Yield Potential as a Function of Oxidizer to Fuel Ratio
3. Mass-Fraction — Time Relationships

4. Yield Potential — Time Relationships
5. The Mixing Function
6. Expected Yield Function — Time Relationship
7. Expected Yield

The paper presented this approach, outlined here, with actual calculated curves, combined with some experimental results to give quantitative information.

The "Seven Chart Approach" as outlined above allows for a systematic procedure in determining the expected yield from liquid propellant explosions and thus guides the experimental work necessary to implement the analytical procedures.

This approach divided the problem into three very distinct parts which can be studied separately and, when combined, give the desired results. The three parts are the determination of the yield potential, the mixing processes analysis, and the ignition and detonation phenomena.

The insight gained into the actual physical phenomena through this approach promises to provide a method of control whereby the hazards from liquid propellant explosions can be considerably reduced.

ACKNOWLEDGMENT

It is with sincere appreciation that the writers express their indebtedness to the National Aeronautics and Space Administration under whose sponsorship (part of contract NAS10-1255) this work was carried out; to the University of Florida; to G. L. Schoessow, F. L. Schwartz, J. A. Wethington, T. M. Reed, R. L. San Martin, C. Williams and to scientists at MFSC, MSC, NASA Headquarters in Washington, BRL and AFRPL.

BIBLIOGRAPHY

1. Farber, E. A., et al., "Feasibility Study to Explore the Explosive Effects of Liquid Propellants to Define the Mathematical Behavior of Physical Processes Involved," Final Report Phase I, Contract No. NAS10-1255, University of Florida, February 1965.

2. Farber, E. A., "A Mathematical Model for Defining Explosive Yield and Mixing Probabilities of Liquid Propellants," Third Space Congress Proceedings, March 1966 (Preceding paper).

3. Deese, J. H., "A Correlation and Hypothesis of LH_2/LO_2/RP-1 Blast Data," Unpublished, January 1963.

4. Arthur D. Little, Inc., "Summary Report on a Study of the Blast Effect of a Saturn Vehicle," February 1962.

5. Aerojet-General Corp., "Blast and Fireball Comparison of Cryogenic and Hypergolic Propellants," Contract No. NAS9-2055, Final Report, 26 June 1964.

6. Mechanical Engineers' Handbook, edited by T. Baumeister, McGraw-Hill Book Co., Inc., 6th Edition, New York, 1958.

7. Obert, E. F., Internal Combustion Engines, International Textbook Company, Second Edition, Pennsylvania, 1960.

8. Arthur D. Little, Inc., "Summary Report on a Study of the Blast Effect of a Saturn Vehicle," February 15, 1962, and some original data obtained from them.

9. Project Pyro., "Monthly Progres; Report - Period ending 29 February 1964."

10. Foust, A. S., et al., Principles of Unit Operations, John Wiley & Sons, Inc., New York, 1960, p. 264.

11. Project Pyro., "Monthly Progress Report - Period ending 31 May 1964," June 9, 1964.

12. Seader, J. D., et al., "Boiling Heat Transfer for Cryogenics," Final Report, Rocketdyne R-5598, May 11, 1964.

13. ASHRAE Guide and Data Book 1961, American Society of Heating, Refrigeration and Air-Conditioning Engineers, Inc., 1961.

14. Handbook of Engineering Fundamentals, edited by O. W. Eshbach, John Wiley and Sons, Inc., Second Edition, New York, 1958.

15. Handbook of Chemistry and Physics, edited by C. D. Hodgman, Chemical Rubber Publishing Co., Forty-First Edition, Ohio, 1960.

16. Chemical Engineers' Handbook, edited by J. H. Perry, McGraw-Hill Book Co., Inc., Third Edition, New York, 1958.

17. Technical Data on Fuel, edited by H. M. Spiers, The British National Committee World Power Conference, Fifth Edition, London, 1952.

18. Fuels and Combustion Handbook, edited by A. J. Johnson, McGraw-Hill Book Company, Inc., New York, 1951.

19. Nelson, W. L., Petroleum Refinery Engineering, McGraw-Hill Book Company, Inc., New York, 1936.

20. Smith, M. L. and Stinson, K. W., Fuels and Combustion, McGraw-Hill Book Company, Inc., New York, 1952.

Appendix

ENGINEERING PROGRESS

AT THE

UNIVERSITY OF FLORIDA

Vol. XXI, No. 8 August, 1967

Technical Paper Series

CHARACTERISTICS OF LIQUID ROCKET PROPELLANT EXPLOSION PHENOMENA

No. 386: *Part III. Studies and Analyses of the Mixing Phenomena of Liquid Propellants Leading to a Yield-Time Function Relationship,* by E. A. Farber and R. L. San Martin.

No. 387: *Part IV. Fireball Hypothesis Describing the Reaction Front and Shock Wave Behavior in Liquid Propellant Explosions,* by E. A. Farber and J. S. Gilbert.

(A Continuing Series of Research Reports on NASA Project NAS 10-1255. Parts I and II appear as Technical Papers No. 346 and No. 347.)

PUBLISHED MONTHLY BY THE

FLORIDA ENGINEERING AND INDUSTRIAL EXPERIMENT STATION

COLLEGE OF ENGINEERING • UNIVERSITY OF FLORIDA • GAINESVILLE

ENTERED AS SECOND-CLASS MATTER AT THE POST OFFICE AT GAINESVILLE, FLORIDA

Characteristics of Liquid Rocket Propellant Explosion Phenomena

A research project initiated in 1964 by Dr. Erich A. Farber, Research Professor of Mechanical Engineering, on liquid propellant rocket explosions, has resulted in the publication of five NASA reports and four technical papers to date in this area. The research is under the sponsorship of the National Aeronautics and Space Administration. The four papers listed below define and discuss the characteristics of liquid rocket propellant explosion phenomena. They are:

I: A Mathematical Model for Defining Explosive Yield and Mixing Probabilities of Liquid Propellants, by E. A. Farber.

II: A Systematic Approach for the Analytical Analysis and Prediction of the Yield from Liquid Propellant Explosions, by E. A. Farber and J. H. Deese.

(Nos. I and II were published in the Proceedings of the Third Space Congress, March, 1966, Canaveral Council of Technical Societies, Cocoa Beach, Florida. Available as Technical Papers No. 346 and No. 347, Florida Engineering and Industrial Experiment Station, Gainesville, Florida.)

III: Studies and Analyses of the Mixing Phenomena of Liquid Propellants Leading to a Yield-Time Function Relationship, by E. A. Farber and R. L. San Martin.

IV: Fireball Hypothesis Describing the Reaction Front and Shock Wave Behavior in Liquid Propellant Explosions, by E. A. Farber and J. S. Gilbert.

(Nos. III and IV, published in this volume as Technical Papers No. 386 and No. 387, were presented at the New York Academy of Sciences conference on explosion hazards in New York City, October, 1966, and will also be published in the Fall of 1967 in the Proceedings of the New York Academy of Sciences.)

Since research on this problem is continuous in nature and considerable effort and time is expended thereon, more papers and reports in this series will be forthcoming.

III

STUDIES AND ANALYSES OF THE MIXING PHENOMENA OF LIQUID PROPELLANTS LEADING TO A YIELD-TIME FUNCTION RELATIONSHIP

by

E. A. Farber, Ph. D.,* and R. L. San Martin, Esq.†

ABSTRACT

This paper presents and discusses four methods which have been developed and are being used by the authors in the study of the mixing phenomenon, an important factor in the explosive "yield" analyses of liquid rocket propellants. The first three methods

A. Film Analysis
B. Wax Cast Analysis
C. Vibration Mixing Analysis

can be classified as simulation study methods since they involve nonexplosive — thus simulated media. The fourth method

D. Thermocouple Grid Analysis

can be used both in simulated as well as explosive tests. These four methods and typical results from these studies are presented.

ACKNOWLEDGMENT

It is with sincere appreciation that the writers express their indebtedness to the National Aeronautics and Space Administration under whose sponsorship (part of contract NAS10-1255) this work was carried out; to the University of Florida and its staff and to Mr. J. H. Deese, Chief, Facilities Technology Office, John F. Kennedy Space Center.

---

* Professor and Research Professor of Mechanical Engineering, University of Florida, Gainesville, Florida.
† Research Associate in Mechanical Engineering, University of Florida, Gainesville, Florida.

INTRODUCTION

In our present-day rocket development it is of utmost importance to be able to predict with sufficient degree of certainty the explosive yield hazards of accidental liquid propellant rocket explosions. This is necessary to properly protect the astronauts, the launch support personnel, and the surrounding facilities. Further insight into the phenomena that lead up to and produce the yield may allow control over these processes and thus the explosive yield from such happenings.

This explosive yield can be defined in terms of TNT equivalency (how many pounds of TNT produce the same effects as one pound of propellant mixture) or preferably as a fraction of the theoretical maximum.

Earlier studies of liquid rocket propellant characteristics[1, 2, 3] have indicated that the study of the characteristics can be divided into a number of subproblems, which can be studied separately and independently and then the results from such studies could be combined to give the answers sought.

Some of these subproblems are the "yield potential" (theoretical maximum), essentially a problem in chemical kinetics, the "mixing function," essentially a problem in hydrodynamics with heat transfer added, and the "delay time," the time between initiation of failure and ignition. These subproblems are under study now and will be reported in separate papers.

The present paper will deal with the second of these factors, the "mixing function," which may be defined as the proportion or fraction of the propellants mixed at any time t. This fraction can be expressed in a number of ways as will be seen in this paper. It can be defined in terms of a contact area or surfaces proportional to this area, in terms of liquid interfaces, of mixing surface profiles, etc. This paper will describe how this was done in various manners by four experimental methods which are independent but complement each other. In many experiments two of these methods were used simultaneously so that the results could be compared for one and the same experiment.

These four methods are

A. The Film Analysis
B. The Wax Cast Analysis
C. The Vibration Mixing Analysis
D. The Thermocouple Grid Analysis

The Film Analysis is a method which depends on high-speed photographic coverage of the mixing phenomena, followed by an analysis and proper interpretation of these records.

The Wax Cast Analysis "freezes" the mixing process at different stages of the process so that the solidified image can be analyzed at a later date and at leisure.

The Vibration Mixing Analysis simulates small fluid elements by different density, different color, differently shaped particles such as marbles, by shaking them on a vibration table for certain lengths of time, and by removing particles periodically simulating such things as evaporation or spill losses. Thus the mixing phenomena can be studied in small incremental steps, simulated by particles as large as marbles or as small as in powders.

The Thermocouple Grid Analysis, the best and most powerful of the four methods, consists of a three-dimensional grid of fine thermocouples, which produces a time record of temperature and its variation at many points in a region under investigation. These readings can be interpreted as will be explained to give insight into the phenomena leading up to and having a hand in producing the yield.

In the following pages these four methods will be discussed in detail, and some of the results which have been obtained will be presented. These results will give an indication of the value of these study methods in investigating the mixing phenomena of liquid rocket propellants. The results presented here are not intended to simulate a particular missile or missile failure but rather to demonstrate how these methods can be employed in the study of the mixing produced by many different missile configurations and types of failures.

THE METHODS

A. Film Analysis

For the application of this method for analysis, it is necessary to obtain a high-speed pictorial record of the mixing phenomena, involving high speed photographic equipment. For the present investigation transparent configurations were chosen and then, by placing mirrors at various angles, three-dimensional views were obtained on the same frame of the high-speed recording film. For non-transparent arrangements, X-ray, Gamma-ray, or tracer techniques could be used in a similar manner. Some of the latter techniques have been used by one of the authors in concentration studies and profile interface studies of two- and three-phase mixtures.[4, 5, 6, 7]

Figure A-1 presents an overall view of the experimental apparatus used in the study of the mixing processes between hot or cold oil and water, hot wax and

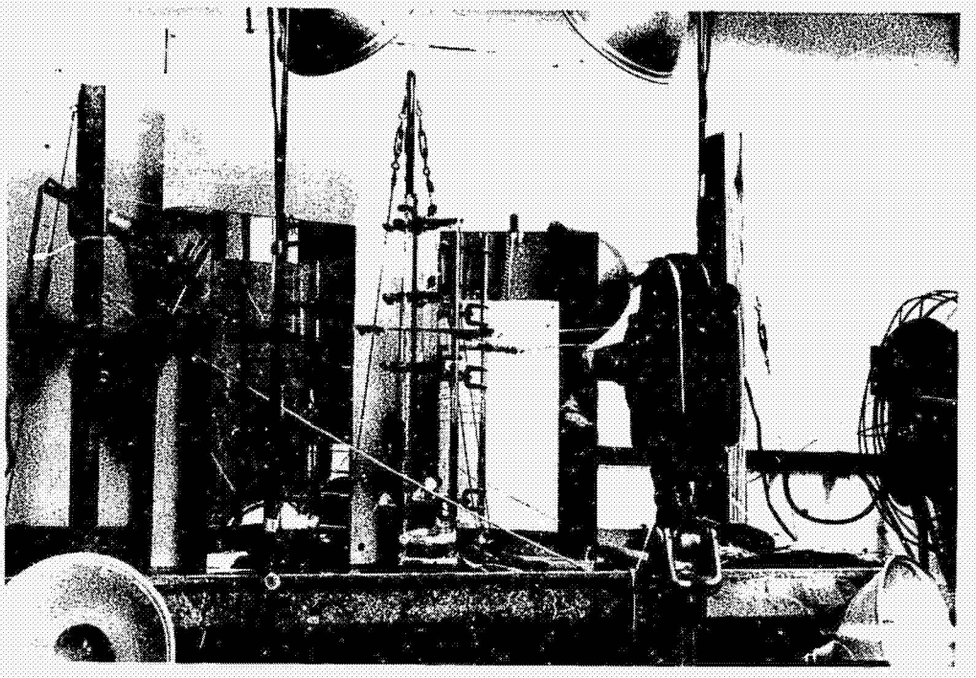

Figure A-1 Experimental Arrangement for Film Analysis

water, LN_2 and kerosene, etc. It consists essentially of a Pyrex glass tube filled to a desired level with one liquid, and another Pyrex tube above filled with the desired amount of the other liquid. A shim stock diaphragm between the two glass tubes holds the upper liquid in place. At time zero the diaphragm is snatched out by a quick motion system so as to remove it almost instantaneously. Slower removal of the diaphragm according to a programmed input can, if desired, simulate a progressive failure. If a complete diaphragm or bulkhead failure is not desired, a second fixed diaphragm can be inserted in addition to the removable one so that when the latter is removed, a desired size opening, at a desired location, remains simulating a particular type of failure.

Figure A-2 shows a number of frames for oil (top) and water, simulating bulkhead failure in a 1 1/2 in. ID tube and an ullage space of 4 [illegible] in. Successive frames taken at 64 frames per second show the progression of the mixing process from three views, 120 degrees apart.

The analysis can be made directly from the frames as projected on a screen or from a more permanent record by either blowing them up on photographic paper or tracing the outlines of the mixing fronts as shown in Figure A-3.

Figure A-3 further indicates the reproducibility of the mixing experiments by showing the traces of three identical runs and how close the total profile areas match.

From the three-dimensional views or traces, the total surface areas were determined by graphically obtaining the perimetric surface of small irregularly shaped discs. The resulting outside surface area, or A_o, can then be plotted versus frame or versus time (see Fig. A-4).

Since there are, however, droplets or particles of one liquid (vapor or solid) surrounded by the other within the space circumscribed by the profile, determined as described above, to get the true contact area between the liquids, these additional surfaces must be taken into account. This was accomplished by a tedious method of counting these droplets, determining their size and surface areas, and adding these new areas to the profile areas. The ratio of the total area to the profile or outside area of any particular frame was defined as the "Turbulence Factor" for this frame. This slow process of determining the total areas or contact areas was shortened considerably later by the very satisfactory approximate method of comparing frames from different runs with standard frames for which the "Turbulence Factors" had been determined carefully, and ascribing the same "Turbulence Factor" to other similarly appearing frames.

-0.016 sec

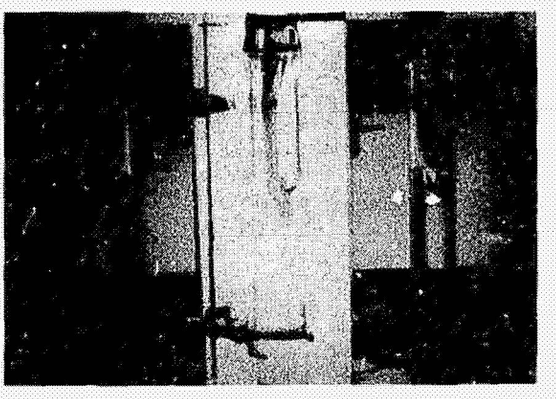

0.063 sec

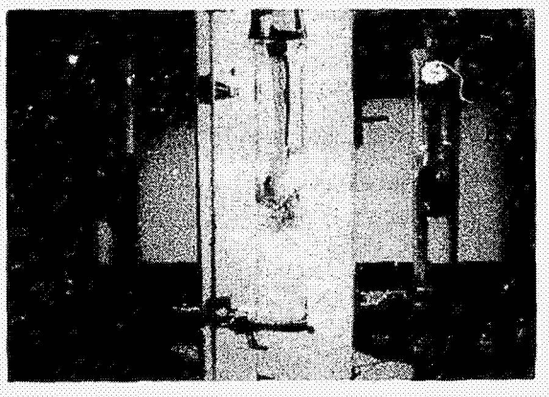

0.14 sec

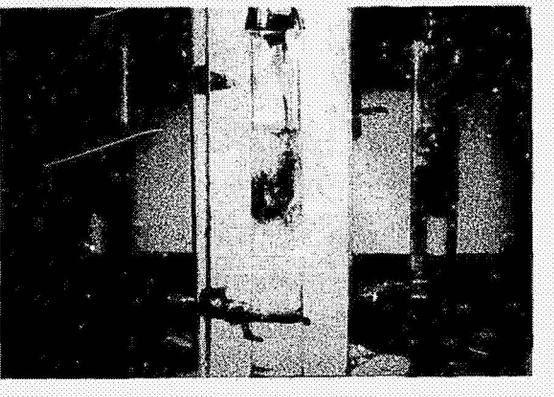

0.22 sec

0.30 sec

Figure A-2 Typical Film Frames Used in Film Analysis

0.38 sec

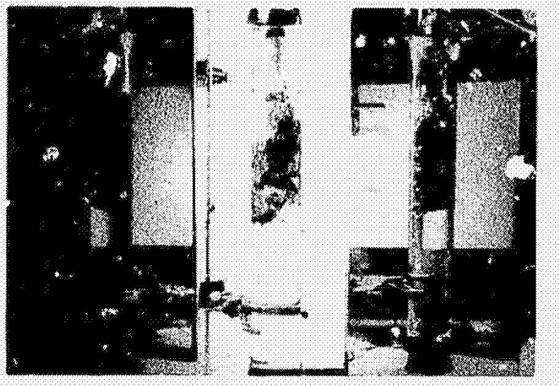

0.45 sec

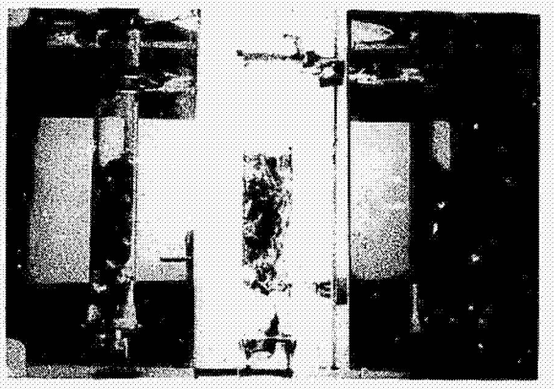

0.53 sec

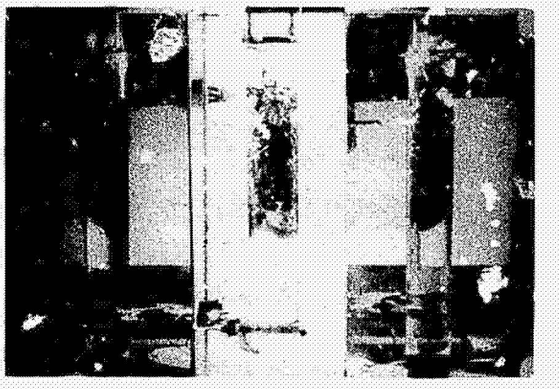

0.61 sec

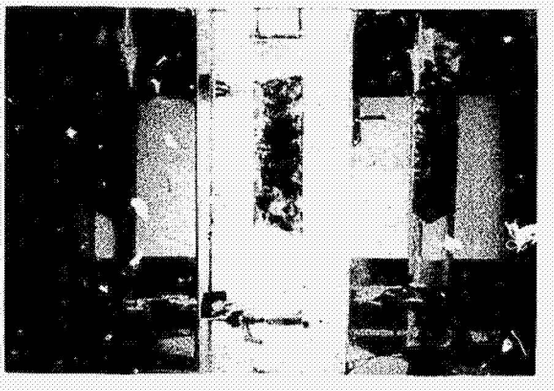

0.69 sec

Figure A-2 (Continued)

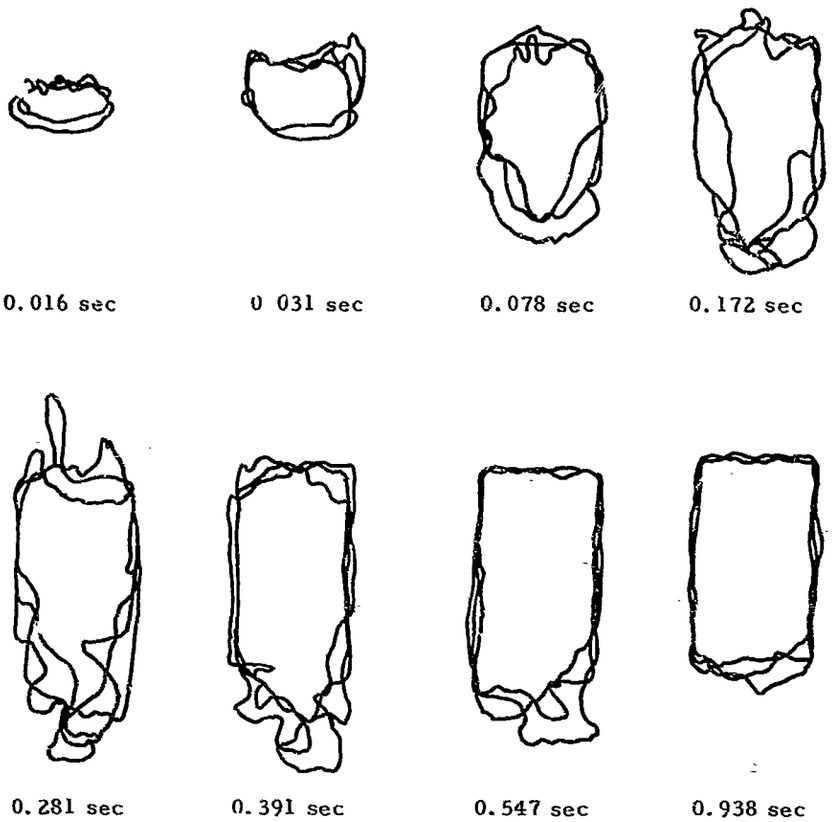

Figure A-3 Superimposed Profile Traces of the Mixing Experiments

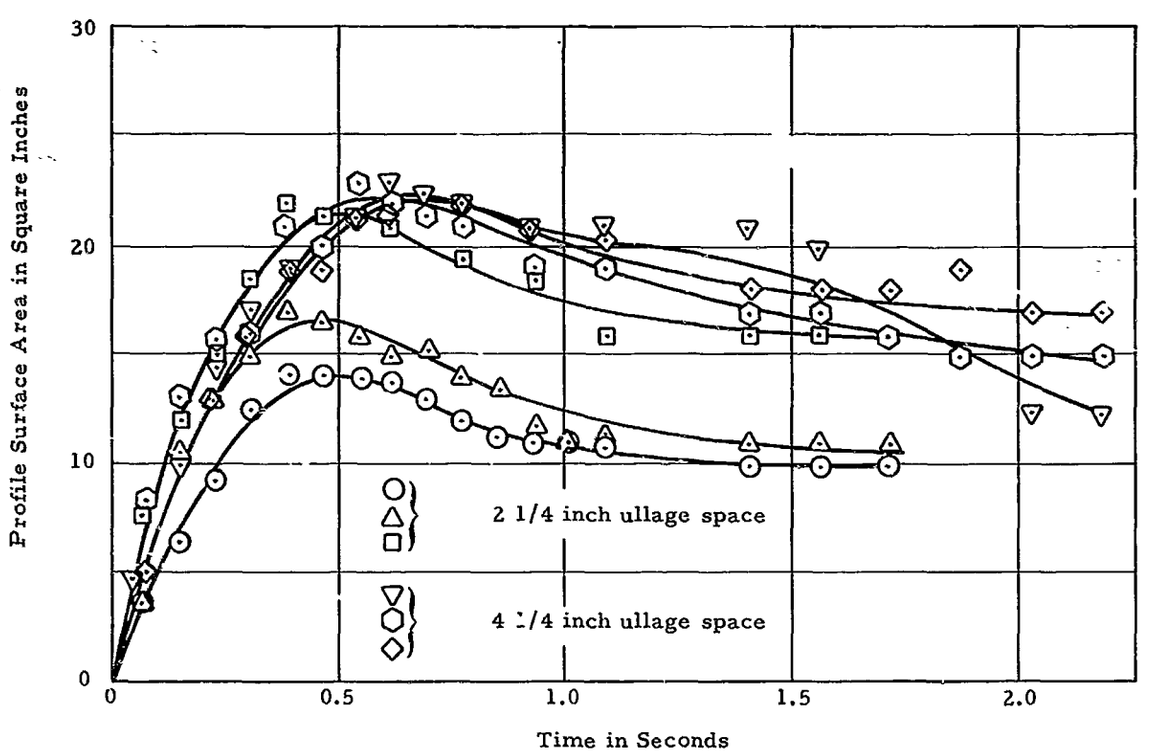

Figure A-4 Profile Surface Area versus Time (Film Analysis)

Figure A-5 presents the "Turbulence Factor" for the runs presented in Figure A-2 and Figure A-3.

Using Figure A-4 and Figure A-5, and combining them, gives the total area or an area directly proportional to the true contact area between the liquids. The result is seen in Figure A-6.

The "Turbulence Factor" has been further substantiated by the Wax Cast Analysis which will be described below.

Figure A-6, in addition to giving the total area, shows the remarkable reproducibility of these experiments. Furthermore, this figure demonstrates the effect of mixing energy. It shows three runs with a 2 1/4 in. ullage space and three runs with a 4 1/4 in. ullage space. Considerably more area is obtained for the 4 1/4 in. ullage space since the upper liquid obtained greater kinetic energy before mixing. In these, as well as all other experiments, it was observed that the reproducibility of mixing increases with the increase in mixing energy.

The Film Analysis as described above proved to be an invaluable aid in the study of the mixing phenomena of liquids. The results, however, were not taken as correct unless they checked with the results of another of the methods described below, simultaneously applied to the same experiment.

In the case of the mixing of hot and cold liquids with temperature differences great enough to produce boiling of one of the liquids, another factor — the "Boiling Factor" — was introduced which accounted for the surface produced by the vapor bubbles of one of the constituents. Similarly a "Freezing Factor" could be introduced. These additional factors were often required when a cryogenic liquid was used as one of the constituents.

A number of different diameter Pyrex glass pipes were used in the mixing studies ranging from 3/4 in. ID to 6 3/4 in. ID's to give a relationship for size. In these experiments the effect of surface tension could be observed since it altered some of the phenomena in the smallest sizes.

B. Wax Cast Analysis

The Film Analysis as described previously was a dynamic method of analysis and the results had to be obtained by interpreting recordings of the actual mixing phenomena through the profile area, turbulence factor, and boiling and freezing factors, to obtain the total area or contact area.

The Wax Cast Analysis allowed the "freezing" of the actual mixing process at various stages of the mixing by mixing hot wax with cold water. By varying the

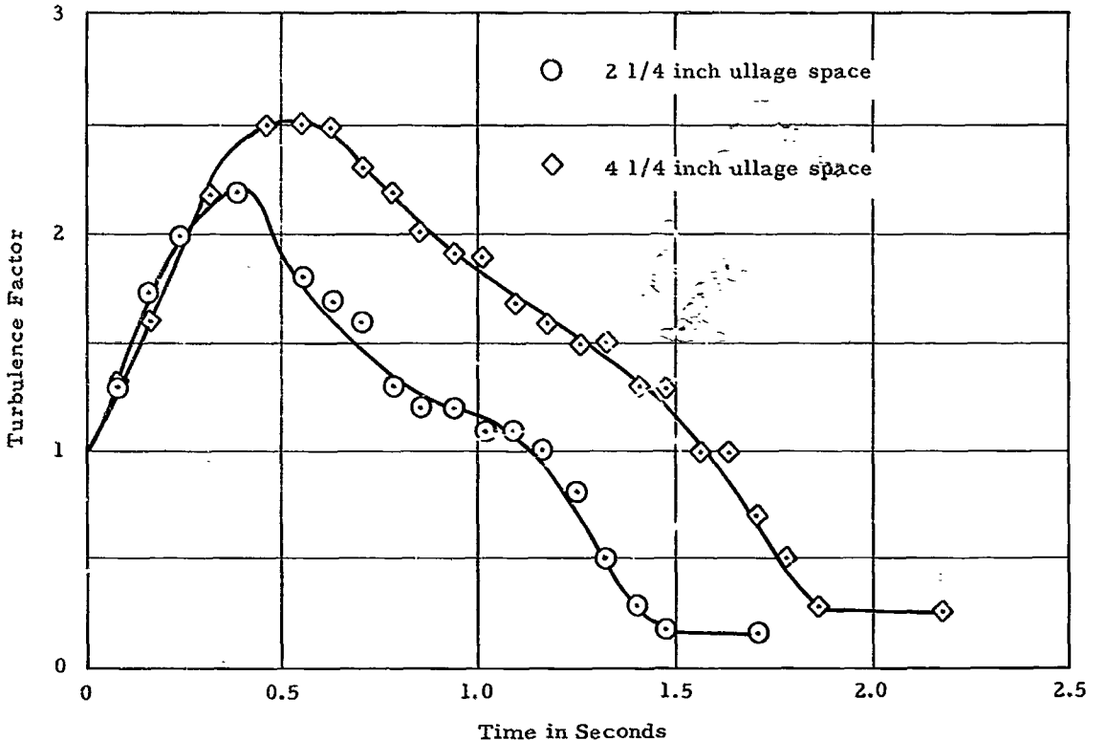

Figure A-5 Turbulence Factor versus Time (Film Analysis)

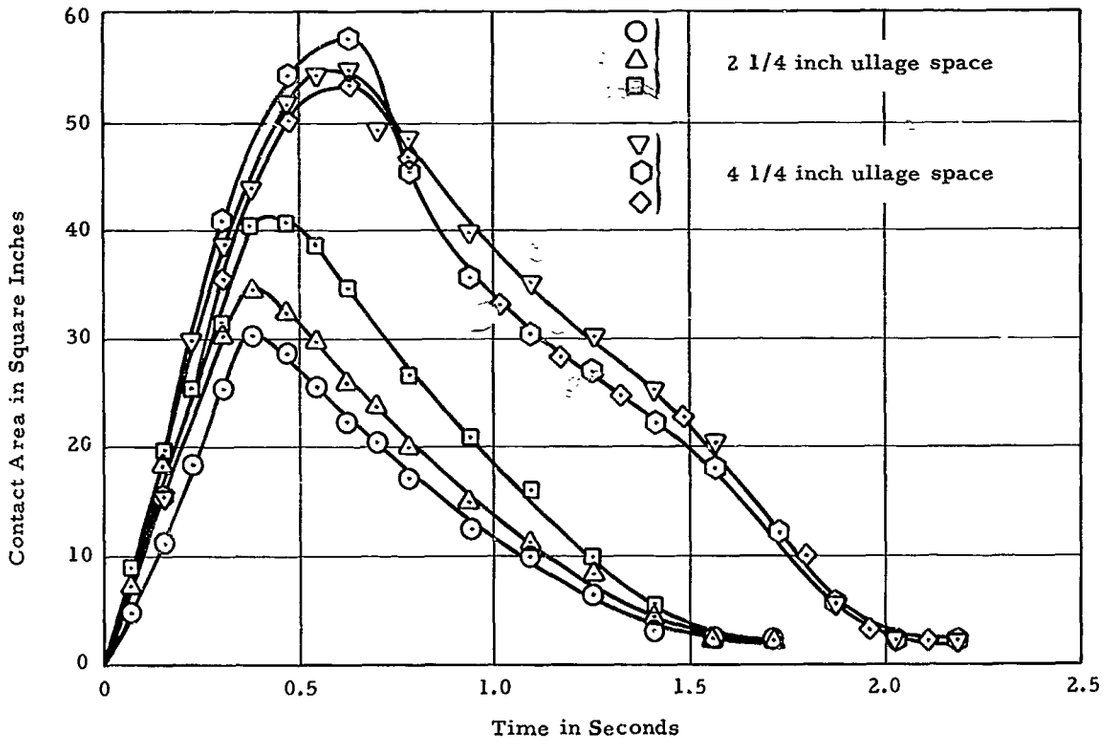

Figure A-6 Contact Area versus Time (Film Analysis)

temperatures slightly the wax would solidify earlier or later in the mixing process and the wax casts obtained in this manner could be analyzed at leisure any time thereafter.

The experimental apparatus and setup for the Wax Cast Analysis is identical with the one for the Film Analysis, and so for many experiments both methods of analysis were used simultaneously and checked against each other.

Figure B-1 shows a series of such wax casts representing a complete experiment. Excellent reproducibility indicated by the Film Analysis allowed the experiments to obtain these wax casts to be carried out identically except for slight variations in temperature. The wax casts indicate the progress of the mixing process. The profile area was determined from these wax casts by two methods: A small (usually in.^{2}) grid was laid out on the surface and then the area determined by counting. This procedure was checked by dipping these samples into paint and letting them dry. By sectioning the samples, determining the thickness of the paint film and its density, after having weighed the sample before coating and after coating, the profile area could be determined. Essentially the same answers were obtained by both methods.

The serially sectioned samples or wax casts in Figure B-2 allowed the total area to be determined by the same method used for the profile area.

The ratio of the total or contact area and the profile area again represented the "Turbulence Factor."

Curves of the profile area versus time (Fig. B-3), the total or contact area versus time (Fig. B-4), and the "Turbulence Factor" versus time (Fig. B-5) were plotted.

The Wax Cast Analysis was primarily used to check the results from the Film Analysis and, after it was found that the results from both analyses were in essential agreement, it was not used further.

C. Vibration Mixing Analysis

Another method by which the mixing processes and phenomena were studied is the Vibration Mixing Analysis. In this method the fluid particles are simulated by solid particles of various sizes, shapes, colors, densities, etc. These solid particles used in various proportions and configurations are mounted on a vibration table and shaken for certain lengths of time. Figure C-1 shows the experimental arrangement simulating spill mixing configuration. Three liquids are represented by different color marbles and are arranged in a desired configuration. Shaking the configuration for predetermined times the marbles will diffuse into each other.

Figure B-1 Typical Wax Casts

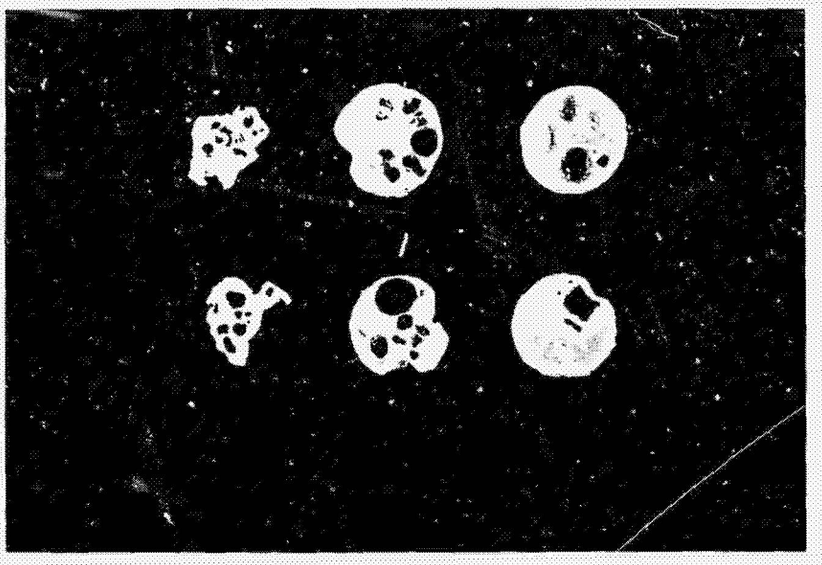

Figure B-2 Serially Sectioned Wax Cast

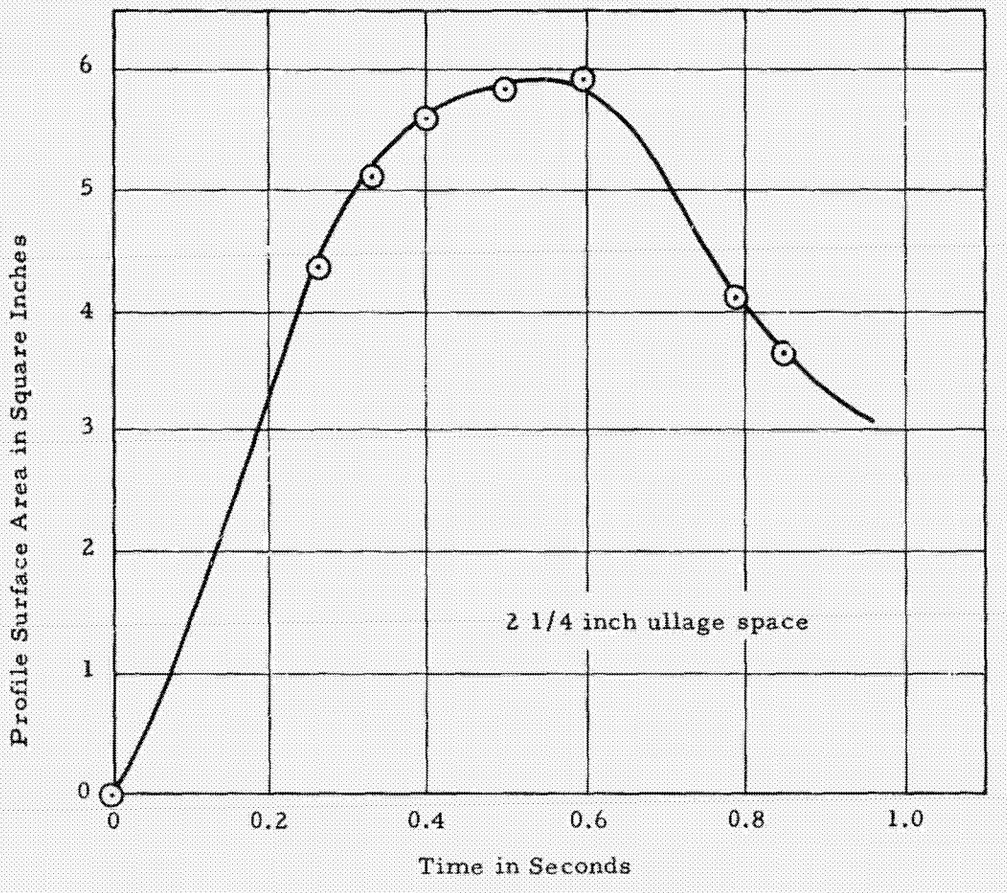

Figure B-3 Profile Surface Area versus Time
(Wax Cast Analysis)

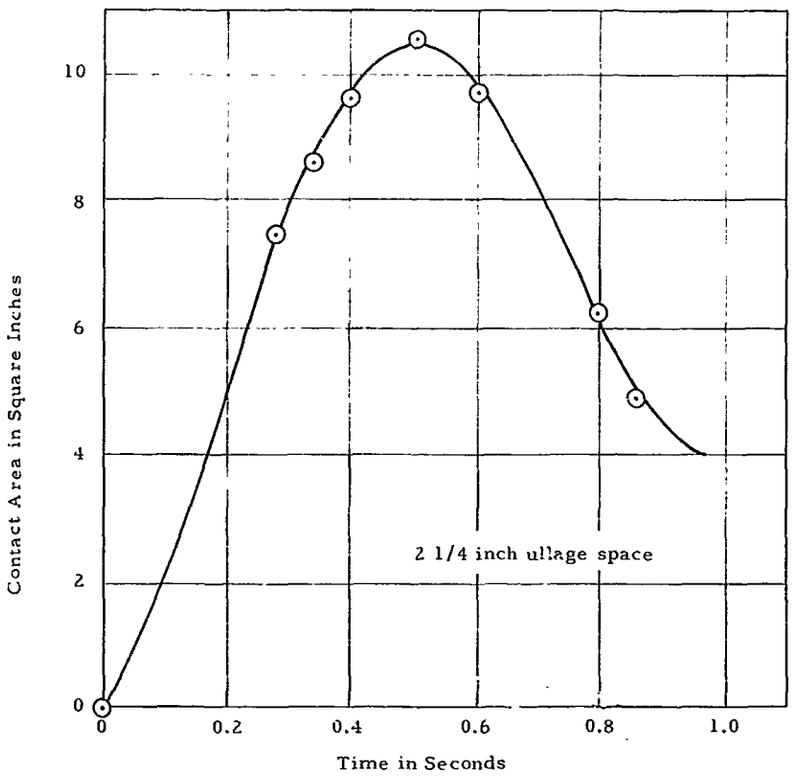

Figure B-4 Contact Area versus Time
(Wax Cast Analysis)

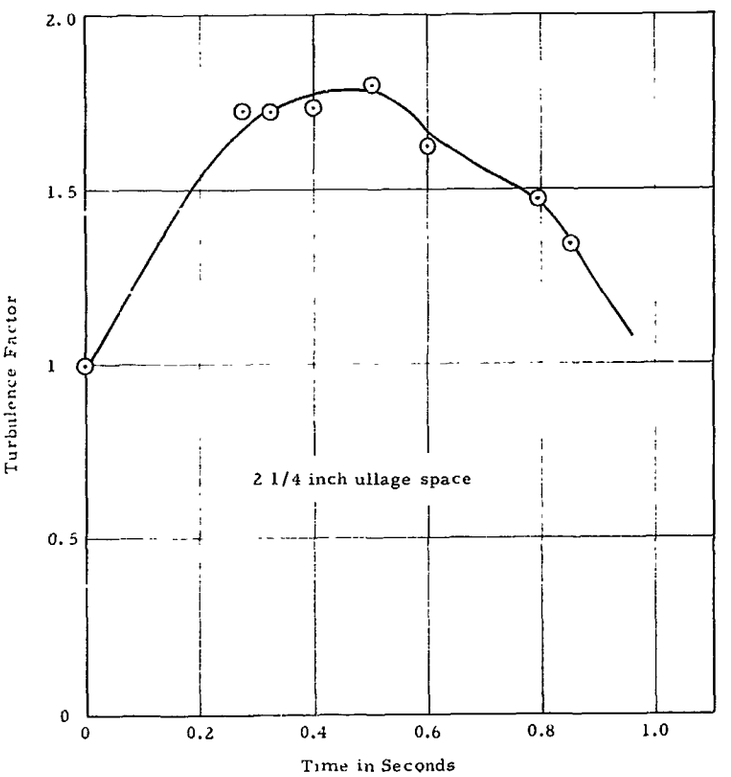

Figure B-5 Turbulence Factor versus Time
(Wax Cast Analysis)

Thus is this manner the mixing process simulated hereby can be studied in steps.

Figure C-2 presents a number of the views representing these steps. Any particular region can be studied in this manner by removing this volume and counting the particles of each of the constituents present. This gives the percentages of each one of these constituents, thus the degree of mixing in this region.

Removal of some of the particles from certain regions as programmed and governed by the fundamental relationships of heat transfer can further account for evaporation losses, taking into account boil-off as part of the mixing process.

In this manner a curve can be plotted for the fraction mixed as a function of time. The time scale is arbitrary since the amplitude and frequency of the shaking table have a pronounced effect on the speed with which the mixing progresses. To find the absolute mixing time either an experiment with liquids or theoretical calculations will give the time scale needed. This absolute time superimposed upon the curve gives the true mixing function-time relationship.

Figure C-3 presents a mixing function curve representing the J-test series of the Arthur D. Little Spill Test Program.[8]

It is interesting to note that all mixing experiments produced the same characteristic shape of the mixing function curve, only the actual values and speed with which the process occurred were different.

D. Thermocouple Grid Analysis

The three methods for studying the mixing process, the Film Analysis, the Wax Cast Analysis, and the Vibration Mixing Analysis are excellent methods for obtaining insight into the phenomena taking place when different liquids mix. They are, however, simulation methods and are not readily applicable to actual explosive mixtures where detonation and explosion would, in most cases, destroy the records.

The Thermocouple Grid Analysis overcomes this difficulty and can, therefore, be considered the most powerful and best of the methods discussed in this paper. It is the best but also the most elaborate, most expensive (and the data reduction the most tedious) of the four methods. For explosive tests, it is, however, the only method which will give information from time zero of the failure up to and beyond the time of ignition.

The heart of this method is a grid of thermocouple junctions spaced throughout the region under study. These can be placed inside the tanks of a missile and extend around it if fireball information and data are desired. A continuous time re-

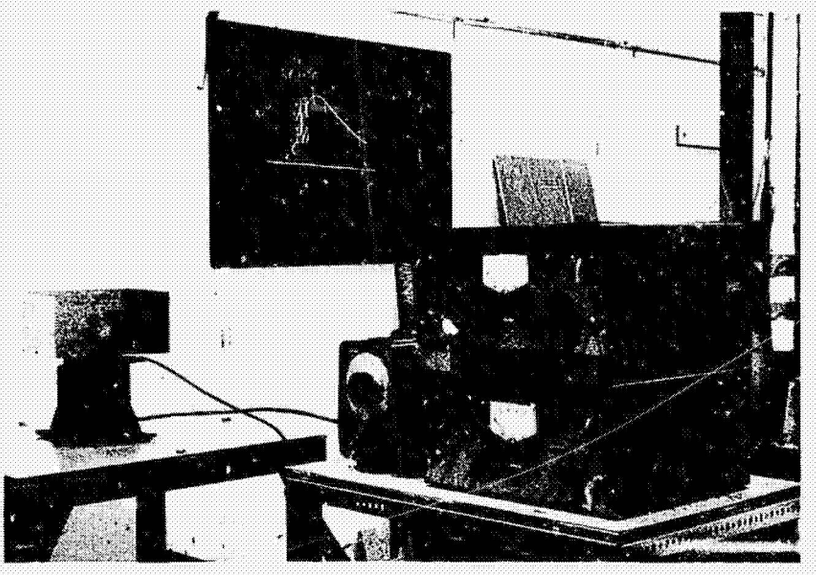

Figure C-1 Experimental Arrangement for Vibration Mixing Analysis

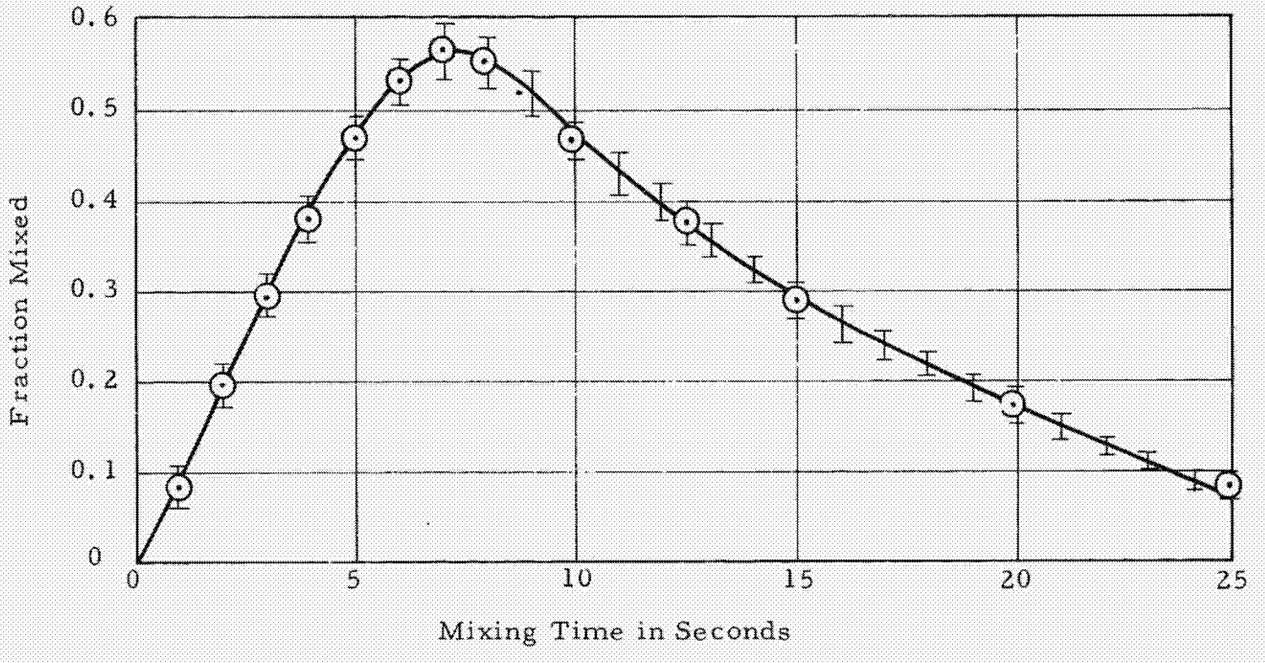

Figure C-3 Mixing Function of Spill Function for Simulated Three Component Liquid Propellant Spill Tests (Vibration Mixing Analysis)

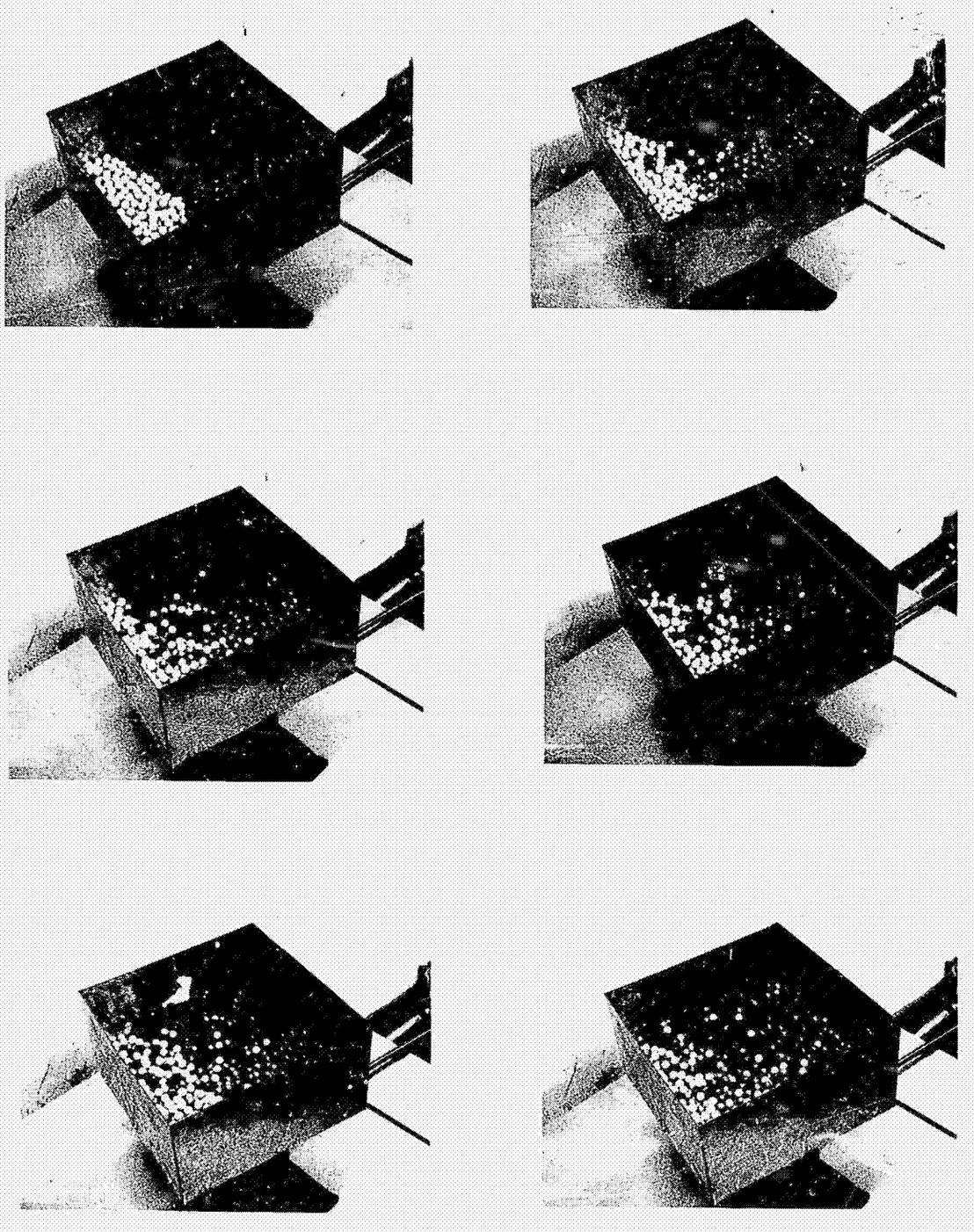

Figure C-2 Successive Stages of Mixing Processes

cord of the signals from the individual junctions is kept for the complete period of the processes under investigation. This method, through its three-dimensional records of the complete time history, can provide a great amount of information with respect to:

1. The three-dimensional mixing front of a particular constituent;
2. The degree of mixing at a particular point;
3. The degree of turbulence at a particular point;

and, in explosive tests, in addition to the above:

4. The location of the point or points of ignition;
5. The time delay from t_o of the mixing to t_o of ignition;
6. The propagation of the reaction front;
7. The propagation of the shock front;
8. The separation of shock front and reaction front, etc.

The experimental arrangement and equipment for the Thermocouple Grid Analysis is the same as that for the Film Analysis and can readily be incorporated into static explosive test series. The only addition necessary is a three-dimensional grid of fine thermocouple junctions giving good response characteristics. Full response times of less than 10 msec have been obtained in our laboratory.

The signals from these thermocouple junctions can be fed to the recording equipment, which may be close by, in inert tests, or at some distance in explosive tests.

The overall experimental arrangement for the work reported upon here is shown in Figure D-1. The experimental apparatus and the recording equipment are shown. All the control experiments using this arrangement, in addition, made use of high-speed camera recordings of the mixing phenomena so as to have a check and comparison between the Film Analysis and the Thermocouple Grid Analysis.

Figure D-2 pictures thermocouple grids which were used in some of these investigations. Our laboratory has the capability of monitoring over 40 individual junctions at present which can be extended to 65 if needed. By high-speed periodic sampling through commutation this capacity can be increased manyfold, but the time continuity of the records has to be sacrificed.

Figure D-3 presents traces obtained from a mixing experiment. All twelve traces in this case correspond to junctions in a vertical plane at three different elevations with four junctions equally spaced in each one of these elevations and arranged in straight lines.

Figure D-3-A presents traces of the mixing of hot oil and water. Figure D-3-B presents traces of the mixing of LN_2 and kerosene.

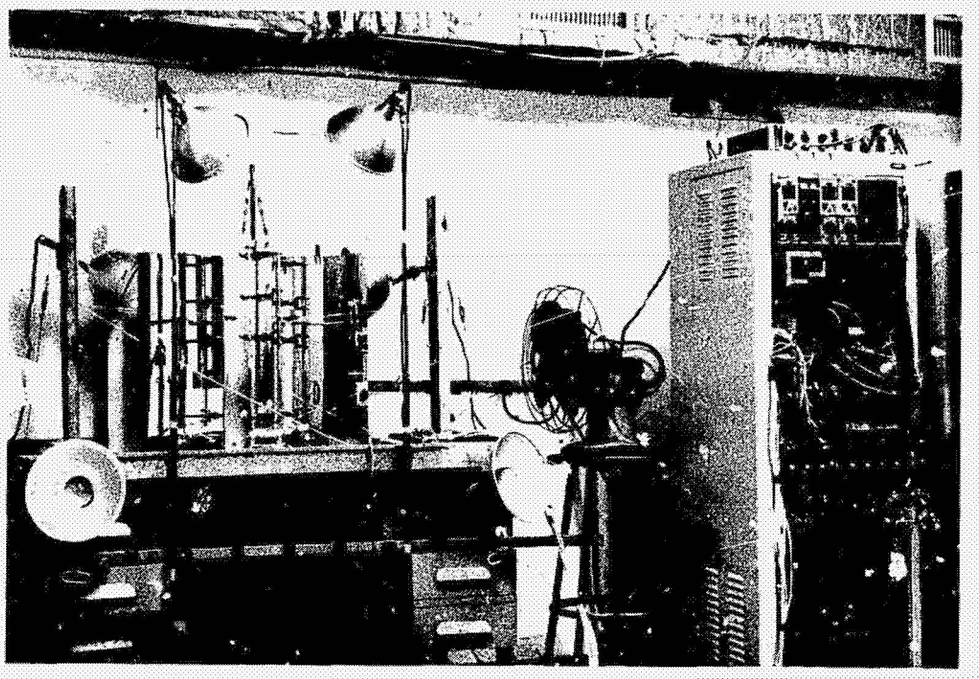

Figure D-1 Experimental Arrangement for Thermocouple Grid Analysis

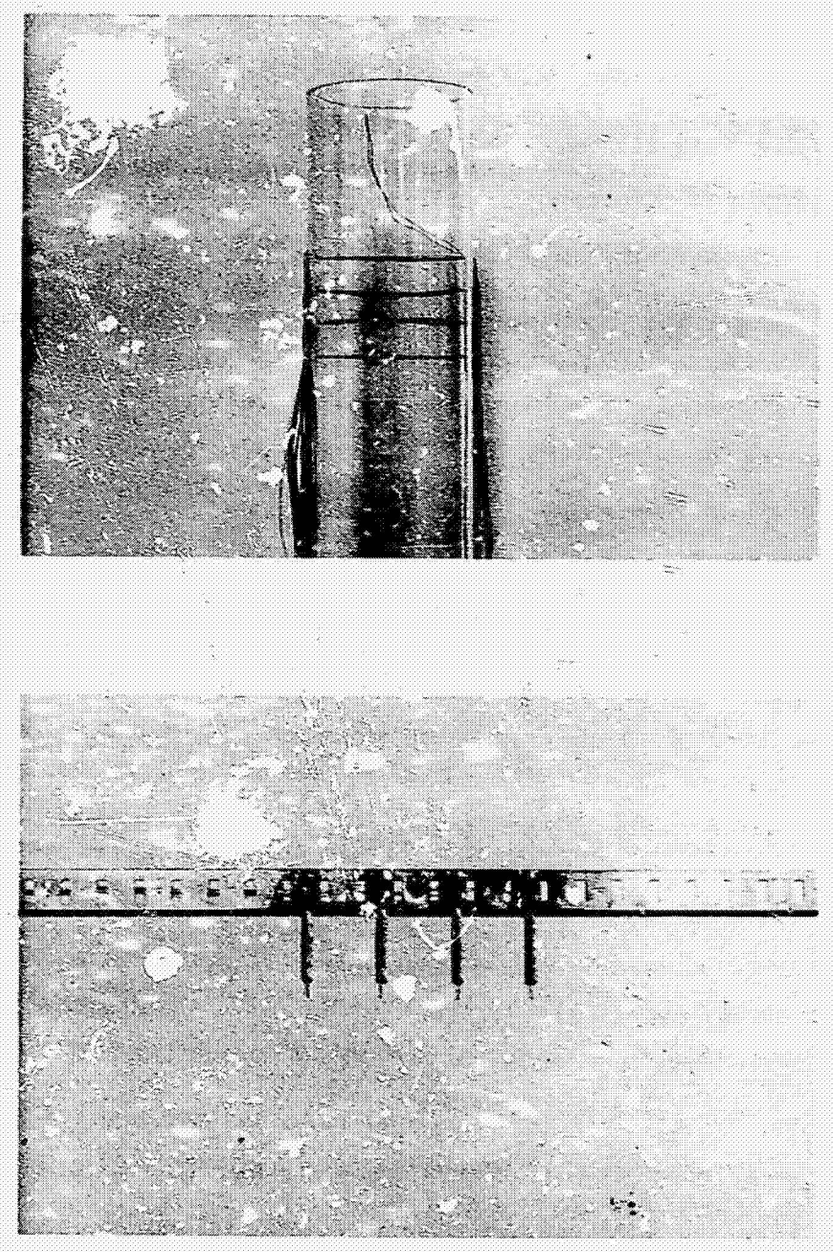

Figure D-2 Typical Sections of Thermocouple Grids

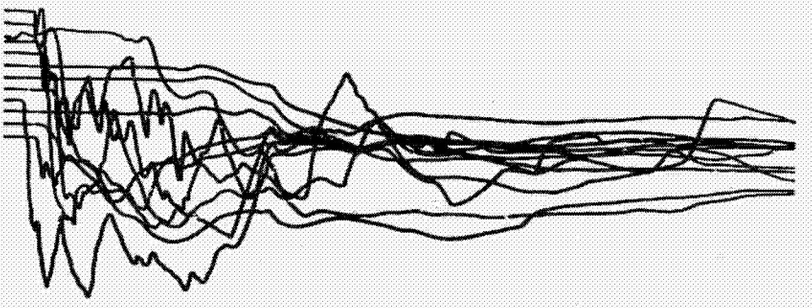

a. Hot Oil and Water

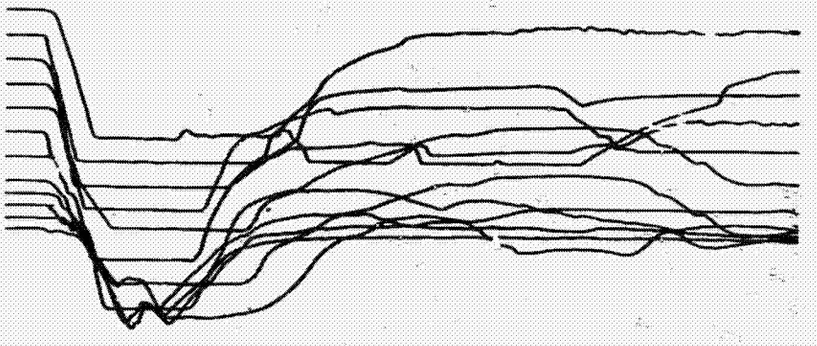

b. Liquid Nitrogen and Kerosene

Figure D-3 Thermocouple Grid Time Traces

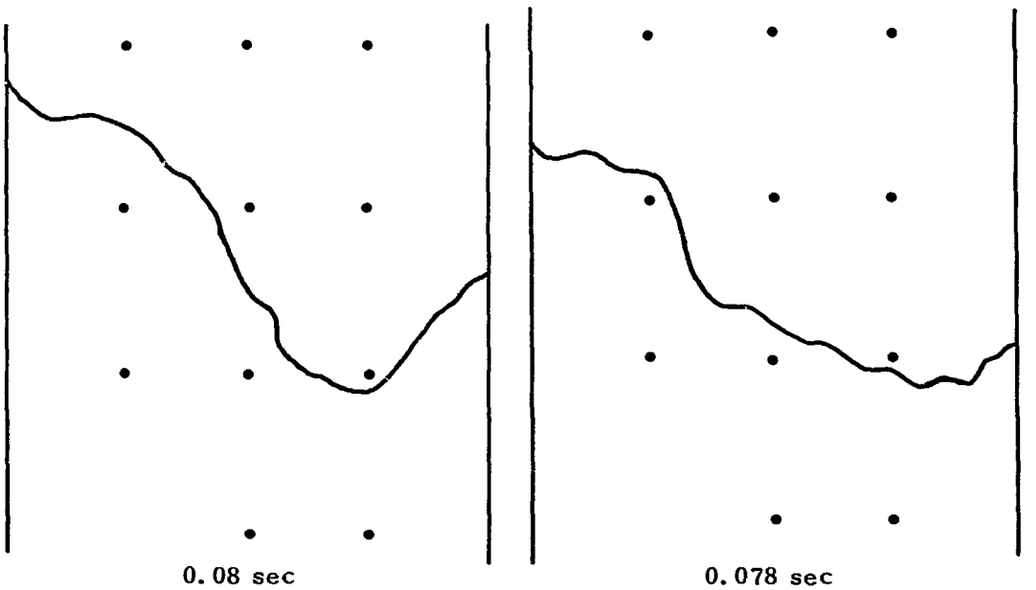

a. Thermocouple Grid Analysis b. Film Analysis

Figure D-4 Comparison of Mixing Profiles Obtained Simultaneously by Thermocouple Grid Analysis and Film Analysis

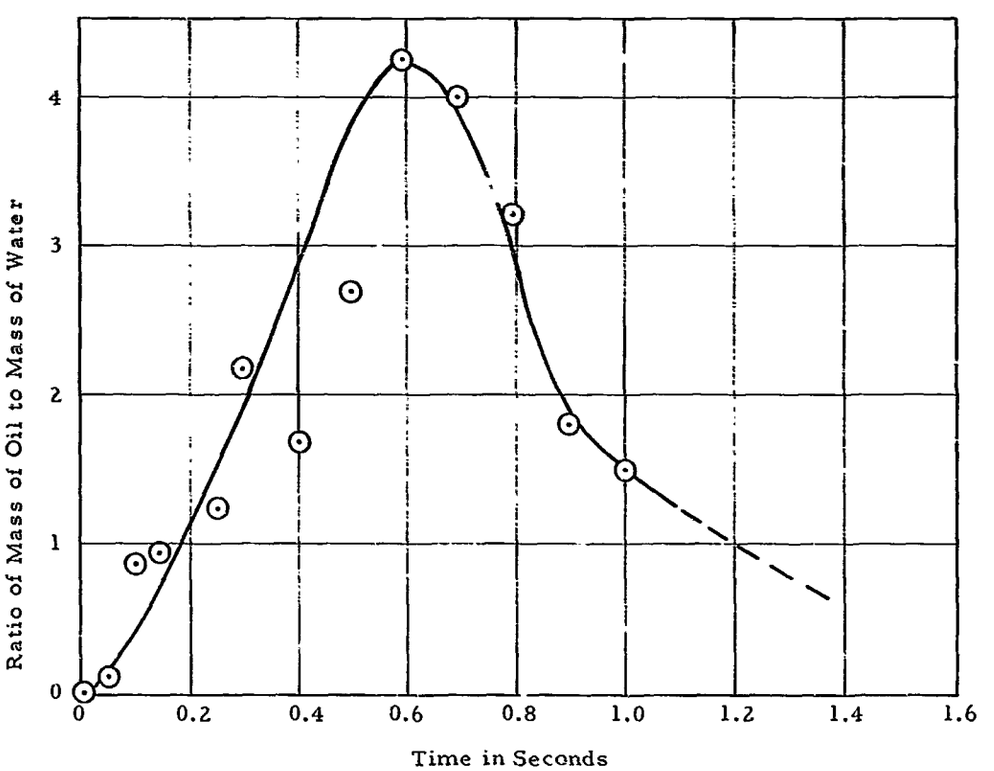

Figure D-5 Mixing Function or Spill Function for Simulated Two Component Liquid Propellant Mixing Test (Thermocouple Grid Analysis)

Figure D-4 presents the resulting mixing profile as determined by interpolation between the junctions of the thermocouple grid at time t.

Figure D-4 also presents the resulting mixing profile of the same hot oil and water experiments as determined by the Film Analysis at the same time t.

It can be seen that the results from both methods of analysis are essentially the same. More and closer space thermocouple junctions would give more points for drawing the mixing profile and would fix this surface with greater reliability.

The degree of mixing at any time, t, around a particular junction can be determined from the time history at this junction by writing the relationship for mass and energy balance at this junction incorporating the laws of thermodynamics, fluid flow, and heat transfer. A computer program to do this is of great help if a considerable number of junctions are involved.

Averaging the conditions around each of the individual junctions can then give the mixing function, the fraction mixed at any time t, Figure D-5.

SUMMARY

The preceding discussion of the four methods which can be employed in investigating the mixing phenomena of liquids to establish a mixing function-time relationship shows the value of these methods, their relative merits, and singular advantages to do the job.

The Film Analysis is relatively simple and easily carried out, but, in its simplest form, the use of light requires transparent containers and rather transparent constituents. In its more sophisticated forms — using shorter wavelength radiation, such as X-ray, Gamma-ray, or tracer methods — the equipment necessary becomes much more complex.

The Wax Cast Analysis allows the checking of the results obtained by the Film Analysis by independently establishing the mixing profile, total or contact area, and turbulence factors.

The Vibration Mixing Analysis provides a method by which, again as in the Wax Cast Analysis, the mixing process can be stopped at any point in its development and studied at leisure.

The Thermocouple Grid Analysis, the most powerful of the four methods, can provide all the information of the above methods (except for stopping the mixing process at any point in its development) and, in addition, can be used in actual missile configuration explosive experiments.

In the manner described above these methods can provide information which

is not available at the present time and, through this information, can give better insight into, and understanding of, the actual happenings during the mixing process and leading up to the explosion of liquid propellant mixtures — information which is needed if we ever hope to control and guide these processes.

REFERENCES

1. Farber, E. A., "A Mathematical Model for Defining Explosive Yield and Mixing Probabilities of Liquid Propellants," Proceedings of the Third Space Congress, March, 1966. (Paper No. I in this series)

2. Farber, E. A. and Deese, J. H., "A Systematic Approach for the Analytical Analysis and Prediction of the Yield from Liquid Propellant Explosions," Proceedings of the Third Space Congress, March, 1966. (Paper No. II in this series)

3. "Blast and Fireball Comparison of Cryogenic and Hypergolic Propellants," Aerojet General Corp., Contract No. NAS 9-2055, Final Report, June, 1964.

4. Farber, E. A. and Richardson, M. R., "The Gamma Ray Densitometer and Concentration Meter," Proceedings of Annual Meeting of Instrument Society of America, April, 1957.

5. Farber, E. A., "200 A Thorium Oxide Slurry Test Loop Density and Concentration Data," Oak Ridge National Laboratory Report, January, 1957.

6. Farber, E. A., "Bubble and Slug Flow in Gas-Liquid and Gas (Vapor)-Liquid-Solid Mixtures," Oak Ridge National Laboratory Report, May, 1957.

7. Farber, E. A., "Bubble and Slug Flow in Circulating Gas-Liquid and Gas-Liquid-Solid Mixtures," Oak Ridge National Laboratory Report, February, 1958.

8. "Summary Report of a Study of the Blast Effect of a Saturn Vehicle," Arthur D. Little, Inc., February 15, 1962.

IV

FIREBALL HYPOTHESIS DESCRIBING THE REACTION FRONT AND SHOCK WAVE BEHAVIOR IN LIQUID PROPELLANT EXPLOSIONS

by

E. A. Farber, Ph. D.* and J. S. Gilbert, Ph. D.†

ABSTRACT

This paper presents a hypothesis describing the reaction front from the time of ignition in liquid propellant mixtures, the resulting buildup and generation of a shock wave, their travel through the mixture to the propellant air interface, and the subsequent separation and separate behavior of the shock wave and the reaction front. The hypothesis was applied to a few liquid propellant explosions for which sufficient high-speed camera coverage was available resulting in quantitative velocity-time graphs, theoretical from time of ignition to after the time of separation of shock wave and fireball, and both theoretical and experimental from that time on. From the discussion of this hypothesis and the method of calculation, it can be seen what experimental information, not available at this time, is needed to verify or possibly modify this hypothesis.

ACKNOWLEDGEMENT

It is with sincere appreciation that the writers express their indebtedness to the National Aeronautics and Space Administration under whose sponsorship (part of contract NAS10-1255) this work was carried out; to the University of Florida and its staff and to Mr. J. H. Deese, Chief, Facilities Technology Office, John F. Kennedy Space Center.

---

*Professor and Research Professor of Mechanical Engineering, University of Florida, Gainesville, Florida.

†Associate Professor of Mechanical Engineering, University of Florida, Gainesville, Florida

INTRODUCTION

With the present emphasis upon space exploration and large manned liquid propellant rocket developments, the problem of liquid propellant explosion hazards has become increasingly important. Much work is being done trying to find methods by which these hazards to the astronauts riding the rocket, to launch support personnel, and to the physical facilities can be predicted.

Some work[1, 2, 3, 4, 5] is and has been done for predicting some of the end results from theoretical studies, supplemented by experimental work looking at the actual phenomena in detail. The present paper will discuss a hypothesis which is intended to give insight into the phenomena taking place in liquid propellant explosions from the time of ignition through the buildup of a detonation wave, the travel of the reaction front and shock wave, the crossing from the liquid-air interface into the air, and then the travel and attenuation of the shock wave and the development and dissipation of the fireball.

For the purpose of this discussion the problem is divided into four parts which together form the "Fireball Hypothesis." These four parts are:

I. The region where ignition produces phenomena that develop into the detonation phenomenon.

II. The region where the reaction front and the shock front travel through the liquid propellants.

III. The liquid propellant-air interface — actually a region where the liquid boundary begins to move and where the reaction front forming the fireball and the shock wave separate.

IV. The region in which the shock wave travels through the atmosphere as an air shock and where the fireball grows and develops separately far behind the shock wave.

Figure 1 is a sketch of the hypothesis showing the four regions, for one case of confinement and yield, etc. These regions are discussed in detail in the following pages.

It might be well to mention that the scales chosen for presenting the four regions in Figure 1 are different for each so as to be able to show the variations occurring in each region. Region III is actually very small; Regions I and II make up the physical space of the liquid propellants, their relative size being a function of the explosive yield obtained from the propellants. Region IV is by far the largest.

Also on a time scale, the phenomena in Region I, II and III will happen in a matter of milliseconds and/or microseconds, while those of Region IV ordinarily

stretch over many seconds. This last fact is also the reason why measurements are available for a good part of Region IV, while they are not for Regions I, II and III.

Another paper[3] reporting upon work covering another phase of the problem of liquid propellant explosion hazards, namely the mixing function, an important factor in the prediction of explosive yields, proposes a method which is believed to be able to give experimental information in Regions I, II and III.

THE FOUR REGIONS

Region I - The Region Where Ignition Produces Phenomena That Develop Into the Detonation Phenomenon

Some time after liquid propellants are brought together, either intentionally or through failure, ignition may occur and usually does occur. At this time of ignition a certain fraction of the total propellants involved is mixed and ready for reaction. Since mixing continues with time, but also evaporation losses occur where cryogenics are involved, the ignition time has a pronounced effect upon the explosive yield[2, 6]. The time of ignition may be essentially a constant for hypergolics or a random function for cryogenic propellants.

The reaction between the propellant components thus initiated will progress rather quickly among those molecules that are ready to react. This may be expressed simply as

$$\frac{dN}{dt} = kN \tag{1}$$

N - number of molecules ready to react

t - time

k - reaction factor

Since the molecules that are ready to react at time, t, must be in "contact" with each other, they can be thought of as located on a "contact area" or "surface" produced by the mixing process. Thus the above equation can also be expressed as

$$\frac{dA}{dt} = kA \tag{2}$$

A - contact area

This contact area, or a surface proportional to it, can be measured experimentally for a particular missile configuration and mode of failure as a function of time. For the purposes here and from a theoretical point of view, it could be con-

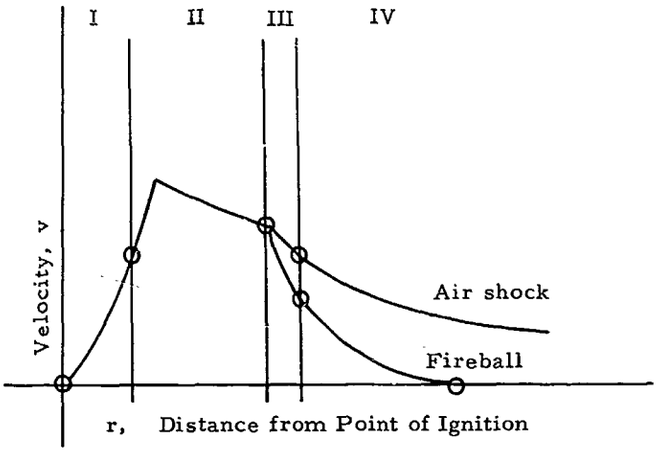

Figure 1 Graphical Representation of Fireball Hypothesis Indicating the Four Distinct Regions

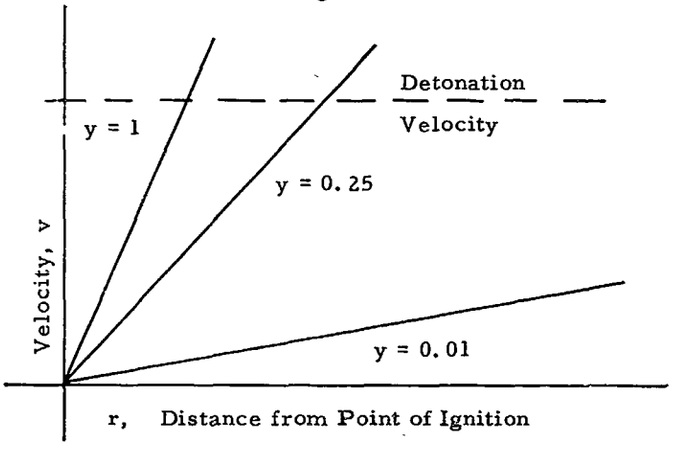

Figure 2A Representation of Fireball Hypothesis in Region I (Reaction Factor = C)

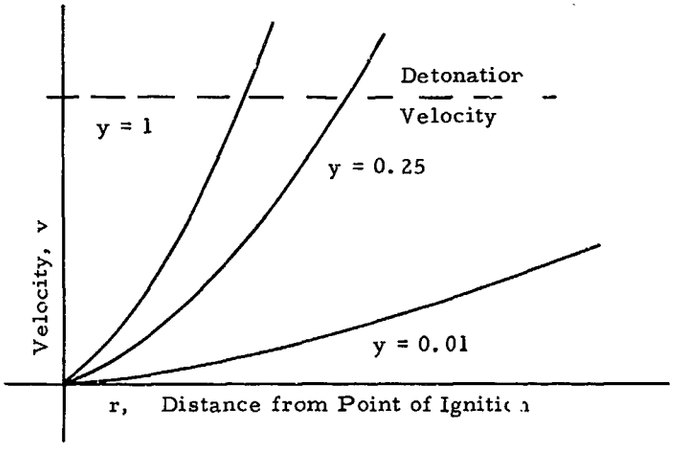

Figure 2B Representation of Fireball Hypothesis in Region I (Reaction Factor = $k_o t$)

sidered spherical for a first approximation, thus assuming the reaction progresses in all directions, which will certainly be true in the initial stages. Thus we can write

$$A = \frac{4\pi r_y^2}{y} = 4\pi r^2 \tag{3}$$

r_y - equivalent radius of actually reacting spherical surface

r - radius of actual total contact area of which only a fraction y reacts

y - yield

Little info mation is available on the reaction factor k in Equation (2). Let us assume that it is a function of time and that it can be expressed as

$$k = k_o t^a \tag{4}$$

where k_o and a are constants.

With this information and the above assumptions Equation (2) can be integrated.

A. For $a = 0$ in Equation (4), Equation (2) can be integrated, and utilizing Equation (3) one obtains

$$v_{y_2} = \frac{r_1\sqrt{y_1}\,k_o}{2e^{\frac{k_o}{2}t_1}}\, e^{\frac{k_o}{2}t_2} \tag{5a}$$

$$r_2 = \frac{r_1}{e^{\frac{k_o}{2}t_1}}\sqrt{\frac{y_1}{y_2}}\, e^{\frac{k_o}{2}t_2} \tag{5b}$$

Where v_{y_2} is the velocity in Region I and r_2 the corresponding radius at which this velocity is reached.

Plotting these parametric Equations (5a) and (5b) as v_y versus r, the part of the Fireball Hypothesis falling into Region I is obtained (Fig. 2A).

B. Repeating the operation of part A but with $a = 1$, making the reaction factor a linear function of time instead of leaving it a constant as in A we obtain

$$v_{y_2} = \frac{r_1\sqrt{y_1}\,k_o}{2e^{\frac{k_o}{2}t_1^2}}\, t_2\, e^{\frac{k_o}{2}t_2^2} \tag{6a}$$

$$r_2 = \frac{r_i}{e^{\frac{k_o}{2} t_1^2}} \sqrt{\frac{y_1}{y_2}} \; e^{\frac{k_o}{2} t_2^2} \tag{6b}$$

Plotting these parametric equations as in A, Figure 2B is obtained.

Other functions can be selected for the reaction factor and with it other velocity rise rate curves can be obtained. The decision as to which relationship represents the true case best (for particular propellants) will have to wait until experimental information, either direct as velocity measurements or indirect in terms of contact area-time measurements, for some of these cases becomes available.

The yield, y, was considered constant or at least an average value in the above calculations. Any other function can be selected in this analysis as soon as there is some justification for it.

It is believed that the above approach gives better insight into the happenings in Region I and allows for the expression of these happenings in a satisfactory manner.

Region II - The Region Where the Reaction Front and the Shock Front Travel Through the Liquid Propellants

In Region II, if the propellants were properly mixed, uniform or smooth propagation of the reaction front and the shock wave would occur. Since this is most likely not the case the traces must be considered average curves since actually they would have small steps, like a stairway, superimposed upon them. These finer points can be added in later on, after the overall hypothesis is developed and assuming that enough information is available to do this.

If the physical system is very small or if the system is essentially unconfined, thus not capable of supporting pressure gradients, then the waves would travel with the velocity of sound as soon as these velocities are reached. Under these conditions the velocity could be considered constant in the Region II with the reaction or detonation and shock traveling together.

Actually confinement, especially in the earlier stages, will build up pressure and temperature due to the reaction taking place and will further increase the front velocities. Assuming the degree of confinement in terms of the masses surrounding the reaction, the pressures and temperatures can be estimated, and from them the wave velocities. Studies[7] have shown however that the velocities in liquids do not increase very fast with increase in pressure so that the original assumption of essentially constant velocity in this region seems justified.

As the traveling waves approach the boundary of the liquids, the confinement decreases, and so the velocity differential between unconfined, or sonic, and the actual velocity decreases. Therefore a maximum velocity will be reached in this region which is a function of confinement, and which is also dependent upon the missile configuration and yield for specific propellants.

Calculations have been made for confinement but seem to be of lesser importance than other considerations.

Figure 3 represents schematically, for a particular condition, the velocity rise and following decrease in Region II.

In Figure 3, detonation velocity is reached at point A. In an unconfined system the velocity may be considered constant until the air-liquid or vapor-air interface is reached. Thus the line AB would represent this case. If confinement is considered, which is naturally highest on the left hand side of the Region II, the wave velocities will still increase until, due to continuous decrease in confinement, they reach a maximum, and then will decrease to a value above or equal to the unconfined system, depending upon what the confinement is at the liquid-air boundary. Thus the actual case will be more closely represented by the curve A-A´-B´.

As mentioned above, present information indicates that these points A´ and B´ are not believed to be far above the line A-B. Vapor inclusion in the system can alter this picture.

The calculations for these curves in Region II are relatively simple. They can be carried out provided the equation of state, heat generation and losses from a certain region, and constant volume processes for complete confinement, or appropriate volume changes for the various degrees of confinement, are considered.

Again verification of this part of the hypothesis must await experimental information.

Region III - The Liquid Propellant-Air Interface, Actually a Region Where the Liquid Boundary Begins to Move and Where the Reaction Front Forming the Fireball and the Shock Wave Separate

When the reaction front and shock front reach the liquid propellant-air interface (or in some cases the boundary of the mixing region within the missile), which most probably has begun to move slightly, two distinct phenomena occur.

A. The shock in the liquid is transformed into a shock wave in air, thus a wave-to-wave phenomena transition, essentially not involving mass transfer.

B. The reaction front, or detonation front, is transformed into a moving mass front, thus a transition from a wave phenomenon to a particle phenomenon.

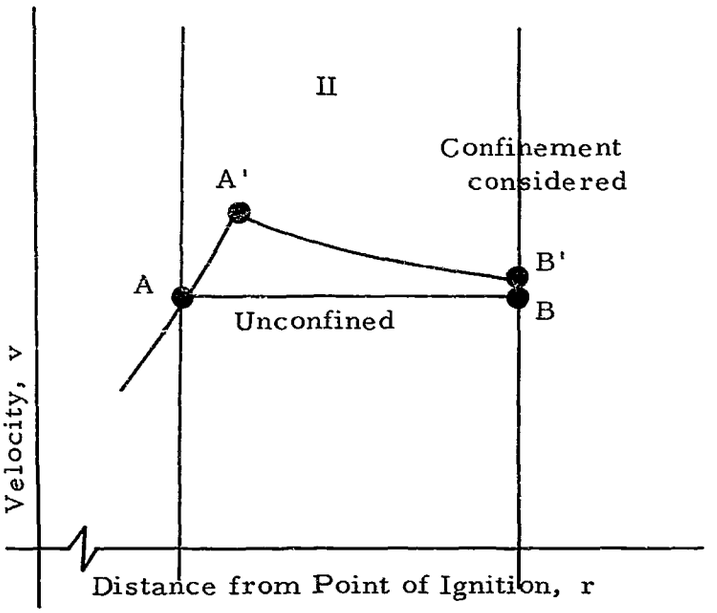

Figure 3 Representation of Fireball Hypothesis in Region II

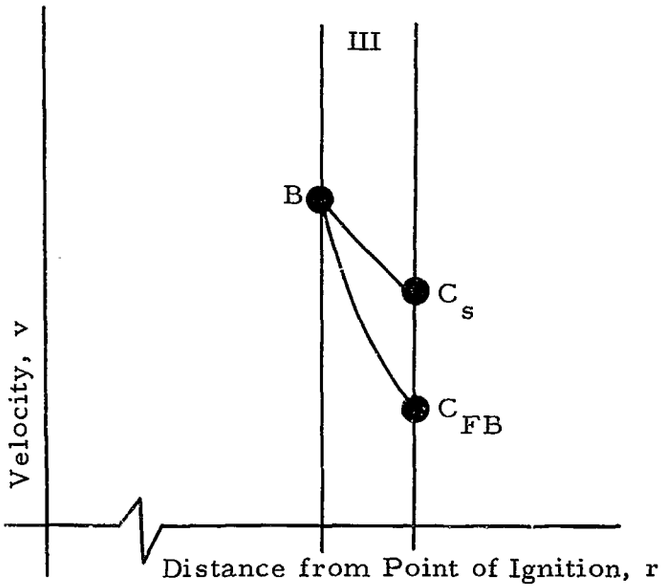

Figure 4 Representation of the Fireball Hypothesis in Region III

It seems that this may well be the reason why at this point the two phenomena, as for instance represented by the velocities, follow their own and different paths.

The shock wave may experience a decrease in velocity as it crosses from the liquid into the air through possibly a small vapor layer. Very little information could be found about the transition of a shock wave from one medium into another and especially for this case where the compressibility is so different.

The reaction front when reaching the interface also as a wave phenomenon will now have to change into a particle phenomenon where the propellant particles have to move out forming the fireball boundary, thus involving tremendous amounts of mass transfer. This transition must produce a rather abrupt change in the velocity in a rather small region.

These phenomena are represented schematically in Figure 4 for Region III.

Calculation of the changes in Region III are very difficult and the numerical results questionable at this time since a number of assumptions are necessary which need experimental verification to lend validity to these results.

However, qualitatively it is believed that this hypothesis fits the happenings and gives further insight into this very complicated process.

Region IV - The Region in Which the Shock Wave Travels Through the Atmosphere as an Air Shock and Where the Fireball Grows and Develops Separately Far Behind the Shock Wave

After separation of the shock wave and the reaction front each of these phenomena follow their own physical laws and relationships.

Fortunately some experimental information is available in this region on both the shock and the fireball. All this information, however, is for considerable distances from the liquid-air interface, and theory again will have to bridge this gap.

Air Shock

The attenuation of the air shock can be approximated by the well-known equations of compressible fluid flow and can be expressed in terms of the pressure ratio across the shock.

$$v_s = c_o \left\{ \frac{\gamma + 1}{2\gamma} \left[\frac{P_2}{P_0} + \frac{\gamma - 1}{\gamma + 1} \right] \right\}^{\frac{1}{2}} \tag{7}$$

where v_s - shock velocity

c_o - velocity of sound at P_0

γ - 1.4 for air

P_2/P_0 - pressure ratio across shock

The pressure ratio can also be expressed in terms of the propellant weight, the yield, the distance from the point of ignition and some constants.

$$\frac{P_2}{P_0} = \frac{10^b}{P_0}\left[\frac{(Wy)^{1/3}}{r}\right]^m + 1 \tag{8}$$

Equation (8) can now be substituted into Equation (7) to obtain the desired relationship, giving the air-shock velocity in terms of the distance from the point of ignition. Spherical geometry was assumed throughout in these derivations and whenever the fireball moved, r was taken as the radius of the fireball. This was necessary since otherwise information like wind velocity, etc. would have to be added into the above equations. Equation (9) is the desired result giving the air-shock relationship for the fireball hypothesis in Region IV.

$$v_s = c_o\left\{\frac{\gamma+1}{2\gamma}\left[\frac{10^b}{P_0}\left(\frac{(Wy)^{1/3}}{r}\right)^m + \frac{\gamma-1}{\gamma+1} + 1\right]\right\}^{\frac{1}{2}} \tag{9}$$

The symbols in Equation (9) have the meanings as defined earlier with b and m constants.

Equation (9) now allows the calculation of the velocity of the air shock at any distance from the missile (Fig. 5).

Fireball Boundary

The fireball boundary can be calculated by utilizing the perfect gas relationships and considering either the spherical or hemispherical configuration. Then considering the heat generated through the chemical reaction processes and the heat losses, the necessary constants describing the process can be evaluated. Information such as that found in the literature[4, 5, 6, 7] is very helpful in this treatment.

Further considering that the heat or energy released minus the amount used in raising the temperature and minus the amount lost produces the kinetic energy which is observed in terms of the velocity at any time t or at any distance r. This is then the fireball velocity as expressed in Equation (10).

$$v_{FB} = \left(\frac{2Q}{m\,4/3\,\pi}\right)^{\frac{1}{2}} \frac{1}{r^{3/2}} = \frac{C}{r^{3/2}} \rightarrow \tag{10}$$

In Equation (10), Q is the energy released and available for acceleration of the mass m. As can be seen the fireball velocity, that is the boundary velocity, is inversely proportional to the 3/2 power of the radius. Q can be expressed in terms of the total weight of the propellants and the thermal yield.

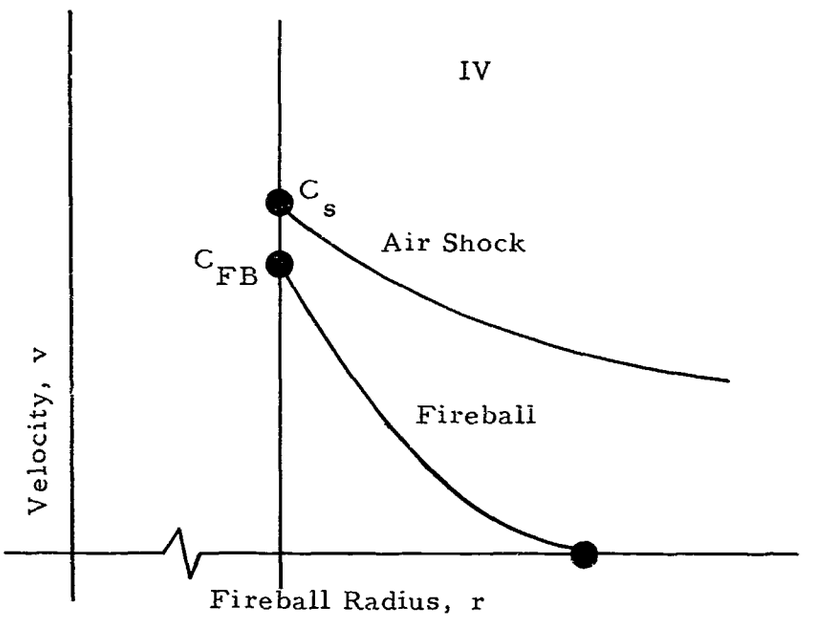

Figure 5 Graphical Representation of Fireball Hypothesis in Region IV

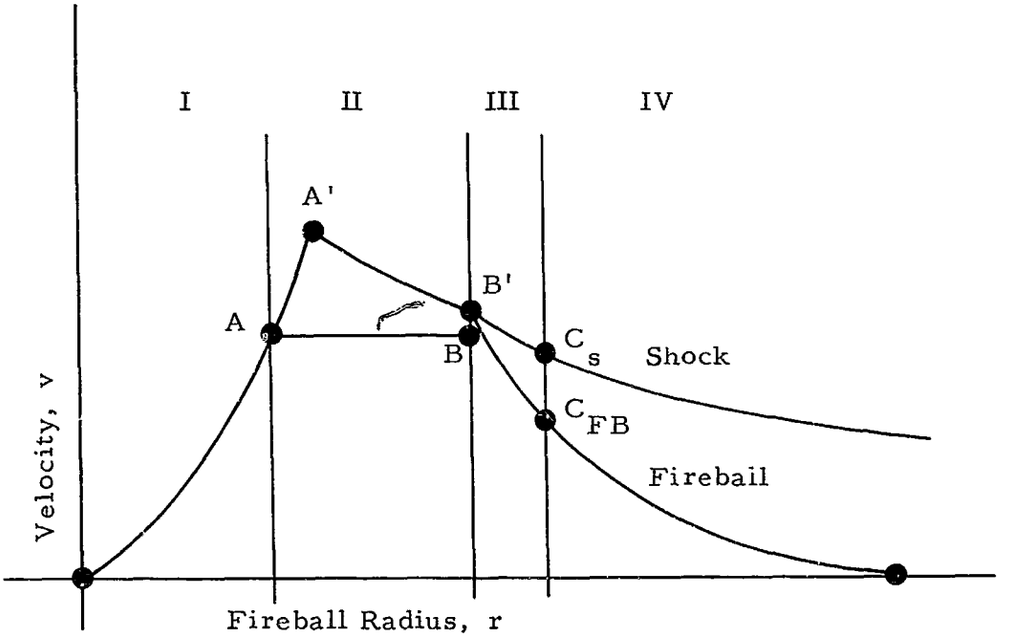

Figure 6 Graphical Representation of the Complete Fireball Hypothesis

Figure 5 represents schematically the shock velocity and the fireball velocity in Region IV, indicating the separate paths which they follow.

It might be well to mention again that in the presentation of the fireball velocity the actual center of the fireball was used as reference rather than the original point of ignition. If that had not been done then the movement, rise of the fireball and drift due to winds and atmospheric conditions would have complicated the presentation.

Complete Fireball Hypothesis

Having discussed the four parts or regions of the complete fireball hypothesis they can be combined to give the complete picture, which is presented in graphical form in Figure 6. The different regions are not plotted to the same scale but rather to a scale which allows the presentation of the variations in each region. This was done by enlarging Region I, and especially Region III, and by shrinking Region II, and especially Region IV.

Figure 6 presents graphically the complete fireball hypothesis for a specific yield. Different yields would change it slightly, specifically the relative sizes of Regions I and II. The higher the yield the smaller is Region I.

The various regions of Figure 6 can be compared with the detailed regions and their discussion under the specific headings, Region I, Region II, Region III and Region IV.

Comparison of Results from the Hypothesis and Some Actual Data

To show how this hypothesis agrees with the sparse experimental information available, films of the S-IV Test were analyzed and analyses from the various reports were used. The hypothesis is plotted in Figure 7 and the available experimental points are superimposed.

The equations used for plotting the calculated curves in Figure 7 were Equations (9) for the air shock velocity and (10) for the fireball velocity.

These equations for the S-IV, where $W = 91,200$ lb, $y = 0.045$ avg., with their constants evaluated, have the following form:

Shock Velocity:

$$v_s = 1100 \left\{ 14 \left[\frac{(91,200 \times 0.045)^{1/3}}{r} \right]^{1.4} + 1.17 \right\}^{\frac{1}{2}} \qquad (9A)$$

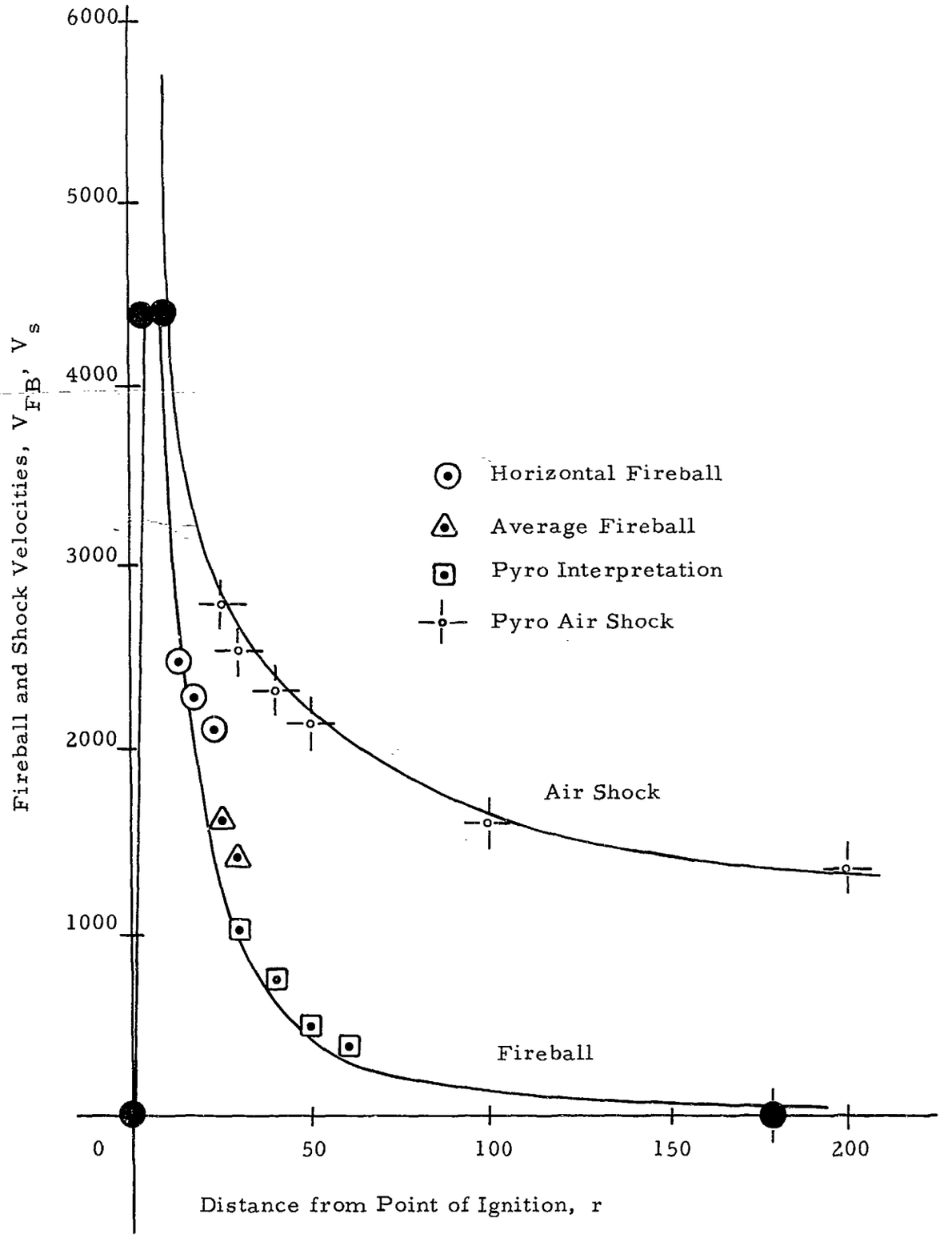

Figure 7 Fireball Hypothesis Applied to the S-IV Experiment with Experimental Points Superimposed upon the Calculated Curves

Fireball Velocity:

$$v_{FB} = \frac{157,500}{r^{3/2}} - 80 \qquad (10A)$$

The results from these equations are the solid curves plotted in Figure 7. In this figure which is plotted to scale, Regions I, II and III are so small that not much detail can be shown.

SUMMARY

In this paper a hypothesis was discussed which seems capable of giving insight into the actual processes taking place from the time of ignition in a liquid propellant rocket explosion till the shock and the fireball have separated and dissipated.

This hypothesis makes it possible to calculate curves for particular missile configurations and yield estimates giving a package for complete analysis.

Some of the assumptions going into the analysis naturally are not on a very firm basis and actual experimental work must be done before this hypothesis can be substantiated or modified.

The thermocouple grid analysis which is discussed as part of another paper[3] seems to be a method which could supply this information.

In the meantime this fireball hypothesis stands as a hypothesis but it seems, from the work done with it, promising and useful in the detailed study and analysis of liquid rocket propellant explosions.

REFERENCES

1. Farber, E. A., "A Mathematical Model for Defining Explosive Yield and Mixing Probabilities of Liquid Propellants," Third Space Congress Proceedings, March 1966. (Paper No. I in this series.)

2. Farber, E. A., Deese, J. H., "A Systematic Approach for the Analytical Analysis and Prediction of the Yield from Liquid Propellant Explosions," Third Space Congress Proceedings, March 1966. (Paper No. II in this series.)

3. Farber, E. A., San Martin, R. L., "Studies and Analyses of the Mixing Phenomena of Liquid Propellants Leading to a Yield-Time Function Relationship," (Paper No. III in this series.)

4. Project Pyro., "Monthly and Quarterly Progress Reports Covering the Liquid Propellant Explosive Test Program including the S-IV Test."

5. Aerojet-General Corp., "Blast and Fireball Comparison of Cryogenic and Hypergolic Propellants," Contract No. NAS9-2055, Final Report, 26 June 1964.

6. Arthur D. Little, Inc., "Summary Rep rt on a Study of the Blast Effect of a Saturn Vehicle," February 15, 1962, and some original data obtained from them.

7. ASME and ASCE "Symposium on Water Hammer," Proceedings, 1933.

8. Van Nice, L. J., Carpenter, J. H., "Thermal Radiation From Saturn Fireballs," TRW Systems Reports, Vol. I and II, December 1965.

9. Goodman, H. J., "Compiled Free-Air Blast Data on Bare Spherical Pentolite," BRL Report, No. 1092, February 1960.

10. Boering, Burkhardt, "Beitraege zur Theorie der Detonation," Deutsche Luftfahrtforschung, No. 1939, April 1944.

11. Technical Data on Fuels, edited by H. M. Spiers, The British National Committee World Power Conference, Fifth Edition, London, 1952.

12. Fuels and Combustion Handbook, edited by A. J. Johnson, McGraw-Hill Book Company, Inc., New York, 1951.

13. Mechanical Engineers' Handbook, edited by T. Baumeister, McGraw-Hill Book Company, Inc., New York, 6th Edition, 1958.

Appendix

C-I (Page 1-12)

ENGINEERING PROGRESS

AT THE

UNIVERSITY OF FLORIDA

VOL. XXI, No. 11 November, 1967

Technical Paper No. 396

CHARACTERISTICS OF LIQUID ROCKET PROPELLANT EXPLOSION PHENOMENA

Part V: Thermocouple Grid Analysis of Two 25,000-Lb LOX/RP Liquid Propellant Explosion Experiments

by

ERICH A. FARBER

Professor of Mechanical Engineering

PUBLISHED MONTHLY BY THE

FLORIDA ENGINEERING AND INDUSTRIAL EXPERIMENT STATION

COLLEGE OF ENGINEERING • UNIVERSITY OF FLORIDA • GAINESVILLE

ENTERED AS SECOND-CLASS MATTER AT THE POST OFFICE AT GAINESVILLE, FLORIDA

CHARACTERISTICS OF LIQUID ROCKET PROPELLANT EXPLOSION PHENOMENA

Part V: Thermocouple Grid Analysis of Two 25,000-Lb LOX/RP Liquid Propellant Explosion Experiments

by

E. A. Farber*

In the studies at the University of Florida to predict the yield obtained from liquid propellant explosions, the problem was divided into the study of three groups of phenomena which offered themselves to separate and independent investigation. When the results of each of these independent investigations are combined, the desired yield value is obtained.[1] These groups are:

I. The Yield Potential Function

II. The Mixing Function

III. The Delay and Detonation Times

The yield potential function (I) is basically controlled by chemical kinetics, the mixing function (II) by the principles of hydrodynamics modified by heat transfer, and the delay and detonation times (III) by characteristic functions for some propellants such as hypergolics and by random processes for others.

Theoretical studies of the above three groups of phenomena have been supplemented by laboratory studies at the University of Florida with mixing studies of fluids simulating the liquid propellants.[2]

In addition to these laboratory experiments with inert fluids the University of Florida group installed instrumentation inside two 25,000-lb tank assemblies of the liquid propellant explosion test series, planned and conducted under Project PYRO at the Air Force Rocket Propulsion Laboratory at Edwards Air Force Base, California. This instrumentation was to measure phenomena following the initiation of failure.

Because of the mode of failure selected by Project PYRO, the region swept through by the star cutter had to be excluded from detailed analysis since any instrumentation in that region would have been destroyed by the cutter before the events occurred which were to be measured.

---

* Professor of Mechanical Engineering, University of Florida

The overall purpose of this instrumentation was to

1. Correlate the mixing phenomena of the true propellants with laboratory mixing experiments using inert fluids for simulation.
2. To substantiate experimentally parts or all of the "Fireball Hypothesis"[3] proposed earlier in these studies.

Specifically it was hoped to be able to determine by this experimental procedure part or all of the following:

After failure but before ignition:

1. The three-dimensional mixing front, or boundary of the mixing region.
2. The degree of mixing at a particular point.
3. The degree of turbulence at a particular point.

After ignition:

4. The location of the point or points of ignition.
5. The time delays from initiation of failure to start of mixing, to ignition.
6. The propagation of the reaction front.
7. The propagation of the shock front.
8. The separation of the shock front and the reaction front.
9. Other phenomena and events obtainable by detailed data analysis.

Only in (2) and (3) above do the thermocouple response characteristics have to be considered since in all other cases only relative time differences are needed.

Excellent data were obtained in both experiments. Advantage was, however, taken of knowledge obtained from the data analysis of the first experiment, No. 278, to obtain the best results possible from the second experiment, No. 282. The main improvements were the moving up of some of the thermocouples higher in the tank and closer to the star cutter, or into the mixing region, since it was found that the star cutter did not travel as far as was previously expected. The recording oscillographs were, in the second experiment, operated at four times the speed of the first experiment to increase the resolution capabilities.

The instrumentation tc accomplish the above consisted of

1. Very fine thermocouples inside the tank.
2. A reference junction box in an underground steel box near ground zero.
3. High speed recording oscillographs.

The sensing elements inside the tank (Fig. 1) consisted of 37 copper-constantan thermocouples, No. 36 gage, shellacked and Teflon-coated. The thermocouples were made so that no excess material was present at the junction and the whole thermocouple looked like a continuous wire with no visible variation at the junction (Fig. 2). A small plastic tube was slipped over the wires to about $\frac{1}{4}$ inch behind the junction and filled with epoxy, both to support the junction preventing relative motion between the wires, and to provide a means for attaching the thermocouple to the support wires inside the tank.

The thermocouples were located in the tank (Fig. 3), so as to give an optimum pattern of the data. They indicated the arrival of events at their location and changes occurring at or in their region.

The leads of the 37 thermocouples (74 individual wires) were guided along the support wires and loosely tied to them about every 8 inches (Fig. 4). This gave the needed support to the fine wires and at the same time allowed them to give, in case they were hit by some small fragments from the shattered glass diaphragm.

The leads were then fed by means of two Cannon plugs through the tank wall, and on the outside by copper-constantan thermocouple cables to the hot reference junctions, located in an underground steel box. From there the signals produced by the thermocouples were carried by copper cables to three CEC recording oscillographs. These recorders were operating at a chart speed of 40 in./sec for experiment 278, and at 160 in./sec for experiment 282.

The data obtained by the above instrumentation and method are shown in Figure 5 for a few thermocouples; 5A giving traces from initiation of failure to some time after detonation; 5B showing only the time increment during which mixing starts and indicating the passage of the reaction and shock fronts.

Preliminary analysis of the data from these two liquid propellant explosion experiments allow the following statements to be made:

1. Experiments No. 278 and 282 were amazingly similar in propellant mixing, ignition and explosion characteristics.

2. Practically all the mixing up to the time of ignition was confined to the volume swept through by the star cutter. This volume as determined from the data was about 12 percent of the total, based upon the RP, giving an upper yield estimate of about 12 percent of the theoretical maximum or somewhat less than 15 percent TNT equivalent.

3. The actual temperatures as recorded by the traces allow the calculation of the degree of mixing by means of a number of simultaneous equations which can most conveniently be solved by computer.

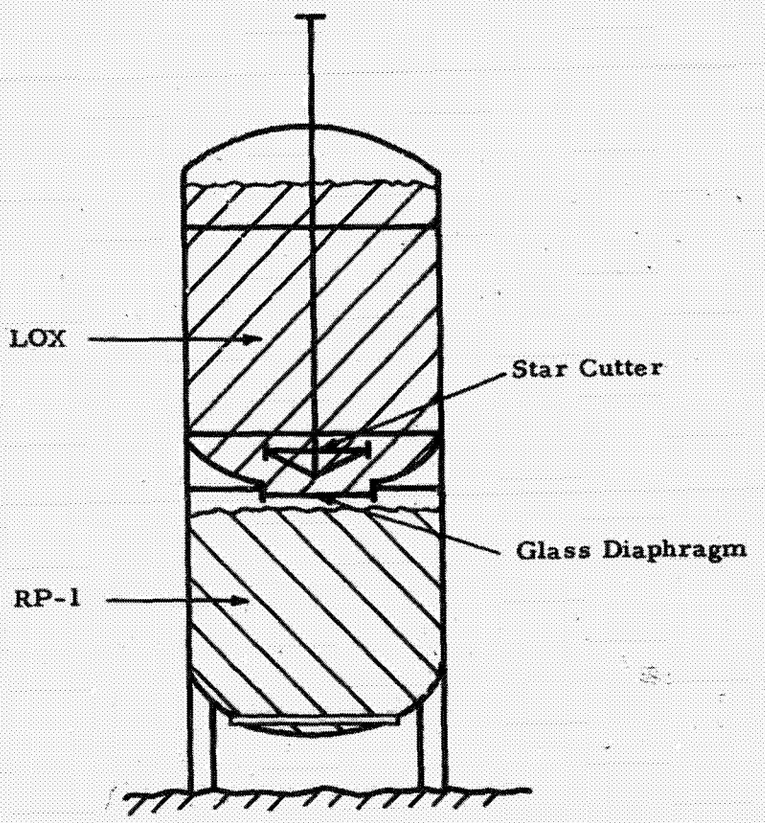

Fig. 1A
Schematic Sketch of 25,000-Lb LOX/RP Tank

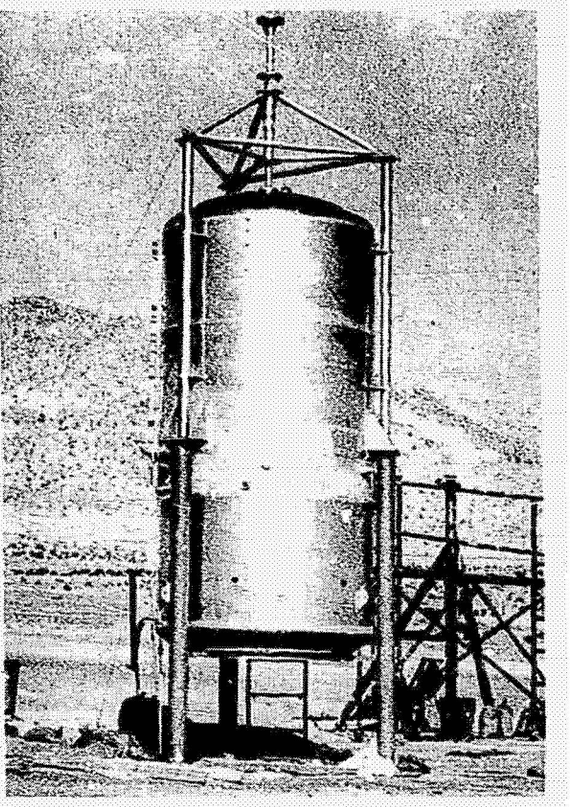

Fig. 1B
25,000-Lb LOX/RP Tank Assembly.
Experiment No. 282

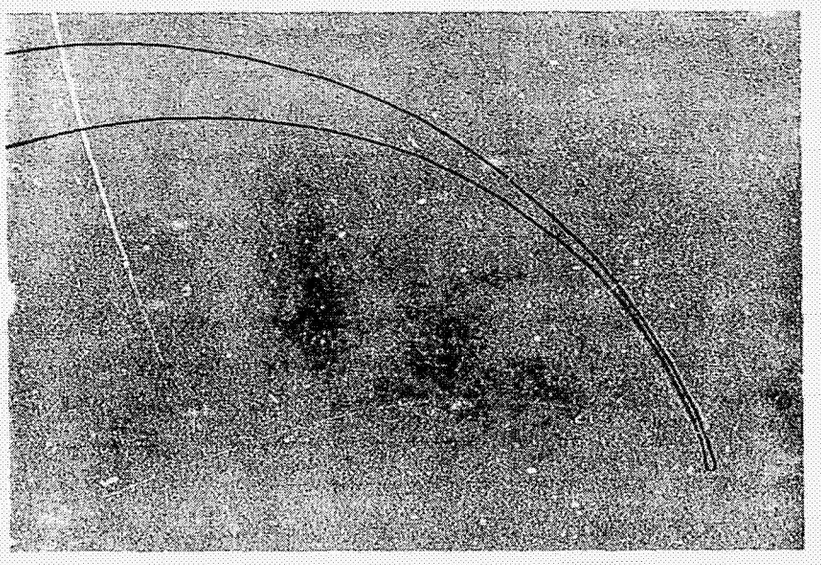

Fig. 2
No. 36 Gage Copper Constantan Thermocouple Sensor

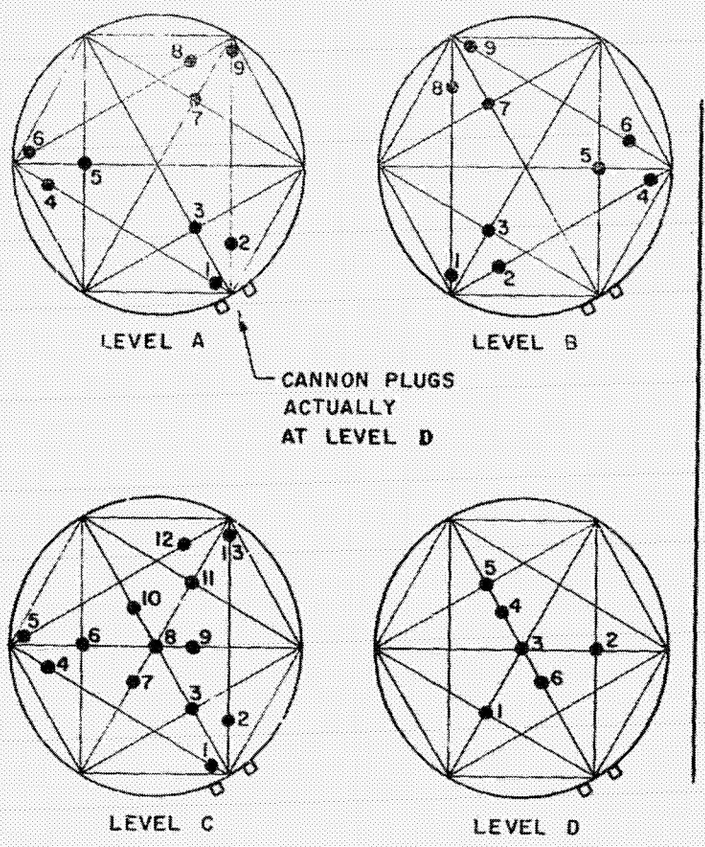

Fig. 3A
Thermocouple Locations. Experiment No. 278.

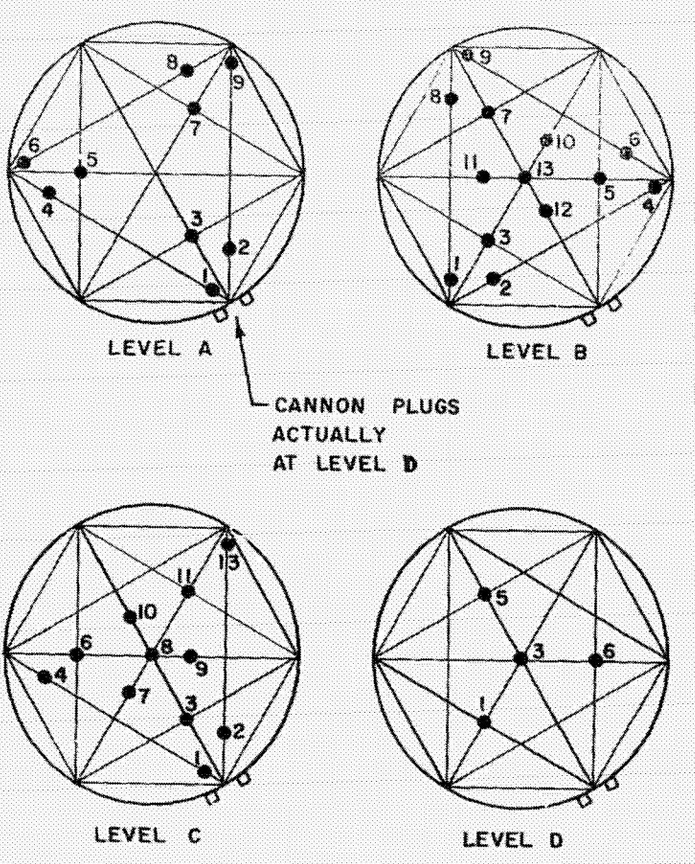

Fig. 3B
Thermocouple Locations. Experiment No. 282.

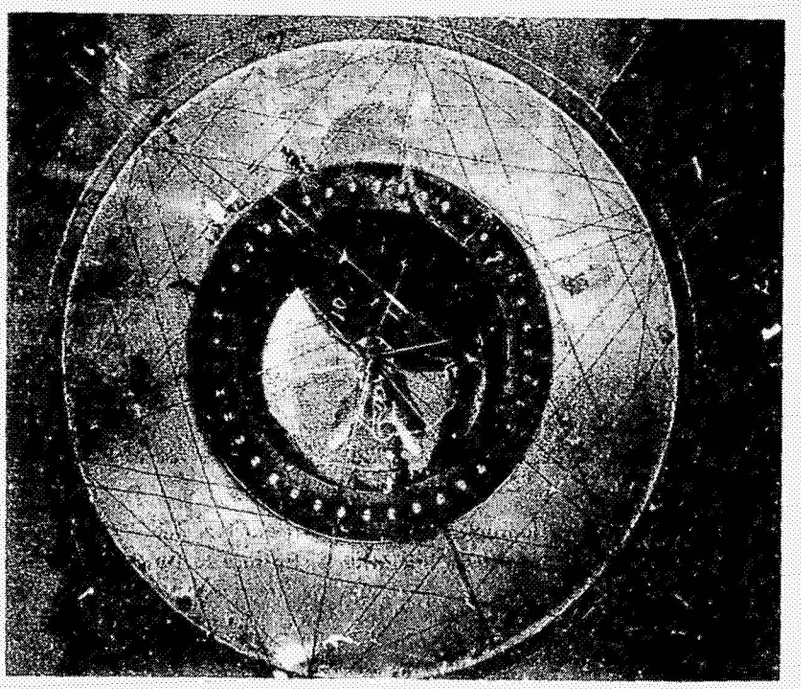

Fig. 4
Thermocouple Grid in Tank

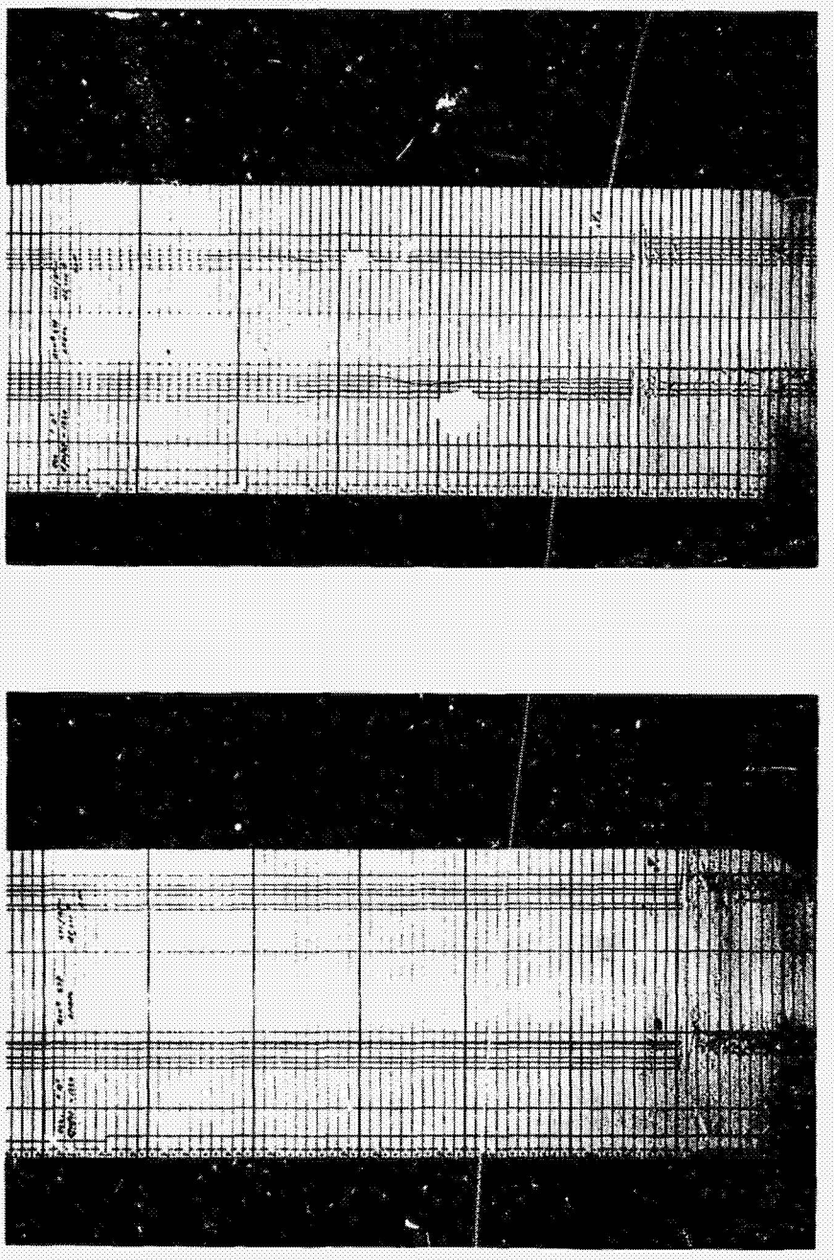

Fig. 5A
Oscillograph Traces. Experiment No. 278.
Complete Interval from Initiation of Failure to Detonation.

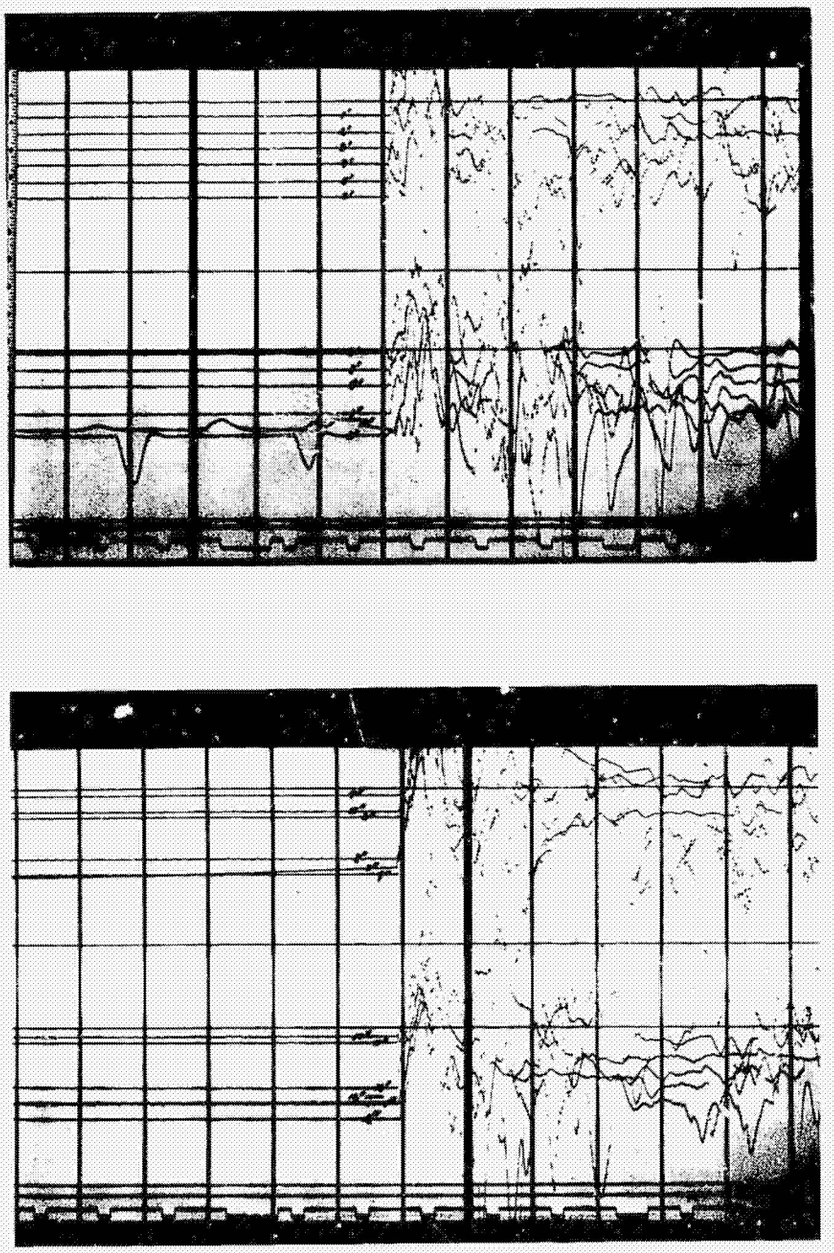

Fig. 5B
Oscillograph Traces. Experiment No. 282.
Ignition and Events Following.

4. The degree of turbulence at a particular point (the points where the thermocouple junctions were located) can be determined from the fluctuations and fine structure of the traces in terms of frequency and amplitude.

5. There was only one point of ignition in each of the experiments and this point was located in each case (Fig. 6A and 6B).

6. The time delays between various events can be determined from the traces. If projected on a screen these times can be read to a 1/1000 of a millisecond. The time delay from failure or firing of the ram to ignition in experiment 278 was 543 milliseconds, and in experiment 282 it was 580 milliseconds (read to the closest millisecond. Greater accuracy is available if desired).

The accurate reading of these delay times also allows the exact determination of the film speeds of the various cameras used. The importance of this is brought out, since none of the cameras operate at their nominal speeds and vary from one time to the next. For instance, the two 4000 fps cameras during experiment 282 were operating actually at 2620 fps and 3750 fps respectively.

7. The propagation velocities of the reaction front could be determined and the preliminary analysis gives the results shown in Figure 7.

8. By careful study of the fine structure of the traces the shock front propagation characteristics can be determined.

9. From (7) and (8) above it can be determined where the two fronts travel together and where and when the shock front leaves the reaction front behind.

10. With the delay times exactly determined, the film speeds are known and with them the volume-time or volume-distance characteristics of the reaction and shock fronts can be determined (Fig. 8).

11. The fine structure of the traces reveals that some of the glass fragments from the shattered diaphragm hit some of the thermocouples in the uppermost of the four layers, but did not damage them, so they recorded this and later events. The glass fragments did not penetrate during their high energy state to the lower layers since the attenuation in the liquid was too great.

12. From the fine structure of the traces, at least three typical shapes are observed. One is where the LOX first arrives, followed by the reaction and shock fronts; another where the reaction and shock fronts are the first events to arrive at the thermocouple, and the third where the shock front seems to pass, closely followed by the reaction front.

The above statements are only a few of the many which could be made and more effort will go into evaluating the data to extract the maximum amount of information possible from these experiments.

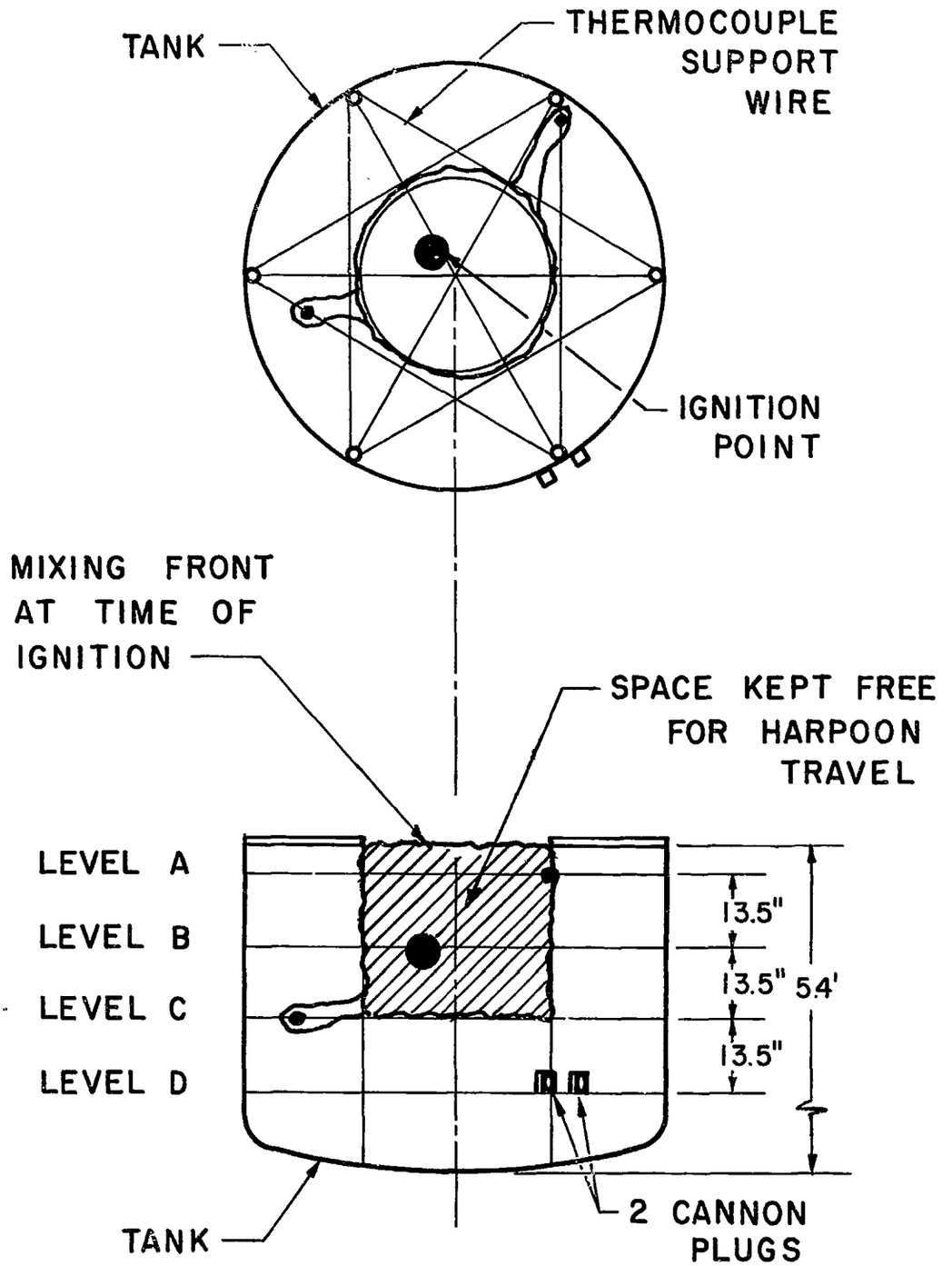

Fig. 6A
Mixing Front and Ignition Point. Experiment 278.

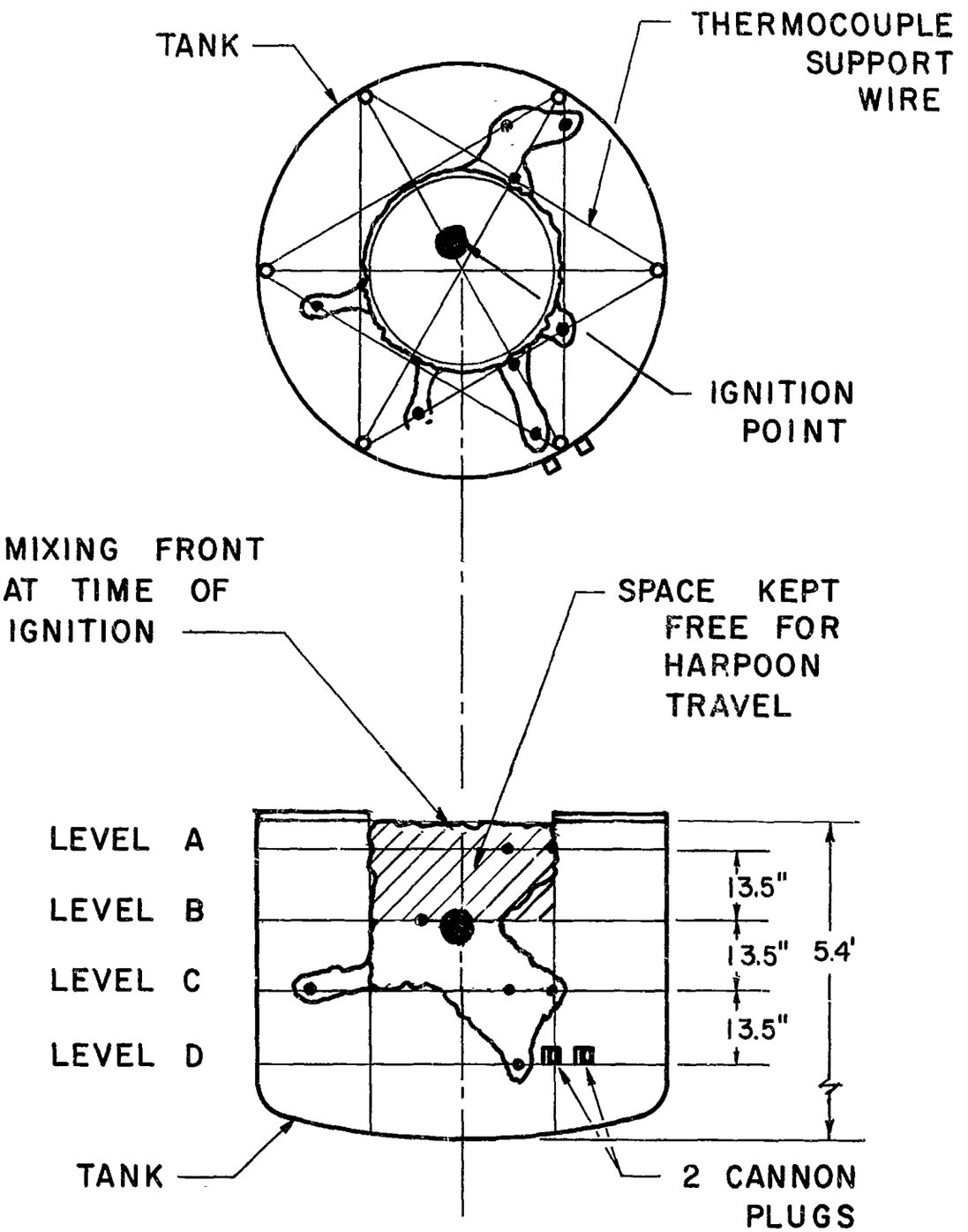

Fig. 6B
Mixing Front and Ignition Point. Experiment 282.

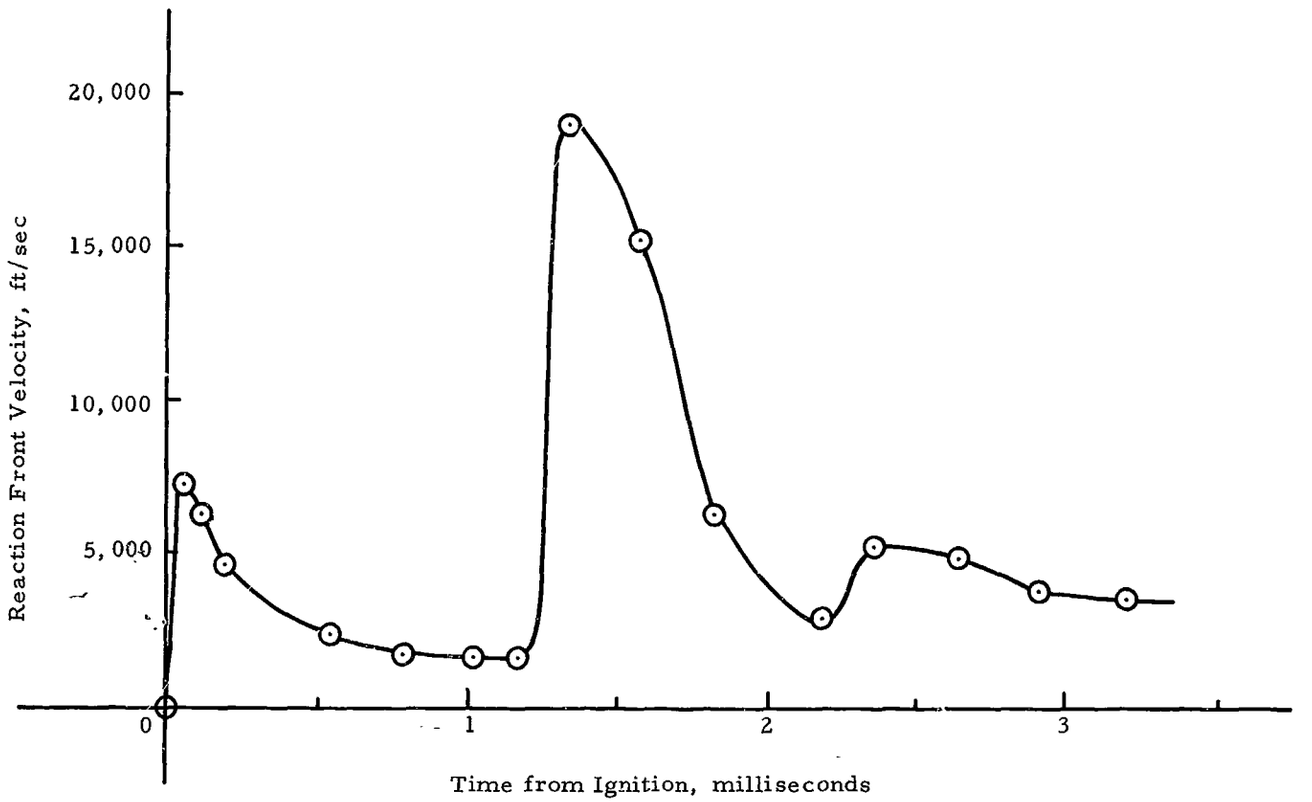

Fig. 7
Reaction Front Velocity as a Function of Time.

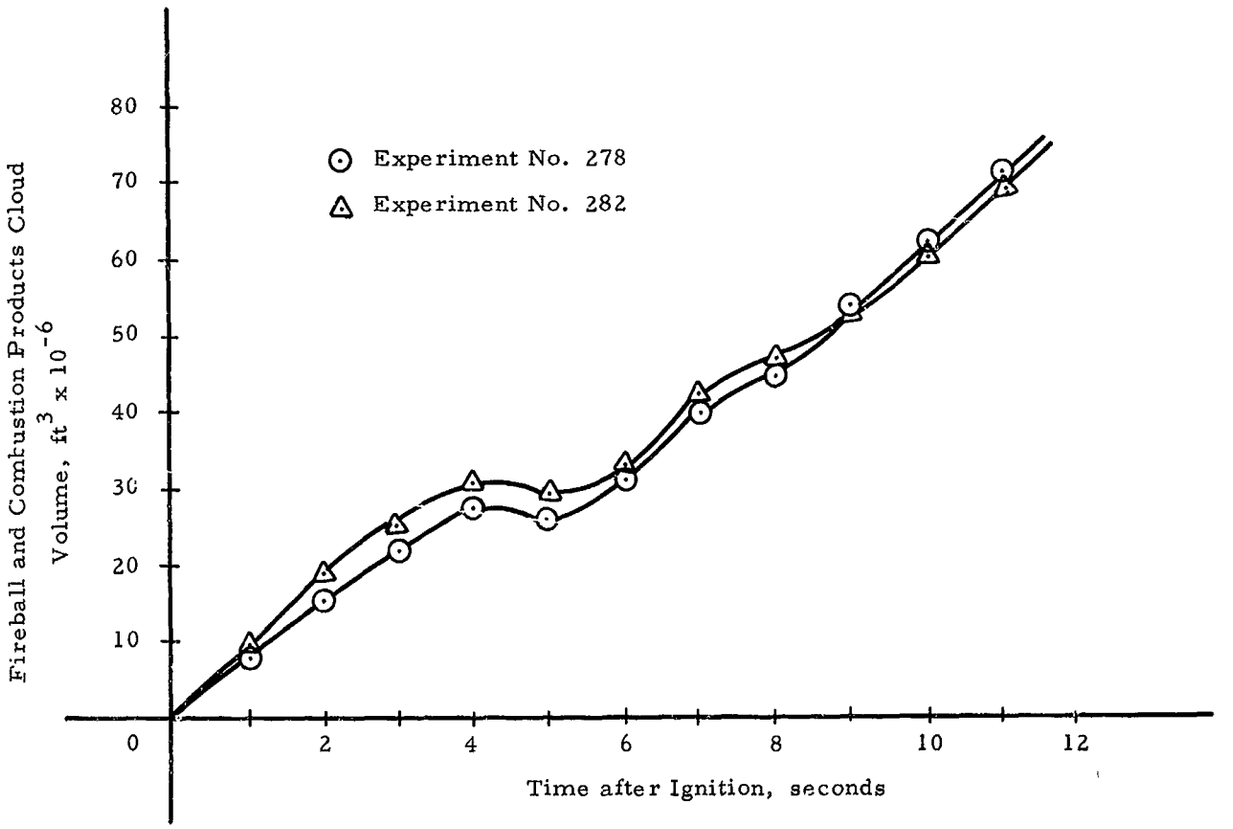

Fig. 8
Fireball and Combustion Products Cloud Volume as a Function of Time.

It is believed that the above data and results to date have demonstrated the applicability of this method of study and this instrumentation in the analysis of liquid propellant explosion characteristics. The application to the two 25,000-lb experiments has added new information and furthermore showed the close correlation between inert liquid mixing experiments and the actual explosion experiments.

The data analysis also allowed the prediction of the yield and substantiated in general the Fireball Hypothesis developed a few years ago by the University of Florida group.

REFERENCES

1. Farber, E. A., et al., "A Systematic Approach for the Analytical Analysis and Prediction of the Yield from Liquid Propellant Explosions," Third Space Congress Proceedings, March, 1966. Available as Technical Paper No. 347, Florida Engineering and Industrial Experiment Station.

2. Farber, E. A., et al., "Studies and Analyses of the Mixing Phenomena of Liquid Propellants Leading to a Yield-Time Function Relationship," New York Academy of Sciences, Explosives Symposium Proceedings, 1967. Available as Technical Paper No. 386, Florida Engineering and Industrial Experiment Station.

3. Farber, E. A., et al., "Fireball Hypothesis Describing the Reaction Front and Shock Wave Behavior in Liquid Propellant Explosions," New York Academy of Sciences, Explosives Symposium Proceedings, 1967. Available as Technical Paper 387, Florida Engineering and Industrial Experiment Station.

4. Farber, E. A., et al., "Fireball and Post-Fireball Composition and Atmospheric Chemistry of Fuel/Oxygen-Fluorine Propellants," NASA Report, Contract NAS10-1255, July, 1967.

ACKNOWLEDGMENTS

It is with sincere appreciation that the writer expresses his thanks to Mr. R. L. Thomas, Jim Wanacheck, R. McQuown and their staff of the Air Force Rocket Propulsion Laboratory, Edwards Air Force Base, California, for their help in preparing and executing the experiments; to Mr. Larry Danielson and Tom Wilder from the Federal Electric Corporation for their help with the instrumentation.

From our staff at the University of Florida thanks are given to Mr. J. D. Ross and F. L. Ebright for their help with the preparation of the thermocouple grid, and to Professor F. W. Klement, Mr. C. F. Bonzon and J. W. Kruck for their help with the analyses of the data.

Last but not least, thanks are given to Mr. John Atkins and Jim Deese from the John F. Kennedy Space Center who, through their administrative actions, greatly aided this project.

Appendix

ENGINEERING PROGRESS

AT THE

UNIVERSITY OF FLORIDA

Vol. XXII, No. 7 July, 1968

Technical Paper Series

CHARACTERISTICS OF LIQUID ROCKET PROPELLANT EXPLOSION PHENOMENA

No. 415A: Part VI. Explosive Yield Estimates for Liquid Propellant Rockets Based Upon a Mathematical Model

No. 415B: Part VII. Interpretation of Explosive Yield Values Obtained From Liquid Rocket Propellant Explosions

by

ERICH A. FARBER

Professor and Research Professor of Mechanical Engineering

(A Continuing Series of Research Reports on NASA Project NAS 10-1255. Parts VI and VII were presented to NASA, April 25, 1968, at Cape Kennedy)

PUBLISHED MONTHLY BY THE

FLORIDA ENGINEERING AND INDUSTRIAL EXPERIMENT STATION

COLLEGE OF ENGINEERING • UNIVERSITY OF FLORIDA • GAINESVILLE

ENTERED AS SECOND-CLASS MATTER AT THE POST OFFICE AT GAINESVILLE, FLORIDA

CHARACTERISTICS OF LIQUID ROCKET PROPELLANT EXPLOSION PHENOMENA

A research project initiated in 1964 by Dr. Erich A. Farber, Research Professor of Mechanical Engineering, on liquid propellant rocket explosions, has resulted in the publication of five NASA reports and seven technical papers to date in this area. The research is under the sponsorship of the National Aeronautics and Space Administration. The seven papers listed below define and discuss the characteristics of liquid rocket propellant explosion phenomena. They are:

I: A Mathematical Model for Defining Explosive Yield and Mixing Probabilities of Liquid Propellants, by E. A. Farber.

II: A Systematic Approach for the Analytical Analysis and Prediction of the Yield from Liquid Propellant Explosions, by E. A. Farber and J. H. Deese.

III: Studies and Analyses of the Mixing Phenomena of Liquid Propellants Leading to a Yield-Time Function Relationship, by E. A. Farber and R. L. San Martin.

IV: Fireball Hypothesis Describing the Reaction Front and Shock Wave Behavior in Liquid Propellant Explosions, by E. A. Farber and J. S. Gilbert.

V: Thermocouple Grid Analysis of Two 25,000-lb LOX/RP Liquid Propellant Explosion Experiments, by E. A. Farber.

VI: Explosive Yield Estimates for Liquid Propellant Rockets Based Upon a Mathematical Model, by E. A. Farber.

VII: Interpretation of Explosive Yield Values Obtained From Liquid Rocket Propellant Explosions, by E. A. Farber.

Since research on this problem is continuous in nature, and considerable effort and time is expended thereon, more papers and reports in this series will be forthcoming.

CHARACTERISTICS OF LIQUID ROCKET PROPELLANT EXPLOSION PHENOMENA

Part VI: Explosive Yield Estimates for Liquid Propellant Rockets Based Upon a Mathematical Model

by

E. A. Farber*

ABSTRACT

This paper demonstrates how the mathematical model,[1,2] developed earlier, can be used to estimate the expected explosive yields, as a result of liquid propellant rocket failures.

The best available data are incorporated and a comparison is made with results obtained from liquid propellant explosion experiments.

The mathematical model, programmed for an IBM-360 computer, used here is described briefly so as to eliminate the need for the references.

INTRODUCTION

The yield from liquid propellant explosions, as a result of missile failures, is of extreme importance in assessing the hazards to astronauts, launch-support personnel, launch-support facilities and surrounding communities. Since explosive tests of large liquid propellant rockets are not practical because of the costs and hazards involved, prediction methods must be used in estimating the expected explosive yields.

A mathematical model was developed by the writer, a few years ago, for this specific purpose. At that time very limited information was available to evaluate the validity of the model. Considerable information has become available since that time. Data were obtained by the writer's University of Florida Group, by instrumenting two 25,000-lb LOX/RP explosive experiments[3] and one 200-lb LOX/RP cold flow and explosive experiment, carried out at the Air Force Rocket Propulsion Laboratory at Edwards Air Force Base, California, which established the yield function-spill function relationship. Only last week the Preliminary Final Report of Project PYRO became available, giving data which were used here to check the results predicted by the model.

This information including the inert mixing experiments, increased the confidence in this model and established it as a very useful tool.

---

*Professor and Research Professor of Mechanical Engineering, University of Florida, Gainesville, Florida.

Yield Function

The yield function, as used for this paper, is defined as the fraction of the theoretically maximum yield which is actually obtained.

$$y = \frac{Y}{Y_{\text{theor. max.}}} \qquad (1)$$

This yield can be expressed as TNT equivalent yield on an energy basis but care must be exercised in predicting damage, since the pressure-time trace for liquid propellants is different from that of TNT, especially in the near field.

Spill Function

The spill function, as used in this paper, is defined as the fraction of the total volume of propellants mixed at any time t, multiplied by some modifying factors.

$$x = \frac{V_M}{V_P} F_T F_B F_F \qquad (2)$$

V_M Propellant Volume Mixed

V_P Total Propellant Volume

F_T Turbulence Factor

F_B Boiling Factor

F_F Freezing Factor

Inert laboratory experiments, utilizing such fluids as water and oil, hot wax and water, hot oil and water, LN_2 and water, LN_2 and kerosene, etc. established the factors F_T, F_B, and F_F.

It was shown that, in the early stages of mixing, these factors have a value near 1 and thus the spill function x is essentially the normalized mixing volume. This latter fact was also established by the explosive experiments of the 25,000-lb LOX/RP and the 200-lb LOX/RP.

Yield Function - Spill Function Relationship

In the development of the mathematical model it was assumed that the relationship between y and x can be expressed as

$$y = \frac{b}{b + c} x^d \qquad (3)$$

where b, c, and d are constants.

Again the explosive experiments of 25,000-lb LOX/RP and the 200-lb LOX/RP cold flow and explosive experiments proved the above relationship valid.

MATHEMATICAL MODEL[1,2]

With the relationship between the yield function (y) and the spill function (x) established, the mathematical model can be formulated, resulting in a statistical function which is capable of incorporating the above y-x relationship, and is able to provide for valid estimating procedures of the parameters involved.[1,2]

The statistical function is a modified Dirichlet bivariate surface with four parameters a, b, c, and d. It is

$$f(x, y) = \frac{d\,\Gamma(a+b+c)}{\Gamma(a)\Gamma(b)\Gamma(c)}\, x^{d-1}(1-x^d)^{a-1} y^{b-1}(x^d-y)^{c-1} \tag{4}$$

where Γ is the gamma function. The only restrictions on this function are that

$$y > 0,\quad x > 0,\quad y \leq x^d,\quad d \neq 0$$

To fully define the above function it is necessary to evaluate the parameters a, b, c, and d on the basis of the particular y-x relationship describing the physical phenomena. This can be done by the following statistical estimating procedure.

Defining

$$u_i = 1 - x_i^d, \qquad v_i = \frac{y_i}{x_i^d} \tag{5}$$

four simultaneous estimation equations can be written for the four parameters a, b, c, and d.[1]

$$\overline{\ln v} = \Psi(b) - \Psi(b + c) \tag{6a}$$

$$\ln \bar{v} = \ln(b) - \ln(b + c) \tag{6b}$$

$$\overline{\ln u} = \Psi(a) - \Psi(a + b + c) \tag{6c}$$

$$\ln \bar{u} = \ln(a) - \ln(a + b + c) \tag{6d}$$

where a bar over an expression indicates the average value of all available values

ln indicates the natural logarithm (base e)

Ψ is Euler's Digamma Function

From this mathematical model, the modified Dirichlet bivariate surface, a wealth of information can be extracted. Some of these are

A. Probability Distribution of the Yield, P_y

$$P_y(y) = \int_{y^{\frac{1}{d}}}^{1} f(x, y)\, dx \tag{7}$$

From this probability distribution, the average yield value can be found as well as confidence limits, indicating that a certain percentage of all yield values lies below the selected yield value.

B. Probability Distribution for the Spill Function, P_x

$$P_x(x) = \int_o^x f(x, y)\, dy \tag{8}$$

This distribution can be analyzed the same way as the one under (A).

C. Confidence Regions for the Yield and Spill

The regions into which a certain percentage of all yield and spill values fall can be obtained by finding the normalized fractional volumes under the probability surface. This requires double integration of the function representing the mathematical model, necessitating the use of a large-scale computer. The integrals are of the form

$$V_{x,y} = \int_o^1 \int_o^x f(x, y)\, dy\, dx \tag{9}$$

for the total volume and with the proper limits for the subvolumes. When plotting y versus x these regions can be seen looking like contour lines on a map.[2]

EXPLOSIVE YIELD ESTIMATION

To use the mathematical model for the estimation and the prediction of expected yield values it is necessary to evaluate the parameters a, b, c, and d.

This was done and it was found that by taking the best available information that the parameters take on the following values:[2]

$$b = 4.0, \quad c = 1.1, \quad d = 1.5$$

a = function of the propellant quantity, (thus can be considered a scaling parameter)

The function for a is plotted in Figure 1 indicating that it is a distorted S curve. The circled points on the curve represent the best information available both in experiments for the smaller quantities and actual liquid propellant rocket failures for the larger quantities.[1,2,3]

The only experiments which were fully instrumented to obtain the yield-spill relationship were the two 25,000-lb LOX/RP explosion tests and the 200-lb LOX/RP cold flow and explosion experiment. The yield-spill relationship which was verified in those experiments was assumed to hold also true in the remainder of the experiments and failures.

The points not circled in this figure represent the a values based upon the PYRO data as presented in the Preliminary Final Report of Project PYRO which was received only one week ago.* It is seen that all a values calculated on the basis of the PYRO data are larger than the values used in the model, except for the 1000-lb LOX/RP CBGS V-V high velocity drop tests. These tests comprise only about 0.5 percent of the total number of tests reported and are not particularly representative of liquid propellant rocket failures.

Figure 1 can be used to predict the most probable parameter a for large-scale rockets such as the Saturn V.

From the figure, it is seen that the value of a increases beyond the last available point, so it can be concluded that it will be greater than 70 for the Saturn V. On the other hand, if the last two points are connected by a straight line its intersection with the Saturn V propellant weight will give an a value which is too large. Thus the actual value of a for the Saturn V must lie between 70 and 97.

Figure 2 shows that the effect of a on the yield is rather small in the range of these large propellant quantities. And so the predicted average yield value for the Saturn V based upon the mathematical model is between 3.5 and 4 percent.

Figure 3 presents the average yield values as predicted by the mathematical model as a function of the propellant weight involved and also gives the 95 percent confidence limit, indicating that 95 times out of 100 the explosive yield for the Saturn V would be less than 9 percent.

The mathematical model as used here included all types of propellants as well as all kinds of modes of failures or experiments.

It is clear that the mode of failure, as well as the propellant type, has a distinct influence upon the actual yield obtained.[5] If only a particular type of failures or a particular type of propellants is to be investigated then only that data can be used for analysis in the mathematical model, and the values of the parameters a, b, c, and d will change. The average explosive yield value should be better in such cases and the confidence limits will be found, in general, closer to the average values.

The last statement indicates that for large-scale liquid propellant rockets it may be desirable to control the mode of failure with a properly designed destruct

*April 18, 1968

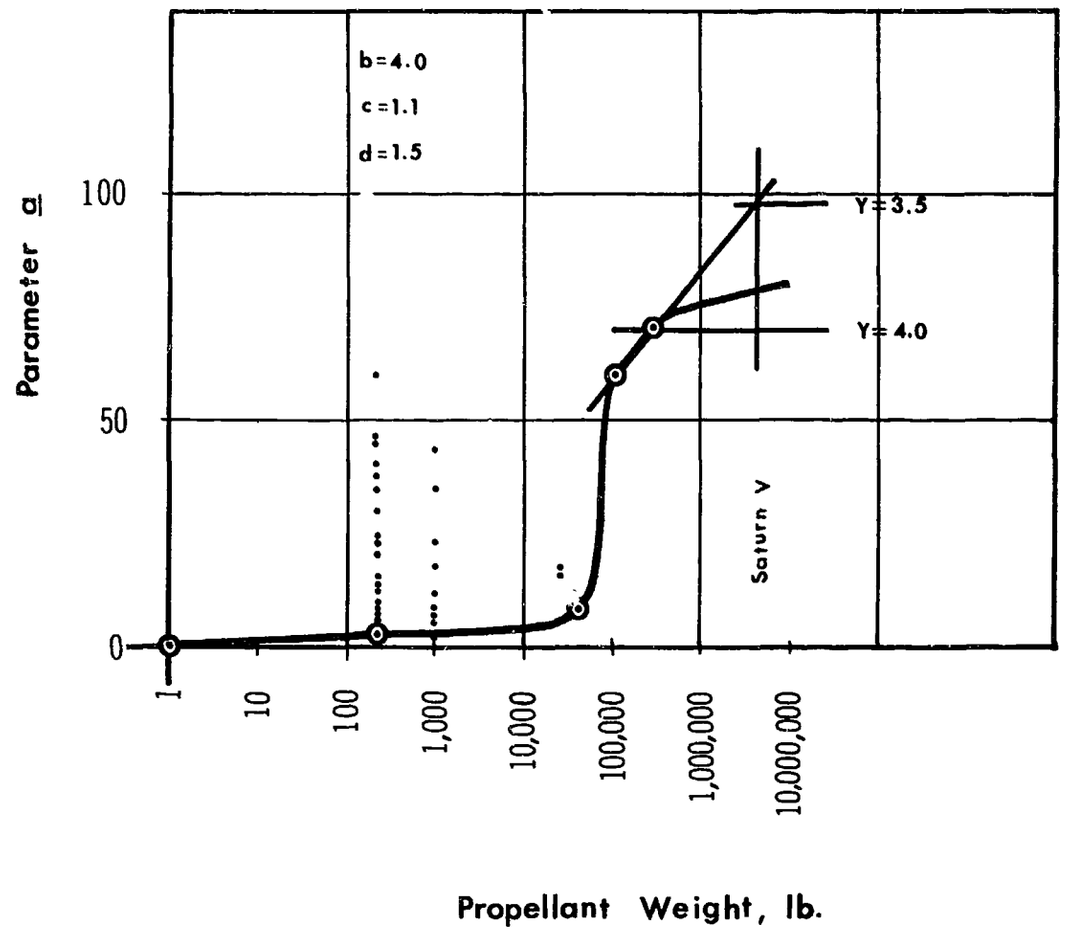

Fig. 1 Parameter a as a Function of Propellant Weight

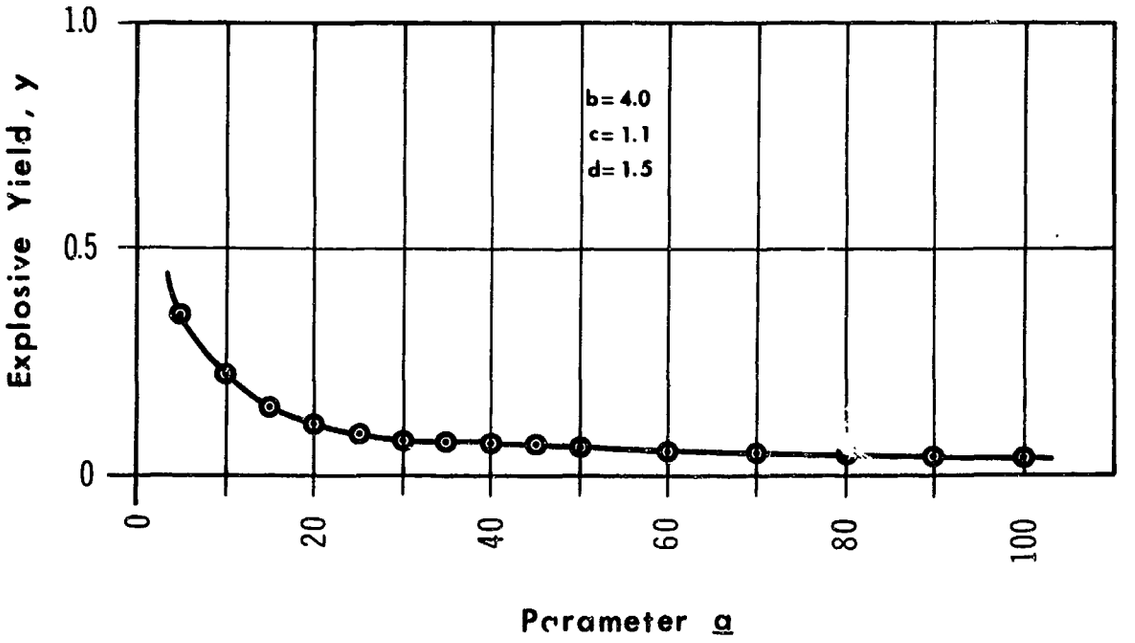

Fig. 2 Effect of Parameter a on Explosive Yield

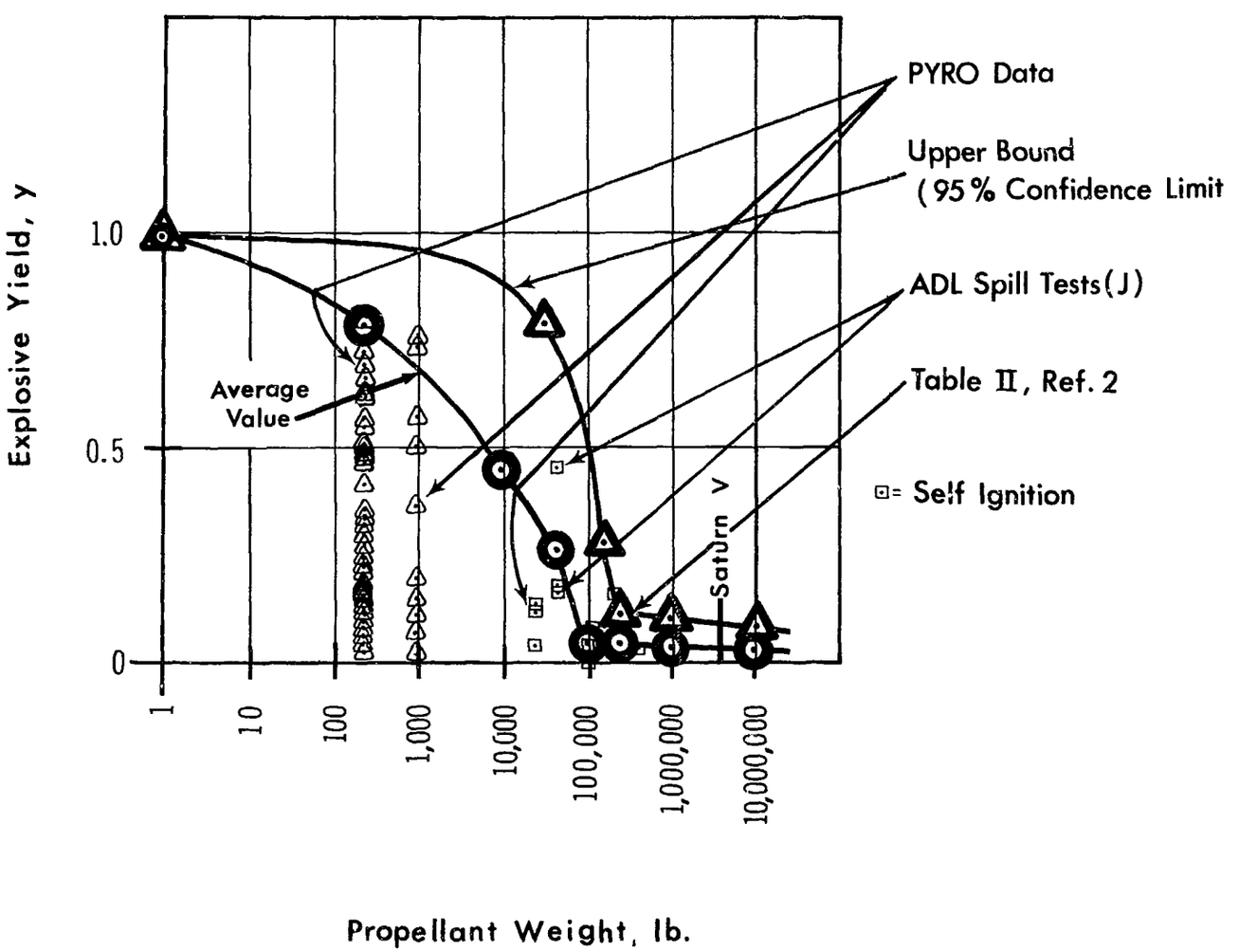

Fig. 3 Estimated Explosive Yield as a Function of Propellant Weight

system, in order to give a minimum explosive yield. With such a procedure the explosive yield value can be lowered and the explosion yield prediction reliability increased.

CONCLUSIONS

1. Since the development of the mathematical model, several years ago, for the estimation and prediction of the expected yield from liquid propellant rocket explosions, much information has become available which increases the confidence in this model.

2. The yield function-spill function relationship was verified by instrumenting two 25,000-LOX/RP explosion experiments and one 200-lb LOX/RP cold flow and explosion experiment.

3. A check of the yields predicted by the model against the experimental results, reported in the Preliminary Final Report on Project PYRO, showed the mathematical model to be conservative in 99.5 percent of the cases and only underestimated a few of the high velocity impact experiments.

4. It seems that the mathematical model can set an upper limit on the expected yield of a large-size liquid propellant rocket for a chosen confidence limit and it can give the average value by conservative extrapolation.

5. All evidence indicates that the mathematical model developed for the prediction of expected yield values is conservative in its predictions.

REFERENCES

1. "Feasibility Study to Explore the Explosive Effects of Liquid Propellants to Define the Mathematical Behavior of the Physical Processes Involved," by E. A. Farber et al, NASA Report, February, 1965.

2. "A Mathematical Model for Defining Explosive Yield and Mixing Probabilities of Liquid Propellants," E. A. Farber, Proceedings of the Third Space Congress, March, 1966.*

3. "Thermocouple Grid Analysis of Two 25,000-lb LOX/RP Liquid Propellant Explosion Experiments," E. A. Farber, Technical Paper No. 396, Florida Engineering and Industrial Experiment Station, Vol. XXI, No. 11, November, 1967.

4. "Studies and Analyses of the Mixing Phenomena of Liquid Propellants Leading to a Yield-Time Function Relationship," E. A. Farber and R. L. San Martin, Proceedings of the New York Academy of Sciences Explosives Symposium, November, 1966.*

5. "Preliminary Final Report of Project PYRO." Received incomplete copy April 17, 1968.

---

* copies also available from the Florida Engineering and Industrial Experiment Station as Technical Papers No. 346 and No. 386 respectively.

CHARACTERISTICS OF LIQUID ROCKET PROPELLANT EXPLOSION PHENOMENA

Part VII: Interpretation of Explosive Yield Values Obtained From Liquid Rocket Propellant Explosions

by

E. A. Farber*

It was mentioned previously that the results obtained by the writer and his associates are in terms of EXPLOSIVE YIELD defined as the fraction of the theoretical maximum (Normalized Yields). In this manner the difficulty of relating one propellant to another, or to other explosives is avoided.

The above difficulty comes from the observation that different propellants and explosives exhibit different pressure-time traces, or relationships, and not enough is known on how to properly correlate one of these traces with another. The most common correlation is made either on the bases of energy release, or over-pressure, or impulse with each of these correlations giving different results especially in the near field.

Since much of the work on liquid propellant explosions is reported in terms of "TNT Equivalent Yields," it was suggested that the writer provide some indication on how the yield values obtained by him could possibly be converted into equivalent TNT values.

Caution must be used when this is done because depending upon the method used different results can be obtained. This same fact is also born out in the yield estimation based upon actual field measurements. Yields obtained and based upon over-pressure measurements are different from those based upon impulse with the difference increasing the closer to ground zero the measurements are taken.

For the purpose of relating the "Normalized Yield" values to "TNT Equivalent" values, the writer used the method given in the "Summary Report on a Study of the Blast Effect of a Saturn Vehicle" by Arthur D. Little, Inc., dated February

*Professor and Research Professor of Mechanical Engineering, University of Florida, Gainesville, Florida.

15, 1962. The results presented on page 70 of the above reference lead to the following correlation:

A. 1 lb of LOX/RP propellant in a 2.25/1 weight ratio is potentially equivalent to 1.23 lb of TNT.

B. 1 lb of LOX/LH_2 propellant in a 5/1 weight ratio is potentially equivalent to 1.52 lb of TNT.

C. 1 lb of LOX/RP/LH_2 propellant in a weight composition of 0.75/0.18/0.07 (Saturn C-2 Configuration) is potentially equivalent to 1.355 lb of TNT.

D. 1 lb of LOX/RP/LH_2 propellant in a weight composition of 0.721/0.244/0.035 (Saturn V Configuration) is potentially equivalent to 1.29 lb of TNT.

On the above bases the values of expected yields as predicted by the Mathematical Model for the Saturn V propellant quantities are:

Saturn V

Normalized Yields	TNT Equivalent Yields
$y_{avg} = 3.8$	$= 4.9$
$y_{0.95} = 9.6$	$= 12.4$

y_{avg} average of all expected yields

$y_{0.95}$ 95% of all the expected yields fall below this value

A further word of caution should be added at this time in case a damage index is attached to these yield values expressed in terms of TNT equivalents. Again because of the difference in the pressure-time traces, a particular liquid propellant explosive yield can be expected to do a different amount and type of damage (especially in the near field) from the TNT explosive yield of the same value. In other words, care should be used in applying these results, taking cognizance of the explosive characteristics of the propellants under consideration.

BIBLIOGRAPHY

1. Farber, E. A., et al. "Feasibility Study to Explore the Explosive Effects of Liquid Propellants to Define the Mathematical Behavior of Physical Processes Involved," Final Report, Phase I, Contract No. NAS10-1255, University of Florida, February, 1965.

2. Farber, E. A., "A Mathematical Model for Defining Explosive Yield and Mixing Probabilities of Liquid Propellants," Third Space Congress Proceedings, March 1966 (Preceding paper).

3. "Thermocouple Grid Analysis of Two 25,000-lb LOX/RP Liquid Propellant Explosion Experiments," E. A. Farber, Technical Paper No. 396, Florida Engineering and Industrial Experiment Station, Vol. XXI, No. 11, November, 1967.

4. "Explosive Yield Estimates for Liquid Propellant Rockets Based Upon a Mathematical Model," E. A. Farber, Technical Paper No. 415A, Florida Engineering and Industrial Experiment Station, Vol. XXII, No. 7, July, 1968.

5. "Interpretation of Explosive Yield Values Obtained from Liquid Rocket Propellant Explosions," E. A. Farber, Technical Paper No. 415B, Florida Engineering and Industrial Experiment Station, Vol. XXII, No. 7, July, 1968.

6. Arthur D. Little, Inc. "Summary Report on a Study of the Blast Effect of a Saturn Vehicle," February, 1962.

7. Wilks, S. S., Mathematical Statistics, John Wiley & Sons, Inc., New York, 1962.

8. Serret, "Cours de Calcul Differential et Integral," Paris, 1907.

9. Gradshteyn and Ryshik, Tablitsy Integralov, Moscow, 1963.

10. Wald, A., Annals of Mathematical Statistics, 11, 1940.

11. "Handbook of Mathematical Functions with Formulas, Graphs, and Mathematical Tables," U. S. Department of Commerce, NBS Applied Mathematics Series -55, 1964.

12. Jahnke, Emde, Lösch, "Tables of Higher Functions," McGraw-Hill Book Company, Inc., New York, 1960.

13. "Preliminary Final Report of Project PYRO." Received incomplete copy April 17, 1968.

14. Information obtained from Lou Ullian, AFETR through informal correspondence and relayed by J. H. Deese.

Bibliography (Continued)

15. E. A. Farber and R. L. San Martin, " Studies and Analyses of the Mixing Phenomena of Liquid Propellants Leading to a Yield-Time Function Relationship," Proceedings of the New York Academy of Sciences Explosives Symposium, November, 1966.

16. Farber, E. A., et al., "Fireball Hypothesis Describing the Reaction Front and Shock Wave Behavior in Liquid Propellant Explosions," New York Academy of Sciences, Explosives Symposium Proceedings, 1967. Available as Technical Paper 387, Florida Engineering and Industrial Experiment Station.

17. Welch, J. E., et al., "The MAC Method," Los Alamos Scientific Laboratory LA-3425, New Mexico, March, 1966.

18. Eichel, F. G., "Electrostatics," Chemical Engineering, March 13, 1967.

19. Van Dolah, R. W. and Burgess, D. S., "Explosion Problems in the Chemical Industry," American Chemical Society, 1968.

20. Van Nice, L. J., et al., "Thermal Radiation from Saturn Fireballs," Volume I, Analysis, TRW Systems, December, 1965.

21. Van Nice, L. J., et al., "Thermal Radiation from Saturn Fireballs," Volume II, Appendices F, G, and H, TRW Systems, December, 1965.

22. Project PYRO, "Monthly and Quarterly Progress Reports," 1963 to present.

23. Huff, V. N., et al., "General Method and Thermodynamic Tables for Computation of Equilibrium Composition and Temperature of Chemical Reaction," NACA TR 1037, U. S. Govt. Printing Office, Washington, D. C., 1951.

24. Houston Research Institute, Inc., "Blast and Fireball Comparison of Cryogenic and Hypergolic Propellants," Contract NAS9-3506, August, 1964.

25. Smith, M. L., et al., "Fuels and Combustion," McGraw-Hill Book Company, New York 1952.

26. Goodman, H. J., "Compiled Free - Air Blast Data on Bare Spherical Pentolite," BRL Report No. 1092, Aberdeen Proving Ground, MD. Feb. 1960.

27. Shaffer, A., Rouseau, J., "Thermodynamical Properties of 24.4K Equilibrium Hydrogen," Airesearch Manufacturing Company, Los Angeles, California, October 1961.

Bibliography (Continued)

28. Deese, J. H., "A Correlation and Hypothesis of LH_2/LO_2/RP-1 Blast Data," Unpublished, January 1963.

29. Stewart, R. B., Timmerhaus, K. D., "Thermodynamic Properties of Cryogenic Fluids," NBS, Boulder, Colorado, 1963.

30. Linde Corp., "Physical Property Equivalents of Some Cryogenic Fluids," 1963.

31. Facilities Engineering and Construction Division, KSC, "Study of Degree of Risk to Launch Area Due to Spilling, Mixing, and Ignition of Cryogenic Propellants," Unpublished, January 1964.

32. Gayle, J. B., "Investigation of S-IV All Systems Vehicle Explosion," MSC, Huntsville, Alabama, NASA TM X-53039, April 27, 1964.

33. Aerojet-General Corp., "Blast and Fireball Comparison of Cryogenic and Hypergolic Propellants," Contract NAS9-2055, June 26, 1964.

34. Foust, A. S., and others, "Principles of Unit Operations," John Wiley & Sons, Inc., New York, New York, 1960.

35. Information obtained from J. H. Deese through informal correspondence.

36. Edwards, J. W. Integral Calculus, MacMillan Company, London, 1896.

37. Mechanical Engineers' Handbook, edited by T. Baumeister, McGraw-Hill Book Company, Inc., 6th Edition, New York, 1958.

38. Obert, E. F., Internal Combustion Engines, International Textbook Company, Second Edition, Pennsylvania, 1960.

39. Seader, J. D., et al., "Boiling Heat Transfer for Cryogenics," Final Report, Rocketdyne R-5598, May 11, 1964.

40. ASHRAE Guide and Data Book 1961, American Society of Heating, Refrigeration and Air-Conditioning Engineers, Inc., 1961.

41. Handbook of Engineering Fundamentals, edited by O. W. Eshbach, John Wiley and Sons, Inc., Second Edition, New York, 1958.

42. Handbook of Chemistry and Physics, edited by C. D. Hodgman, Chemical Rubber Publishing Company, Forty-First Edition, Ohio, 1960.

43. Chemical Engineers' Handbook, edited by J. H. Perry, McGraw-Hill Book Company, Inc., Third Edition, New York, 1958.

Bibliography (continued)

44. Technical Data on Fuel, edited by H. M. Spiers, The British National Committee World Power Conference, Fifth Edition, London, 1952.

45. Fuels and Combustion Handbook, edited by A. [illegible]. Johnson, McGraw-Hill Book Company, Inc., New York, 1951.

46. Nelson, W. L., Petroleum Refinery Engineering, McGraw-Hill Book Company, Inc., New York, 1936.

47. Farber, E. A. and Deese, J. H., "A Systematic Approach for the Analytical Analysis and Prediction of the Yield from Liquid Propellant Explosions," Proceedings of the Third Space Congress, March, 1966.

48. "Blast and Fireball Comparison of Cryogenic and Hypergolic Propellants," Aerojet General Corp., Contract No. NAS 9-2055, Final Report, June, 1964.

49. Farber, E. A. and Richardson, M. R., "The Gamma Ray Densitometer and Concentration Meter," Proceedings of Annual Meeting of Instrument Society of America, April, 1957.

50. Farber, E. A., "200 A Thorium [illegible] Slurry Test Loop Density and Concentration Data," Oak Ridge National Laboratory Report, January, 1957.

51. Farber, E. A., "Bubble and Slug Flow in Gas-Liquid and Gas (Vapor) - Liquid-Solid Mixtures," Oak Ridge National Laboratory Report, May, 1957.

52. Farber, E. A., "Bubble and Slug Flow in Circulating Gas-Liquid and Gas-Liquid-Solid Mixtures," Oak Ridge National Laboratory Report, February, 1958.

53. ASME and ASCE "Symposium on Water Hammer," Proceedings, 1933.

54. Boering, Burkhardt, "Beitraege zur Theorie der Detonation," Deutsche Luftfahrtforschung, No. 1939, April 1944.

55. Farber, E. A., et al., "Fireball and Post-Fireball Composition and Atmospheric Chemistry of Fuel/Oxygen-Fluorine Propellants," NASA report, Contract NAS10-1255, July, 1967.

56. Farber, E. A., et al., "A Bibliography of Authoritative Sources Defining the Physical and Chemical Properties of Fluorine and its Oxidizing Mixtures and Compounds," Part I, Contract NAS10-1255, University of Florida, April 1965.

Bibliography (Continued)

57. Farber, E. A., et al., "A Bibliography of Authoritative Sources Defining the Physical and Chemical Properties of Fluorine and its Oxidizing Mixtures and Compounds," Part II, Confidential, Contract NAS10-1255, University of Florida, April 1966.

58. Farber, E. A., et al., "Thermocouple Grid Method Applied to Studying Liquid Mixing," Contract NAS10-1255, University of Florida, March 1966.

59. High, R. W., "The Saturn Fireball," New York Academy of Sciences, Explosives Symposium Proceedings, 1967.

60. Fletcher, R. F., "Characteristics of Liquid Propellant Explosions," New York Academy of Sciences, Explosives Symposium Proceedings, 1967.